

TC175.2
.A34
1993

DISSERTATION

VERTICAL SORTING WITHIN DUNE STRUCTURE

Submitted by

Mohamed M. M. Abdel-Motaleb

Civil Engineering Department

In partial fulfillment of the requirements

for the Degree of Doctor of Philosophy

Colorado State University

Fort Collins, Colorado

Spring, 1993

Date Due

INTERLIBRARY LOAN		
#	-106	
4 WEEKS USE; NO RENEWAL		
VERTI	SEP 11 2000	CTURE

BRODART, INC. Cat No. 23 233 Printed in U.S.A.

In partial fulfillment of the requirements
for the Degree of Doctor of Philosophy
Colorado State University
Fort Collins, Colorado
Spring, 1993




COLORADO STATE UNIVERSITY

November 24, 1992

WE HEREBY RECOMMEND THAT THE DISSERTATION PREPARED UNDER OUR SUPERVISION BY MOHAMED M. M. ABDEL-MOTALEB ENTITLED VERTICAL SORTING WITHIN DUNE STRUCTURE BE ACCEPTED AS FULFILLING IN PART, REQUIREMENTS FOR THE DEGREE OF DOCTOR OF PHILOSOPHY.

Committee on Graduate Work









Advisor



Department Head

TC 175.2
A34
1993

ACKNOWLEDGEMENTS

The writer wishes to express his sincerest gratitude and appreciation to his major professor, Dr. J. Gessler, for the excellent guidance, advice, and the continuous encouragement he provided throughout the experimental work, the analysis and interpretation of the results, which to a large extent has made the completion of this study possible.

The writer's grateful appreciations are extended to Drs. E. V. Richardson and A. Molinas, members of the writer's graduate committee, for their assistance and encouragement. The writer also wishes to thank Dr. D.W. Zachmann, a member of the writer's graduate committee, for his assistance and encouragement. Special thanks are due to Dr. C.F. Nordin for his help reviewing the original draft of the dissertation and his suggestions are gratefully acknowledged.

The writer expresses his gratitude to the Egyptian Ministry of Public Works and Water Resources, Dr. M. Abu-Zeid; Chairman of the Water Research Center, Dr. Ahmed Khafagy; Director of the Soil Mechanics Research Institute, for giving him this opportunity to study at Colorado State university. He also thanks the USAID mission in Cairo and the Water Research Center project, Contract number 263-0132-C-5060, at Colorado State University for providing the financial support during his research.

The writer extends his thanks to the Water Research Center project's staff for their keen help and support during this research; and also Jenifer Davis for her help during the typing.

A special gratitude and dedication for this work is due to my wife Entesar and to my son Kareem for their support, patience and encouragement throughout this research. Finally, thanks be to my God without whom nothing can be achieved.

*This work is dedicated to
my wife Entesar and my son Kareem*

ABSTRACT OF DISSERTATION

VERTICAL SORTING WITHIN DUNE STRUCTURE

Vertical sorting of sediment mixtures within dune structures was measured experimentally by conducting three types of experiments: running water experiments, still water experiments, and air experiments. Five different sediment mixtures with known initial gradations were used. The median grain diameters for the five sediment mixtures were between 0.35 mm and 0.86 mm, the geometric standard deviations of the same sediment mixtures were between 2.30 and 2.9.

In the running water experiments, each experiment was continued until the dunes were fully developed down the flume. Then each dune was sampled along several horizontal layers. In the still water experiments, a delta shape was deposited, foreset by foreset, following one another in a continuous way. In the air experiments, the sand mixture was deposited as in the still water experiments. These experiments were to study the effect of the gravitational force on the vertical sorting process.

The results of the running water experiments showed clearly demonstrated the vertical sorting process (vertical reduction in the sediment grain diameter) within the two-dimensional dunes. Also, the still water and air experiments showed the importance of the hydrodynamic force on the sorting process. A prediction equation relating the

median grain diameter within the dune structure in the vertical direction to the back flow velocity on the lee face of the dune and the submerged weight of the sediment particle was used to calculate the vertical median grain diameter for the two-dimensional dune and compared with the measured data. Five dimensionless parameters were tested to correct the error in the predicted values. The dimensionless grain diameter gave the best result.

Other sets of laboratory and field data for a point bar and three-dimensional dunes showed the sorting phenomenon. Calculated values for the vertical median grain diameter for the three-dimensional dune computed using the prediction equation agreed reasonably well with the observed values.

Mohamed M. M. Abdel-Motaleb
Civil Engineering Department
Colorado State University
Fort Collins, Colorado 80523
Spring, 1993

TABLE OF CONTENTS

CHAPTER 1	INTRODUCTION	1
CHAPTER 2	SORTING PROCESSES IN RIVERS	6
2.1	Four Sorting Processes	7
2.2	Predicting Bed Forms	11
2.3	Gravitational Sliding and Granular Flow	14
2.4	Delta Deposits	19
2.5	Zones of Flow Downstream of a Dune	26
2.6	Evidence of Vertical Sorting	28
2.7	Sorting in Point Bars and Dunes	34
CHAPTER 3	THE VERTICAL SORTING PROCESS	37
3.1	Physical Background	37
3.1.1	Pattern of flow in front of the dune	37
3.2	Explanation of Enrichment Stoss Side with Fine Material	38
3.3	Development of Lamination in the Lee Face	40
3.4	Proposed Mechanism	41
3.5	Proposed Relationship Between the Vertical Sorting and Dune Size	44
CHAPTER 4	EXPERIMENTAL SETUP AND PROCEDURE	48
4.1	The Flume	48
4.2	Individual Measurements	50
4.2.1	General	50
4.2.2	Flow depth	51
4.2.3	Discharge	52
4.2.4	Slope	52
4.3	Bed Sample	53
4.3.1	General	53
4.3.2	Bed Sample Procedure	55
4.4	Sediment Mixture	56
4.5	Procedure	62

CHAPTER 5	RESULTS AND ANALYSIS OF EXPERIMENTAL DATA	66
5.1	Calculation of Average Bed Shear Stress	66
5.2	Experimental Results	70
5.2.1	Running Water Experiments	70
5.2.2	Still water experiments	85
5.2.3	Air Experiments	90
5.2.4	"Eight-foot" Flume Experiment	93
5.3	Prediction of Vertical Size Distribution of a Dune Structure	94
5.3.1	Developing the Theoretical Equation	94
5.3.2	Effect of the Median Diameter on the Formula	110
5.4	Predicting the Vertical Median Grain Diameter Procedure	124
5.5	Prediction of Vertical Grain Size for a Three-dimensional Dune	131
5.6	Field Data	133
CHAPTER 6	SUMMARY, CONCLUSIONS, AND RECOMMENDATIONS	138
6.1	Summary	138
6.2	Conclusions	140
6.3	Recommendations for Future Research	142
REFERENCES	144
APPENDIX A	SIZE DISTRIBUTION CURVES FOR THE DUNE LAYERS	149
APPENDIX B	SHEAR STRESS CALCULATIONS	183

LIST OF FIGURES

Figure 2.1.	Relation of bed form to stream power and median fall diameter of bed sediment (after Simons and Richardson, 1966)	12
Figure 2.2.	The complete lines indicate shear stress and the broken lines indicate pressure (after Bagnold, 1954)	17
Figure 2.3.	Inclined flume (after Bagnold, 1954)	18
Figure 2.4.	Size characteristics of sand used in experiments (after Jopling, 1965)	20
Figure 2.5.	The upper diagram illustrates the dispersion and sorting of particles in the downstream direction as a function of differential settling velocity. The lower diagram illustrates the dispersion of one size class of particle as a function of height above the bed of the stream. Note the collective settling of the assorted particle sizes carried along the bed of the stream in the zone of heavy sediment concentration (after Jopling, 1965).	23
Figure 2.6.	Zones of the flow downstream of a ripple, dune or sand delta on the basis of its turbulence properties (after Allen, 1968)	27
Figure 2.7	Magnitude of the turbulence downstream of a dune (after Allen, 1968)	29
Figure 2.8	Position of samples (after Brush, 1965b)	31
Figure 2.9.	Foreset lamina in dune structure which consists of several laminae	33
Figure 2.10.	Grain size distribution of the two fractions (after Ribberink, 1983)	33
Figure 2.11	Point bar on the East Fork river, Wyoming. Note the dunes in the foreground	36
Figure 2.12	Sediment size distributions over the point bar shown in Figure 2.12.	36
Figure 3.1.	Flow pattern over a lee face of a ripple (after Reineck and Singh, 1975)	39
Figure 3.2.	Flow pattern and sedimentation processes on the lee side of a ripple (after Reineck and Singh, 1975)	39
Figure 3.3.	Proposed internal structure of a dune	43
Figure 3.4.	Photograph of foreset bedding in a large sand wave along the Orinoco river (McKee, 1989, Fig. 16)	46

Figure 4.1.	Schematic diagram for the experimental flume (after Rathbun et al., 1969)	49
Figure 4.2.	Design curve for sample of mass m (ISO standards, 1983)	54
Figure 4.3.	Schematic diagram for the bed sampler	55
Figure 4.4.	Size distribution curves for sand mixtures number 1, 2 and 3	60
Figure 4.5.	Size distribution curves for sand mixtures number 3, 4 and 5	61
Figure 4.6.	Diagram showing the deposition of each sand foreset using a funnel	64
Figure 5.1.	Variation in dune height to dune length ratio with bed shear stress for different grain sizes (after Fredsøe, 1982)	69
Figure 5.2.	Variation in dune height to water depth ratio with bed shear stress for different grain sizes (after Fredsøe, 1982)	69
Figure 5.3.	Size distribution curves for dune layers (Dune #1, Mixture #1)	73
Figure 5.4.	Actual median grain diameter for a dune layer (Mixture #1)	74
Figure 5.5.	Actual median grain diameter for dune layer (Mixture #2)	75
Figure 5.6.	Actual median grain diameter for dune layer (Mixture #3)	76
Figure 5.7.	Actual median grain diameter for dune layer (Mixture #4)	77
Figure 5.8.	Actual median grain diameter for a dune layer (Mixture #5)	78
Figure 5.9.	Normalized average geometric standard deviation in the vertical direction (Mixture #1)	80
Figure 5.10.	Normalized average geometric standard deviation in the vertical direction (Mixture #2)	81
Figure 5.11.	Normalized average geometric standard deviation in the vertical direction (Mixture #3)	82
Figure 5.12.	Normalized average geometric standard deviation in the vertical direction (Mixture #4)	83
Figure 5.13.	Normalized average geometric standard deviation in the vertical direction (Mixture #5)	84
Figure 5.19.	Three-dimensional dune pictures (8 ft. flume)	95
Figure 5.20.	Size distribution curves for dune layers (Dune #1, 8 ft. flume)	96
Figure 5.21.	Size distribution curves for dune layers (Dune #2, 8 ft. flume)	97
Figure 5.22.	Size distribution curves for dune layers (Dune #3, 8 ft. flume)	98
Figure 5.23.	Size distribution curves for dune layers (Dune #4, 8 ft. flume)	99
Figure 5.24.	Dune definition sketch	101
Figure 5.25.	Standardized dimensionless velocity diagram	104
Figure 5.26.	Predicted and actual median grain diameter for a dune layer (Mixture #1)	105
Figure 5.27.	Predicted and actual median grain diameter for a dune layer (Mixture #2)	106
Figure 5.28.	Predicted and actual median grain diameter for a dune layer (Mixture #3)	107
Figure 5.29.	Predicted and actual median grain diameter for a dune layer (Mixture #4)	108
Figure 5.30.	Predicted and actual median grain diameter for a dune layer (Mixture #5)	109

Figure 5.31.	Relation between the error in the predicted median grain diameter for each dune layer and the grain diameter	112
Figure 5.32.	Relation between the error in the predicted median grain diameter for each dune layer and the dimensionless shear stress	116
Figure 5.33.	Relation between the error in the predicted median grain diameter for each dune layer and the dimensionless shear stress due to grain resistance	117
Figure 5.34.	Relation between the error in the predicted median grain diameter of each dune layer and the dimensionless shear stress due to form drag	118
Figure 5.35.	Relation between the error in the predicted median grain diameter for each dune layer and the boundary Reynolds number	120
Figure 5.36.	Relation between the error in the predicted median grain diameter for each dune layer and the dimensionless grain diameter	121
Figure 5.37.	Relation between the error in predicting the median diameter for each dune layer and the dimensionless shear stress	122
Figure 5.39.	Predicted, modified, and actual median grain diameter for a dune layer (Mixture #1)	125
Figure 5.40.	Predicted, modified, and actual median grain diameter for a dune layer (Mixture #2)	126
Figure 5.41.	Predicted, modified, and actual median grain diameter for a dune layer (Mixture #3)	127
Figure 5.42.	Predicted, modified, and actual median grain diameter for a dune layer (Mixture #4)	128
Figure 5.43.	Predicted, modified, and actual median grain diameter for a dune layer (Mixture #5)	129
Figure 5.44.	Standardized normalized geometric standard deviation in the vertical direction	130
Figure 5.45.	Predicted values for the median grain diameter for the 8 foot flume dunes and the actual values	134
Figure 5.46.	Size distribution curves for four samples along the back and the lee face of a water dune (after McKee, 1989)	135

LIST OF TABLES

Table 2.1.	Measured and calculated speed of a moving sand front under gravity force (After Bagnold, 1954)	19
Table 2.3.	Grain size data for glacial outwash sand and gravelly sand (after Jopling, 1965)	22
Table 2.4.	Grain size data for silica 17 sand (after Jopling, 1965)	22
Table 2.5.	Grain size data for ipswich sand (after Jopling, 1965)	22
Table 2.2.	Values of d_{50} at different positions in the dune structure (after Brush, 1965)	31
Table 4.1.	Grain size distribution for sand mixture #1	57
Table 4.2.	Grain size distribution for sand mixture #2	57
Table 4.3.	Grain size distribution for sand mixture #3	58
Table 4.4.	Grain size distribution for sand mixture #4	58
Table 4.5.	Grain size distribution for sand mixture #5	59
Table 5.1.	Summary of the measured data for running water experiments . . .	67
Table 5.2.	Summary of the measured data for still water and air experiments	67
Table 5.3.	Calculated values for bed shear stress, shear stress due to grain resistance, and shear stress due to form drag	68
Table 5.4.	The ratio between the predicted median grain diameter and actual median grain diameter value	115
Table 5.5.	The values of dimensionless shear stress, dimensionless shear stress due to grain resistance, dimensionless shear stress due to form drag, boundary Reynolds number, and dimensionless grain diameter	115

NOTATIONS

a	=	constant
A	=	cross-sectional area
A_b	=	area related to the bed
c_a	=	mean concentration of sediment at an arbitrary reference elevation a
c_s	=	volume concentration of the sediment
c_y	=	mean concentration of sediment at a certain y
c_α	=	numerical constant
d_o	=	total depth
d_s	=	representative size of bed material
d_{si}	=	median grain diameter at layer i
d_{50p}	=	predicted median grain diameter
d_{50m}	=	median grain diameter of sediment mixture
d_{ave}	=	average flow depth
d_{50}	=	median grain diameter
D_*	=	dimensionless particle diameter
E	=	numerical constant
F_b	=	bed friction factor
F_d	=	drag force
F_f	=	friction force
F_g	=	submerged weight of particle
F_L	=	lift force
F_s	=	seepage force in the stream bed
F_w	=	wall friction factor
Fr	=	Froude number
g	=	acceleration of gravity
k	=	Van Karman coefficient
k_s	=	d_{6s} is the grain roughness of the bed
L	=	distance downstream of reference station
p	=	wetted perimeter
p_b	=	wetted perimeter related to the bed

pp	=	repulsive pressure
P_o	=	probability density function of grain size distribution of mixture
$q(d_s)$	=	probability that grain size d_s will not be removed
Q_s	=	sediment discharge
Q_w	=	water discharge
r	=	hydraulic radius for the whole section
r_b	=	hydraulic radius associated with the bed
r_{bd}	=	hydraulic radius associated with τ_{bd}
r_{bg}	=	hydraulic radius associated with τ_{bg}
R_*	=	boundary Reynolds number
S_c	=	shape factor for the stream cross-section
S_e	=	slope of energy gradient
S_p	=	shape factor of the particle
S_r	=	shape factor for the stream cross-section
S_w	=	water surface slope
S_1	=	thickness of laminar sublayer
T	=	applied shear stress
T_g	=	internal resisting grain shear stress
u_s	=	mean velocity of sand particle
u_*	=	shear velocity
U_w	=	average velocity of flow
ν	=	kinematic viscosity of water
w	=	fall velocity at any elevation y above the bed
W	=	weight of particle at distance L from reference station
W_o	=	weight of particle at reference station
y	=	elevation above the bed
α	=	constant angle related to particle collision
β	=	coefficient relating the sediment diffusion coefficient to the momentum diffusion coefficient
γ	=	specific weight of water
γ_s	=	specific weight of sediment
γ_w	=	specific weight of the fluid
λ	=	linear concentration of sediment which equals d_s / s (s is the free distance between two particles)
μ	=	dynamic viscosity of water
ρ	=	density of water

ρ_s	=	density of sediment
σ	=	standard deviation
σ_g	=	geometric standard deviation
τ	=	mean bed shear stress
τ_b	=	bed shear stress
τ_{bd}	=	shear stress results due to irregularities in the bed
τ_{bg}	=	shear stress results from grain resistance
$\tau_c(d_s)$	=	critical shear stress for grain size d_s
τ_*	=	dimensionless shear stress
τ_{*g}	=	dimensionless shear stress due to grain resistance
τ_{*d}	=	dimensionless shear stress due to form drag

CHAPTER 1

INTRODUCTION

The reduction of rock material as a consequence of denudation and weathering of the earth's crust has been of interest to geologists for a long time. Of still greater interest is the transportation of this movable material--boulders, gravel, sand, and silt--by the action of gravity, wind, and water. It is these erosion, transportation, and depositional phenomena that have developed our alluvial plains, river valleys, loess deposits, desert dunes, and sand seas. Erosion and sedimentation are important environmental problems. Watershed control, river mechanics, and the improvement of navigation and dredging techniques take into account many of the principals related to transport of sediment.

Sediment transport occurs in natural stream beds at least in part as bed load. A striking feature of many of these natural stream beds is the distortion of these beds into trains of waves. For low Froude numbers, these bedforms (waves) are typically classified as ripples or dunes, depending on the bed morphology and flow conditions. Their equilibrium (fully developed) shapes are determined by interaction between the flow, the bed geometry, and sediment transport field. Thus the bedform is created by the flow, and conversely, the flow is acted on by the bedform.

Furthermore, a detailed physical understanding of these flow, sediment and bed interactions comprises the basis for developing better methods for computing effective

roughnesses of channels in which ripples or dunes are present. Two of the features of the flow-bedform interaction are cross stratification and sorting processes. An understanding of these phenomena is also a part of making accurate predictions of sediment transport and its composition on rippled and duned beds. This makes an understanding of the interaction between the flow and the bed morphology of considerable importance to engineers interested in rivers and streams with erodible beds. Similarly, geologists and sedimentologists attempting to interpret paleoenvironmental conditions using primary sedimentary structures preserved in the stratigraphic record must have the ability to relate the observed geometric features of those bedforms to the flow conditions that created them. Also, geologists are interested in determining the way which the earth's crust was folded, for example, in a sedimentary deposit which has been folded and eroded, which way was up and which way was down (see, for example, discussions by Middleton, 1965 and Brush, 1965a).

Sediment sorting is one of the bedform characteristics which is not physically fully understood despite the attention of earlier researchers of the mid-sixties, such as Brush (1965b), Jopling (1964, 1965), McKee (1965) and others. In general, sorting is the fundamental process which leads to the formation of primary sedimentary structures and textures in an alluvial channel. According to Brush (1965b, p. 25) "Fall velocity, turbulence, diffusion, gravitational sliding, and shear stresses in proximity to the stream bed reflect the physical controls which lead to temporal and spatial segregation of sediment particles by size, and which interact with the population characteristics of the particle distributions available."

A physical understanding of how sorting contributes to the sediment deposited structure will enhance our understanding of the environment in which the sediment has been deposited. In addition, one of the benefits of studying the vertical sorting in dunes is to understand that as the dune moves over the river bed it keeps a layer of coarse particles that cover the non-moving layer of the bed. This protects the layer in case the sediment is stopped, for example, by a dam or any hydraulic structure. If it is stopped, the dune will erode until the coarsest layer is reached. The erosion will then stop unless the shear stress reaches a critical value able to destroy even this armored type layer.

Another aspect of understanding this phenomenon is that it is a step further toward the relationship between the grain size distribution within the dune structure and the shape of the dune. If there is a relationship, much of the research on form drag of dunes may become somewhat unnecessary. But before going to this step, the phenomenon of vertical sorting needs to be documented and explained.

The objectives of this study were to investigate the major factors influencing vertical sorting within individual dunes, to experimentally measure the vertical size distribution within a dune structure, and on the basis of the results, to develop a method to predict the vertical size distribution within a two-dimensional dune structure, assuming a median grain diameter, d_{50} , of the sediment mixture, a geometric standard deviation, σ_g , of the mixture, and a mean velocity of the reach containing the dunes.

The goal of this research was achieved by conducting a series of physical experiments in a laboratory flume using 5 different sediment mixtures with known initial gradations. Three types of experiments were conducted: running water experiments,

still water experiments, and air experiments. In the running water experiments, the experiment was kept running until well developed dunes formed over the length of the flume bed under uniform sediment and hydraulic conditions. The experiment ran for about 12 to 24 hours depending on the mixture type. After the dunes showed little change in shape with time, the experiment was stopped and the sampling of the dune began. The second set of experiments, with still water, were necessary to separate the effect of the gravitational sliding only from the effect of hydraulic forces in the vortex zone, downstream of the dune. In these experiments the dune was deposited mechanically foreset by foreset, until an adequate length for sampling had been reached. Then the dune was sampled using the same technique described for the running water experiments. The air experiments were conducted for the same reason as the still water ones, i.e. to separate the effect of the hydrodynamic forces from the gravitational force. The same procedure for the deposition of the still water dune was used to deposit the air dune. The reason for the air experiments was to remove the effect of submerged weight (water experiments) on the sorting process.

Chapter 2 presents previous experimental, theoretical, and historical field studies of the vertical size distribution of sand mixtures and the factors that affect this process. Chapter 3 gives an interpretation of the vertical sorting phenomenon, and proposes mechanisms that controls these processes and how they might vary with size of the dunes. Chapter 4 briefly describes the flume used in the experiments, methodologies used in the measurements of the hydraulic parameters, the sediment mixtures, and the procedures used to collect the data in the study. Chapter 5 is devoted to the analysis

and interpretation of the experimental data and includes data collected by other researchers. An equation to predict the vertical size distribution of the sediment mixture of a two-dimensional dune structure is presented. At the end of the chapter there is a comparison between data from a three-dimensional dune and the predicted values based on this research. Chapter 6 contains a summary, the conclusions and some recommendations. Appendix A contains the size distribution curves for the dunes of the five mixtures, and other data. Graphs for the corrected values of the predicted median diameter within the dune structure using two different correction factors, dimensionless shear stress due to grain resistance, and dimensionless grain diameter. Appendix B contains methods used for side-wall corrections and for computations of the bed shear stress and shear stress related to the grain roughness.

CHAPTER 2

SORTING PROCESSES IN RIVERS

Sediment transport by wind and water and the sorting processes associated with sediment transport have been studied by geologists, scientists, and engineers for at least 150 years. Geologists were primarily interested in interpreting the geologic record and in determining the depositional environments of sedimentary rocks. Middleton (1965) and Reineck and Singh (1975) provide excellent historical reviews from the geologist's perspective. Bagnold (1941) focused on the physics of wind-blown sands and later (1954) on the physics of granular shear flows, and much of what is known today about these processes is based on the foundation that he laid. Engineers were concerned mostly with traditional problems of river engineering--navigation, channel stabilization, deposition in reservoirs and erosion and armoring downstream--and much of their work was directed to practical application (see Graf, 1971, for a review of early work in river hydraulics and sediment transport). The investigation of these various disciplines proceeded more-or-less independently until the early 1960's, when concerted efforts were undertaken to integrate fluid mechanics, sediment transport, sedimentology, and geology into a hydrodynamic relation of primary sedimentary structures (Middleton, 1965). Since then, much of the important work on fluvial and eolian processes has been carried out by earth scientists, as demonstrated in the review volume by Reineck and Singh (1975) and the book "Wind as a Geologic Agent" by Greeley and Iverson (1987).

For this study, attention is focused on sorting associated with sediment transport by water, specifically the sorting that occurs in individual dune structures. Vertical sorting associated with the development of point bars has been studied in considerable detail, and the sorting in individual dunes has been observed by several investigators, as will be shown in subsequent discussion, but not much is known about the specific mechanisms involved. The following section of this chapter reviews some of the important work on sorting processes that lead to this investigation.

2.1 Four Sorting Processes

There are four kinds of sorting in river processes. The first one is the longitudinal sorting which occurs along a river over long distances, for example, in the Mississippi or Colorado rivers. The second one is 'selective erosion' leading to armoring. The third one is vertical sorting in suspended sediment load. The last one is vertical sorting in bed sediment structures, such as ripples or dunes.

Longitudinal sorting. Studies of river bed materials have shown that the size of particles forming the beds of rivers gradually decrease in size in the downstream direction. This reduction in size is related to channel geometry, sediment transport, and flow variables such as the velocity. Many researchers worked on the prediction of this size reduction as early as the nineteenth century. One of these researchers was Sternberg (see Reineck and Singh, 1975, p. 114), who presented a relationship sometimes referred to as his "abrasion law". This relation is:

$$W = W_o e^{(-E L)} \quad (2.1)$$

where:

W = weight of the particle at distance L from a reference station,

W_o = weight of the particle at the reference station,

E = numerical constant, and

L = distance downstream of the reference station.

But Lane (1955) presented the following relation:

$$Q_s d_s \sim Q_w S_e \quad (2.2)$$

where:

Q_s = sediment discharge,

Q_w = water discharge,

S_e = slope of energy gradient, and

d_s = representative size of bed material.

A decrease in slope therefore will lead to a decrease in size of bed material. The relationship is very useful to predict the effect of man's work on river response.

Armoring. This is the process in which the fine particles of the bed material are most easily transported by the flow; the coarse particles tend to remain on the bed. If the drag force of the flow is not sufficient to move these coarse particles after a while, no further erosion can take place on the bed because of the natural armoring of the bed that occurs. If the drag force caused by the flow acting on the coarsest particles is

greater than the resisting force provided by the particles, the material will be transported. No armoring can take place under these circumstances.

Gessler (1970, 1971) suggested that the size distribution of the armor coat can be obtained from:

$$P_a = \frac{\int_{d_s \text{ Min}}^{d_s} q(d_s) P_o d d_s}{\int_{d_s \text{ Min}}^{d_s} q(d_s) P_a d d_s} \quad (2.3)$$

where:

P_o = probability density function of the grain size distribution of the mixture, and

$q(d_s)$ = probability that grain size d_s will not be removed.

Then:

$$q(d_s) = \frac{1}{\sigma\sqrt{2\pi}} \int_{-\infty}^{\frac{\tau_c(d_s)}{\tau} - 1} \exp\left[-\frac{x^2}{2\sigma^2}\right] dx \quad (2.4)$$

where:

σ = standard deviation,

$\tau_c(d_s)$ = critical shear stress for grain size, d_s , and

τ = mean bed shear stress.

Vertical sorting in suspended sediment. The concentration of suspended sediment load both within a given size fraction and more pronouncedly for the entire sample, at a certain level, tends to decrease rapidly with elevation above the reference (Brush, 1965a). The equation which describes the suspended sediment-concentration profile in steady two-dimensional open channel flow (Rouse, 1950) is:

$$\frac{c_y}{c_a} = \left[\frac{d_w - y}{d_w - a} \frac{a}{y} \right]^{\frac{w}{\beta k u_*}} \quad (2.5)$$

where:

c_y = mean concentration of sediment at a certain y ,

w = fall velocity at any elevation y above the bed,

c_a = mean concentration of sediment at an arbitrary reference elevation, a ,

d_w = total depth,

β = coefficient relating the sediment diffusion coefficient to the momentum diffusion coefficient,

k = van Karman coefficient ($k \approx 0.4$), and

u_* = shear velocity.

Iteratively for a number of size fractions within any specific particle-size distribution, the vertical sorting characteristics of the suspended sediment can be determined (Brush, 1965b).

Vertical sorting within bedform structures. This type of sorting arises as the result of bed load deposition on the downstream faces of sand waves or along and over the surface of point bars. Some work has been done on sorting in point bars, but there

are no predictive equations for vertical sorting in dunes. In fact, the only reports there are which showed some attention to this topic by researchers are a few descriptions of what they saw during experimental runs or samplings of deposited sediment in the natural environment. The importance of vertical sorting arises from the need to calculate bed-load transport for a sediment mixture. Most of the sediment bed load calculations assume that the sediment is sufficiently uniform leading to a single representative grain size. In some cases this assumption is not sufficient. For example:

- 1 - In many rivers the bed material is not uniform. It may have a geometric standard deviation, σ_g , bigger than 1.6.
- 2 - On most river beds where sediment transport is occurring, there are bedforms, transport layer, and the distribution of the particles within the bedform structure decreases in the vertical direction. This distribution affects the bed load characteristics. Thus, predicting bed form is an important component in identifying sorting processes.

2.2. Predicting Bed Forms

Bed configurations in alluvial channels may be classified as small scale features, ripples, dunes, antidunes, and flat bed, and large scale features, alternate bars in straight channels, and point bars that form on the inside of bends in meandering channels.

Many empirical methods exist for predicting the occurrence of bed forms. Simons and Richardson (1966) relate bed configurations to particle size and stream power as shown in Figure 2.1.

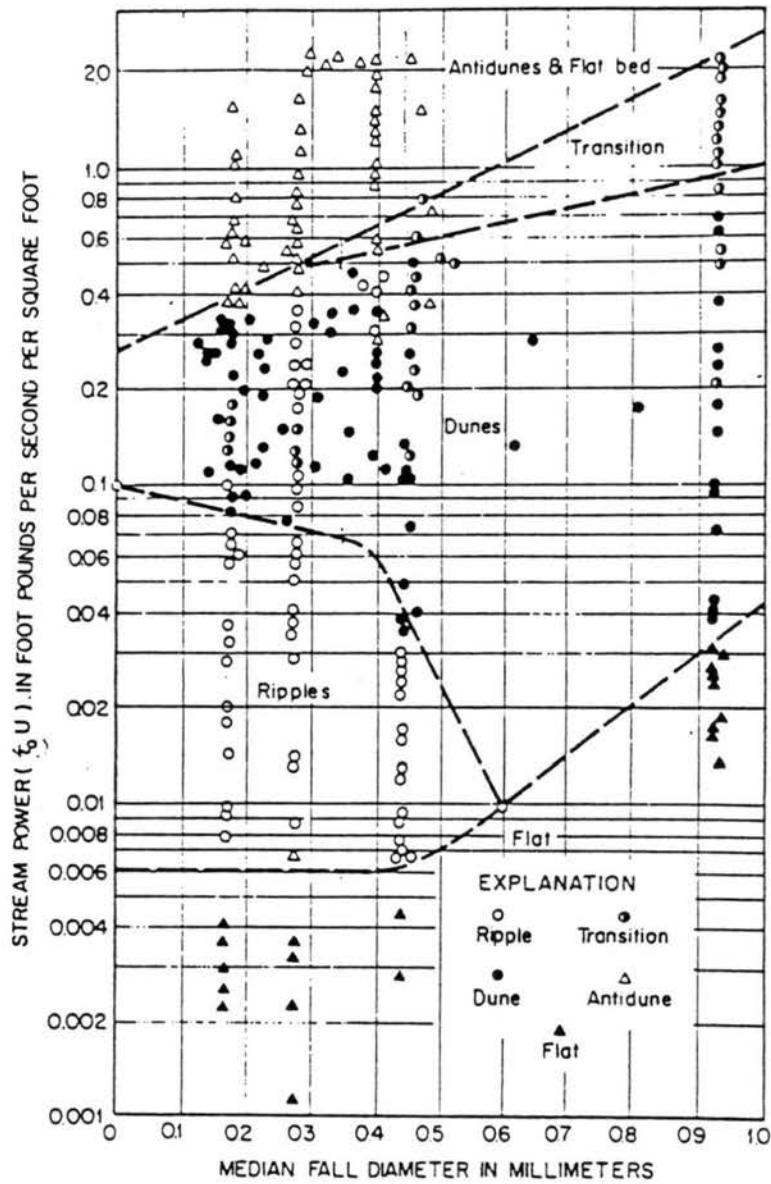


Figure 2.1. Relation of bed form to stream power and median fall diameter of bed sediment (after Simons and Richardson, 1966).

Other empirical relations developed from dimensional reasoning and empirical data are given by Yalin (1977, Figure 7.29) and van Rijn (1984, Figs. 2 and 3). These empirical relations are useful for prediction, but they do not provide much insight about the mechanisms responsible for the formation of sand waves. For that, mathematical models involving stability analysis are more appropriate.

The models for stability analyses are complicated, but the ideas applied to a sand bed are fairly simple. A flat sand bed with water and sediment flowing over it is stable if a small perturbation at the bed is dampened. If a small perturbation grows and generates a series of sand waves, the bed is unstable. Pioneering work in stability analysis was carried out by Kennedy (1963), who used two-dimensional potential flow and a simple relation between sediment transport rate and velocity near the bed. Engelund (1970) introduced real fluid properties and a more reasonable sediment transport function. For purposes here, the most important work was by Fredsøe who developed a model to predict dune length and height as function of grain size, flow depth, and dimensionless grain shear stress (Fredsøe, 1982, Figs. 5,6 and 8). Fredsøe (1978) also re-analyzed the origin of meandering and braiding in terms of stability analyses drawing heavily on the theoretical treatment of flow and bed topography in channel bends by Engelund (1974). A complete treatment of the theoretical developments and many appropriate references are given by Fredsøe (1984).

2.3 Gravitational Sliding and Granular Flow

The bed load sorting which occurs in alluvial sand bed channels arises as a result of bed load transport over the upstream faces of sand waves, ripples or dunes. As a duned bed migrates slowly downstream, a number of sorting processes operate on it. The combined effects of the various types of sorting are due to diffusion of sand particles at the crest of the dune, eddies, turbulence and backflow in the mixing zone, erosion on the back of the dunes, and gravitational sliding of the sediment at the lee face of the dune. Sorting due to gravitational sliding at the lee face of the dune has been described by Bagnold (1941).

This description of the avalanching down the lee face of a desert dune by Bagnold (1941) can also be applied to the sorting process of dunes. In a later and more quantitative approach Bagnold (1954) investigated the nature of the sliding of sand grains in the air down a trough at the angle of repose and predicted the speed of the front. The applied shear stress, T , on any plane, y , below the upper, free, surface of the sand is:

$$T = \rho_s g \sin\beta \int_y^0 c dy \quad (2.6)$$

where β is the angle of bed with the horizontal.

In anticipation of the fact that the very low viscosity of the fluid, in this case air, puts the internal resisting grain shear stress, T_g , in the inertia region, conditions for steady flow require that:

$$T = pp \tan \alpha_i \quad (2.7)$$

$$pp = a \rho_s \lambda^2 D^2 (du/dy)^2 \cos\alpha \quad (2.8)$$

$$a \rho_s \lambda^2 D^2 (du/dy)^2 \sin\alpha = \rho_s g \sin\beta \int_y^0 c dy \quad (2.9)$$

Finally,

$$\frac{du}{dy} = \sqrt{\frac{g \sin\beta}{a \sin\alpha}} \sqrt{\frac{\int_y^0 c dy}{\lambda d_s}} \quad (2.10)$$

where:

pp = repulsive pressure,

α = constant angle related to particle collision,

u = mean velocity of the sand particle,

y = elevation above the bed,

g = acceleration of gravity,

c = volume concentration of the sediment,

d_s = particle diameter,

λ = linear concentration of sediment which equal D/s (s is the free distance between two particles),

a = constant, and

ρ_s = density of the grains.

Observation by Bagnold shows that the visible grains at the free surface are about as closely packed as they are in random static piling, for which $c = 0.6$ for most natural sands. Since the grains below cannot be appreciably more closely packed, c must be

constant with depth; so $\int c dy = 0.6y$, and λ probably has a value corresponding to the limit 22.3 for spheres. Bagnold used, $\lambda = 17$, and the value of a $\sin\alpha$ from (Figure 2.2) is 0.076. Since T is seen to increase very rapidly with λ at these very high concentrations, the real figure may well be twice this. But taking a $\sin\alpha$ as 0.076, Equation (10) becomes:

$$\frac{du}{dy} = \sqrt{\frac{0.6 \sin\beta}{0.076} \frac{g^{1/2} y^{1/2}}{\lambda d_s}} = 0.165 \sqrt{g \sin\beta} \frac{y^{1/2}}{d_s} \quad (2.11)$$

and

$$u = 0.667 \times 0.165 \sqrt{g \sin\beta} \frac{y^{3/2}}{d_s} \quad (2.12)$$

A fairly uniform quartz sand of mean grain diameter 0.035 mm was allowed to flow down the simple flume shown in Figure 2.3 (Bagnold). By raising the reservoir gate a given distance a sand flow of any required height could be started, and could be stopped by closing the gate. The passage of repeated flows was found to leave the level of the sand bed constant to within one grain diameter. The height, y , of the flow above this level was measured together with the speed. The angle, θ , was constant at 33 degrees. The results by Bagnold are given in Table 2.1. The calculated values were 50% larger than the measured speed. From Equation 2.10 it can be seen that the square-root of grain diameter is inversely proportional to the shear stress as given by the velocity gradient. So as the grain of mixed sizes are sheared together, Bagnold suggested that the largest tend to drift toward the zone of least shear strain, e.g, toward the free surface of gravity flow, and the smaller grains toward the zone of greatest shear

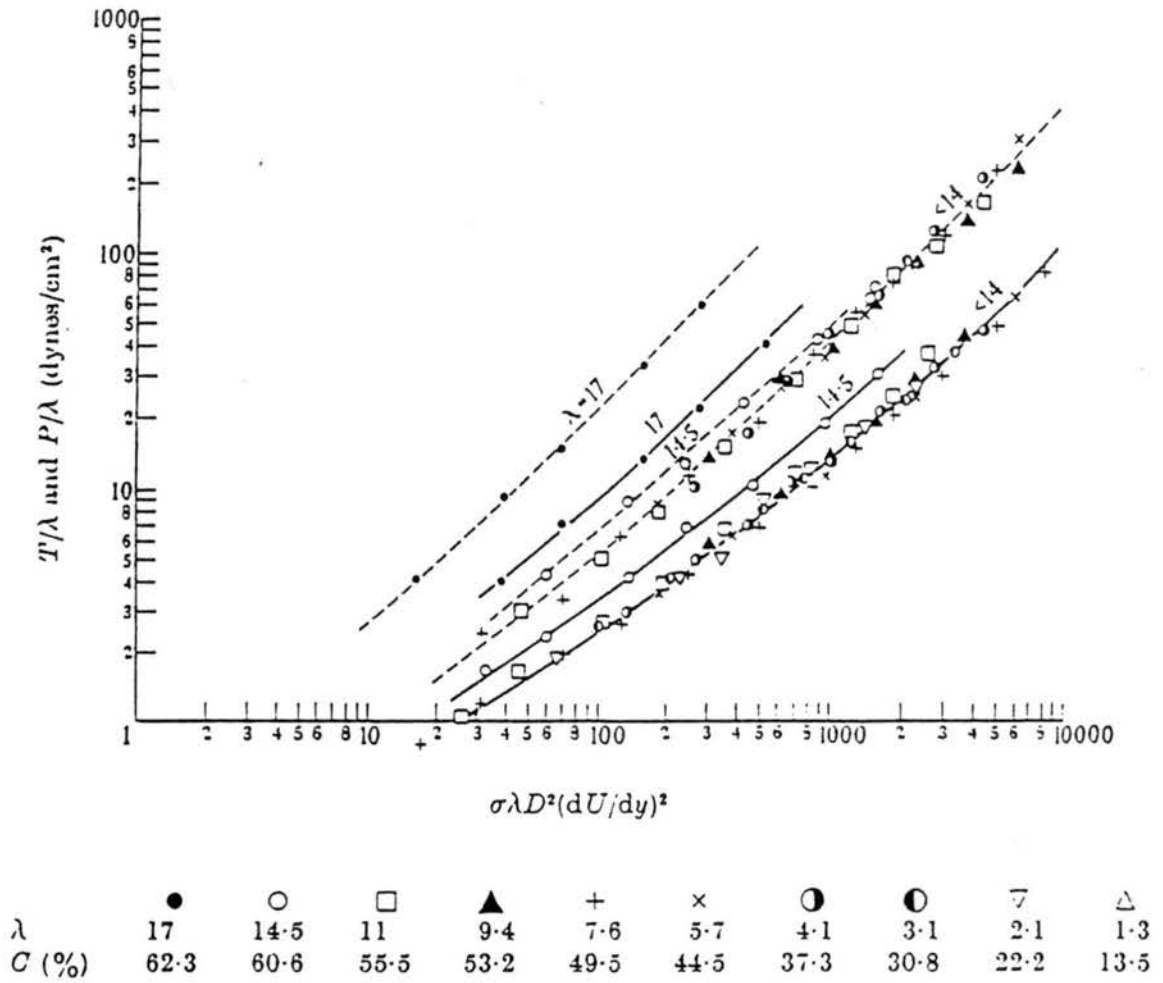


Figure 2.2. The complete lines indicate shear stress and the broken lines indicate pressure (after Bagnold, 1954).

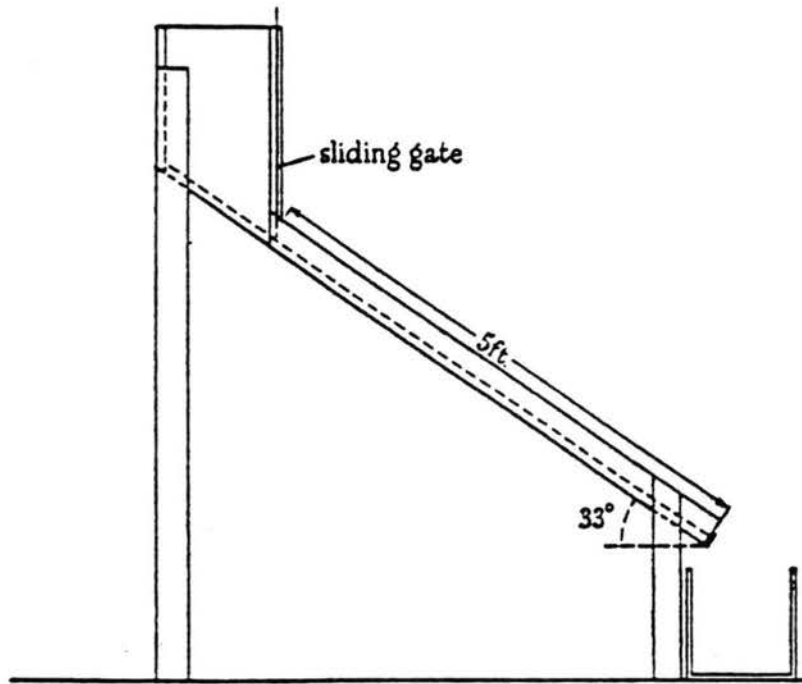


Figure 2.3. Inclined flume (after Bagnold, 1954).

Table 2.1. Measured and calculated speed of a moving sand front under gravity force (After Bagnold, 1954).

Flow Height y (cm)	Measured Speed (cm/sec)	Calculated Speed (cm/sec)	Calculated Speed to Measured speed
0.50	17.20	26.40	1.53
0.65	27.50	38.80	1.41
0.75	30.00	48.00	1.60
0.90	39.00	63.00	1.61

strain. Thus in avalanches down a dune front, the particles tend to become sorted perpendicularly to the plane of sliding. However, it is important to note that no experimental or field data was presented by Bagnold to show this kind of sorting.

2.4 Delta Deposits

Jopling (1965) studied the movement and dispersion of particles in the flow transition over the foreset front of a tabular unit of cross-bedding (micro-delta). A number of experiments were carried out using a transition flow regime with Froude number of about 1 to 1.8 (upper regime) so no bedforms developed on the back of the delta. The experiments were designed to study the grain size distribution in a cross-bedding deposit (delta deposit) using four types of sand mixtures (Figure 2.4). The sampling procedure was designed with the following objectives:

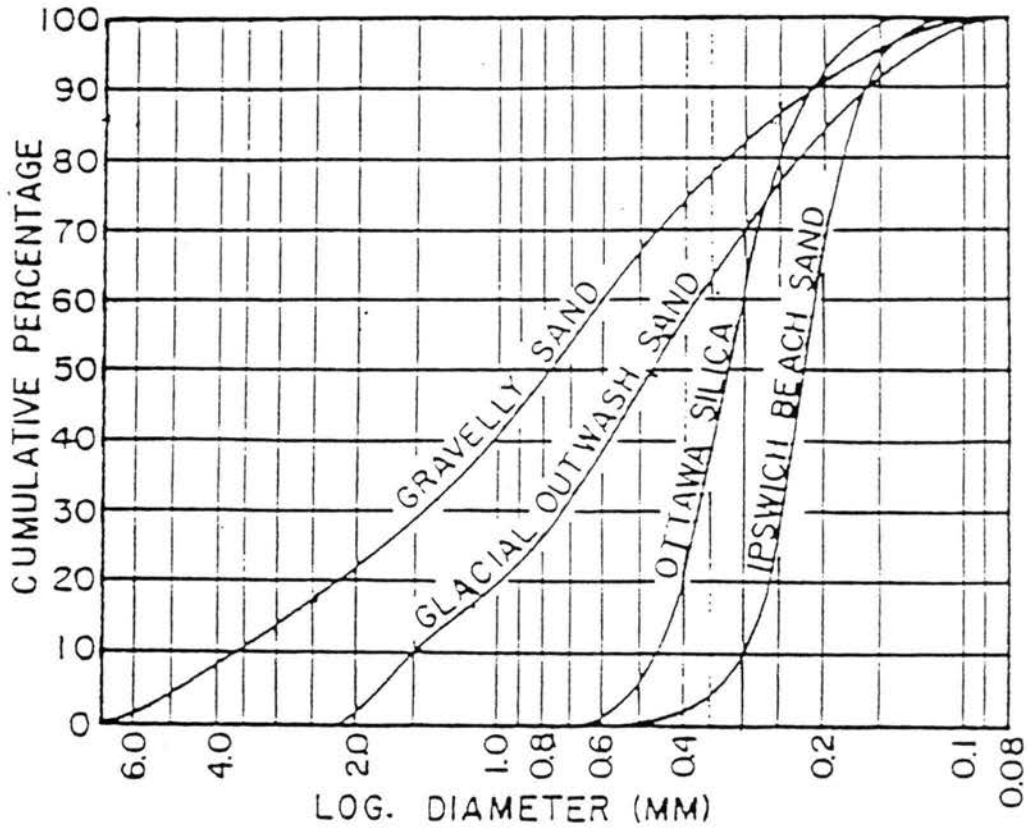


Figure 2.4. Size characteristics of sand used in experiments (after Jopling, 1965).

- 1 - Determining of the downslope distribution of grain sizes in the foreset bedding,
- 2 - Relating the distribution of grain sizes within the bottomset bedding to the flow pattern over the delta front,
- 3 - Explaining the origin of the toset bedding, and
- 4 - Comparing the overall size grading characteristics for the various sets.

The various sets were sampled for bulk grain size composition only after relatively uniform conditions of sediment transport had been established. The results are given in Tables 2.2, 2.3 and 2.4.

Jopling reporting that the sand grain composition of the topset deposition was generally finer than foreset deposition (Figure 2.5). Tables 2.2, 2.3 and 2.4 indicate a tendency for the heavier and larger grains to roll over the finer grains; that is, there was a selective transport in the downstream direction leaving a residue of finer topset beds. The gravelly sand and glacial outwash sand were exceptions; the sand grain composition of the topset deposition was coarser than that for the foreset deposition (Table 2.2). This phenomenon was difficult to interpret according to Jopling because of the short length of the flume and the exaggerated entrance effects. Such conditions prevent the establishment of a true equilibrium in sediment transport. In spite of these experimental limitations, Jopling has commonly observed in field occurrences that the topset deposition is somewhat finer grained than the foreset deposition.

Table 2.3. Grain size data for glacial outwash sand and gravelly sand (after Jopling, 1965).

Set Name	Glacial Outwash Sand Run # 1 Median Grain Diameter (mm)	Gravelly Sand Run # 1 Median Grain Diameter (mm)
Topset	0.40	1.08
Upper Foreset	0.33	0.56
Middle Foreset	0.41	0.70
Basal Foreset	0.57	1.42
Toeset	-----	-----
Bottomset	0.18 (at Toe) 0.15 (18 in. From Toe)	0.13 (at toe)

Table 2.4. Grain size data for silica 17 sand (after Jopling, 1965).

Set Name	Run # 1 Median Grain Diameter (mm)	Run # 2 Median Grain Diameter (mm)	Run # 3 Median Grain Diameter (mm)
Topset	-----	0.28	0.28
Upper Foreset	0.33	0.32	0.35
Middle Foreset	0.35	-----	-----
Basal Foreset	0.34	0.34	0.34
Toeset	-----	0.28	0.29
Bottomset	0.26 (at Toe)	0.24 (24 in. from Toe)	-----

Table 2.5. Grain size data for ipswich sand (after Jopling, 1965).

Set Name	Run # 1 Median Grain Diameter (mm)	Run # 2 Median Grain Diameter (mm)	Run # 3 A Median Grain Diameter (mm)
Topset	0.20 0.25	-----	0.21 0.29
Upper Foreset	0.27	0.22	-----
Middle Foreset	0.24	0.22	-----
Basal Foreset	0.21	0.23	0.27
Toeset	0.20	0.20	0.22
Bottomset	(6 in. from toe) 0.18 (18 in. from toe)	(8 in. From toe) 0.19 (16 in. from toe)	0.18 (30 in. from toe)

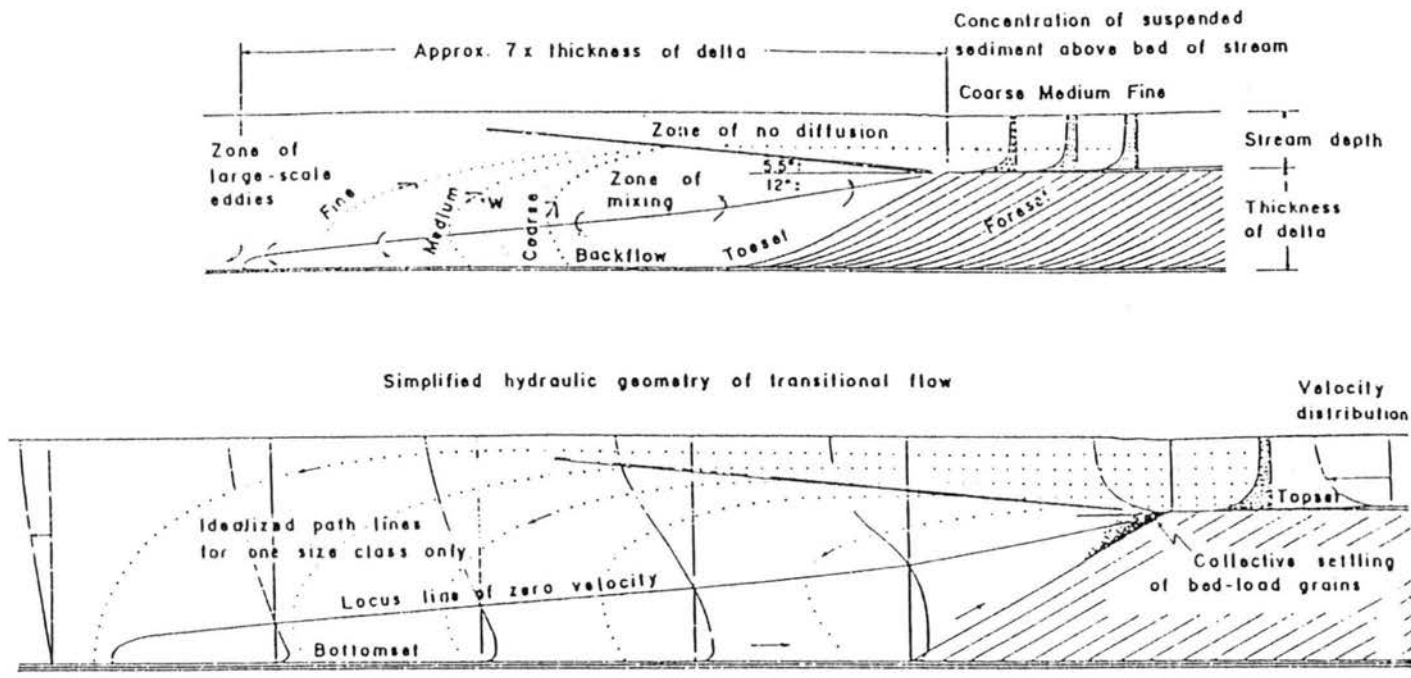


Figure 2.5. The upper diagram illustrates the dispersion and sorting of particles in the downstream direction as a function of differential settling velocity. The lower diagram illustrates the dispersion of one size class of particle as a function of height above the bed of the stream. Note the collective settling of the assorted particle sizes carried along the bed of the stream in the zone of heavy sediment concentration (after Jopling, 1965).

Concerning foreset deposits, some of the data of Jopling can be cited in summary form. For the gravelly sand and glacial outwash sand, the median grain size increased down the foreset slope (Table 2.2). These sands, which were the coarsest and most poorly sorted of all the test sands, were deposited as angular units of cross-bedding with foreset laminae abutting bottom sets of fine silty sand. Although the coarse fraction of the sediment load was selectively deposited at the top of the foreset slope as wedge until this wedge becomes unstable, the process of slip reversed this distribution in the downslope direction. Jopling believes that this phenomenon could probably be explained in terms of Bagnold's (1954) dispersive pressure theory, which is that the dispersive pressure caused by grain collisions forces the larger particles towards the surface of the slip face, where greater freedom of movement prevails. Tables 2.2, 2.3 and 2.4 show the results of the sampling. There is a tendency for the median grain diameter to increase downslope.

In reference to bottom set and toset deposits, Jopling said that from the field observation the bottom sets are finer grained than the other sets mentioned before (Tables 2.2, 2.3 and 2.4). It is also evident from the grain size data that tosets form a transitional link between foreset and bottomset deposits.

Jopling (1964) proposed the following mechanics of sorting: that the finer material carried in suspension settles as a more or less continuous 'rain' of eletritus on the foreset slope and over the bottomset bed. On the other hand, the coarser material carried as bed load accumulates on the upper foreset slope as a metastable wedge and periodically slips down the foreset slope under the influence of gravity. This process,

Jopling thought, results in the down slope redistribution of the larger grain sizes, and it therefore produces a layer of coarser material on the foreset. The finer material is overridden and buried by this new layer of coarser material (in this study, only delta deposition and the existence of a suspended load were reported).

Concerning ripple or dune regime, there are two kinds of depositions: one horizontal (parallel) bedding and the other cross-bedding (Jopling, 1964). The origin of the dune cross-lamination can be adequately explained in terms of the processes previously cited: differential particle trajectory, pulses in trajectory behavior, segregational tendencies along the transport surface (back of the dune), and dispersive pressure. Later the theory of cross-lamination will be discussed, but here it can be said that the origin of the horizontal bedding is related to the divergent flow pattern and the flow separation that occurs at the crests of the traveling dunes. The troughs located between the dunes function as sediment vorticity traps for the removal and segregation of part of the fine material carried in suspension near the bed of the stream.

Jopling believed that the fine material deposited in the irregular trough zones forms a thin, irregular, bed which is overridden and buried by the slow advance of dune foresets, concomitant with some scour, reworking and redeposition. Most of the coarser material carried as bed load is caught on the dune foreset where it is periodically redistributed downslope by slip movements. In an aggrading sequence the base of the dune deposit may be left behind as a residual layer overlying the scoured bed of finer material. For a slowly aggrading deposit, the repetition of this cycle results in a bedding structure. As aggradation continues, concomitant with a slow upward shift in

the level of dune and trough migration, many of these thin layers are devoid of internal structure and would be classified as horizontal beds.

The sorting mechanism described above differentiates the depositing sediment into fine and coarser layers, even for conditions that are uniform. But in Jopling's experiments, a sorting of sand grains in the downslope direction was commonly observed for high standard deviation sand mixture. As a general rule, however, there was no well-defined sorting of grain size into a layered (bedded) arrangement parallel to the foreset slope, as was mentioned earlier. A point needs to be questioned: If the discharge is constant (uniform flow), how can it be that each time the dune passes a certain point it leaves the bottom layer ?. That would mean that the bed thickness would always increase in height, under uniform flow and sediment conditions. This is not likely, because under a certain flow condition the dune will be in equilibrium condition after a certain time, which means that the slope and the sequence of the dune is the same with time.

2.5. Zones of Flow Downstream of a Dune

Based on experimental evidence, Allen (1968) reported that deposits formed in the lee of ripples, dunes and sand deltas depend for their properties on the behavior of grains when subjected to fluid shearing, turbulent diffusion, and gravity slip. The flow downstream of a ripple, dune or sand delta can be divided into four zones on the basis of its turbulence properties (Figure 2.6). The external flow is of moderate turbulence intensity compared with the mixing region of free shearing, in which turbulence is

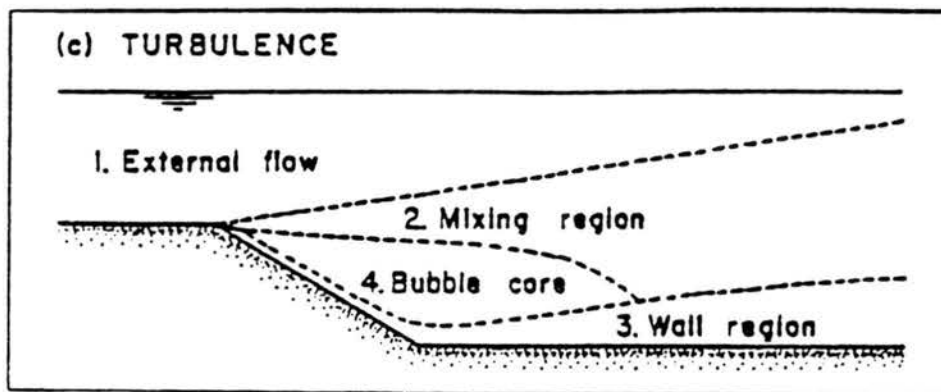


Figure 2.6. Zones of the flow downstream of a ripple, dune or sand delta on the basis of its turbulence properties (after Allen, 1968).

generated to a much greater extent. The fluid in the mixing region displays a rapid change of mean velocity with normal distance, and there is an inflection point in the velocity profile. The fluid layer which occupies the mixing region is unstable and rolls up into vortices. Freymuth (1966), has discussed vortices as being at first spatially periodic and representing a pseudo-turbulence, that is, they are small at the start of the rolling-up process, but gradually increase in size and power as they convect down the mixing region.

Allen said that at a certain critical distance from separation, the vortices themselves become unstable and proceed to break down into random turbulence. The extent of generation and magnitude of the turbulence, periodic and otherwise, can be gauged from the representative plot in Figure 2.7 of the root mean square value of the fluctuating velocity component, u' , parallel to the x direction. The third region of the flow, that close to the wall, is one in which the turbulence convected to the bed is dissipated. A further dissipation of turbulence occurs in the core of separation bubble (loosely called an eddy or roller). Allen points out that the grading of avalanched sediments is not wholly the result of the avalanching process, since the settling of grains is a continuous affair.

2.6. Evidence of Vertical Sorting

Brush (1965b) studied the formation of primary sediment structures in and along an alluvial channel sand bed which occurs as result of interaction between gravity, the physical characteristics of the sediment and fluid as well as the hydraulic environment.

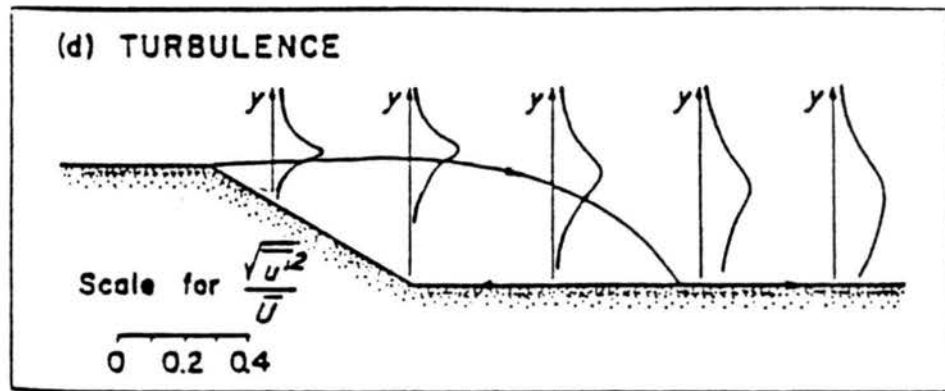


Figure 2.7 Magnitude of the turbulence downstream of a dune (after Allen, 1968).

The occurrence of many of these structures in channel beds resulted from the presence of ripples, dunes, bars, and antidunes on the bed. However, the actual process by which recognizable structures developed arises from sorting of sediment with respect to size, shape, and density along the bed and within the stream. The settling rates of the particles, turbulent diffusion, gravitational sliding, and boundary shear stress contributed to the sorting processes.

Brush (1965b) took local surface samples from the dune surface of several experimental runs in a large recirculating flume. These samples were taken at the crest, at the half of the dune back height, at the toe of the dune, and at a point in the lowest portion of the trough which occurs immediately downstream from a dune (Figure 2.8). In addition, he took a number of core samples and surface samples for the entire dune surface. The reason for taking both core and surface samples was to find the median diameter of the entire dune structure. The sand used for this study had a mean diameter of 0.37 mm. A similar but much less extensive study had been made earlier by Brush in the flume at Colorado State University during several runs made by Simons and Richardson in 1962 for sand of 0.45 mm in diameter and with a standard deviation of about 1.6 (uniform sand). The results of Brush's two studies are shown in Table 2.5.

According to Brush, finer sizes occur in the trough due to settling from the suspension of the material passing over the crest of the dune and subsequently caught in the stable eddy zone. Also, Brush reported that an equally important aspect of the sorting is that the larger particles tend to reach the bottom of the dune in greater concentrations because they would meet fewer obstructions in their downward movement

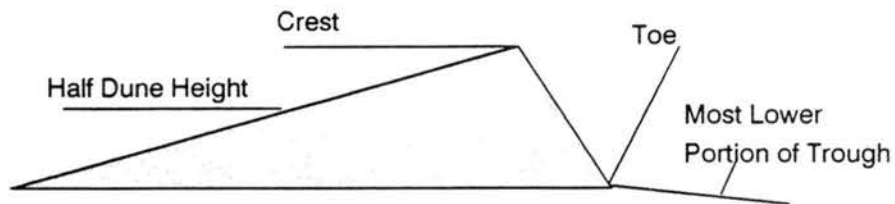


Figure 2.8 Position of samples (after Brush, 1965b).

Table 2.2. Values of d_{50} at different positions in the dune structure (after Brush, 1965).

Mixture	1 ($d_{50} = 0.73$ mm)	2 ($d_{50} = 0.45$ mm)
d_{50} at crest	0.311 mm	0.43 mm
d_{50} at half dune height	0.365 mm	0.47 mm
d_{50} at the toe	0.461 mm	0.55 mm
d_{50} at the most lower portion of trough	0.267 mm	0.39 mm

(gravitational sorting). Schematically, the sorting in an inclined stratum of a dune is shown in Figure 2.9. Each of these sorting processes contribute to recognizable portions of the primary sedimentary structures of cross stratification.

Moving into the era of computers, Ribberink (1983) conducted a study in the framework of a research project concerning the development of a mathematical model for morphological computations of rivers in the case of nonuniform sediment. The study consisted of series of laboratory experiments in a straight flume , 40 m long, 0.5 m wide and 0.5 m deep, under steady uniform equilibrium conditions with a restriction to bed load transport and dune regime. The flume was fed upstream by different mixtures of two very narrow sieve size fractions (Figure 2.10). During each experiment the total amount and composition of input mixture, the water discharge, and the downstream water level were kept constant. When equilibrium was reached, in addition to regular registrations of water and bed level, the dunes were sampled.

In order to measure the composition of the sediment mixture in the transport layer of the bed to get data for verification of a component of the semi-empirical components of the mathematical model, which is the transport formula per size fraction, a bed sampling technique was developed. Before the sampling took place, the water flow was stopped leaving approximately 0.2 m of water on top of the bed. Thin wall pipes (wall thickness about 1 mm and 10 cm in diameter) were slowly pressed into the bed near a dune crest until the concrete bottom of the flume was reached. This pressing had to be done slowly in order to avoid too large a disturbance of the bed. Using a hollow tube (inner diameter about 1 cm) the sediment was siphoned out of the pipe,

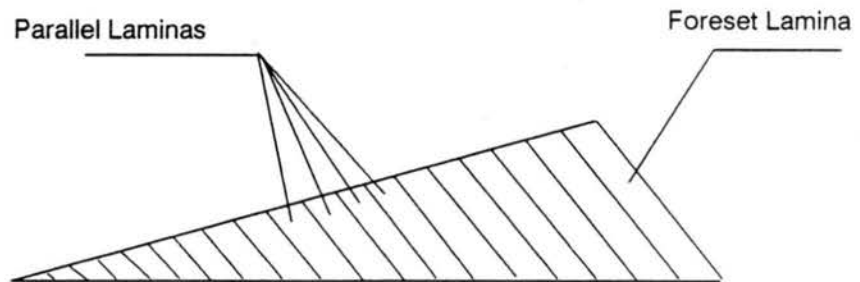


Figure 2.9. Foreset lamina in dune structure which consists of several laminas.

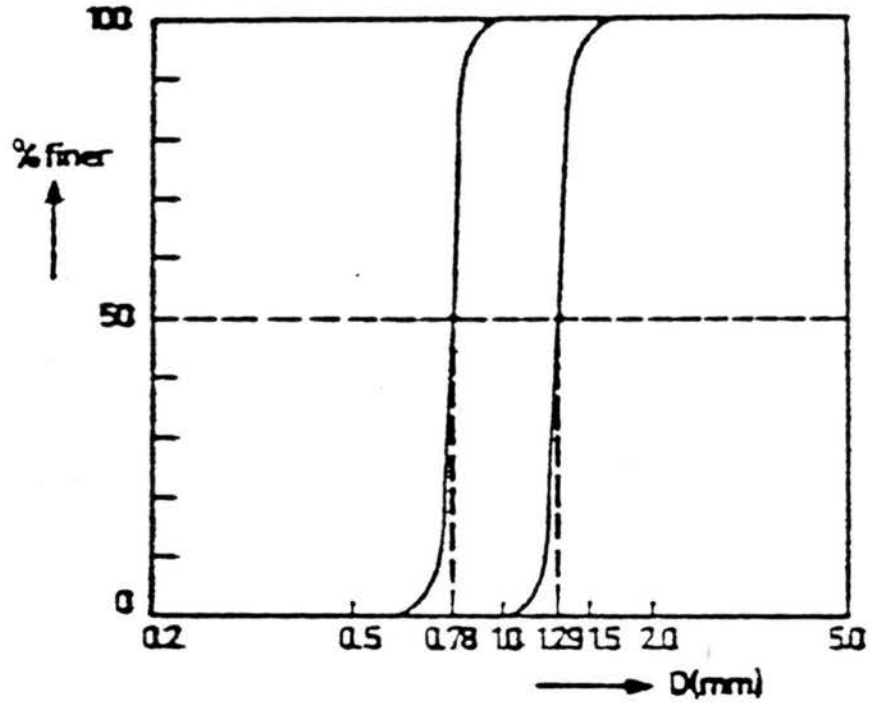


Figure 2.10. Grain size distribution of the two fractions (after Ribberink, 1983).

layer by layer (thickness of each layer was about 0.5 cm) into a sieve tray. The main results of the experiments follow are as follows:

- 1 - Vertical sorting of size fractions occurred in all experiments. At the steep lee side of the dunes, the coarse size fraction was more often deposited at the lower level than the fine size fraction. Differences in volume concentration per size fraction up to 30% occur between upper and lower layers.
- 2 - A transition layer was found which was generally below the propagation dunes, had a relatively coarse composition and a thickness of about 0.1 to 0.5 H, where H is the average dune height. Exchange of size fractions between this layer and the upper bed layer occurred on a much longer time scale than the dune period.

Ribberink also pointed out that vertical sorting in bed forms not only occurs in laboratory conditions but also takes place in natural conditions. Ribberink reported that Zanke (1976) found similar vertical sorting of a wide range of grain size mixture in the Weser river in Germany.

2.7 Sorting in Point Bars and Dunes

Many studies have been carried out to describe flow in a bend and sediment sorting that results in development of a point bar (Engelund, 1974; Odgaard, 1982; Ikeda et al., 1987). In these models, it is assumed that the radial forces on a particle moving downstream along the bar are zero, that is, the drag on a sediment particle due to secondary flow up the surface of the bar is just equal to the particle's weight

component down the bar's surface. The secondary flows are strongest on the outside of the bar and decrease along the bar surface toward the inner bank, so there is a sorting of sediments, from coarse to fine, from the outer to inner side of the bar (or from bottom to top, in case a core sample is taken vertically through the bar).

These ideas are well supported by empirical evidence. For example, samples were collected over a point bar in the East Fork river in Wyoming, Figure 2.11. The size distributions of the samples, plotted in Figure 2.12, show clearly the sorting process (C. Nordin, 1992, personal communication).

The flow downstream of the lee face of a dune is probably more complicated than the secondary flow in a bend, but it is postulated for this study that a similar mechanism, a balance between fluid drag from reverse flow up the face of the dune and the particle's weight component along the face, is a major factor leading to the vertical sorting observed by Brush (1965b) and Ribberink (1983).



Figure 2.11 Point bar on the East Fork river, Wyoming. Note the dunes in the foreground.

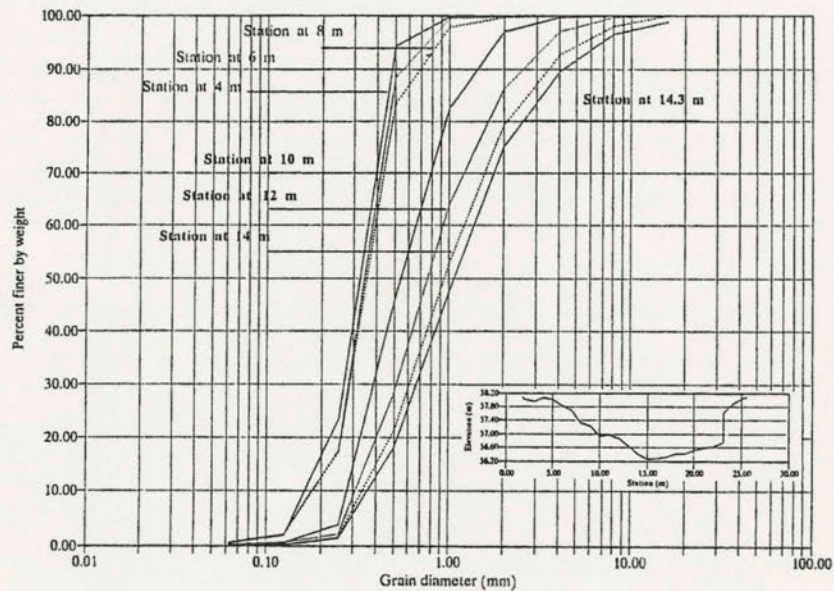


Figure 2.12 Sediment size distributions over the point bar shown in Figure 2.12.

CHAPTER 3

THE VERTICAL SORTING PROCESS

3.1 Physical Background

Before explaining how the vertical sorting may develop within the dune structure, it is useful to review how the flow pattern helps to develop the kind of vertical sorting in which a decrease in the median grain diameter occurs in the vertical direction within the dune structure. Much of this review in Sections 3.1-3.3 is taken directly or paraphrased from Reineck and Singh (1975, p. 17-22).

3.1.1 Pattern of flow in front of the dune.

The lee side of the dune can be divided into three major hydrodynamically different zones as shown in Figure 3.1 and 3.2: the zone of no diffusion, the zone of mixing, and the zone of backflow. Some other researchers such as Allen (1968), divided the latter zone into two zones: the eddy core and the wall region, as mentioned in Chapter 2.

Zone of no diffusion. Reineck believe that this zone may be regarded as a part of the stream flow that carries sediment in suspension over and behind the foreset slope (lee slope). Its velocity distribution is similar to that of the upstream flow, but with a progressive truncation in the downstream direction.

Zone of mixing. This zone is characterized by macroturbulence. The fluid which occupies the mixing region is unstable and rolls up into vortices. The fluid in the zone of mixing displays a rapidly changing distribution of the velocity profile (Figure 3.1). The separation of the flow from the foreset boundary results in the generation of a reverse circulation which is directed toward the toe of the foreset and up the foreset slope. The zone of mixing acts also as a sediment vorticity trap for catching some of the sediment settling out from the zone of no diffusion. At the beginning the vortices are spatially periodic and represent a pseudo turbulence. They are small at the start of the rolling-up process, but gradually increase in size and region. At a certain critical distance from separation ($2/3$ of the distance of the next dune stoss side according to Reineck and Singh, 1975), the vortices themselves become unstable and begin to break down into random turbulence.

Zone of backflow. This zone shows a reversal of direction of the flow. When vortices originating in the mixing zone reach the zone of backflow, they develop a counter current flowing along the bottom set and up the lee slope. The backflow may attain velocities as large as 20% to 25% of the average down-current velocity (Reineck and Singh, 1975, p. 18). Some of the grains moving in the backflow (in suspension) may be caught back in the eddies of the zone of mixing.

3.2 Explanation of Enrichment Stoss Side with Fine Material

At the point of flow reattachment on dune's stoss side, transport is in the downstream direction only where grains move by sliding, rolling, saltation and

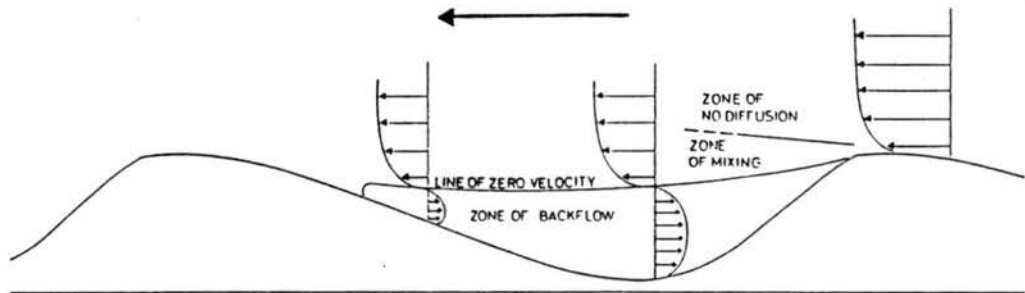


Figure 3.1. Flow pattern over a lee face of a ripple (after Reineck and Singh, 1975).

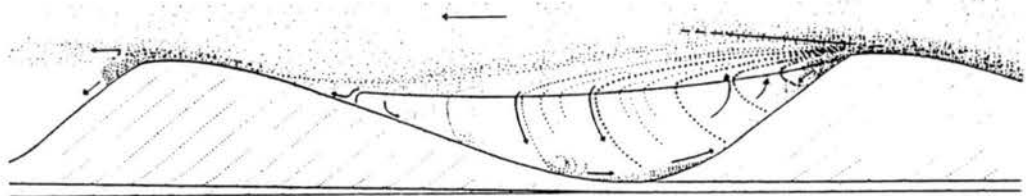


Figure 3.2. Flow pattern and sedimentation processes on the lee side of a ripple (after Reineck and Singh, 1975).

suspension. Sand grains move in an irregular pulsating movement along and up the stoss side. The bigger grains have a large area exposed to running water, and so they are taken away easily. However, the smaller grains are also transported away as they become exposed to the flow after the shielding by the bigger particles has been removed. Even then, a sorting of the sediment takes place. Finer grains settle down into the intergranular pore spaces. The net result is that on the stoss side a relative enrichment by finer grains takes place.

3.3 Development of Lamination in the Lee Face

In the development of this deposited structure, the vertical decrease in the grain size, from bottom to top, in the dune structure and the fine material in the toe and the bottomset both started with the heavy-fluid layer which is formed on the back of the dune. When this layer reaches the crest of the dune (highest point in the dune structure), the coarse particles (the flow cannot carry them behind the crest) form a wedge, and the fine particles which the hydrodynamic force of the flow is able to carry behind the crest of the dune, continue moving as suspended particles to the lee side of the dune. If the fine particles go to the zone of no diffusion, they continue to the next dune. The particles which are heavier than that go to the zone of mixing, where they are caught in the eddies of this zone and may settle at the toe or at the bottomset. Also some of these particles will travel upstream due to the backflow current.

Returning to the wedge, it contains the coarse particles of the sediment mixture; that is the particles which the flow can not carry as suspended load. Also within this

wedge are fine particles which are shielded by the coarse particles. As time passes the accumulation of sediment in this wedge becomes big enough to make this wedge unstable. The result is the avalanching of this material down the slope of the lee side of the dune. Each avalanche forms a foreset lamina, and within this foreset lamina the sediment particles are rearranged. This rearrangement is a function of the size of the particle and the hydrodynamic force on the particle. The driving force of each particle is, in this case the weight component in the direction parallel to the lee slope. On the other hand, the forces which resist the movement of the particle are the friction force, which is a function of the angle and the material of the slope, and the drag force which is a function of the backflow. Considering that all the particles have the same friction and are exposed to about the same velocity from the reverse flow up the lee face of the dune, the particles which have more weight will reach the bottom of the slope faster and so forth. This process is continuous as long as the flow and the sediment conditions are proper to form a dune. Following is a proposed mechanism for the development of the dune structure.

3.4 Proposed Mechanism

For this discussion, assume equilibrium conditions of the flow and the sediment meaning that the average sediment bed load at a certain section of the dune and the sediment characteristics are the same over a period of time (in a statistical sense). In other words, the turbulence pulses affected by the amount of sediment bed load or its size characteristics will not be considered.

If the dunes migrate without change in size and shape, an observer can see that each dune is self-sufficient; that is, no bed load comes from the upstream dune to contribute to the deposition of any foreset lamina of the downstream dune. It has been found by means of the experimental results reported in Chapter 5 that the deposited sand within the structure of a single dune contains almost the same material as the original sediment mixture, except for the small amount of fine material which the mixture loses as suspended load. The meaning of this result is that the eroded material from the back of the dune, which is assumed to be deposited in one single foreset lamina on the lee face should be the same as the original sand mixture. If the eroded sediment material were not the same each time, the composite of each dune could not be the same as the original mixture.

From the above discussion, one can argue that various size fractions within one-foreset lamina accumulate in each unit area (trapezoid), Figure 3.3, with mostly coarser particles in the lowest trapezoid, slightly finer particles in the trapezoid above this, and so on up to the crest of the dune. That happens continuously each time a foreset lamina is deposited and because the dune consists of many foreset laminae beside each other, these unit areas which have about the same size distributions and are equal in height will form horizontal layers, as shown in Figure 3.3. Each layer, which extends from the stoss side where particles are deposited contains its own characteristic particle size distribution.

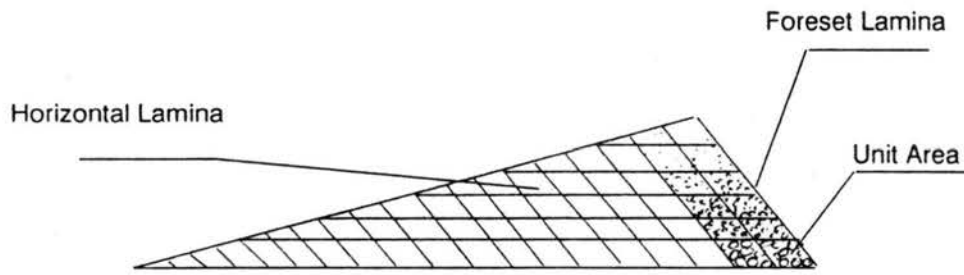


Figure 3.3. Proposed internal structure of a dune.

Furthermore, the idea of self-sufficiency is supported by the observations of the two dimensional dune shape during each experiment which was not changing during an experiment. Each foreset lamina within the dune structure is reduced in height from full dune height (at time of deposition) to eventually zero, as erosion occurs in the back of the dune. Thus, at the crest of the dune is the finest material, while further upstream, lower levels of foreset lamina are exposed, with progressively coarser material, until the last foreset lamina is reached, which contains the coarsest sand grains. Under equilibrium conditions, erosion from the tops of these remaining foreset lamina occurs such that the accumulated sediment load passing the crest of the dune has again a grain size distribution of the original mixture.

For this study the following assumptions were made:

- 1 - The lee face is at incipient failure, that is, it is at the angle of repose,
- 2 - Sediment transport rate is small, so most particles roll or slide down the lee face unimpeded by friction. Gravity and fluid forces are the main component that lead to vertical sorting along the lee face, and
- 3 - Bulk flow down the lee face as described by Bagnold (1954) at small transport rates is not very important.

These assumptions may not hold for larger features or for large sediment transport rates.

3.5 Proposed Relationship Between the Vertical Sorting and Dune Size

In the previous section, it was assumed that each foreset lamina has the same particle size distribution. For small-scale features formed in laboratory flumes, this is

probably a good assumption. Groups of particles eroded from the upstream face of the dune will move and disperse as bedload at different velocities, depending mostly on their sizes. The mean particle velocities will be comparable to the flow velocities near the bed (Einstein, 1950). The larger particles, being exposed to larger velocities near the bed, will move faster than the smaller particles. Rathbun and Nordin (1972) report mean particle velocities over a flat bed to vary from about 2 to 15 percent of the mean flow velocity. Thus, the larger particles eroded from the lower parts of the upstream dune face will overtake and mix with the finer particles eroded from higher along the dune face, and the size distribution of material moving over the crest is more-or-less constant. Under these conditions, any lamination that develops along the lee face of the dunes would be weak and probably could not be distinguished visually (see, for example, Reineck and Singh, 1975, Fig. 9). However, the same conditions probably do not apply in rivers. McKee (1989, p. B10) examined the cross stratification in large dunes along the Orinoco river and reported that "A widespread and characteristic feature of stratification in most sand-wave deposits along the Rio Orinoco is an alternation of coarse and fine grain sizes in the foreset bedding of tabular-planar sets." (see Figure 3.4).

Several features may be responsible for the alternation of coarse and fine laminae observed by McKee:

- 1 - These may reflect changes in river stage with concurrent changes in transport capacity,

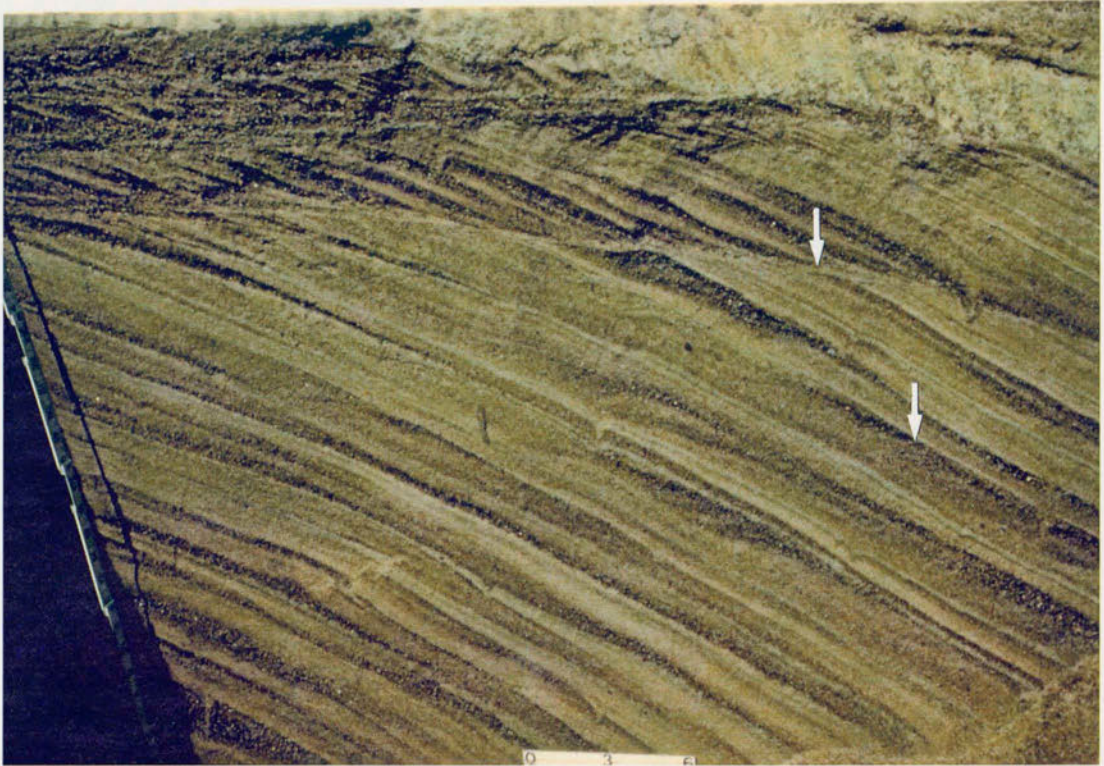


Figure 3.4. Photograph of foreset bedding in a large sand wave along the Orinoco river (McKee, 1989, Fig. 16).

- 2 - The time scales of transport and dispersion may be such that groups of particles of different sizes arrive at the crest of the dune at different times, and
- 3 - Under most conditions, flow along the back of a dune is stable and similar to flow over a flat bed. However, under some conditions, the bed along the back of the dune is unstable, so that a small perturbation (from differential erosion and transport, for example) grows and generates secondary waves on the back of the large feature. These secondary waves are more-or-less self contained, so groups of particles of different sizes, depending on where along the back of the dune the secondary waves formed, arrive at the crest at different times.

The relative importance of these factors remains to be determined.

Even where alternating fine and coarse lamina exist, the vertical sorting phenomenon will still occur in each lamina and within the total dune structure. In order to obtain a representative size distribution of any horizontal layer of the dune, it is necessary to sample across many foreset laminae.

CHAPTER 4

EXPERIMENTAL SETUP AND PROCEDURE

The experimental flume used to study the vertical sorting in dune structures which arise as a result of the bed load transportation over the upstream faces of the sand dunes in nonuniform sand mixture is in the Hydraulics Laboratory at the Engineering Research Center of Colorado State University. This chapter briefly describes the flume, the individual measurements, the sediment mixtures, and the description of the operational procedures.

4.1 The Flume

The flume used in these experiments is the same one used by Rathbun et al. (1969). It is a tilting closed circuit flume made of 1.91 cm plexiglass (Figure 4.1). The dimensions of the flume are 10 m long, 0.2 m wide, and 0.2 m deep. It recirculates water and sediment. The flume bed slope can be adjusted by screw jack at the upstream end. Water is pumped from a plexiglass tank, 0.953 m long, 0.635 m wide, 0.635 m deep, at the downstream end of the flume by a 3 HP variable speed pump through a 11.43 cm plexiglass pipe line to the head box where flow straightening tubes are placed to reduce the turbulent eddies induced at the flume entrance and by the pump. Also a rectangular floating wood board was placed on the water surface just downstream of the

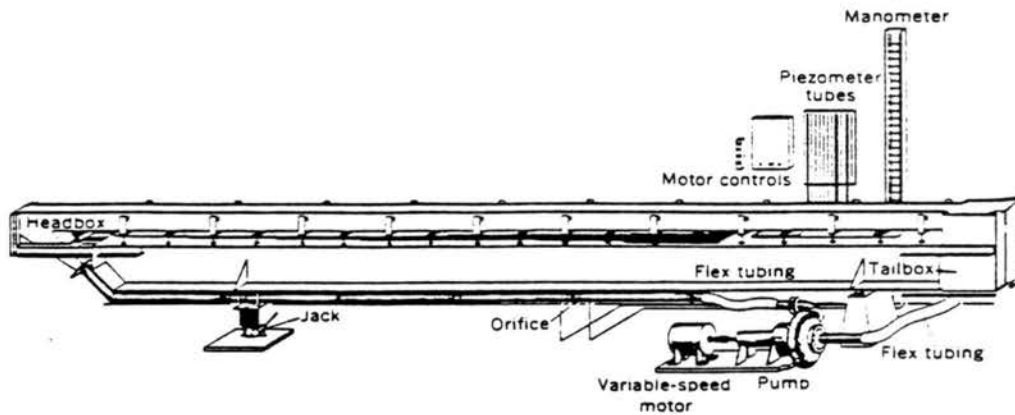


Figure 4.1. Schematic diagram for the experimental flume (after Rathbun et al., 1969).

head box to reduce surface waves. The flow in all runs of this study was subcritical to get low regime conditions and this was subject to downstream control.

A bottom-hinged, adjustable, inclined steel gate is located at the downstream end of the flume to maintain uniform flow conditions, and to control the water depth. There is an instrument plexiglass carriage running longitudinally on the flume top and a part that moves laterally as well so that, with a point gage mounted on the instrument carriage, any position in the flume can be reached. The measurements for this research, flow depth, bed and water surface slopes, were taken at sixteen different stations at 0.46 m intervals along the flume. Station one was at 1.804 m downstream from the head box, and the last station was at 1.04 m upstream of the end of the flume.

4.2 Individual Measurements

4.2.1 General

As the main objective of this research was to predict the vertical sorting in the dune structure in sediment mixture, it was necessary to choose flow variables which could be considered to have the best correlation to the problem. Simons and Richardson (1966) reported a comprehensive study of variables affecting bedforms and flow characteristics, their dependency and independency, and the conditions in which a dependent variable changes into an independent one, or vice versa.

These principle variables involved in the analysis of the flow in alluvial channels are:

$$F_1 (u, d, s_e, \rho, \mu, g, d_{50}, \sigma, \rho_s, s_p, s_r, s_c, f_s) = 0 \quad (4.1)$$

where:

u = average velocity of flow,

d = average flow depth,

s_e = slope of the energy grade line,

ρ = density of water,

μ = dynamic viscosity of water,

g = gravitational acceleration,

d_{50} = median diameter of the bed material,

σ = measure of the size distribution of the bed material,

ρ_s = density of sediment,

s_p = shape of the particles,

s_r = shape factor for the reach of the stream,

s_c = shape factor for the cross section of the stream, and

f_s = seepage force in the bed of the stream.

Based on the above equation, it was felt sufficient to consider all the hydraulic conditions, which were slope, depth of the flow, channel geometry and discharge. Because of the nonuniformity in the shear stress distribution resulting from the difference in roughness between the flume bed and walls, a method, which will be discussed in a later chapter, was needed to correct the calculated bed shear stress to account for this wall effect.

4.2.2 Flow depth

Usually in the case of nonuniform material, bed irregularities especially when bedform is considered, affect the accuracy of measurements because the theoretical bed surface is not known and the bed reading at any section actually depends on the position of the needle tip of the point gage relative to the larger grains on the bed. One possible way of reducing such error was attempted by taking three different point gage readings across the width at each of the sixteen test sections. The recorded bed reading was actually the average of three readings. The corresponding water surface readings at every section were determined and the depth of the flow was calculated as the average difference between the water surface and the bed surface at the specified test sections. The depth of the flow was measured from the top of the grains to the water surface. The error in measuring the average depth was highly affected by bed irregularities. One

would expect the absolute error in the measured depth to be in the same order of magnitude as the maximum grain size on the bed.

4.2.3 Discharge

The discharge range from the pump is from 0.0 to approximately 0.0224 m³/sec and is controlled by three switches which control the three-phase motor of the pump; the discharge in each stage can be adjusted by means of a valve in the return line of the flume. Discharge is measured on a manometer by reading the difference in pressure head upstream and downstream of a calibrated orifice-meter mounted in the return pipeline. There are two manometers, each containing a different type of fluid: one is filled with water for low discharges and the other with mercury for high discharges. It can be reasonably assumed that an error of about $\pm 3\%$ can be expected in the measured discharge.

4.2.4 Slope

Slope has always been one of the most difficult quantities to measure and because of the one-to-one dependency of the calculated mean bed shear stress and the measured slope, it was important to reduce the error in the measured slope. For this reason it was necessary to fix a datum which could be easily reached by the point gage on the instrument carriage so that all measurements could be taken to the greatest accuracy of the point gage, 0.3 mm. For the purpose of fixing the datum, the elevations of sixteen points along the centerline of the plastic flume bed were determined relative to a fixed

point using a surveyor's level and rod. The readings of three independent readers were taken and an average was calculated. With the elevations of the fixed points known, the corresponding point gage readings to the points were determined, and after the procedure mentioned in Flow Depth, Sec. 4.2.2, the bed elevations relative to the fixed points were determined. The bed slope was then calculated through a regression analysis as the slope of the line of best fit.

Similarly, the water surface slope was determined as the slope of line of best fit through the range of measured water surface elevations. The water surface slope was checked by using a manometer board consisting of five plastic tubes each 0.61 m long with 0.95 cm inner diameter. The error in slope was due to the error in the level readings on the surveying rod, where the resolution is 0.3 mm.

4.3 Bed Sample

4.3.1 General

In order to measure the composition of the sediment mixture in the transport layer (dune) of the bed, the bed sampling technique by Ribberink (1983) was used after changing the procedure to remove the weak points. This sampling by Ribberink was to first press thin walled pipes (diameter = 10 cm) slowly at the dune crest into the bed. Then the sample was taken layer by layer. The layer thickness of 0.5 cm results in samples of approximately 60 gm dry weight. The way of taking the sample and the weight of the sample are not ideal. First the pressing process of the 10 cm pipe into the

sand disturbs the layering of the sediment especially in view of the small size of the sample (10 cm diameter).

Second, the weight of Ribberink's samples were considered to be small according to ISO standards (1983). Figure 4.2 shows the mass m of the total sample to be analyzed for various levels of accuracy. If d_{84} is about 1 mm, high accuracy requires a sample of approximately 0.2 kg, or about three times the amount analyzed by Ribberink.

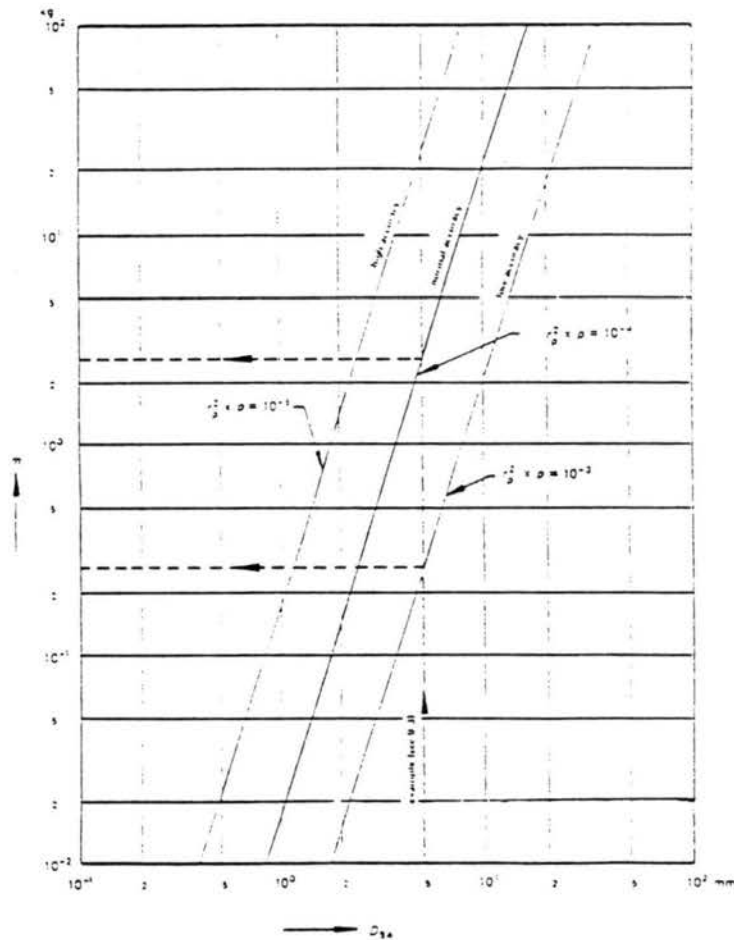


Figure 4.2. Design curve for sample of mass m (ISO standards, 1983).

4.3.2 Bed Sample Procedure

At the end of each run, the water flow was stopped leaving approximately 10 cm of water on the top of the bed. A glass tube (outer diameter 1 cm) mounted on the end of the point gage was used to siphon the sediment (Figure 4.3). Connected to this glass tube was a rubber tube to carry the sediment to the sieve tray. On the rubber line there was a clamp to control the flow of water through the rubber line, so the sand structure would not be destroyed by the siphoning procedure. The siphoning tube could be positioned anywhere above the dune by means of the instrument carriage which could be moved along the flume. The point gage was used to read the layer thickness before the siphoning process was started. In most cases the layer thickness was about 5 mm and extended across the flume and along the entire dune. The weight of the sample varied according to the layer length but the minimum weight was about 600 gm, and the number of layers depended on the dune height.

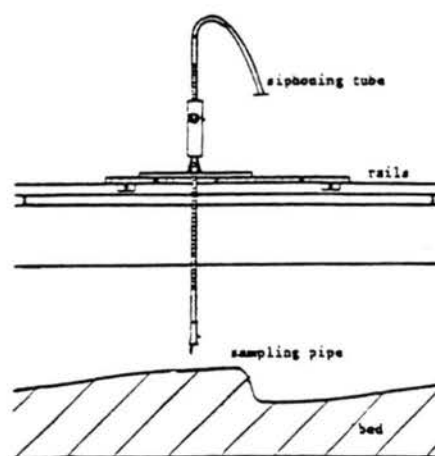


Figure 4.3. Schematic diagram for the bed sampler.

4.4 Sediment Mixture

There are no specific requirements that need to be met in the determination of the initial grain size distribution for the sediment mixture. Five different sediment mixtures were used in these experiments, consisting of two kinds of sediment (sand) materials which were obtained in bulk quantities.

The procedure to make each mixture was as follows. First the gradation curve of each sediment kind had to be known, that done by taking seven one-kg samples from seven different locations and then by sieving them using thirteen different square-opening sieves, ($\sqrt{2}$ scale) each eight inches in diameter, placed on top of each other. Then each sample was shaken for about five minutes in a mechanical shaker. Each size fraction in each sample was weighed and then added up for all seven samples to provide the percentage by weight of that size in the mixture. This procedure was repeated for the second sediment material. From the gradation curve for sediment material the d_{50} , the d_{16} and the d_{84} were known. Mixing the two sediment materials by weight percentage, the first three mixtures were obtained.

The last two mixtures were obtained by first sieving the two sediment materials on a 1.65 mm sieve and the remainder on that sieve was removed. After that the two sediment materials were mixed by weight percentage to get the final mixtures. The characteristics of the five mixtures is shown in Tables 4.1, 4.2, 4.3, 4.4 and 4.5, and their gradation curves are shown in Figures 4.4 and 4.5. After proper mixing of the two sediment materials, another three samples from each mixture were taken and sieved to get the final shape of the gradation curve for the mixture.

Table 4.1. Grain size distribution for sand mixture #1.

Sieve Diameter (mm)	Retaining Weight (gm)	Passing Weight (gm)	% Passing
4.76	0.0	2999.01	100
2.38	45.06	2953.95	98.49
1.19	460.54	2493.41	83.14
0.833	323.10	2170.31	72.37
0.6	203.91	1966.40	65.57
0.5	87.54	1878.86	62.65
0.42	106.64	1772.22	59.09
0.295	506.58	1265.64	42.20
0.125	1237.14	28.50	0.95
0.074	16.70	11.80	0.39
0.063	3.18	8.62	0.29
R	8.62	0.0	0.0

Table 4.2. Grain size distribution for sand mixture #2.

Sieve Diameter (mm)	Retaining Weight (gm)	Passing Weight (gm)	% Passing
4.00	0.0	2173.50	100
2.38	1.10	2172.40	99.95
2.00	2.80	2169.60	99.82
1.40	91.80	2077.80	95.59
1.00	387.00	1690.80	77.79
0.71	391.50	1299.30	59.78
0.50	178.00	1121.30	51.59
0.355	185.00	936.30	43.08
0.25	469.00	467.30	21.49
0.18	344.50	122.80	5.65
0.125	91.00	31.80	1.46
0.09	21.20	10.60	0.49
0.063	7.30	3.30	0.15
R	3.30	0.0	0.0

Table 4.3. Grain size distribution for sand mixture #3.

Sieve Diameter (mm)	Retaining Weight (gm)	Passing Weight (gm)	% Passing
4.76	0.0	1999	100
2.38	36.33	1962.67	98.18
1.19	452.65	1510.02	75.54
0.833	311.69	1198.33	59.95
0.60	183.69	1014.64	50.76
0.5	59.02	955.62	47.80
0.42	60.55	895.07	44.78
0.295	258.29	636.78	31.85
0.125	621.81	14.97	0.75
0.074	9.07	5.90	0.29
0.063	1.59	4.31	0.22
R	4.31	0.0	0.0

Table 4.4. Grain size distribution for sand mixture #4.

Sieve Diameter (mm)	Retaining Weight (gm)	Passing Weight (gm)	% Passing
4.00	0.0	3126.10	100
2.38	0.0	3126.10	100
2.00	0.10	3126.00	99.99
1.40	113.00	3013.00	96.38
1.00	745.00	2268.00	72.55
0.71	725.00	1543.00	49.36
0.50	282.00	1261.00	40.34
0.355	205.00	1056.00	33.78
0.25	388.50	667.50	21.35
0.18	421.00	246.50	7.89
0.125	174.50	72.00	2.30
0.09	47.00	25.00	0.79
0.063	16.00	9.00	0.29
R	9.00	0.0	0.0

Table 4.5. Grain size distribution for sand mixture #5.

Sieve Diameter (mm)	Retaining Weight (gm)	Passing Weight (gm)	% Passing
4.76	0.0	2997.99	100
2.38	63.93	2934.06	97.87
1.19	897.41	2036.65	67.93
0.833	611.97	1424.68	47.52
0.60	347.16	1077.52	35.94
0.50	89.52	988.00	32.96
0.42	75.01	912.99	30.45
0.295	268.29	644.70	21.50
0.125	628.29	16.41	0.55
0.074	10.51	5.90	0.197
0.063	1.59	4.31	0.144
R	4.31	0.0	0.0

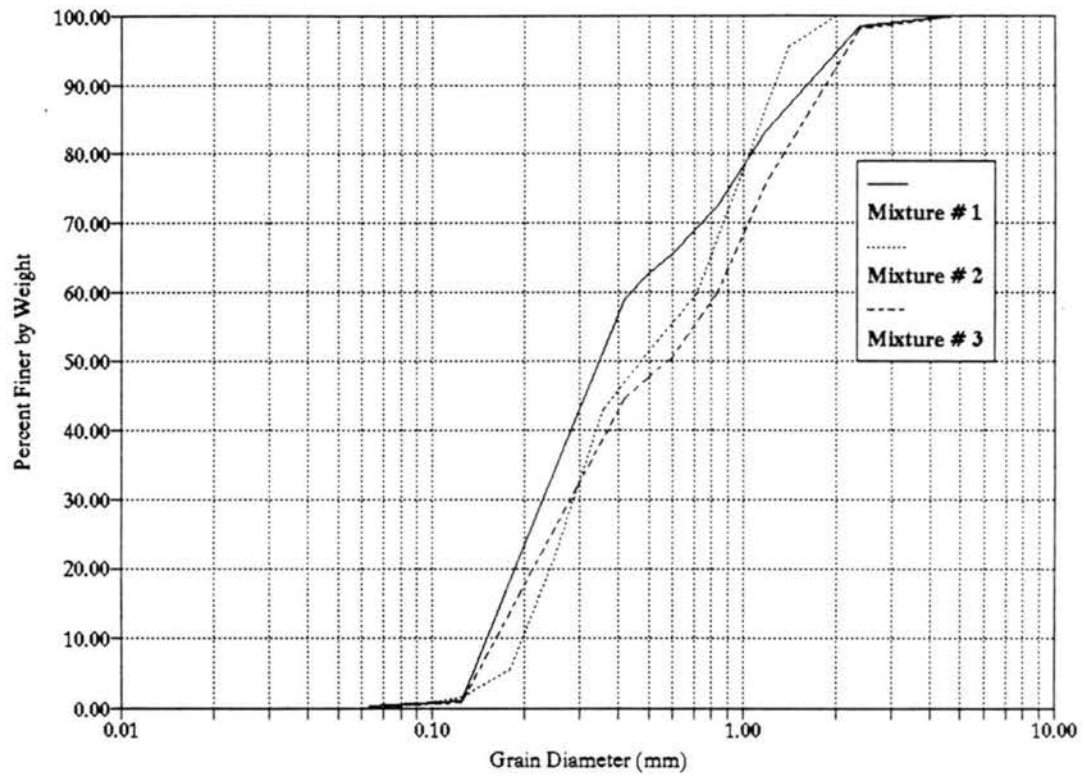


Figure 4.4. Size distribution curves for sand mixtures number 1, 2 and 3.

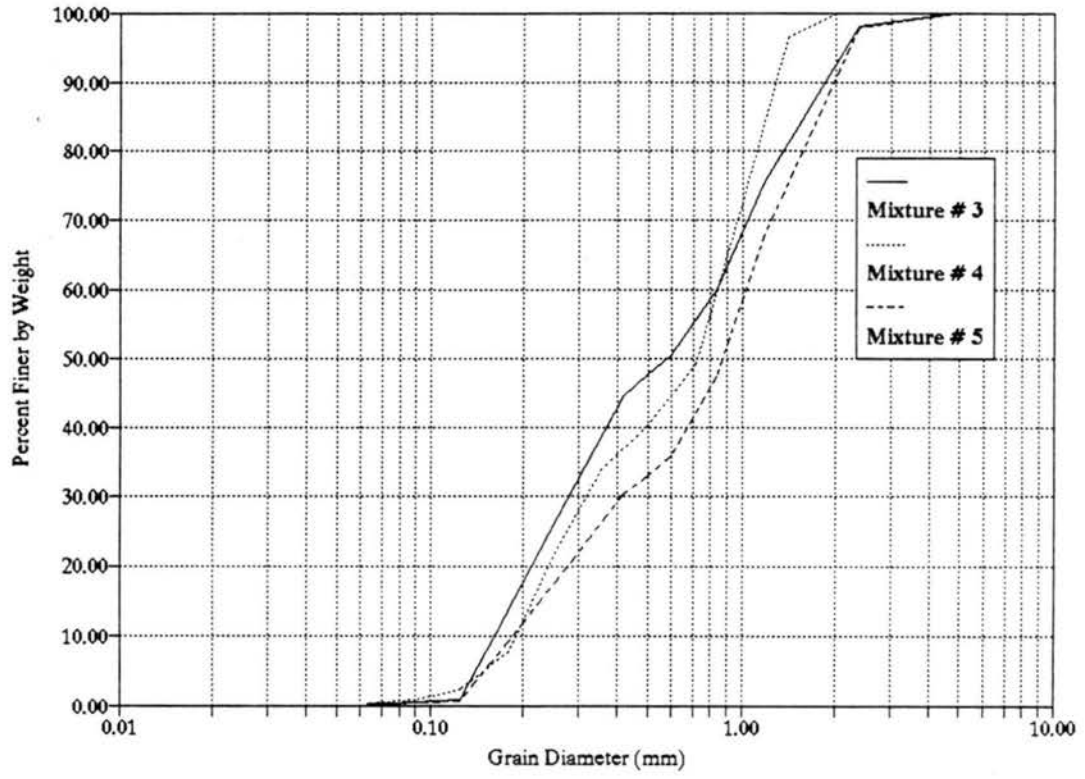


Figure 4.5. Size distribution curves for sand mixtures number 3, 4 and 5.

The median diameters and geometric standard deviations of the fine mixtures are as follows:

Mixture	d_{50}	σ_g
1	0.35	2.85
2	0.45	2.30
3	0.60	2.90
4	0.72	2.30
5	0.86	2.68

Each sediment mixture was loaded into the flume to a depth of 11 cm with special care to avoid segregation of larger grains. The bed surface was leveled using a flat plexiglass plate the same width as the flume connected vertically to the instrument carriage by two screws. The bottom edge of the flat plate was adjusted to the required elevation of the bed surface, and the carriage was then pushed by hand carefully and very slowly to produce a smooth plane surface with the required thickness over the entire length of the sediment bed. The edges were then smoothed using a hand trowel.

4.5 Procedure

There were three types of experiments, each with a different procedure. The first one involved running water, the second, still water, and the third air. The first procedure was as follows: Before the experiment was begun, the d_{50} of the mixture was known and the slope set by using the Simons and Richardson (1966) graph (Figure 2.1) so the depth and discharge could be approximately predicted. The slope of the flume bed was adjusted appropriately. When the sand was put in, it took the slope of the flume. Then clear water was pumped into the flume at a very low rate, the discharge

gradually increased with continuous adjustment of the downstream gate to establish uniform flow conditions at each gradual increase in the discharge. In each run the bed configuration was assumed to have reached equilibrium when the bedforms had not only developed fully down the flume but also had ceased to show overall change in size or geometry with time. Runs continued for about 24 to 48 hours to ensure sufficient time for attainment of equilibrium. During this time, readings for bed level, water surface, and discharge were taken several times. Just before stopping the run, these readings were taken for a last time. After flow was stopped, then the samples were taken from three or four dunes in the middle section of the flume.

The second procedure (experiment with still water) was as follows: First, a wooden foreset of a dune was put on the flume bed. Then clear water was pumped into the flume. As the water level was rising, the downstream steel gate was adjusted until a proper depth of water was reached. After that the pump was stopped, the controlling valve was closed and the downstream steel gate was sealed to keep the water level stable during the experiment. The water depth was about 2 cm higher than the dune height needed. The sand mixture was poured into the flume using a wooden funnel with the same width as the flume width (Figure 4.6). The sand was poured into an inclined layer with an angle equal to the angle of repose of the sand mixture. The funnel was as low as possible to the water surface in order to remove the impact factor of the sand mixture grains on these already deposited. After reaching an appropriate dune length, the dune was sampled layer by layer.

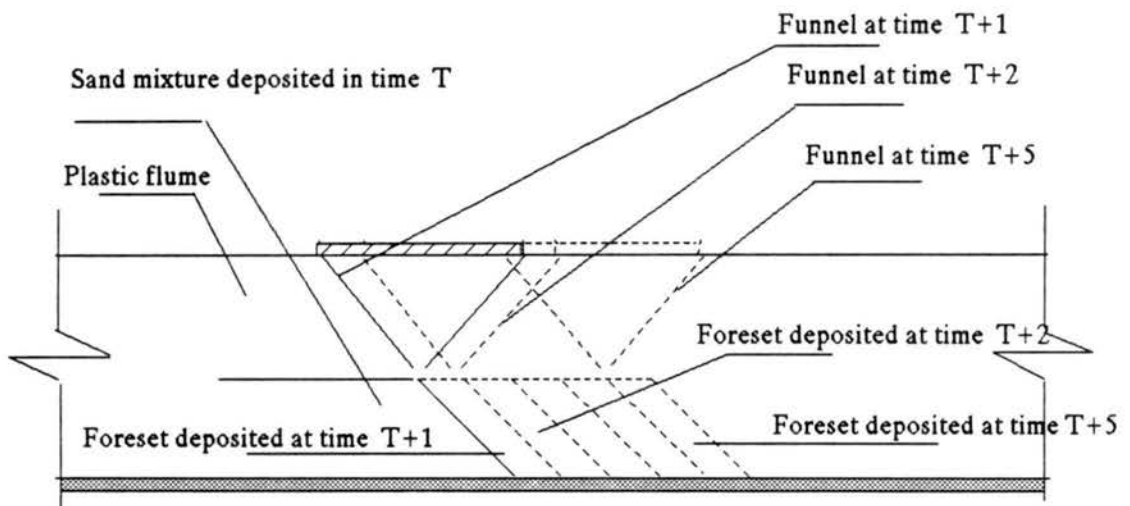


Figure 4.6. Diagram showing the deposition of each sand foreset using a funnel.

The third procedure (experiment with air) was the same as the experiment with still water but with air as the media in which deposition occurred. To sample the dune layers using the same siphoning method as before, the dune was covered completely with water. In order to do that without distorting the dune structure, a very slow water discharge was pumped into the flume, while at the same time a hose with almost the same discharge was put downstream of the dune, so that the level of water upstream and downstream was the same. Slowly the dune layers were submerged in water. Then the pump was stopped, the controlling valve was closed, and the downstream steel gate was sealed. After these steps the sampling of the dune layers was started.

CHAPTER 5

RESULTS AND ANALYSIS OF EXPERIMENTAL DATA

The main objective of this study was to find a method that could predict the vertical sorting in dune structures in non-uniform sediment mixtures. To carry out this goal, a set of water- and sediment-related variables were measured as described in Chapter 4. These variables included the grain size distribution of the original mixture, the water discharge, Q_w , the average water depth in the flume, d_{avg} , the final water surface slope, S_w , and the grain size distribution of the vertical dune layer samples.

Tables 5.1 and 5.2 contain the experimental data of the flume measurements for the eleven experiments: six experiments with running water, three experiments with still water, and two experiments with air. Five mixtures were used in these 11 experiments. One of these experiments, #4.1, was a duplication of experiment number four under almost the same conditions to verify that the grain size distribution of the vertical dune layers of the same mixture under the same hydraulic conditions could be reproduced. The grain size distribution curves are shown in Appendix A.

5.1 Calculation of Average Bed Shear Stress

The calculations of the average bed shear stresses, τ_b , and the shear stresses related to the grain roughness, τ_{bg} , and to the dune shape, τ_{bd} , were based on a modified Einstein analysis proposed by Vanoni and Brooks (1957) for flumes with

Table 5.1. Summary of the measured data for running water experiments.

Run No.	d_{50} (mm)	σ_g	d_{ave} (cm)	Q_w (m/sec)	S_w	S_e	F_r	Dune Height H (m)	Dune Length L (m)
RW-1	0.35	2.85	18.5	0.021	0.0024	0.0022	0.43	0.040	1.07
RW-2	0.45	2.3	17.1	0.022	0.0028	0.002	0.49	0.030	0.91
RW-3	0.60	2.9	16.1	0.021	0.0022	0.002	0.53	0.030	0.91
RW-4	0.72	2.3	17.8	0.022	0.0024	0.0022	0.46	0.035	0.91
RW-4.1	0.72	2.3	17.8	0.022	0.0023	0.0022	0.46	0.035	0.91
RW-5	0.86	2.68	17.8	0.022	0.0027	0.0025	0.47	0.030	1.07

Table 5.2. Summary of the measured data for still water and air experiments.

Run No.	d_{50} (mm)	σ_g	depth of Water (cm)
ST-1	0.86	2.68	8.0
ST-2	0.86	2.68	16.0
ST-3	0.86	2.68	30.0
AIR-1	0.86	2.68	16.0
AIR-2	0.86	2.68	30.0

hydraulically smooth walls. The principal assumption is that the cross sectional area can be divided into two parts, A_b (bed area) and A_w (wall area) in which the streamwise component of the gravity force is resisted by the shear force exerted in the bed and walls, respectively. Also, it is assumed that the mean velocity and energy gradient are

the same for A_b and A_w , and that the Darcy-Weisbach flow formula could be applied to each part of the cross section as well as the total cross section. The details of this method are given in Appendix B. The calculated values of the bed shear stress and shear stress due to grain resistance and form drag are presented in Table 5.3.

Table 5.3. Calculated values for bed shear stress, shear stress due to grain resistance, and shear stress due to form drag.

Run No.	d_{ave} (cm)	Q_w (m ³ /sec)	S_e	V (m/sec)	τ_b (N/m ²)	τ_{bg} (N/m ²)	τ_{bd} (N/m ²)
RW-1	18.5	0.021	0.0022	0.57	2.52	0.97	1.55
RW-2	17.1	0.022	0.002	0.64	1.97	1.26	0.71
RW-3	16.1	0.021	0.002	0.65	1.43	1.33	0.10
RW-4	17.8	0.022	0.0022	0.62	2.34	1.31	1.03
RW-4.1	17.8	0.022	0.0022	0.62	2.34	1.31	1.03
RW-5	17.8	0.022	0.0025	0.62	2.80	1.46	1.34

Fredsøe's theoretical relation (Fredsoe, 1982) were used to check the experimental results of H/L and H/h_w and τ_{*g} in this study. The $(H/L)_a$ and $(H/h_w)_a$ and τ_{*g} for each mixture were plotted in Figure 5.1 and Figure 5.2. The τ_{*g} values were less than 0.2 which means that all the sediment has been assumed to be carried as a bed load according to Fredsøe. From Figure 5.1, the results show that $(H/L)_a$ ratio is between 0.17 and 0.22 which gives a better agreement with the curve in Figure 5.2.

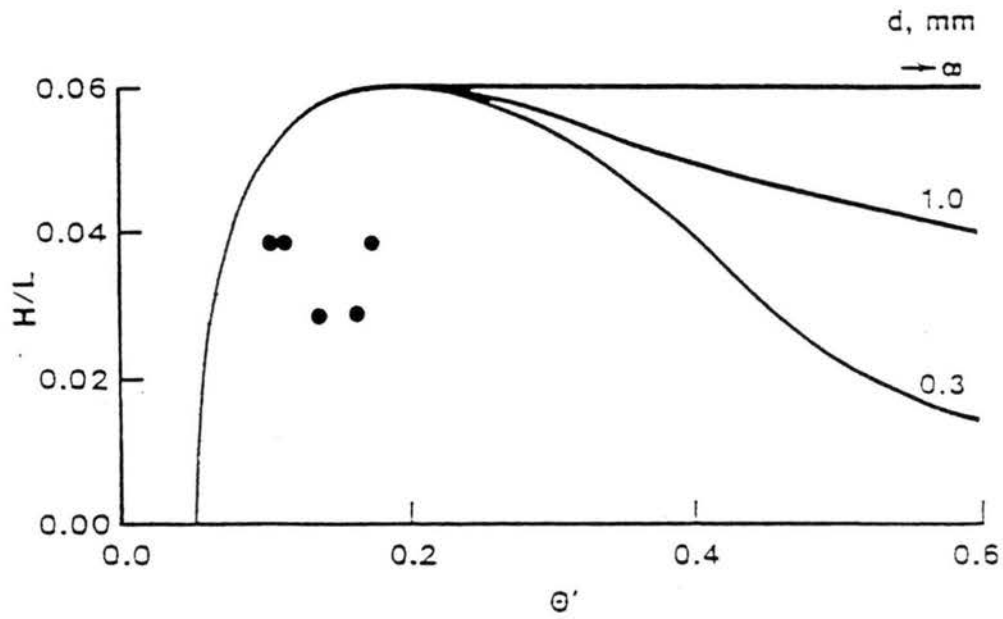


Figure 5.1. Variation in dune height to dune length ratio with bed shear stress for different grain sizes (after Fredsøe, 1982).

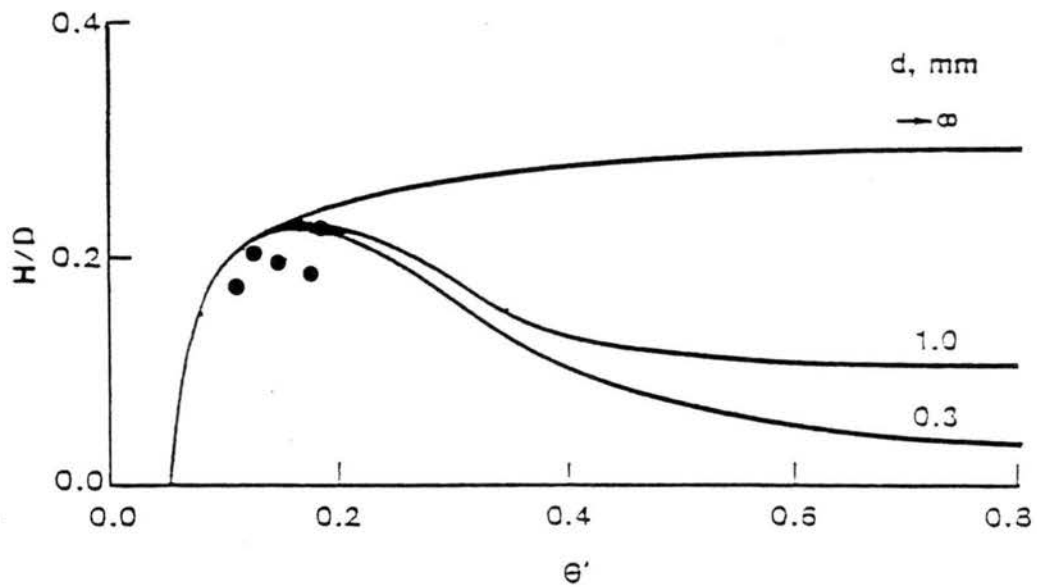


Figure 5.2. Variation in dune height to water depth ratio with bed shear stress for different grain sizes (after Fredsøe, 1982).

The reasons that the experimental results do not follow the curves in Figures 5.1 and 5.2 may be because:

- 1 - These curves were derived for a single size sediment material, 0.3mm 1 mm, but the sediment material which has been used in this study was nonuniform, and
- 2 - The width of the flume which was used in this study was narrow, 20 cm, which may have affected the shape of the dune.

5.2 Experimental Results

5.2.1 Running Water Experiments

As mentioned in Chapter 4 in the experimental procedure, the experiment was kept running until the dunes had developed fully down the flume. Using five sediment mixtures with the characteristics described earlier, each one was sampled in the same way to study the vertical sorting, which gives information about the transport of sediment bed load characteristics per size fraction. Vertical sorting gives additional information about the size characteristics of the sediment bed load moving on a channel bed with the existence of bedform, and will give an idea about the contribution of each size fraction in the sediment bed load. Also, it is an important step toward studying the effect of vertical sorting on the shape of the dune.

Mixtures #1, 3 and 5 showed a geometric standard deviation (σ_{gm}) of 2.85, 2.9 and 2.68 resulting in a difference of about 7% between the smallest and the largest value. On the other hand, the median diameter (d_{50m}) of the three mixtures was 0.35 mm, 0.6 mm and 0.86, mm resulting in a difference of about 60% between the

lowest value and the largest one. Also the ratio between the maximum and the minimum grain size diameter for the three mixtures was 26.5. The other two mixtures (Mixtures #2 and #4) both had a geometric standard deviation (σ_{gm}) of 2.3, and median diameters (d_{50m}) of 0.47 mm and 0.72 mm, with the maximum grain diameter reduced to 1.65 mm, so that the ratio between the maximum and the minimum grain size diameter for these two mixtures was reduced to 13.22.

The purpose of changing the median diameter (d_{50m}) for Mixture #1, 3 and 5 within a spectrum wider than that for the geometric standard deviation (σ_{gm}), which was almost constant, was to minimize the effect of the geometric standard deviation (σ_{gm}) and to study the effect of the median diameter (d_{50m}). That is to see if the median diameter (d_{50m}) for each non-uniform sediment mixture material could be a factor in the sorting process. Also the ratio between the maximum grain size diameter and the minimum grain size diameter might give an indication of the particle diameter range within each sediment mixture in the sorting process. The geometric standard deviation (σ_g) for Mixtures #2 and #4 was reduced to about 20% less than Mixtures #1, #2 and #3 to see if there was a change in the sorting process due to this reduction or whether it would follow the same pattern as for Mixtures #1, #3 and #5, and the median diameter (d_{50}) was chosen to be less than 0.6 mm for Mixture #2 and to be higher than 0.6 mm for Mixture #4. Also the ratio of the maximum grain diameter to the minimum grain diameter was reduced to almost half the ratio for Mixtures #1, #3 and #5.

From the grain size distribution of each layer of the different dunes from different mixtures, there was clear evidence of the vertical sorting within the entire

length of the dune structure, which supports the idea presented in Chapter 3 of how each grain size of the sediment bed load is deposited within the dune structure. Figure 5.3, which is one of 22 graphs presented in Appendix A, shows that the dune layers were distinctive one from another and also an increase of d_{50} of each layer downward. Figures 5.4, 5.5, 5.6, 5.7 and 5.8 showed the average variation of d_{50} for each mixture as a function of y/d , where y is the distance from the highest point of the dune to the point where the layer is sampled, and d is the total height of the dune, which is the summation of the thickness of the layers. For Mixture #1 the ratio between the median diameter (d_{50}) at the lowest layer ($y/d = 0.0$) and the median diameter (d_{50}) at the top of the dune ($y = d$) was 2.6, for Mixture #3 this ratio was 2.36, and 1.67 for Mixture #5. The ratios for Mixture #2 and #4 were 2.38 and 1.45.

It appeared that as the d_{50} of the mixture decreased, this ratio increased and vice versa. Further, these results did not follow the pattern of the geometric standard deviation for any of the five mixtures. For example, the first mixture, which had a geometric standard deviation (σ_{gm}) 2.85, had a ratio between the lower layer grain diameter and the upper layer grain diameter equal to 2.6. On the other hand, the second mixture had a geometric standard deviation equal to 2.3, which is less than the first one, but the ratio between the lower grain diameter and the upper grain diameter was 2.38.

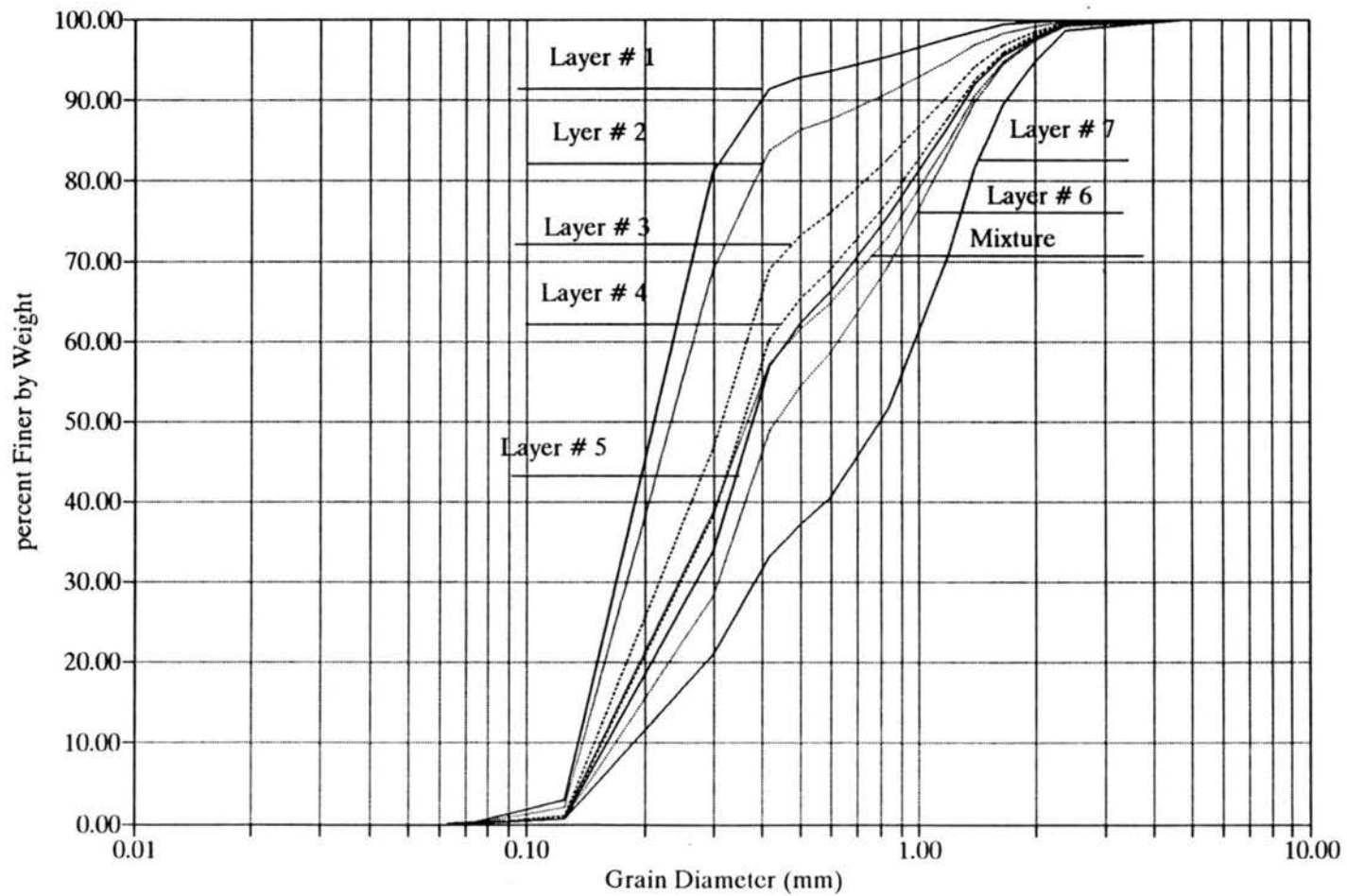


Figure 5.3. Size distribution curves for dune layers (Dune #1, Mixture #1).

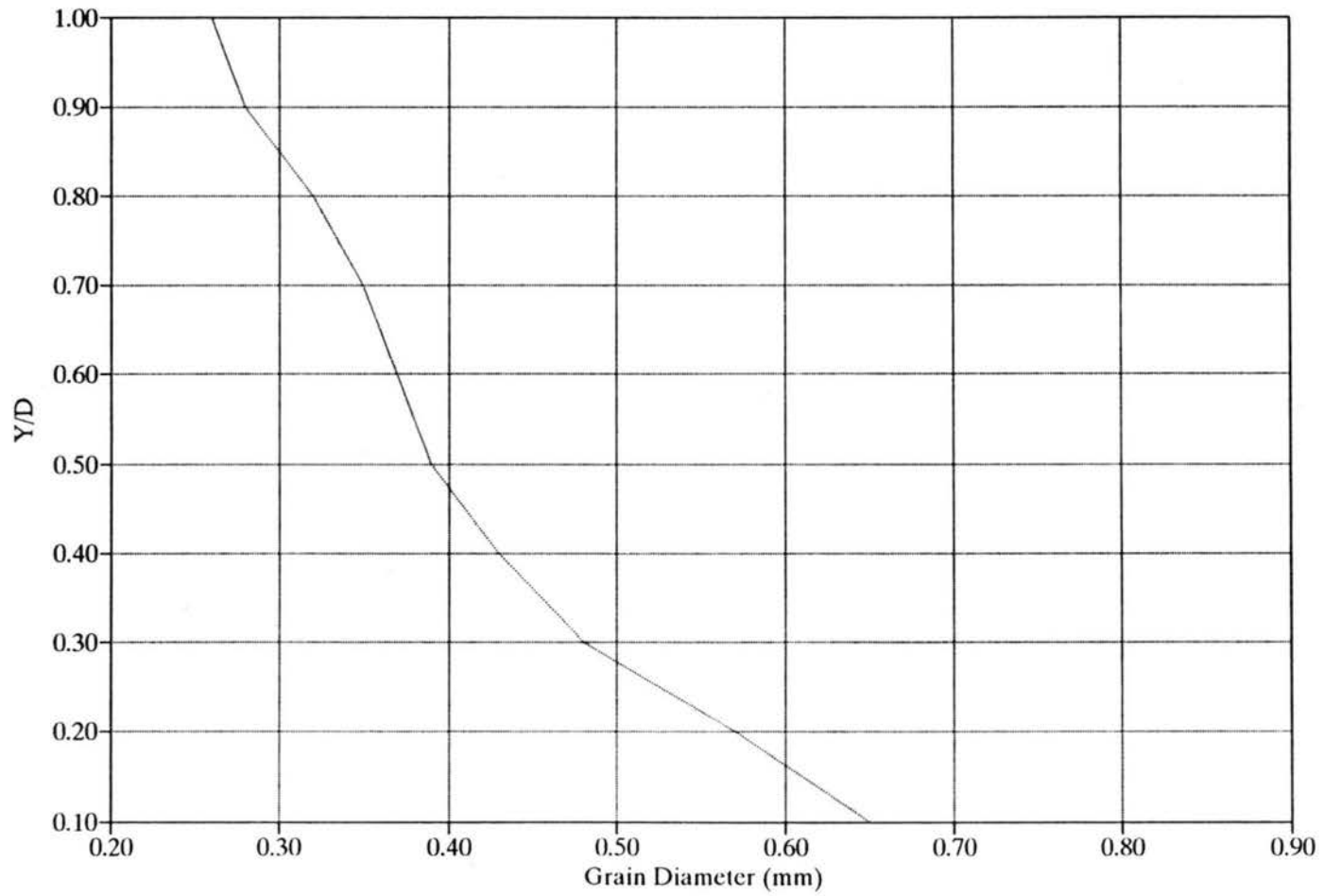


Figure 5.4. Actual median grain diameter for a dune layer (Mixture #1).

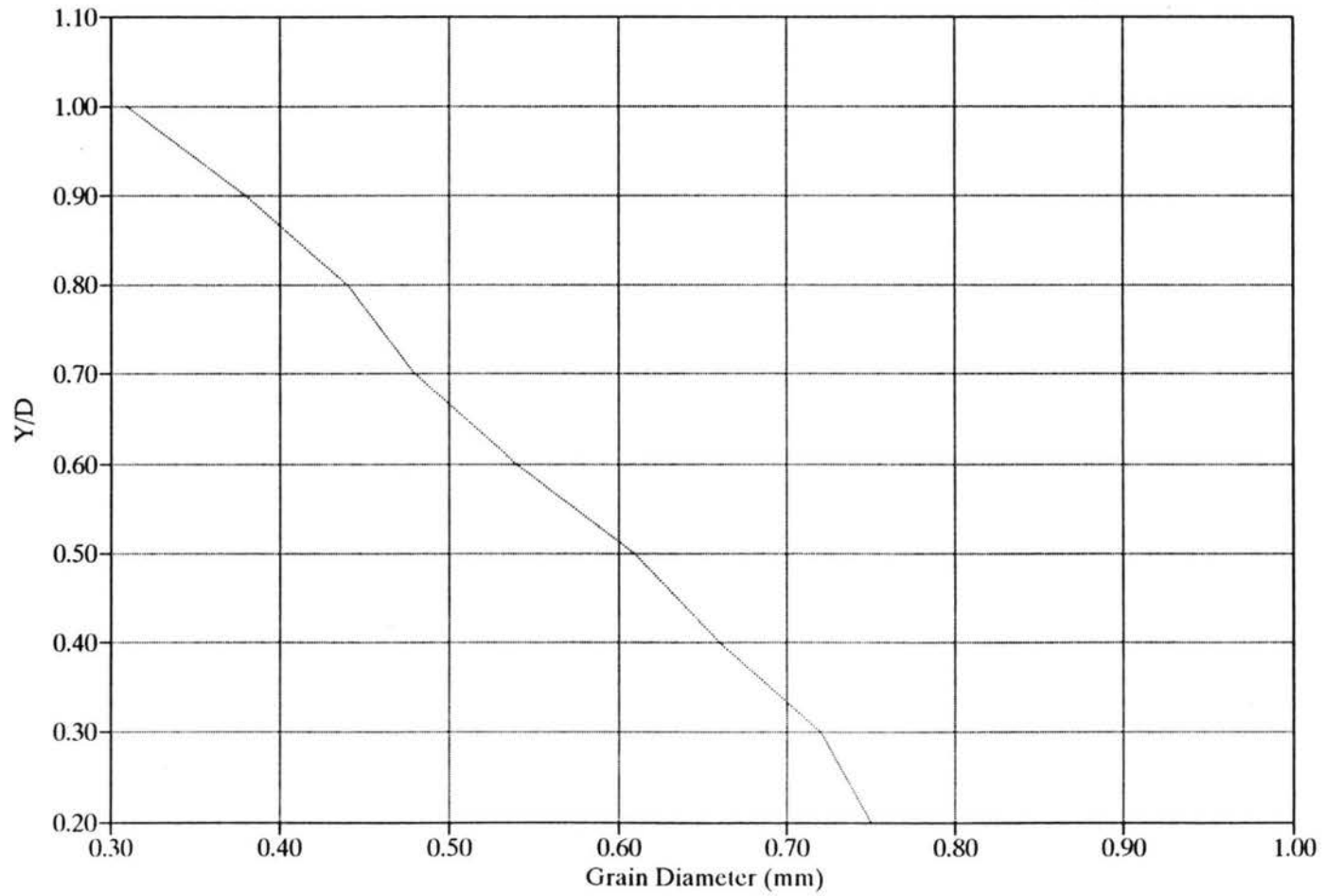


Figure 5.5. Actual median grain diameter for dune layer (Mixture #2).

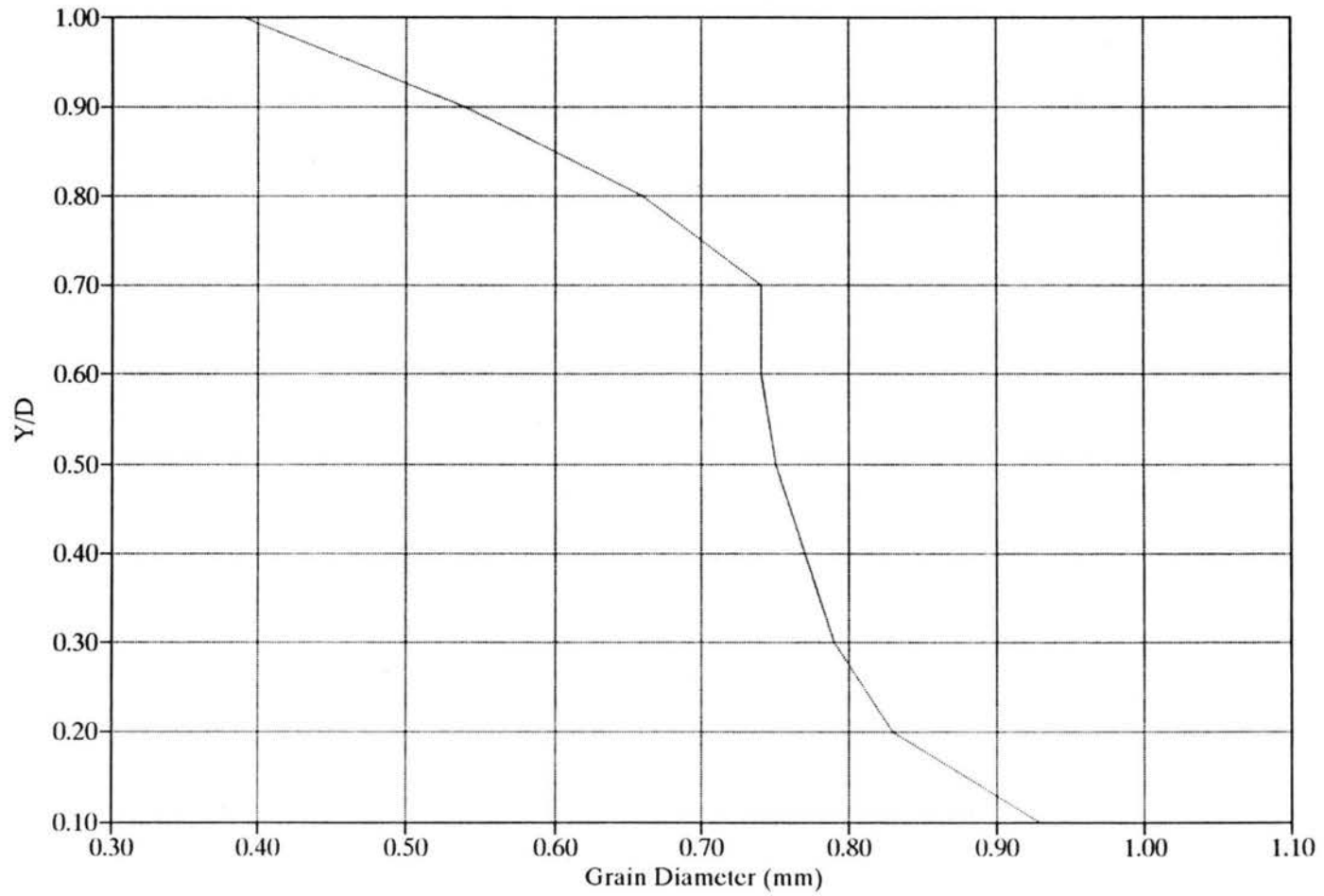


Figure 5.6. Actual median grain diameter for dune layer (Mixture #3).

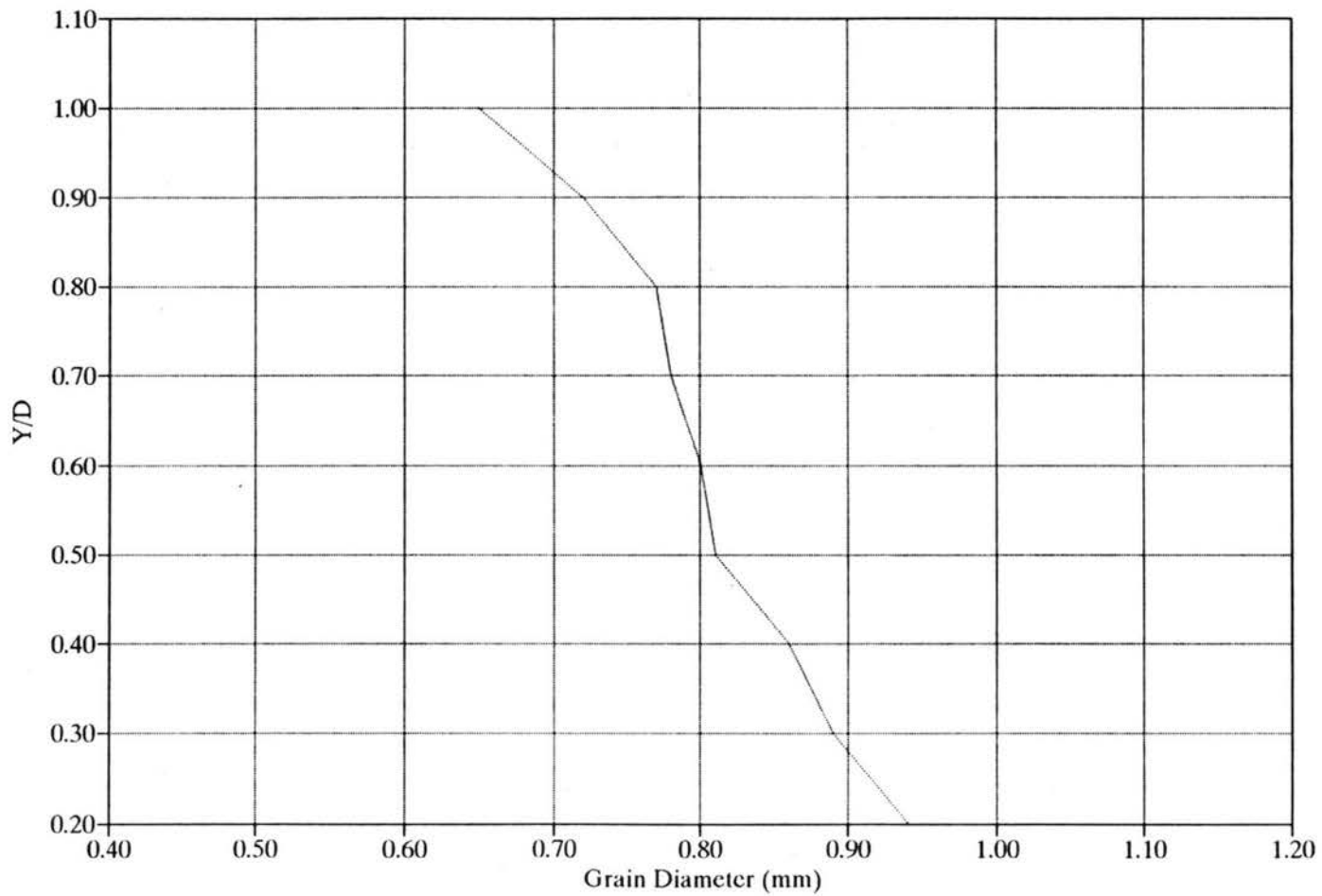


Figure 5.7. Actual median grain diameter for dune layer (Mixture #4).

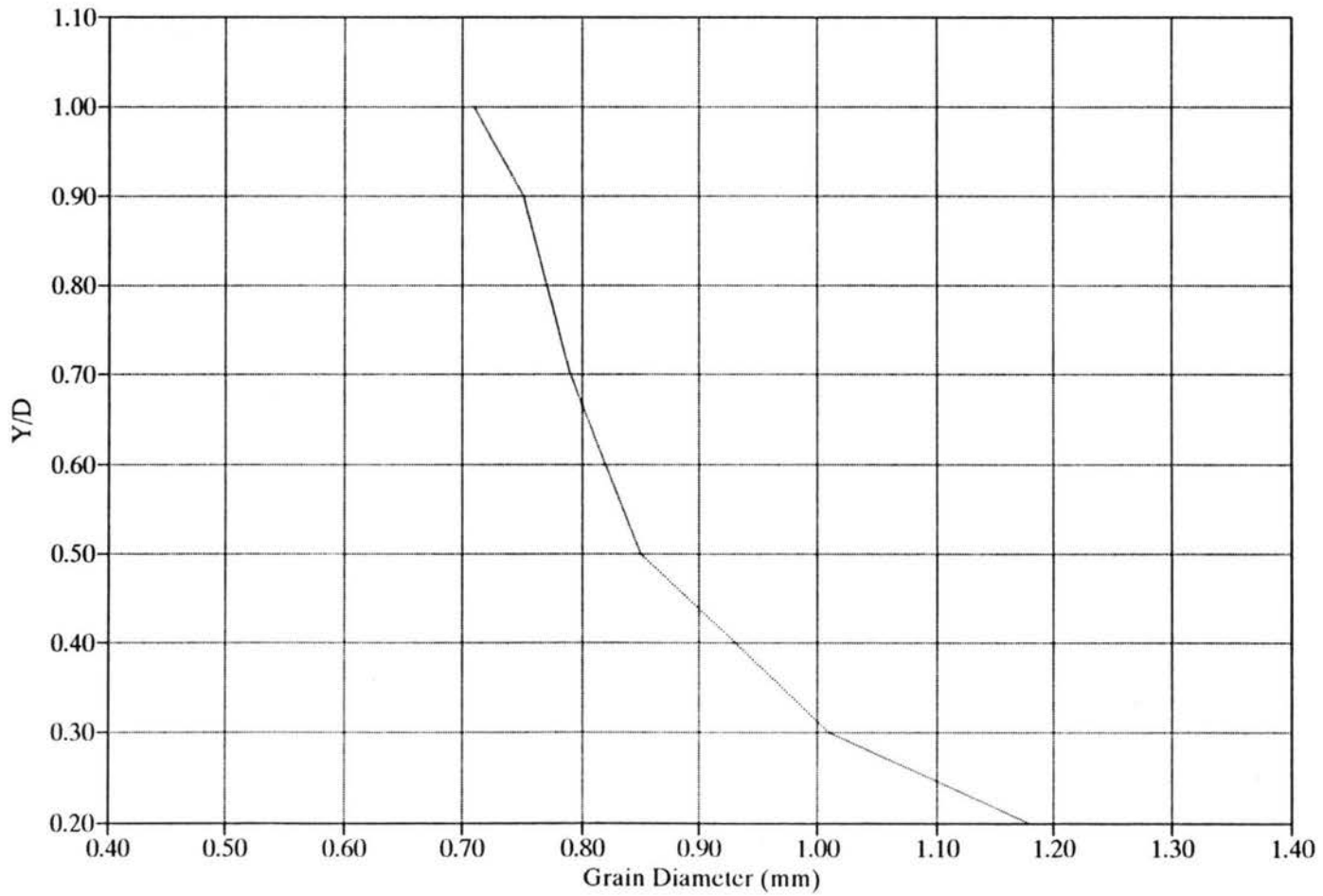


Figure 5.8. Actual median grain diameter for a dune layer (Mixture #5).

The same ratio was equal to 2.36 for Mixture #3, which had a geometric standard deviation of 2.9, and also the fourth and fifth mixtures, which have a geometric standard deviation equal to 2.3 and 2.7. This ratio was then equal to 1.45 and 1.67, respectively. From these results, it can be seen that the geometric standard deviation is not a major factor in this ratio, which is an indication of the vertical sorting.

Figures 5.9, 5.10, 5.11, 5.12 and 5.13 show the normalized average geometric standard deviation (σ_{gal}/σ_{gm}) in the vertical direction from top ($y/d = 1$) to bottom ($y/d=0.0$) for each dune layer, over the geometric standard deviation for each of the five mixtures. The Mixture #1 has a normalized geometric standard deviation ($\sigma_{gal}/\sigma_{gm1}$) values equal to 0.62 at the top and 0.85 at the bottom, Mixture #2 has $\sigma_{gal}/\sigma_{gm2}$ values equal to 0.8 and 0.9; for the top and the bottom, the values of $\sigma_{gal}/\sigma_{gm3}$ for Mixture #3 are 0.82 and 0.7. Also the values of the $\sigma_{gal}/\sigma_{gm4}$ for Mixture #4 are 0.9, 0.75 for the top and the bottom, Mixture #5 has $\sigma_{gal}/\sigma_{gm5}$ values equal to 0.82 and 0.62 for the top layer and the bottom layer of the dune. This is a pattern which can be related to the median grain diameter (d_{50m}) of each mixture, not to the geometric standard deviation (σ_{gmi}) of each mixture. This pattern is: when the median grain diameter (d_{50m}) of a mixture is less than 0.6 mm the geometric standard deviation (σ_{gal}) increases from top to bottom, and the d_{50m} is greater than 0.6 mm the σ_{gal} decreases from top to bottom regardless of the original geometric standard deviation (σ_{gmi}) for each mixture.

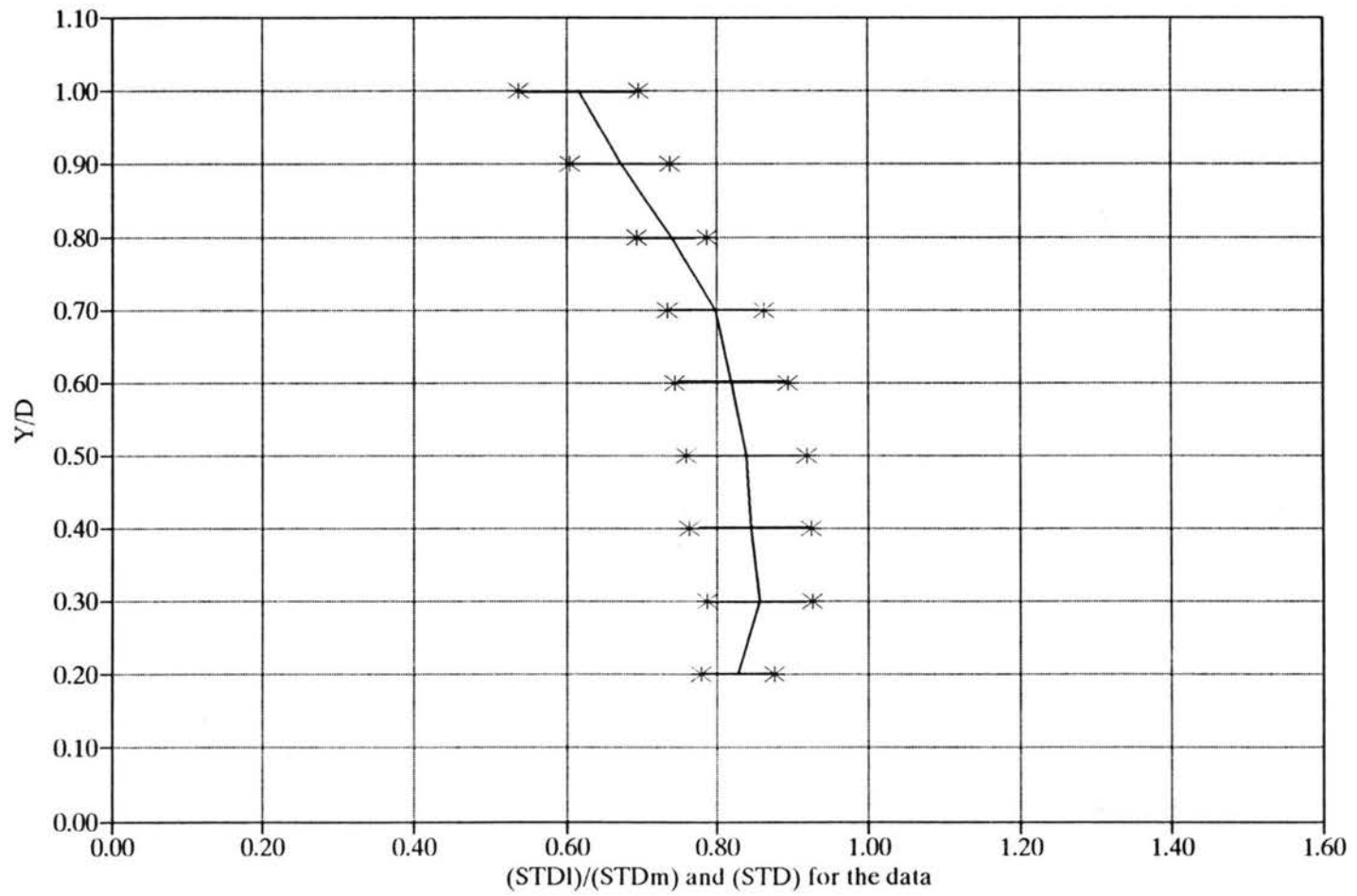


Figure 5.9. Normalized average geometric standard deviation in the vertical direction (Mixture #1).

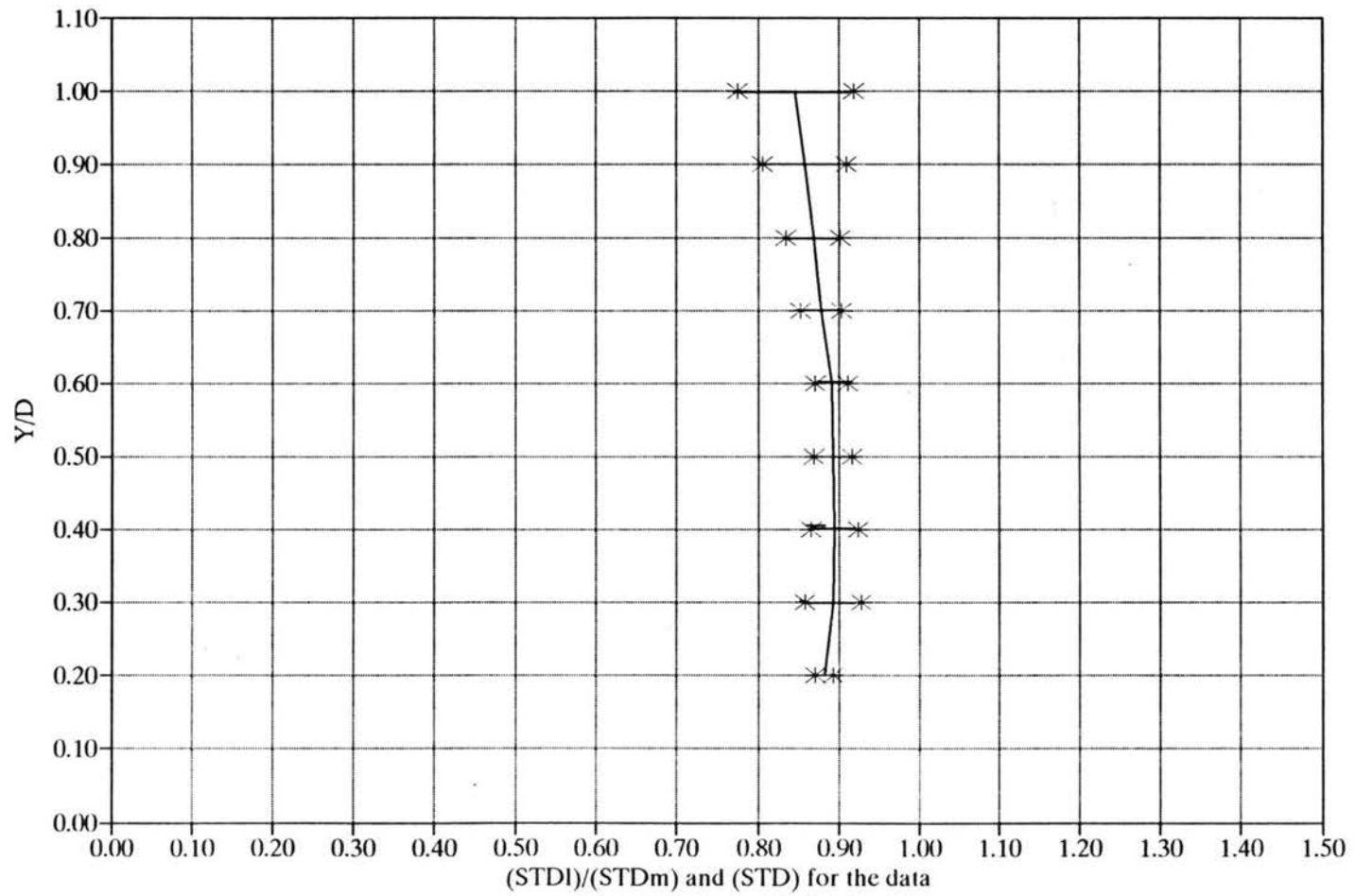


Figure 5.10. Normalized average geometric standard deviation in the vertical direction (Mixture #2).

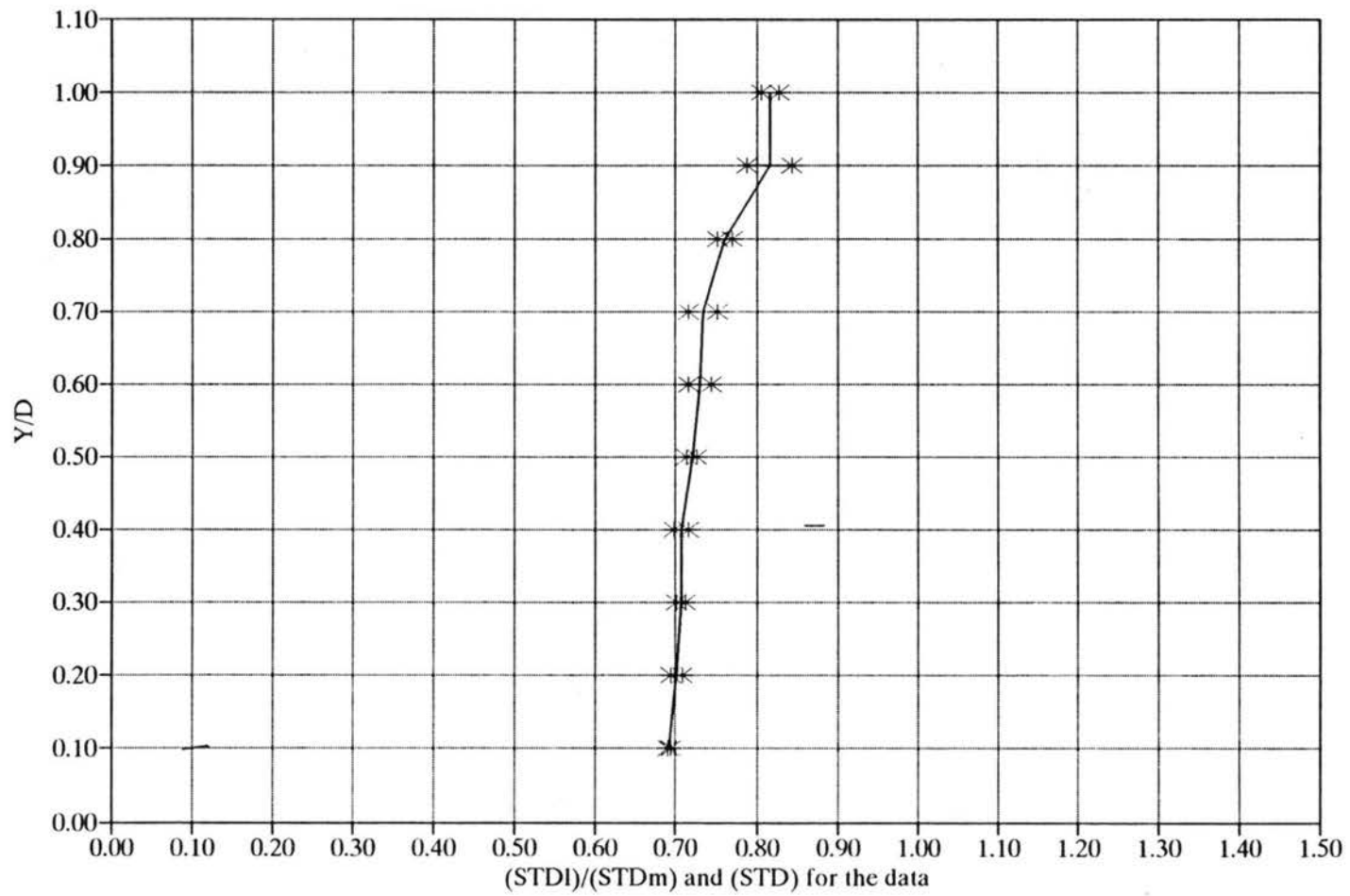


Figure 5.11. Normalized average geometric standard deviation in the vertical direction (Mixture #3).

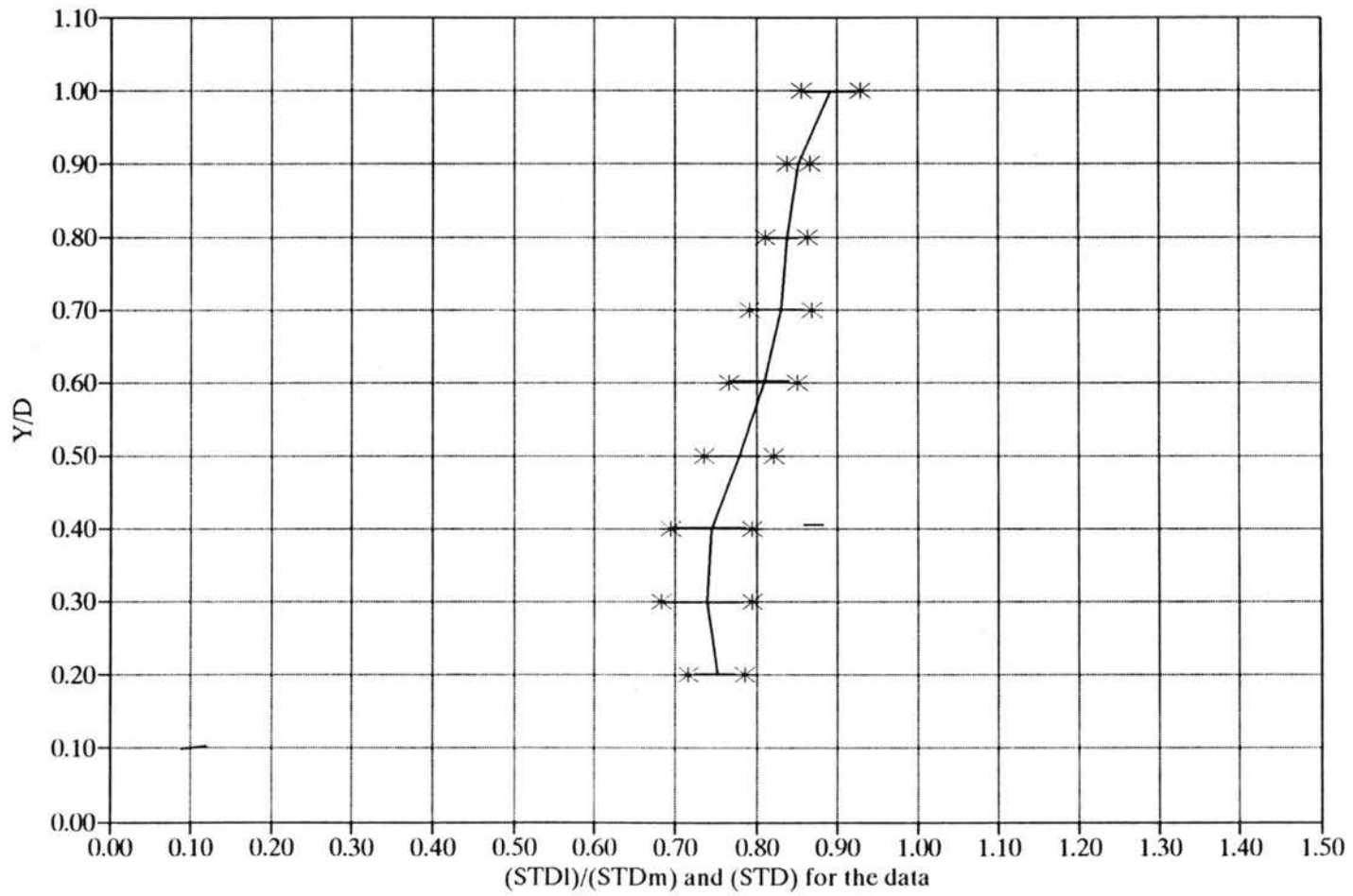


Figure 5.12. Normalized average geometric standard deviation in the vertical direction (Mixture #4).

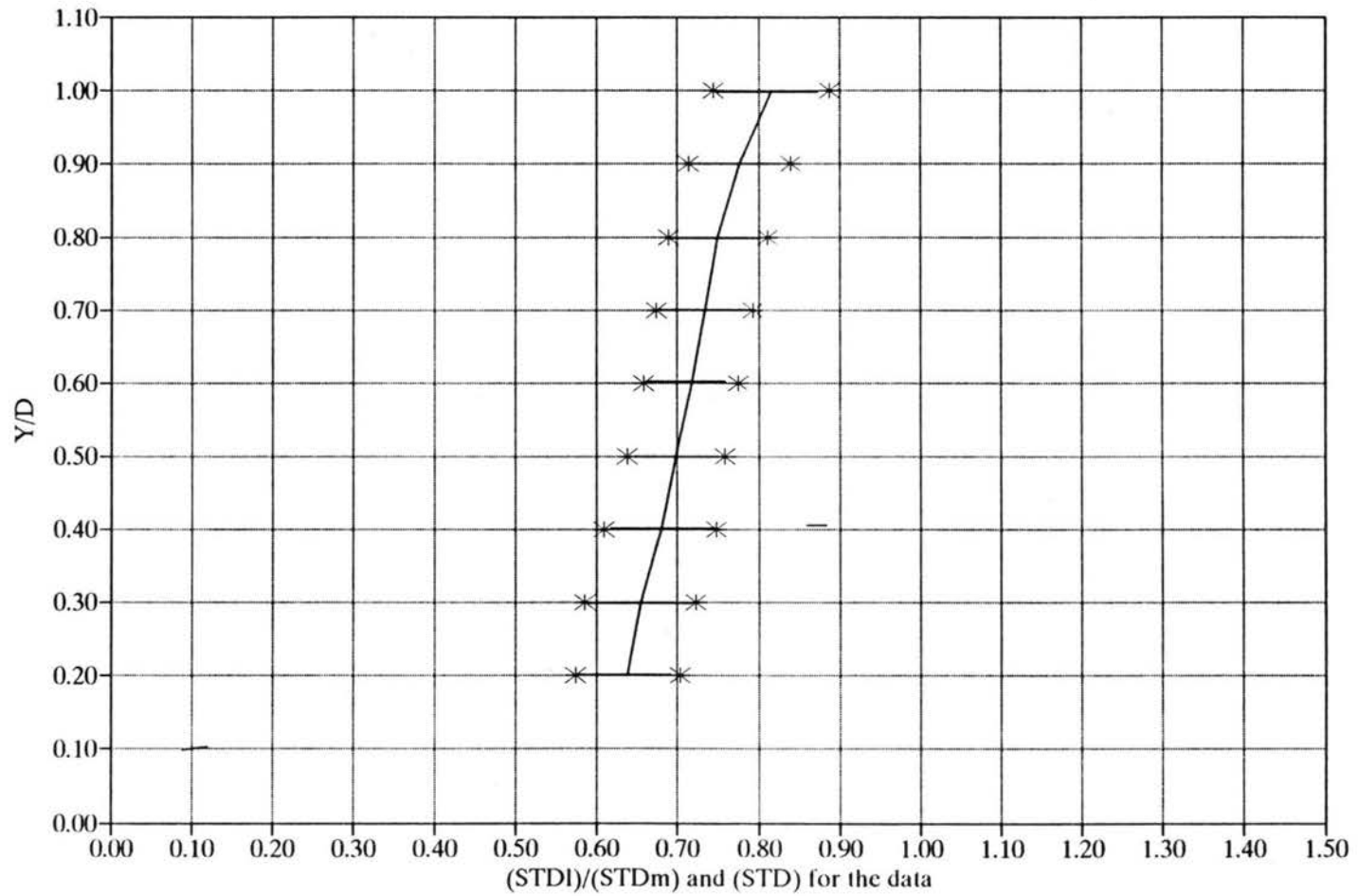


Figure 5.13. Normalized average geometric standard deviation in the vertical direction (Mixture #5).

5.2.2 Still water experiments

One of the five mixtures, #5, $d_{50} = 0.86$ mm and $\sigma_{gm} = 2.67$, was used to study the vertical sorting process (vertical decrease in sand grain size within the dune) in still water. The main reason for this kind of experiment was to remove the effect of the hydrodynamic forces in order to study the effect of the gravitational force only on the vertical sorting process.

Three experiments were run using the same sand mixture as was described in Chapter 4. The water depth for the first experiment was 0.1 m and the sand deposit was a delta type shape more than a dune type shape. That was accomplished by depositing foreset lamina after foreset lamina by moving a funnel with the same width as the flume in the downstream direction in a continuous movement so the same avalanching process that occurs during the deposition of each foreset in the running water experiment was duplicated but without the effect of the hydrodynamic forces. The height of the deposited sand was 0.08 m; this height was chosen to be as close as possible to the running water dune height and at the same time could be practically done. Also the water depth was chosen to be 20 mm higher than the deposited sand so that when the sand mixture for each foreset lamina was poured through the funnel opening over the previously deposited foreset lamina, it would settle as soon as possible duplicating what happens in the running water experiments during the gravitational sliding. After a proper length of deposited sand mixture was reached, the same sampling technique described in Chapter 4 was used. Eleven layers, each one 5 mm thick were sampled.

The results of the sieve analysis are shown in Figure 5.14. From this figure, it is clear that there was no sorting at all within the dune structure. All grain size distribution curves were almost falling on top of each other. Variations were probably due to noise in the complex technique. The reason for the lack of vertical sorting may be that the length of the lee slope, which is a function of the height of the dune, was not long enough to give the gravitational sliding a chance to develop the sorting of the sand particles. Based on this conclusion, the next stage was to do another experiment but with a deposited sand mixture height higher than in the first experiment.

The height of the deposited sand for the second experiment was double that of the first experiment, 0.16 m, so the length of the lee slope was increased and the water depth raised to 0.18 m. There were 11 layers, each 14 mm thick. The results of the sieve analysis of this experiment are shown in Figure 5.15. From this figure, the dune layers started to spread out from each other more than in the first experiment, but the sorting was still not clear despite the increased height of the dune.

The next logical step was to do another experiment but with a dune height of 0.30 m, almost double the second experiment, with a water depth of 0.32 m. The results of the sieve analysis for this experiment, shown in Figure 5.16, shows clear evidence of the vertical sorting within the deposited sand structure. The first six layers did not show a clear sorting process, maybe because the distance on the lee slope from the top of the dune to each layer of the first six layers was still insufficient to show the

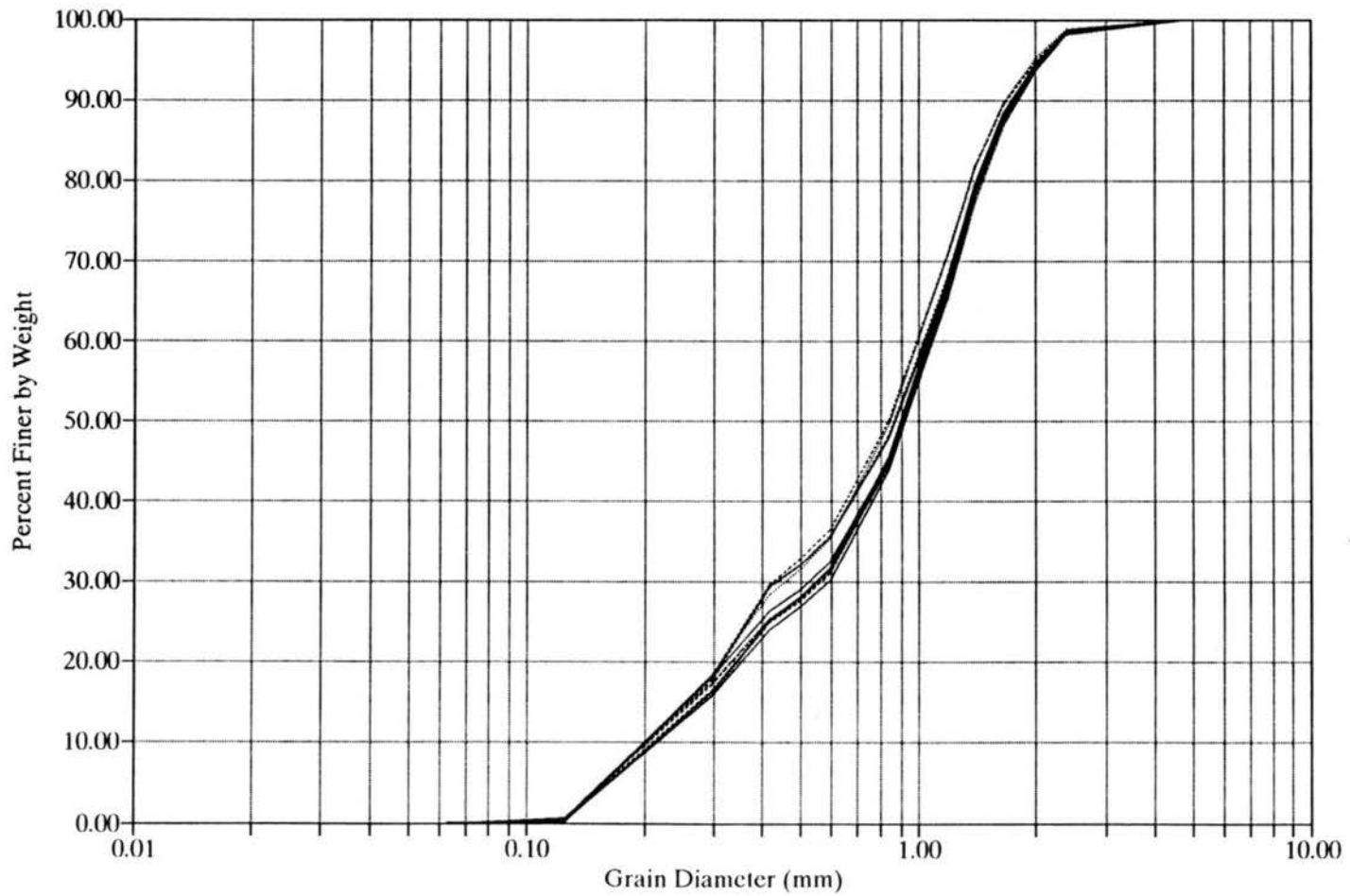


Figure 5.14. Size distribution curves for horizontal layers of delta type deposition in still water (delta height = 0.08 m).

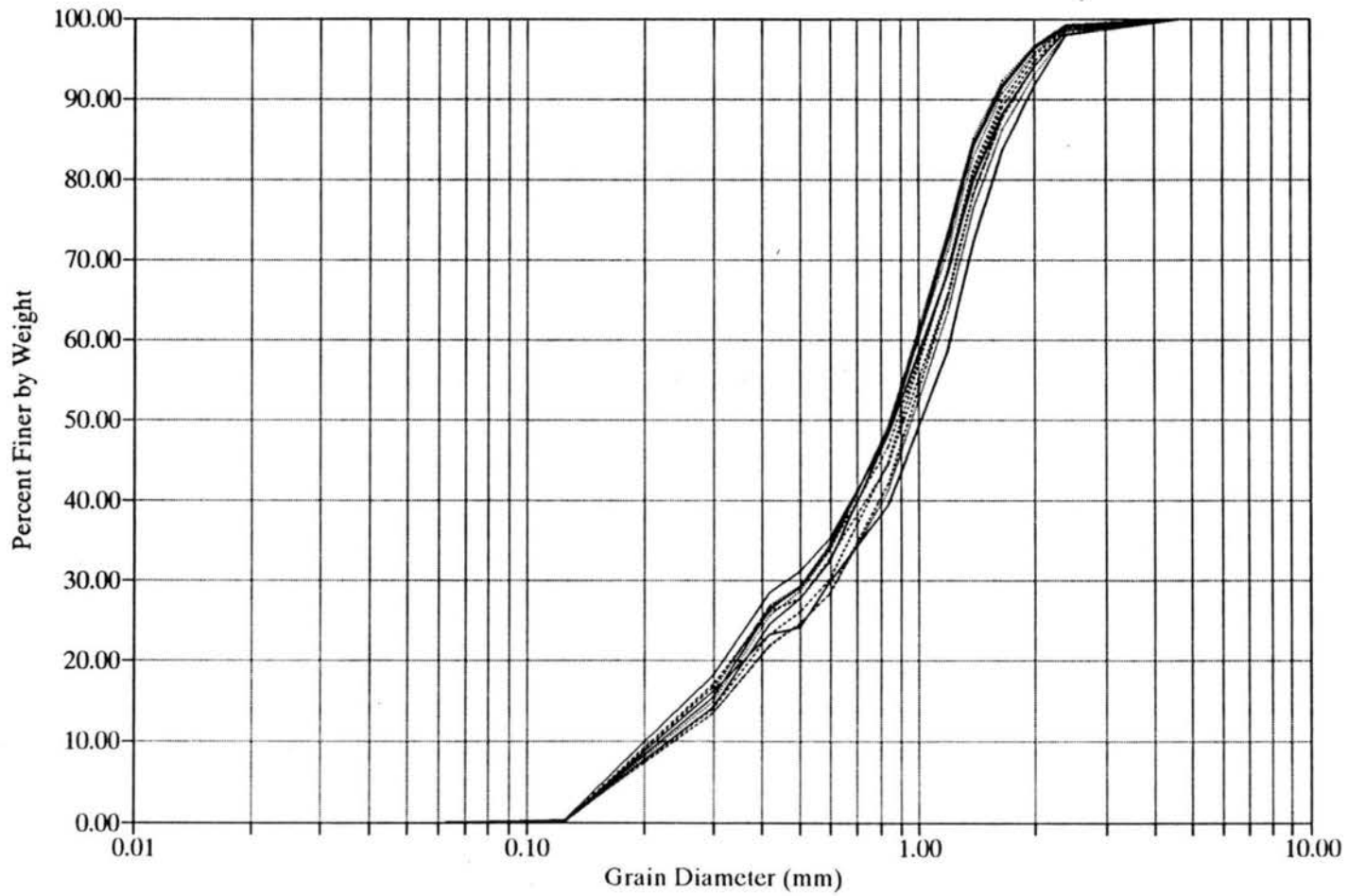


Figure 5.15. Size distribution curves for horizontal layers of delta type deposition in still water (delta height = 0.16 m).

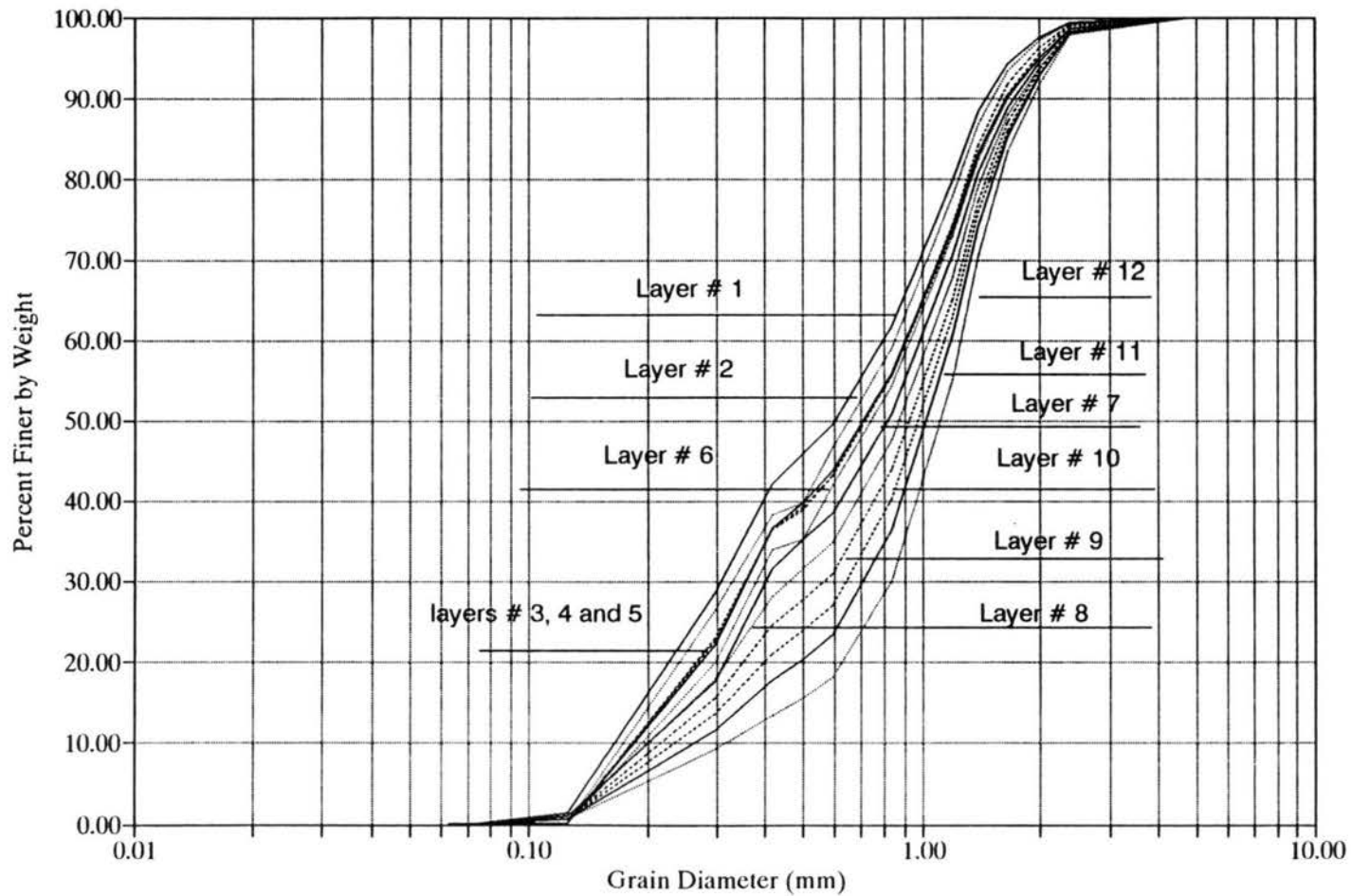


Figure 5.16. Size distribution curves for horizontal layers of delta type deposition in still water (delta height = 0.3 m).

effect of the velocity and gravitational forces on the individual sand grains, but as the lee slope distance was increased these forces worked as in the lower five layers, which gave no doubt of this process.

From the above results it can be concluded that to get sorting in a relatively thick layer of granular flow the deposited sand height needs to be higher than that for running water experiments. One can certainly conclude from these experiments that hydrodynamic forces are important in the sorting process.

5.2.3 Air Experiments

For more evidence on the role of gravitational force in the sorting process, another set of experiments was conducted using the same sediment mixture. But the depositing, using the same technique as in the still water experiments of the sand, was in air. Two experiments were conducted. The deposited delta shape height of the first experiment was 0.16 m and the number of layers was, as before, 11 layers, each 14 mm thick. Figure 5.17 shows the sieve analysis results for each layer. The grain size distribution curves of these layers fell almost on top of each other, indicating very little vertical sorting in the dune structure. So the next step, as with the still water experiments, was to increase the dune height. The height of the deposited sand delta of the second experiment was 0.30 m, and the 11 layers were sampled (see Figure 5.18). The top six layers, as in the third still water experiment, showed no vertical sorting of the sand. But as the lee slope length, which is a function in the height of the

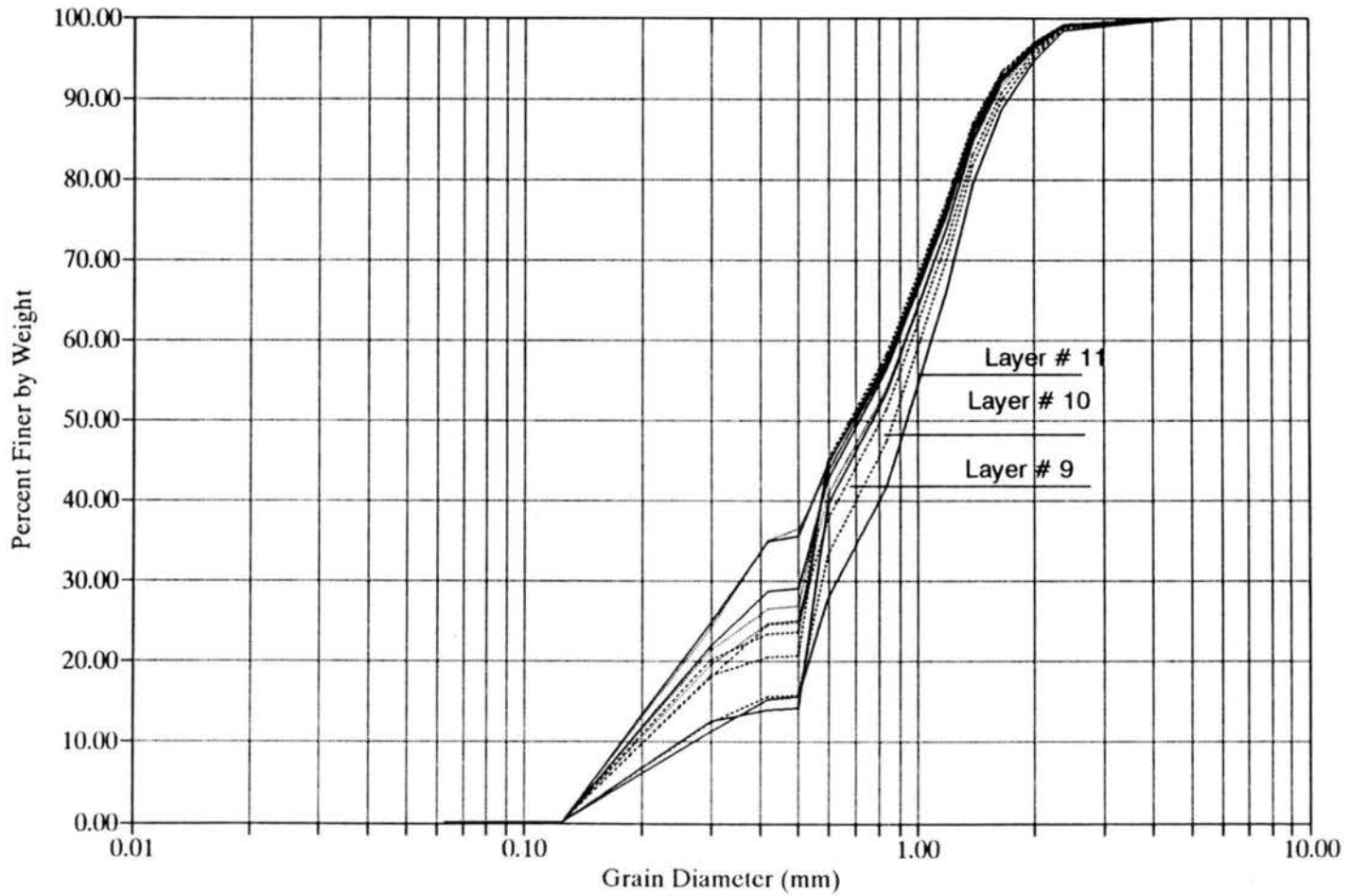


Figure 5.17. Size distribution curves for horizontal layers of delta type deposition in air (delta height = 0.16 m).

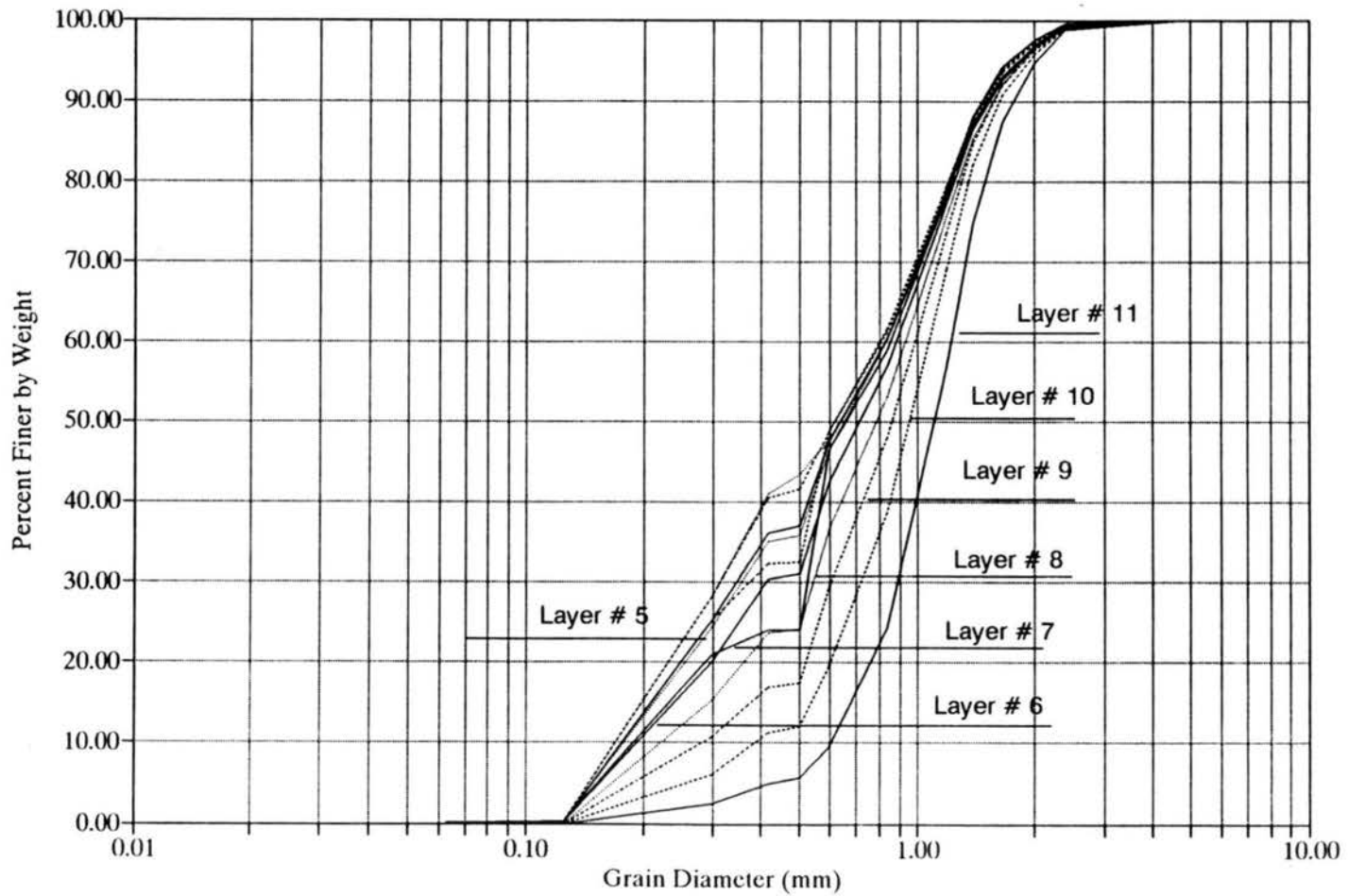


Figure 5.18. Size distribution curves for horizontal layers of delta type deposition in air (delta height = 0.3 m).

deposited sand, increased, the sorting process seemed to develop. From these two experiments with two different depositional environments, one can conclude that the hydrodynamic forces are important in the vertical sorting process within the dune structure.

5.2.4 "Eight-foot" Flume Experiment

All the dunes that were sampled in the flume used in this study were two-dimensional dunes. Because the dunes in natural rivers and channels are three-dimensional, it was very important to sample three-dimensional dunes to prove that the same process occurs. The opportunity to get this data was made possible by Dr. Albert Albert Molinas, at Colorado State University, who was working on a project to study the scour around piers in an eight-foot flume. During one of his runs, the flow conditions were favorable to forming a dune on the bed of the flume. This flume was a recirculating type, 2.44 m wide (8 ft), 0.61 m deep, and 45.7 m long. The flow could be varied from 0.0 to 0.623 cms by use of 2 pumps and a control valve on the discharge lines. The slope of the flume could be adjusted from 0.0 to 1.5 percent by screw jacks.

The flow characteristics of this run were 0.453 cms discharge, 0.304 m depth, and 0.58 mps velocity. The sediment mixture was not the same all over the flume because the study required a change of the sediment mixture around each pier. The sampling technique which was used was as follows:

Using a very thin steel plate with a very sharp edge, each dune was sampled by pushing the steel plate in very slowly, so the sand structure of the dune was not

disturbed. The thickness of each layer was about 3 cm. Pictures of the dunes that were sampled and the flume bed are shown in Figure 5.19. The results of the sieve analysis of each one of the four dune layers were shown in Figures 5.20, 5.21, 5.22 and 5.23. Figure 5.20 shows four layers, its d_{50} varying between 0.35 mm and 0.55 mm. For the second dune (Figure 5.21), which was upstream of the first one, the d_{50} was between 0.6 mm and 1.5 mm. The third dune (Figure 5.22), which was the smallest, has d_{50} of 0.6 mm and 0.8 mm, and the last one (Figure 5.23) had a d_{50} between 0.55 mm and 1.5 mm. These results show that the vertical sorting occurs within the three-dimensional dunes typical of natural conditions, much the same as in the two-dimensional dune.

5.3 Prediction of Vertical Size Distribution of a Dune Structure

5.3.1 Developing the Theoretical Equation

The hydrodynamic forces acting on a sediment particles on the lee side of the dune are the submerged weight of particle, the lift force, the drag force and friction force. These forces are defined by the following equations:



Figure 5.19. Three-dimensional dune pictures (8 ft. flume).

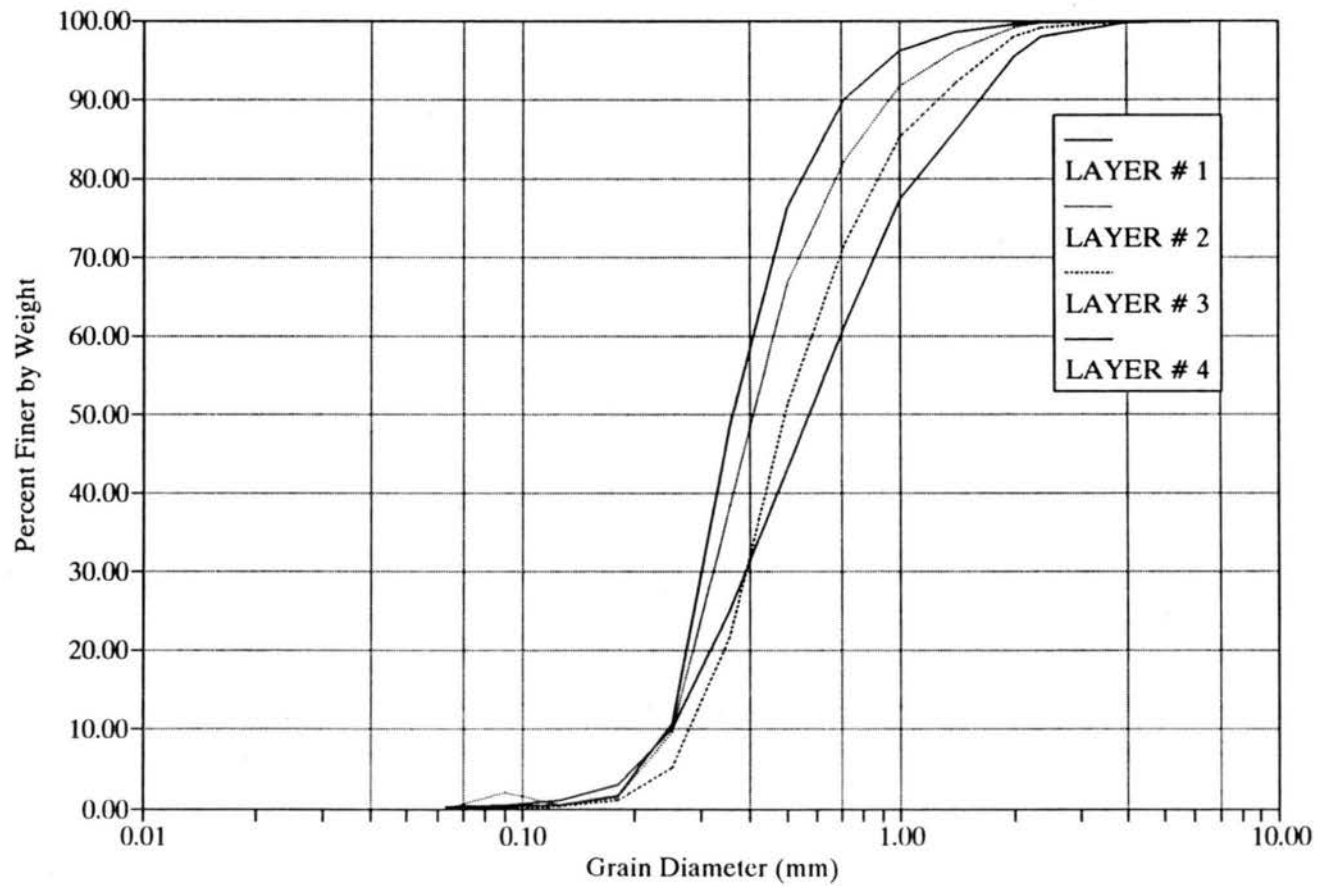


Figure 5.20. Size distribution curves for dune layers (Dune #1, 8 ft. flume).

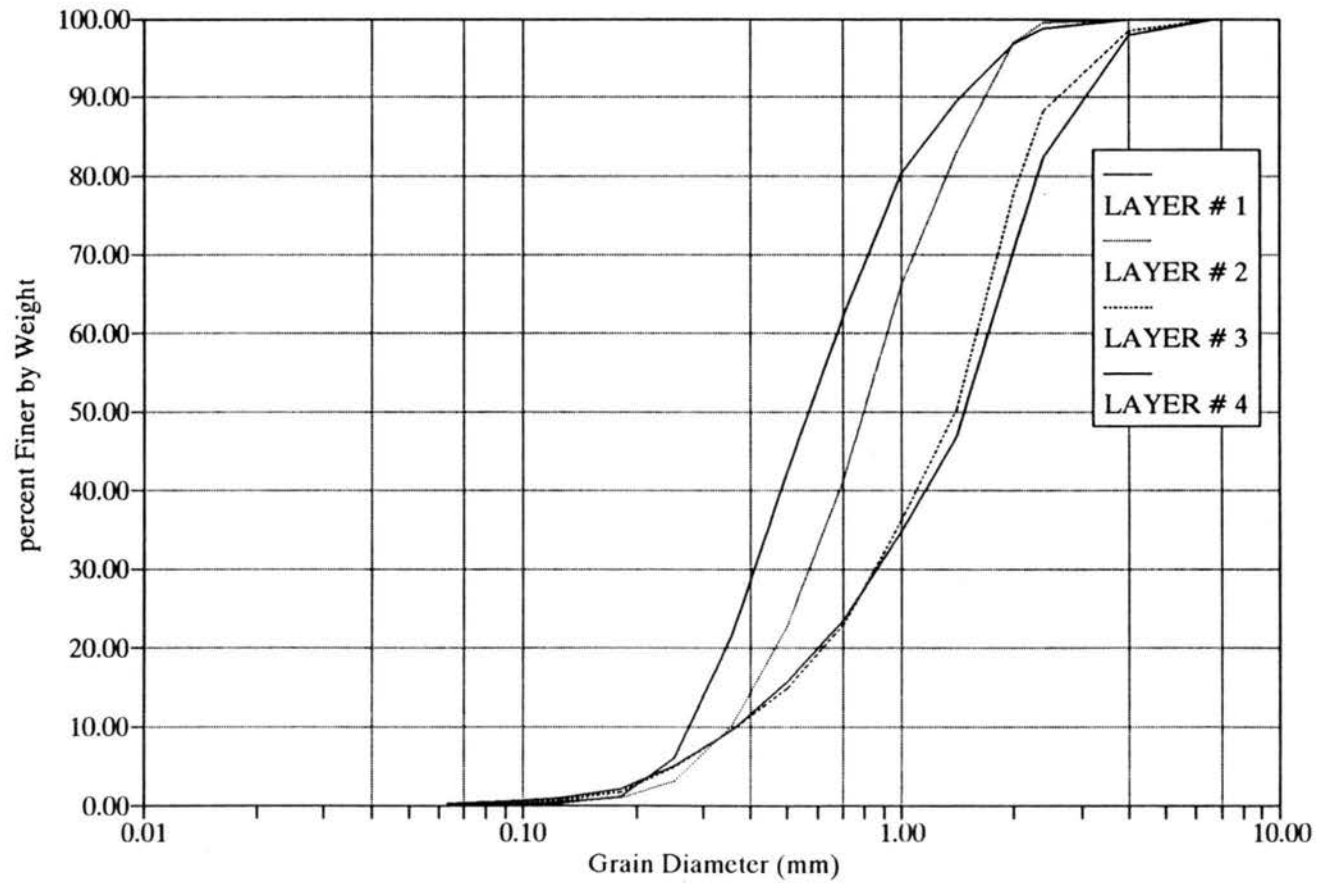


Figure 5.21. Size distribution curves for dune layers (Dune #2, 8 ft. flume).

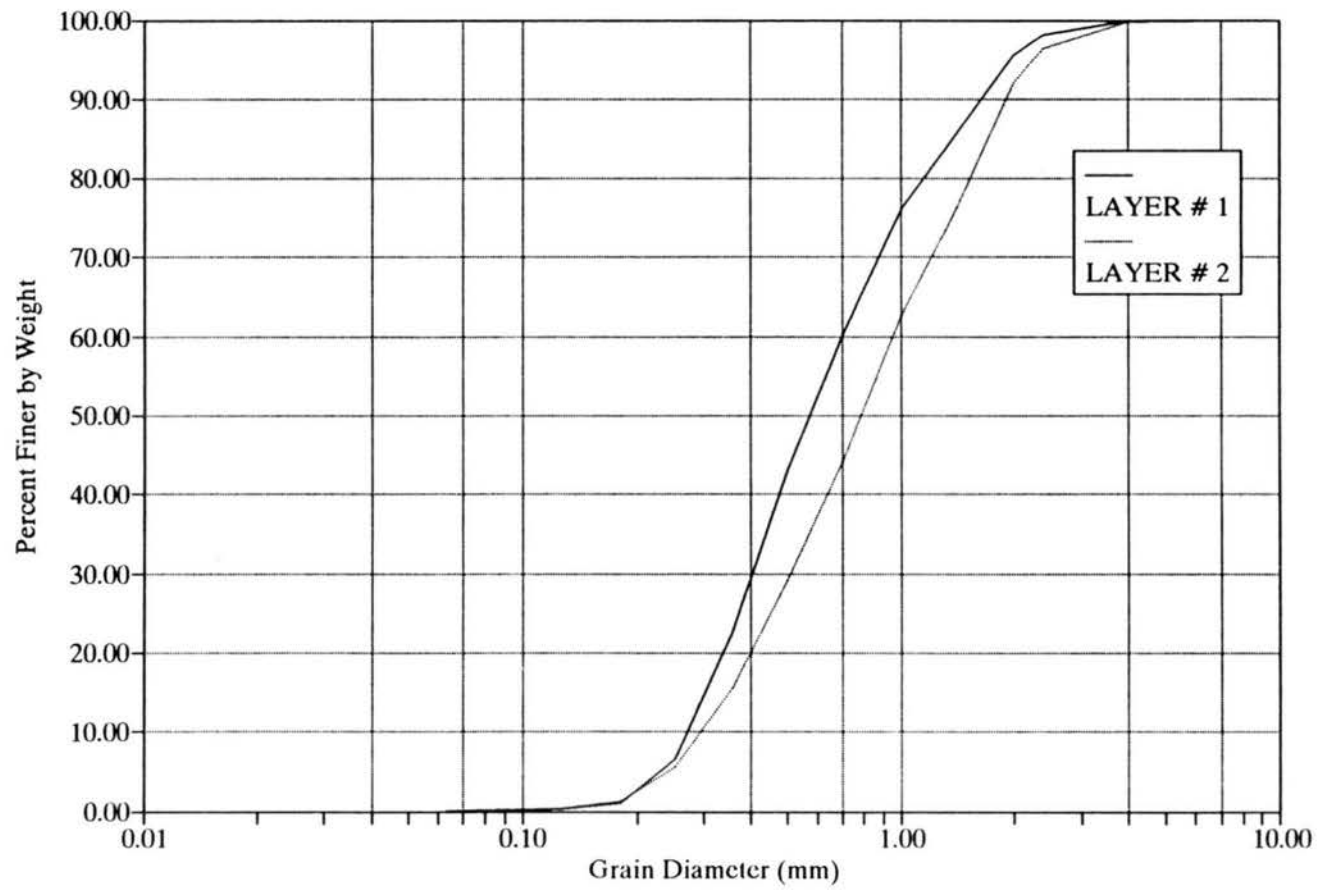


Figure 5.22. Size distribution curves for dune layers (Dune #3, 8 ft. flume).

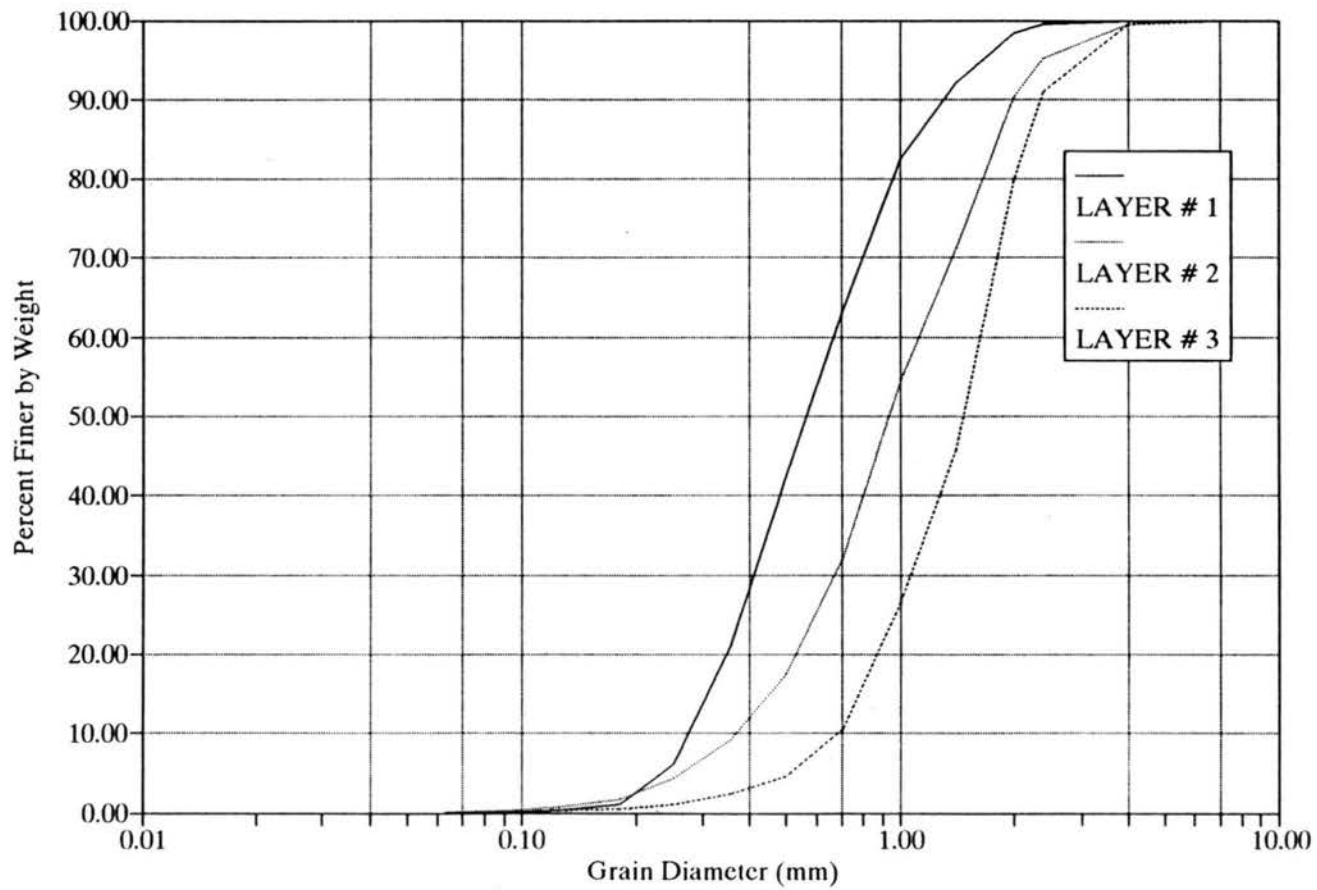


Figure 5.23. Size distribution curves for dune layers (Dune #4, 8 ft. flume).

$$F_{dj} = c_d \rho u^2 d_{si}^2 \quad (5.1)$$

$$F_{Li} = c_L \rho u^2 d_{si}^2 \quad (5.2)$$

$$F_{gj} = c_g (\gamma_s - \gamma) d_{si}^3 \quad (5.3)$$

$$F_{ff} = c_f F_{gi} \quad (5.4)$$

Usually the lift force does not appear explicitly in the theoretical analysis because the lift depends on the same variables as drag, and the constants in the resulting equations are determined empirically. This procedure automatically considers the effect of lift.

The sum of the forces in the direction parallel to the lee side slope of the dune by considering the particles on the dune lee slope (Figure 5.24) can be written as:

$$\sum F_j = m a_j \quad (5.5)$$

so substitute Equations 5.1 - 5.4 into Equation 5.5, the following equation can be obtained:

$$F_{ff} + F_{dj} - F_{gj} = m a_j \quad (5.6)$$

Assume that the right hand side of the Equation 5.6 is small, almost zero, and that the acceleration of the particle is also small because of the effect of the back flow on the particle, which is in the up-slope direction. Also assume that the particle moving down slope almost does not contact the lee slope, so the friction force can be dropped. The final equation can be as follows:

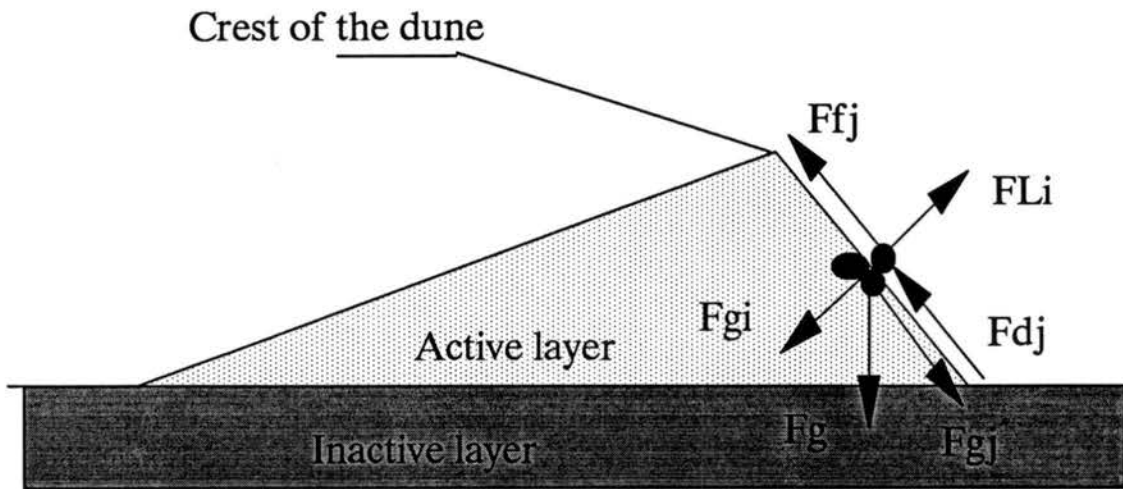


Figure 5.24. Dune definition sketch.

$$c_g (\gamma_s - \gamma) d_{si}^3 = c_d \rho u^2 d_{si}^2 \quad (5.7)$$

or

$$u^2 = c \frac{(\gamma_s - \gamma)}{\rho} d_{si} \quad (5.8)$$

or

$$u^2 = c g \left(\frac{\rho_s}{\rho} - 1 \right) d_{si} \quad (5.9)$$

This constant c which will be determined experimentally includes the constants c_d and c_g . To get this constant, the velocity of the back flow at the lowest point of the lee side of the dune should be known. Jopling (1965) reported that this velocity varied between 20 and 33 percent of the mean flow velocity. Also Nelson and Smith (1989) reported this velocity to be 20 percent of the mean flow velocity. So due to the uncertainty in measuring this value due to the flow conditions in the lee side of the dune, an assumption was made. This assumption was that the mean velocity above the crest of each dune controls the velocity of the back flow at the lowest point of the lee side of the dune. The ratio between the velocity at the crest and the mean flow velocity for the 22 dunes was about 1.1. So this assumption is over estimating the back flow velocity at the lowest point of the lee side by about 3.33 times the actual back flow velocity, assuming that the difference between the back flow velocity at the lowest point of the dune and at the crest is equal 0.33. But that assumption will be good because the constant in Equation 38 will be found empirically during the calibration. Also, the d_{50} of the same layer was also known from the size distribution curve for each dune. Thus,

the constant c could be determined. This procedure was done for each dune in each experiment. An assumed normalized vertical velocity distribution could be drawn based on the above assumption. A standardized normalized vertical velocity diagram (Figure 5.25) was obtained so it could be used in the prediction process.

The flow velocity for the experiments varied between $0.55 \text{ m}^3/\text{s}$ and $0.64 \text{ m}^3/\text{s}$, which is a good range to form dunes as was shown by H.P. Guy et al. (1965). They used velocities between $0.52 \text{ m}^3/\text{s}$ and $0.67 \text{ m}^3/\text{s}$, almost in the same range. The standardized vertical velocity distribution for the back flow at the lee side of the dune was calculated. Also, the average value for the 22 constants was used as a fixed constant for the final equation. Finally, to predict the size distribution of a dune structure, the following equation was used:

$$d_{si} = \frac{u_i^2}{22.53 g \left(\frac{\rho_s}{\rho} - 1 \right)} \quad (5.10)$$

where d_{si} is the median diameter of the i th layer and u_i is the velocity at that layer.

The above equation (5.10) and the standardized vertical velocity diagram were used to predict the size distribution for the five mixtures. After that the vertical size distribution were calculated for the five mixture. The predicted values are compared with the actual vertical size distribution as shown in the Figures 5.26, 5.27, 5.28, 5.29 and 5.30. The mixtures which had d_{50} of less than 0.6 mm had predicted values higher

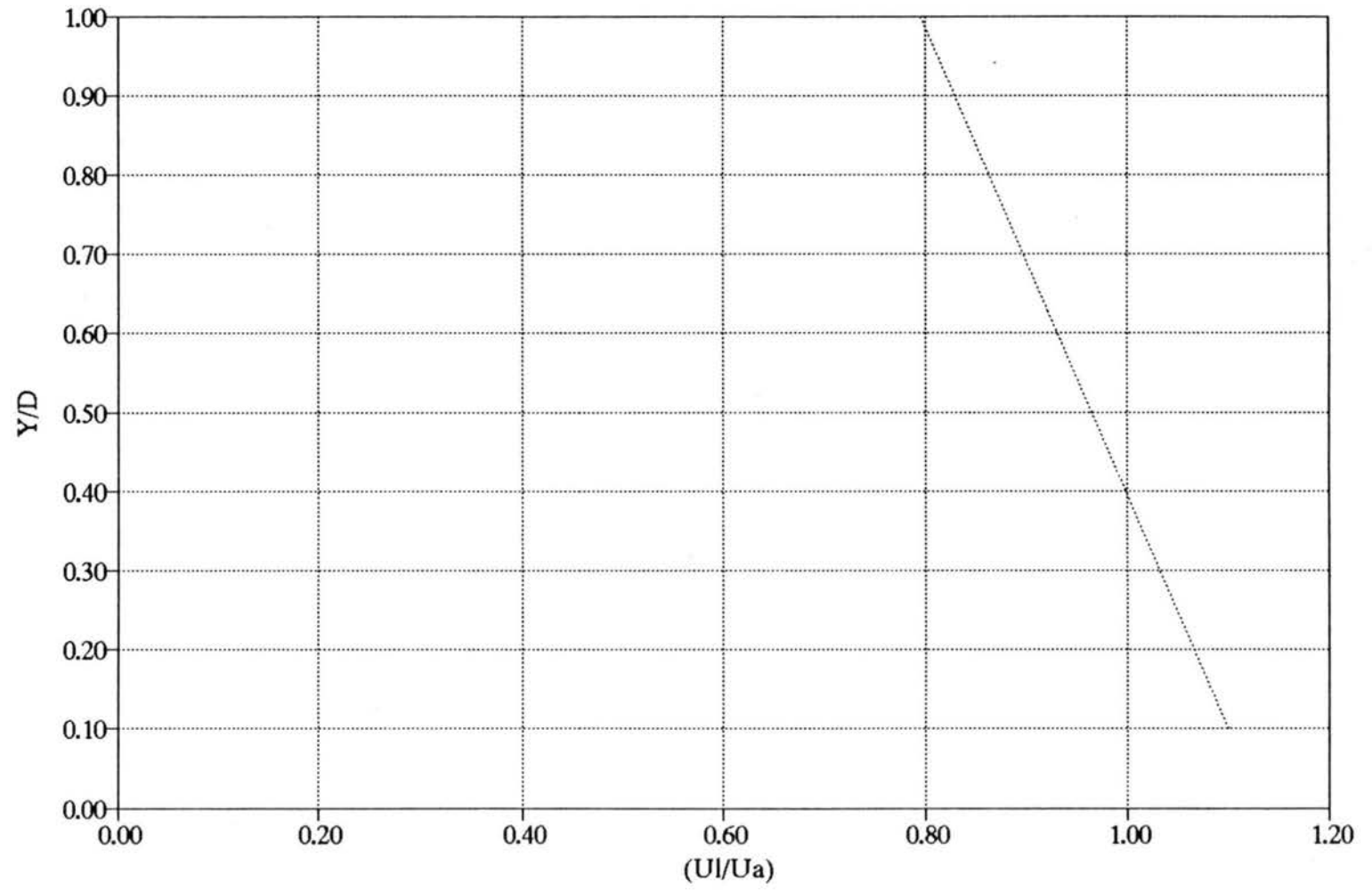


Figure 5.25. Standardized dimensionless velocity diagram.

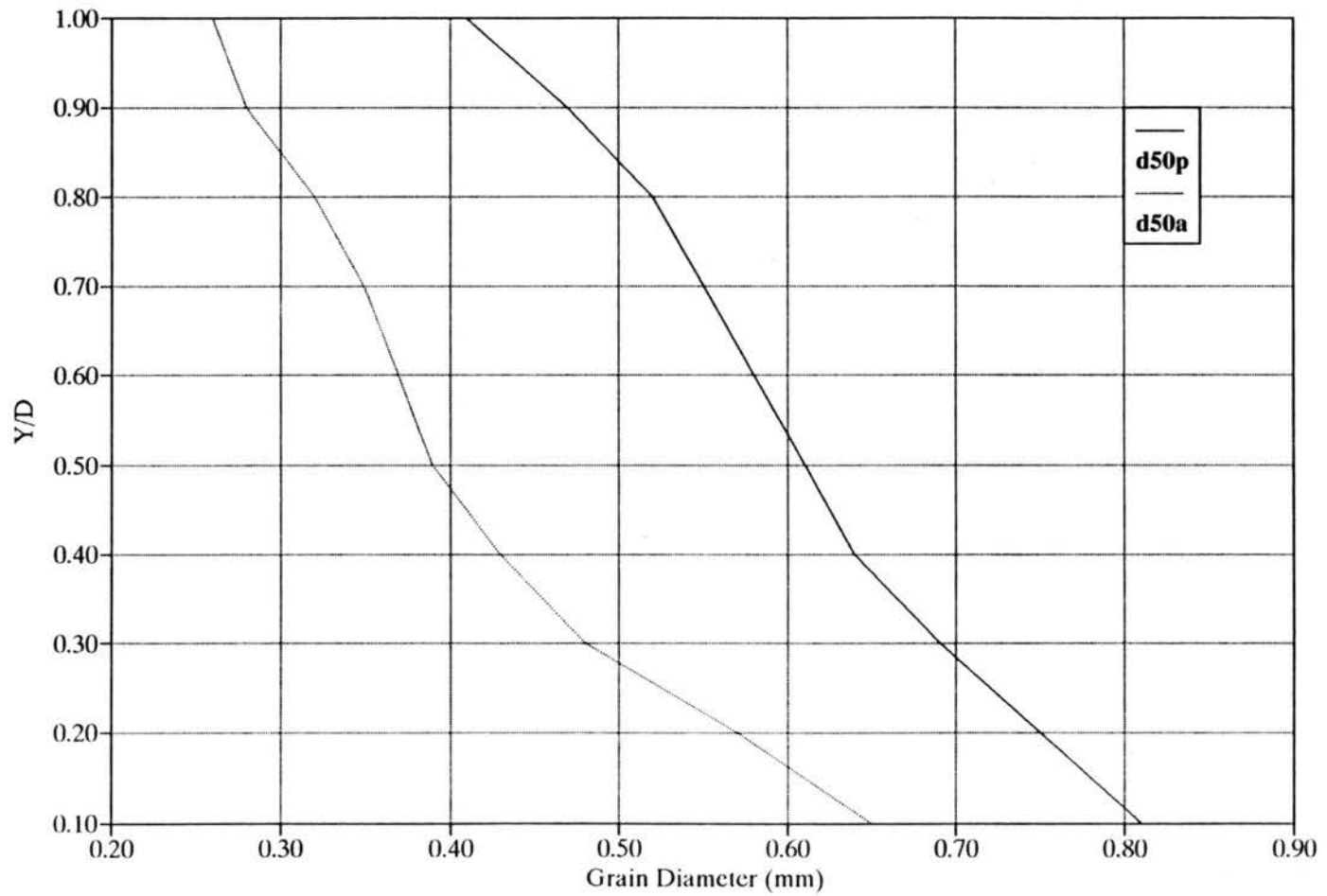


Figure 5.26. Predicted and actual median grain diameter for a dune layer (Mixture #1).

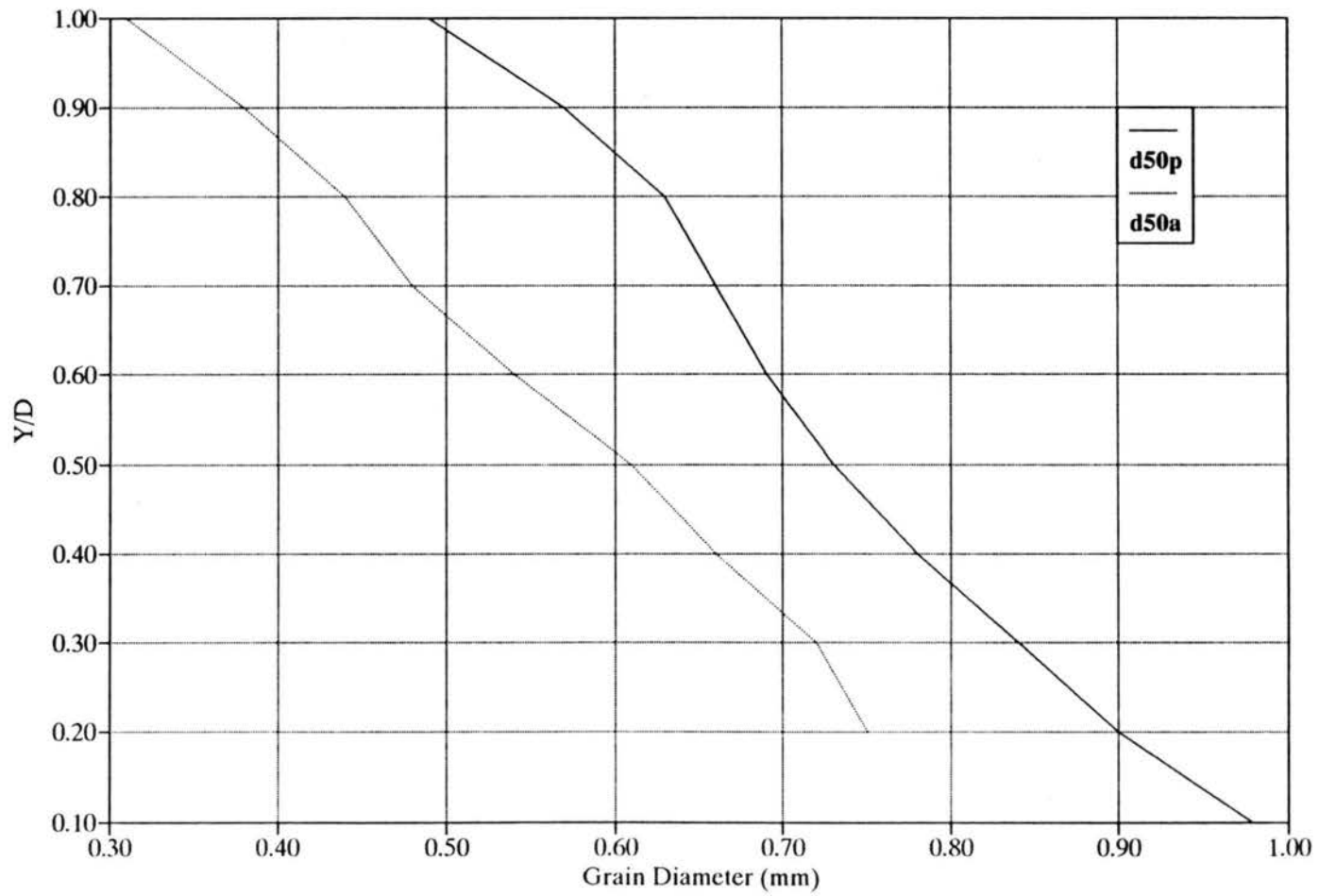


Figure 5.27. Predicted and actual median grain diameter for a dune layer (Mixture #2).

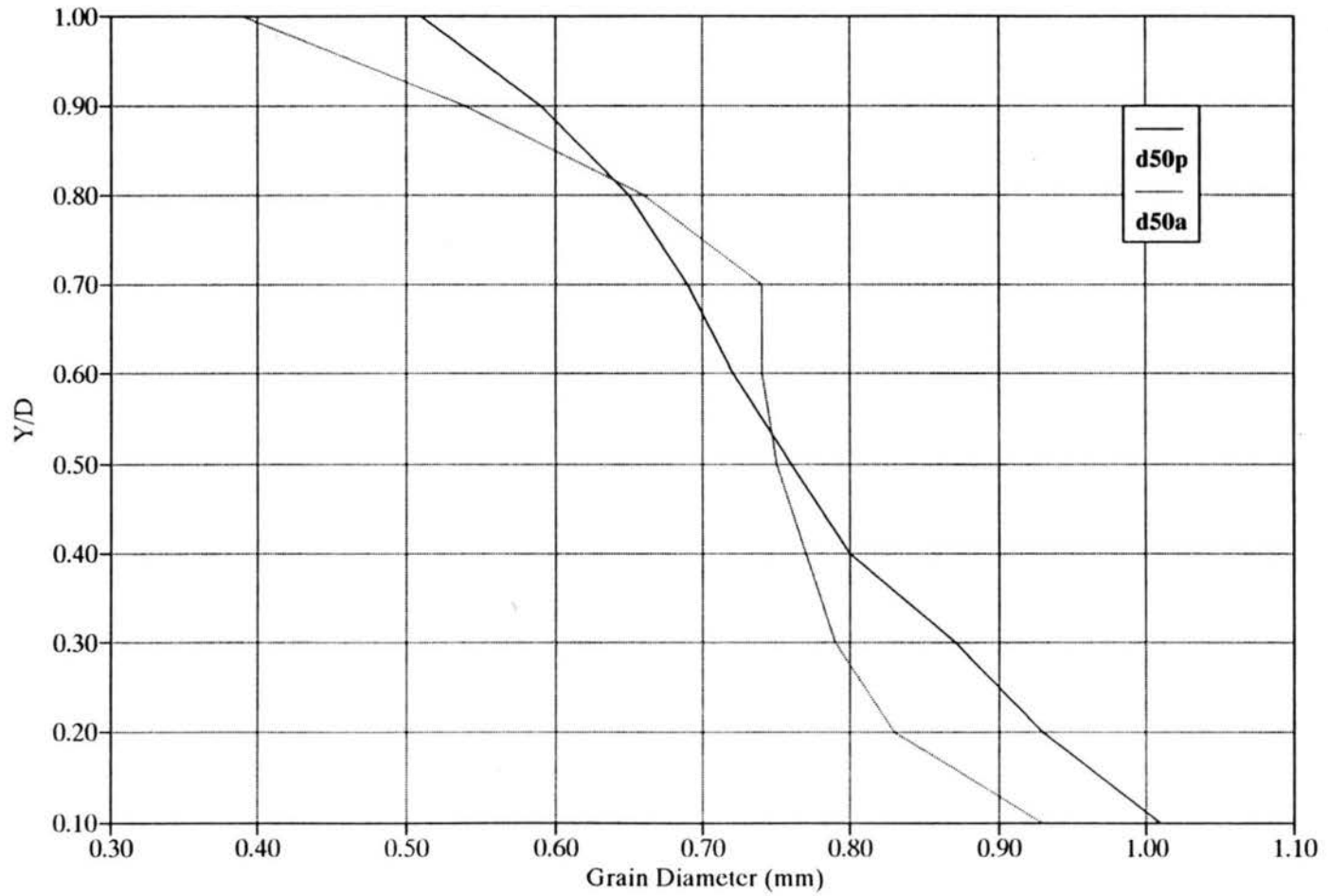


Figure 5.28. Predicted and actual median grain diameter for a dune layer (Mixture #3).

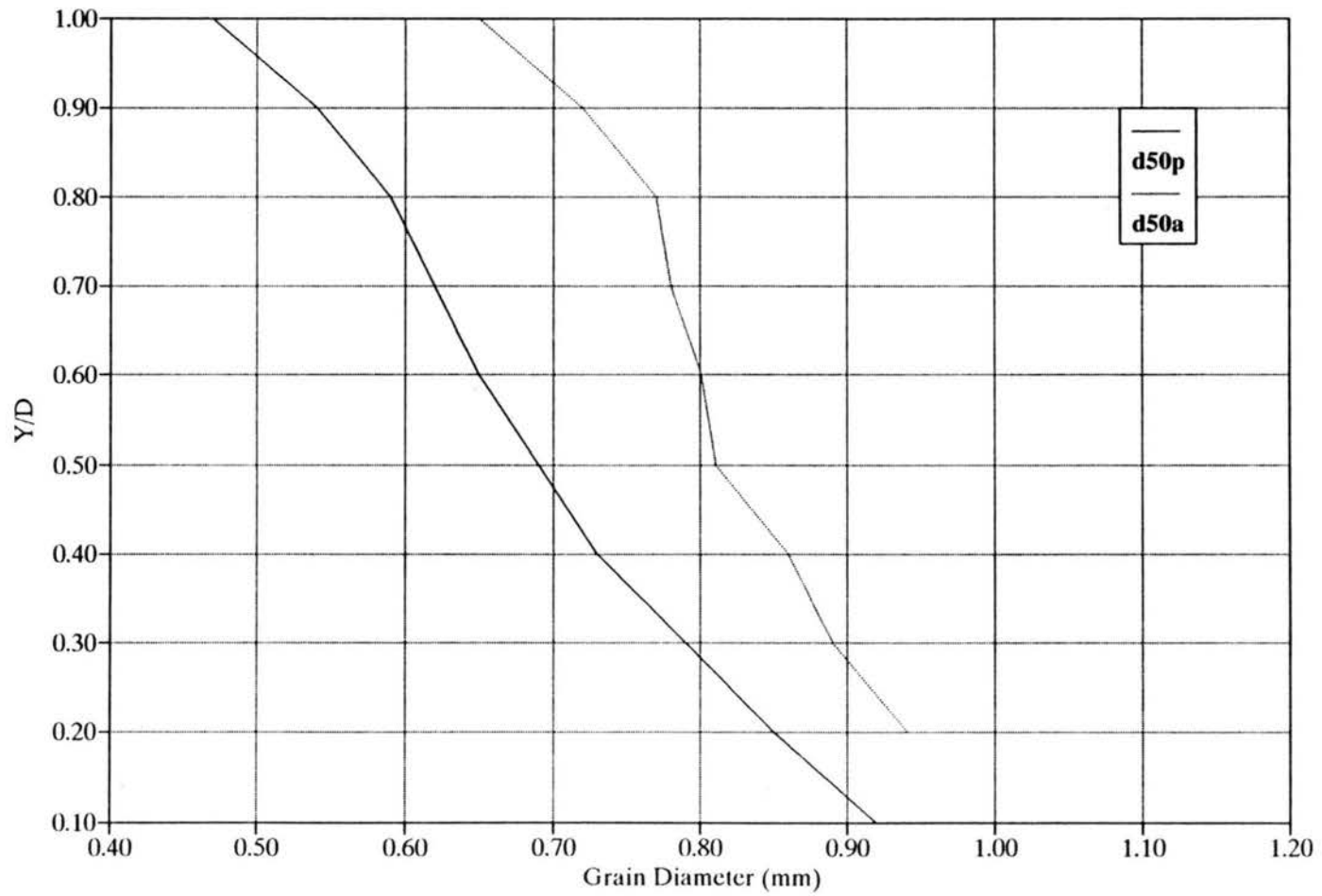


Figure 5.29. Predicted and actual median grain diameter for a dune layer (Mixture #4).

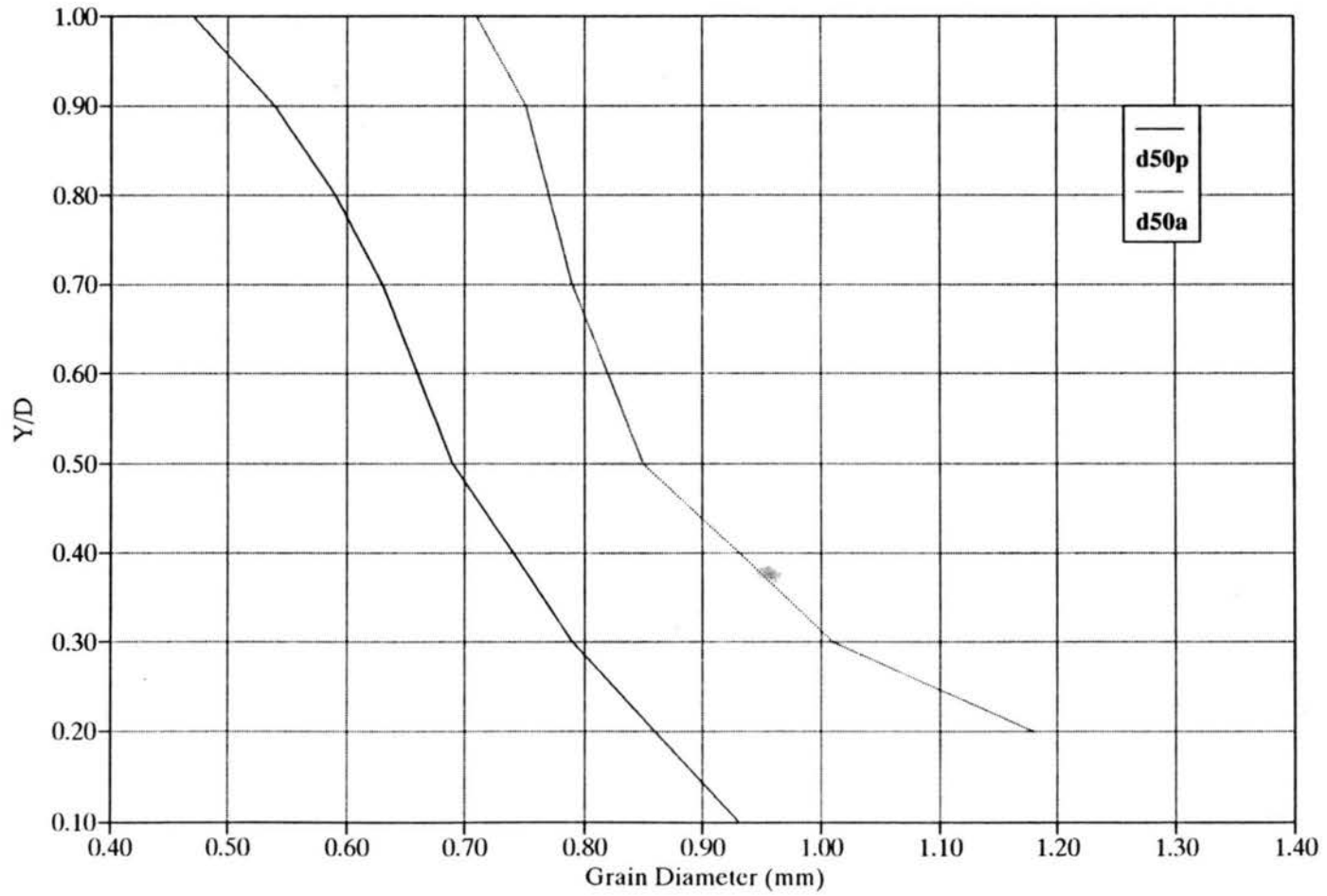


Figure 5.30. Predicted and actual median grain diameter for a dune layer (Mixture #5).

than the actual data, at d_{50} equal 0.6 mm, both the predicted and the actual values were almost the same.

For the mixtures which had a d_{50} of more than 0.6 mm, the predicted values were lower than the actual values. For example, the two mixtures which had the same standard deviation, (σ_g) equal to 2.3 but the d_{50} was different, 0.47 mm and 0.72 mm. The first one was over-predicted and the second one was under-predicted regardless of the standard deviation. In addition there were two mixtures that had a small difference in the d_{50} , 0.72 mm and 0.87 mm, but had a standard deviation of 2.8 and 2.3. These two were over-predicted; in fact the difference was almost 20% in the standard deviation and in the d_{50} but the mixtures behaved according to the d_{50} , not to the standard deviation. From the above results, there is an indication that the σ_{gm} is not as important as the d_{50} for the prediction of the vertical sorting.

The following step was taken to correct this error in the prediction values, that is, to consider the effect of the d_{50} of each mixture.

5.3.2 Effect of the Median Diameter on the Formula

The previous analysis in this chapter shows that the geometric standard deviation (σ_g) of the mixture did not affect the vertical size distribution of the dune layers. But on the other hand, the median diameter (d_{50}) for each sand mixture was found to be the controlling parameter for the vertical size distribution within the dune structure. In other words, the error in the predicted value of the median diameter (d_{50p}) is a function in the d_{50} of the sand mixture as in the following equation:

$$\frac{d_{50p}}{d_{50a}} = f(d_{50m}) \quad (5.11)$$

where d_{50a} is the actual median diameter of each dune layer, and d_{50m} is the median diameter of each mixture. A graph between a d_{50m} for each mixture and the ratio d_{50p}/d_{50a} is drawn in Figure 5.31. The graph shows a smooth pattern moving from the first mixture at the far left of the graph to the next one according to the increase in median diameter of each mixture. Also, as the d_{50m} increased, the ratio d_{50p}/d_{50a} decreased. Therefore, this graph which showed the relationship between these two parameters, could be developed by means of a regression analysis. The only problem was that the relationship is not dimensionless.

So the next step was to find a dimensionless parameter representing the median diameter of each mixture to correct the error in the ratio d_{50p}/d_{50a} for each layer, which should be almost one. Five dimensionless parameters were tested. The following five equations define these parameters:

$$\tau_* = \frac{\tau_b}{(\gamma_s - \gamma) d_s} \quad (5.12)$$

$$\tau_{*g} = \frac{\tau_{bg}}{(\gamma_s - \gamma) d_s} \quad (5.13)$$

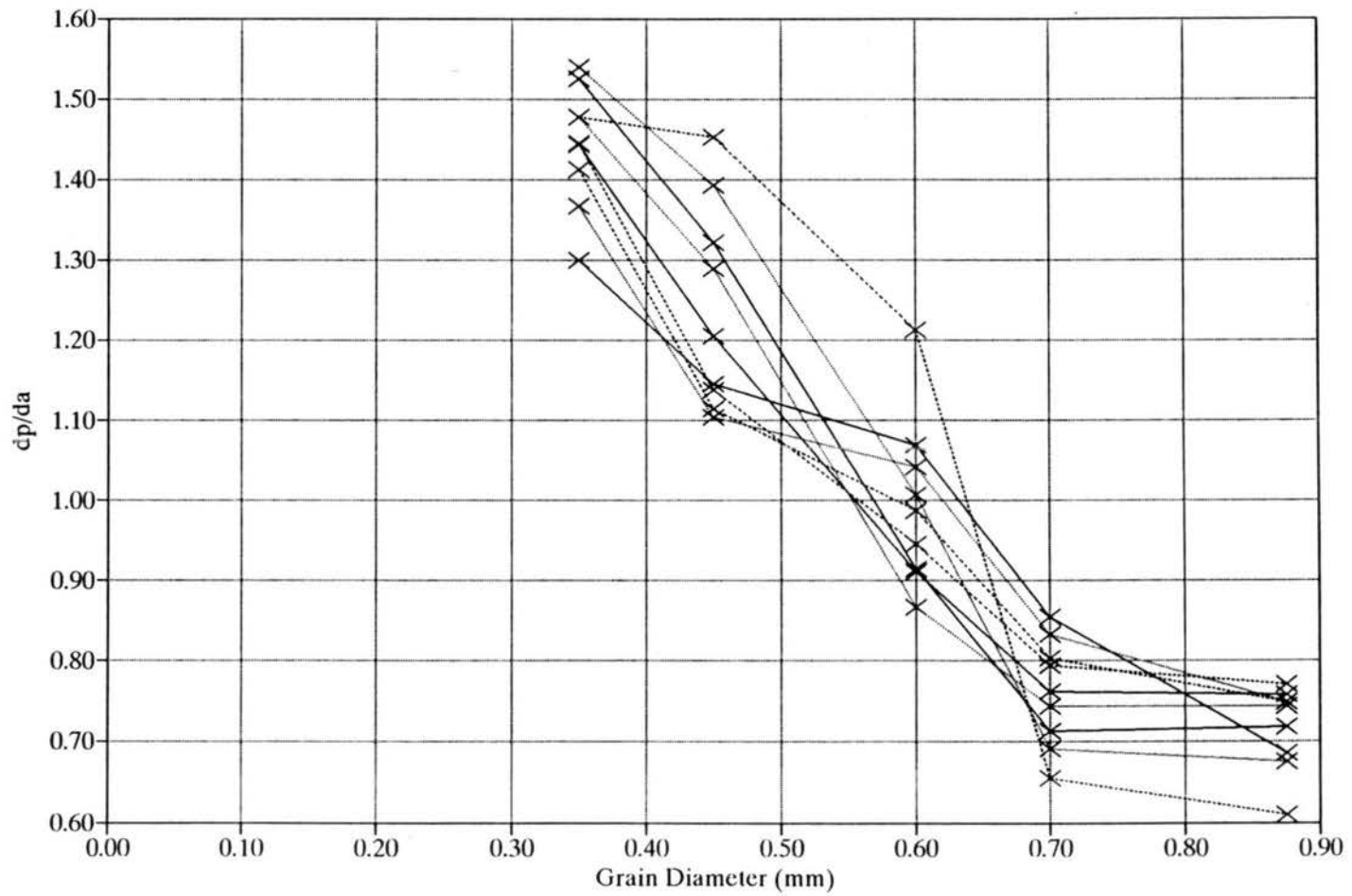


Figure 5.31. Relation between the error in the predicted median grain diameter for each dune layer and the grain diameter.

$$\tau_{*d} = \frac{\tau_{bd}}{(\gamma_s - \gamma) d_s} \quad (5.14)$$

$$R_* = \frac{u_* d_s}{\nu} \quad (5.15)$$

$$D_* = d_{50m} \left[\frac{g \left(\frac{\rho_s}{\rho} - 1 \right)}{\nu^2} \right]^{1/3} \quad (5.16)$$

where:

τ_* = dimensionless shear stress,

τ_b = bed shear stress,

γ_s = specific weight of the bed material,

γ = specific weight of water,

τ_{*g} = dimensionless shear stress due to the grain resistance,

τ_{*d} = dimensionless shear stress due to the form drag,

R_* = boundary Reynolds number,

ν = kinematic viscosity of water,

u_* = shear velocity which equal to $\sqrt{\tau_o/\rho}$,

D_* = dimensionless particle diameter, and

g = acceleration of gravity.

The first four parameters were used by Shields (1936) in his diagram but in different format. The fifth parameter was used by many researchers, such as Gessler (1967), van Rijn (1984), and others. Table 5.4 shows the values of the ratio d_{50p}/d_{50m} for each mixture and Table 5.5 contains the values of the five parameters, τ_* , τ_{*g} , τ_{*d} , R_* and D_* . Figure 5.32 shows the relationship between d_{50p}/d_{50a} and τ_* for all the data; each mixture has one value of τ_* , so all the points for each layer are lined above each other. The finest mixture, $d_{50m}=0.35$ mm, is at the right end of the graph, and, according to decreasing τ_* values, the second mixture, $d_{50m}=0.42$ mm, is next. That is true for the third mixture too, but for the last two mixtures that is not the case : as the ratio of d_{50p}/d_{50a} decreases the τ_* value increases.

The second parameter, which is the dimensionless shear stress due to grain resistance, is related to the d_{50p}/d_{50a} ratio, as shown in Figure 5.33. It shows a reasonable relationship between the τ_{*g} and the error ratio better than that between τ_* and the same ratio. But the problem is the calculation of the values of τ_{*g} which takes a long time. Also, many parameters should be known before starting the calculations of τ_{*g} . The third relationship between τ_{*d} and the error of the prediction of the median diameter (Figure 5.34) looks like the first relationship between the τ_* and the same ratio. That gives an idea about how the shear stress due to the form drag is affecting the bed shear stress, therefore, when that part of the shear stress is removed the remaining part gives a better correlation for the relation between it and the d_{50p}/d_{50a} ratio.

Table 5.4. The ratio between the predicted median grain diameter and actual median grain diameter value.

Run No.	dp/da at 0.2 Y/D	dp/da at 0.3 Y/D	dp/da at 0.4 Y/D	dp/da at 0.5 Y/D	dp/da at 0.6 Y/D	dp/da at 0.7 Y/D	dp/da at 0.8 Y/D	dp/da at 0.9 Y/D	dp/da at 1 Y/D
RW-1	1.3	1.367	1.412	1.444	1.443	1.477	1.524	1.54	1.477
RW-2	1.154	1.104	1.115	1.138	1.205	1.288	1.322	1.393	1.452
RW-3	1.069	1.042	0.987	0.946	0.912	0.868	0.915	1.007	1.212
RW-4	0.903	0.881	0.849	0.843	0.812	0.796	0.765	0.747	0.713
RW-4.1	0.855	0.834	0.804	0.795	0.763	0.745	0.713	0.691	0.656
RW-5	0.686	0.75	0.75	0.772	0.759	0.744	0.719	0.676	0.61

Table 5.5. The values of dimensionless shear stress, dimensionless shear stress due to grain resistance, dimensionless shear stress due to form drag, boundary Reynolds number, and dimensionless grain diameter.

Run No.	τ_*	τ_{*g}	τ_{*d}	R_*	D_*
RW-1	0.442	0.175	0.279	19.742	4.442
RW-2	0.3	0.169	0.094	23.338	5.711
RW-3	0.128	0.14	0.01	23.836	7.615
RW-4	0.209	0.115	0.09	38.461	8.884
RW-4.1	0.209	0.115	0.09	38.461	8.884
RW-5	0.2	0.107	0.098	50.595	11.105

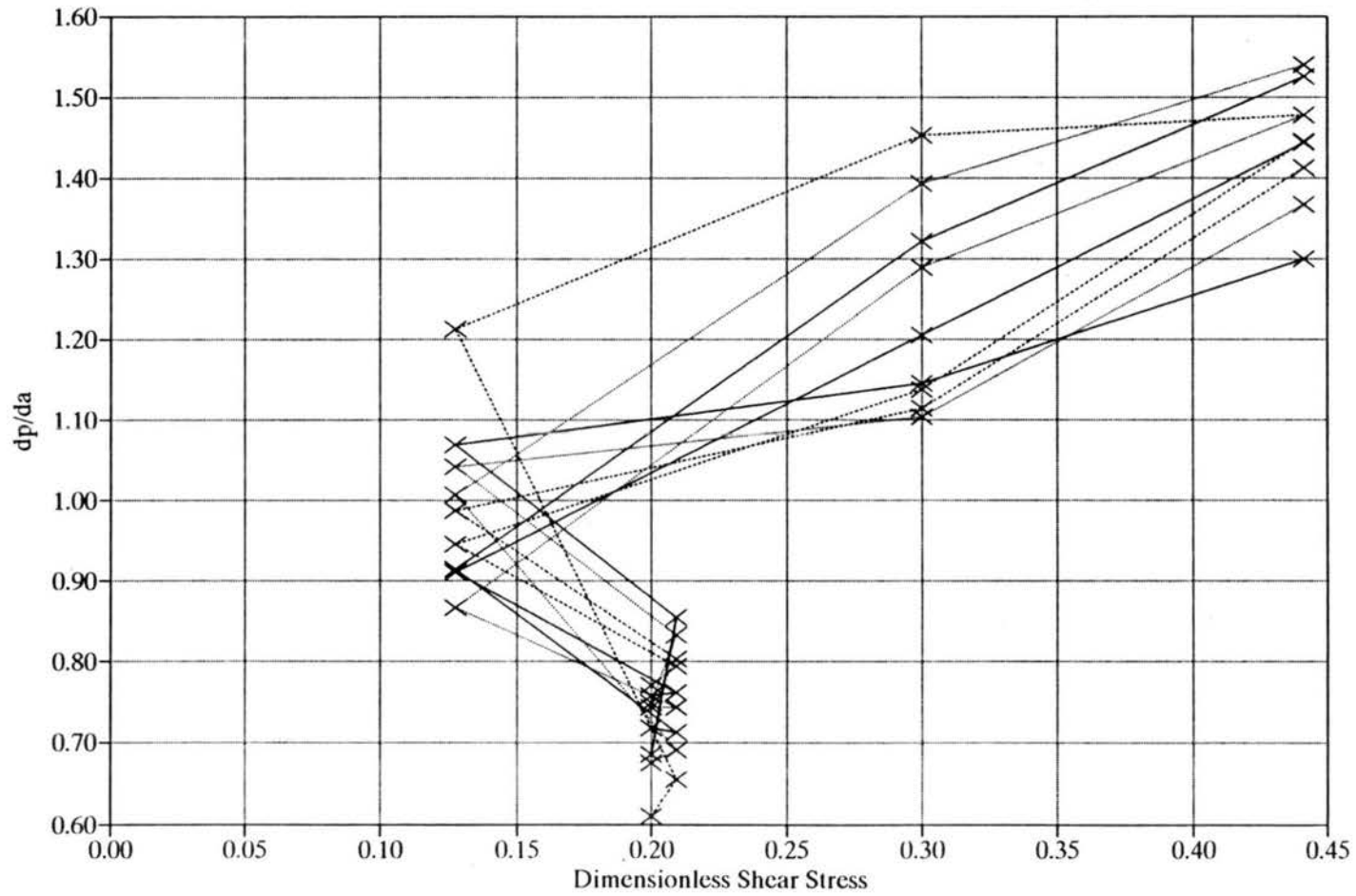


Figure 5.32. Relation between the error in the predicted median grain diameter for each dune layer and the dimensionless shear stress.

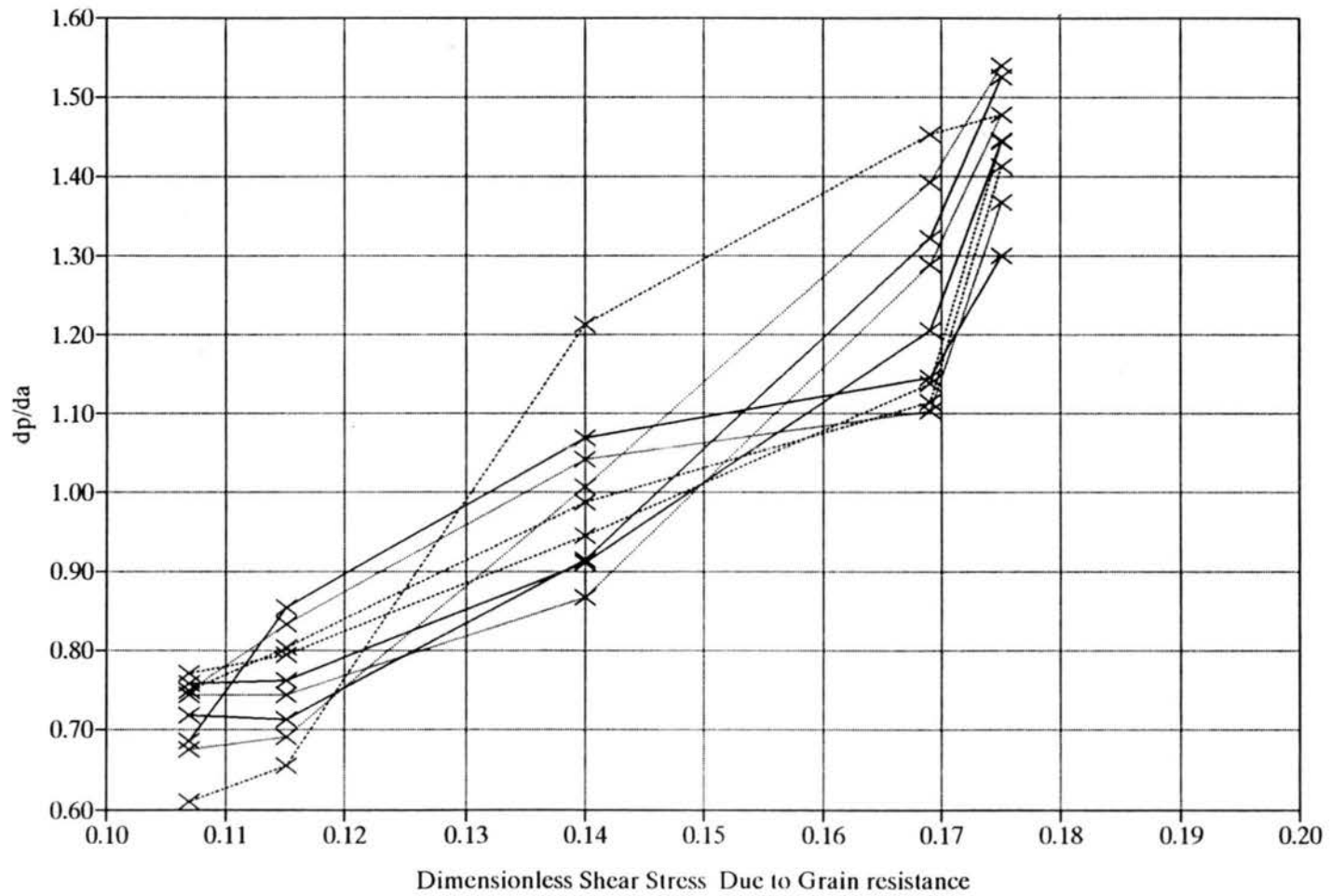


Figure 5.33. Relation between the error in the predicted median grain diameter for each dune layer and the dimensionless shear stress due to grain resistance.

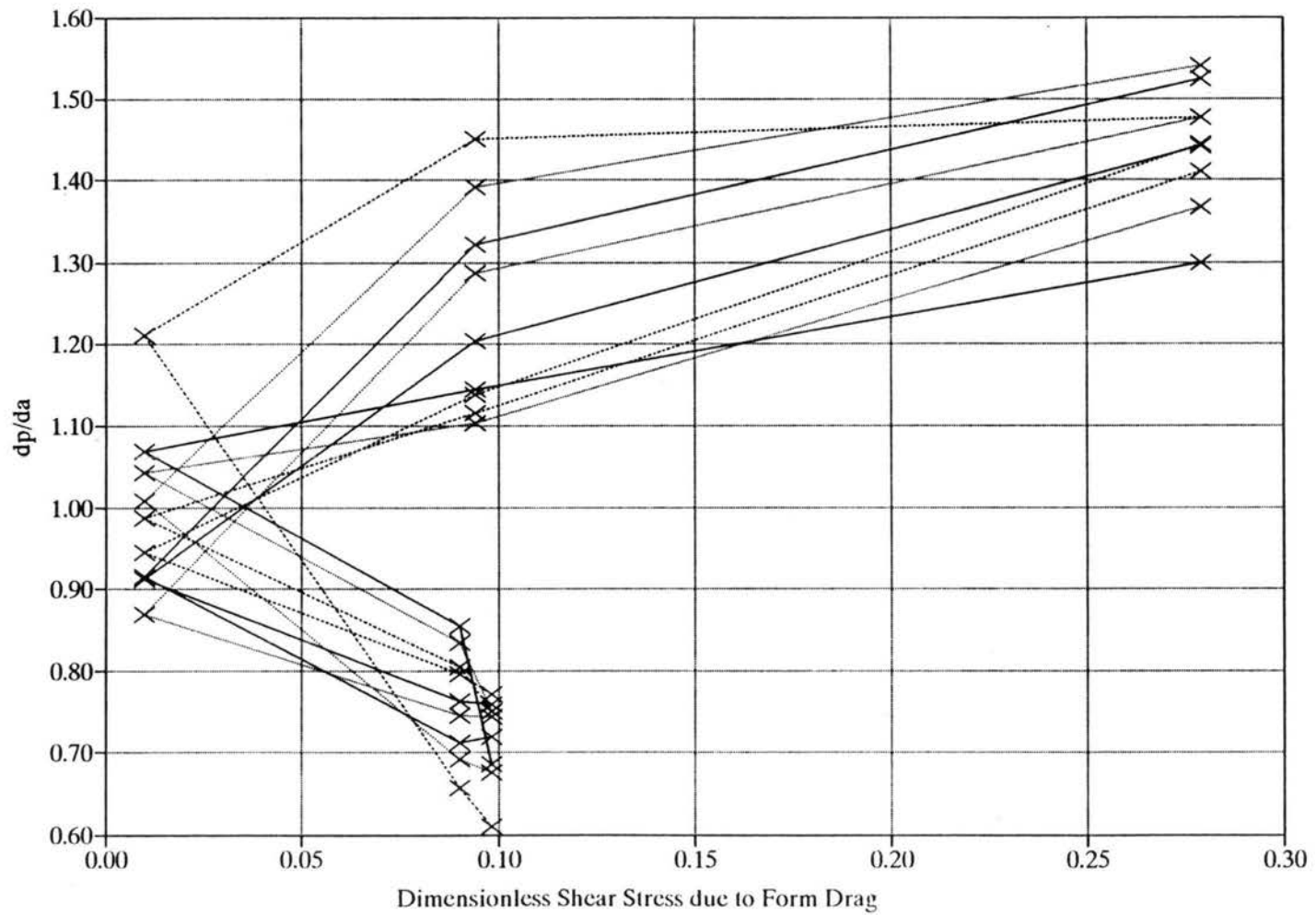


Figure 5.34. Relation between the error in the predicted median grain diameter of each dune layer and the dimensionless shear stress due to form drag.

The fourth graphic relationship (Figure 5.35) which is between d_{50p}/d_{50a} and R_* behaves in a logical pattern; that is, as the d_{50m} and R_* increase, the ratio of d_{50p}/d_{50a} decreases. The only problem is that there is a jump in the graph between the second mixture and the third mixture. Although the second graph gives a better relation than the first one, it still is not good enough to be used. The last dimensionless parameter, D_* , is plotted versus d_{50p}/d_{50a} in Figure 5.36. In this figure the first mixture, $d_{50}=0.35$ mm, is at the far left of the graph. As the D_* and d_{50m} increase, the d_{50p}/d_{50a} decreases, and the transition from one mixture to another one is smoother than before, and match the graph between d_{50m} and d_{50p}/d_{50a} .

A regression analysis was then used to get a curves which fit within the range of all the data were presented in the Figures 5.33 and 5.36. Figures 5.37 and 5.38 show the curves which were developed. The equations which represents these curves are:

$$\frac{d_{50p}}{d_{50a}} = (21.83 - 667.75\tau_{*g} + 7808.60\tau_{*g}^2 - 39834.42\tau_{*g}^3 + 75248.92\tau_{*g}^4)^2 \quad (5.17)$$

$$\frac{d_{50p}}{d_{50a}} = 3.477 - 0.970 \sqrt{D_*} + 0.00033 D_*^3 \quad (5.32)$$

Figures 5.35 and 5.36 give an acceptable pattern between the d_{50p}/d_{50a} values and the values of τ_{*g} and D_* , but Figure 5.38 matches the graph between the d_{50p}/d_{50a} and the median diameter d_{50mi} for each mixture, also Figure 5.34 needs less calculation than

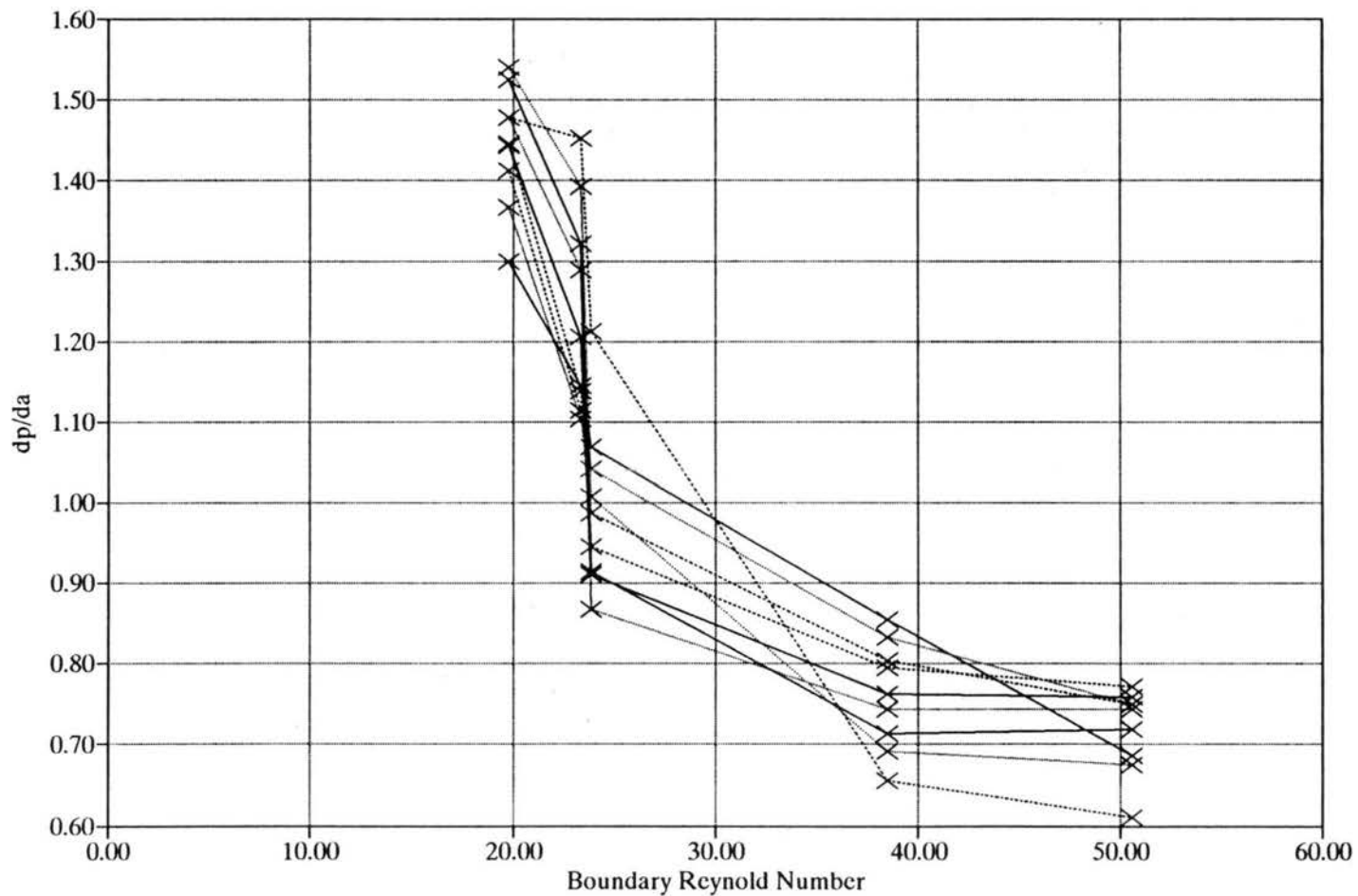


Figure 5.35. Relation between the error in the predicted median grain diameter for each dune layer and the boundary Reynolds number.

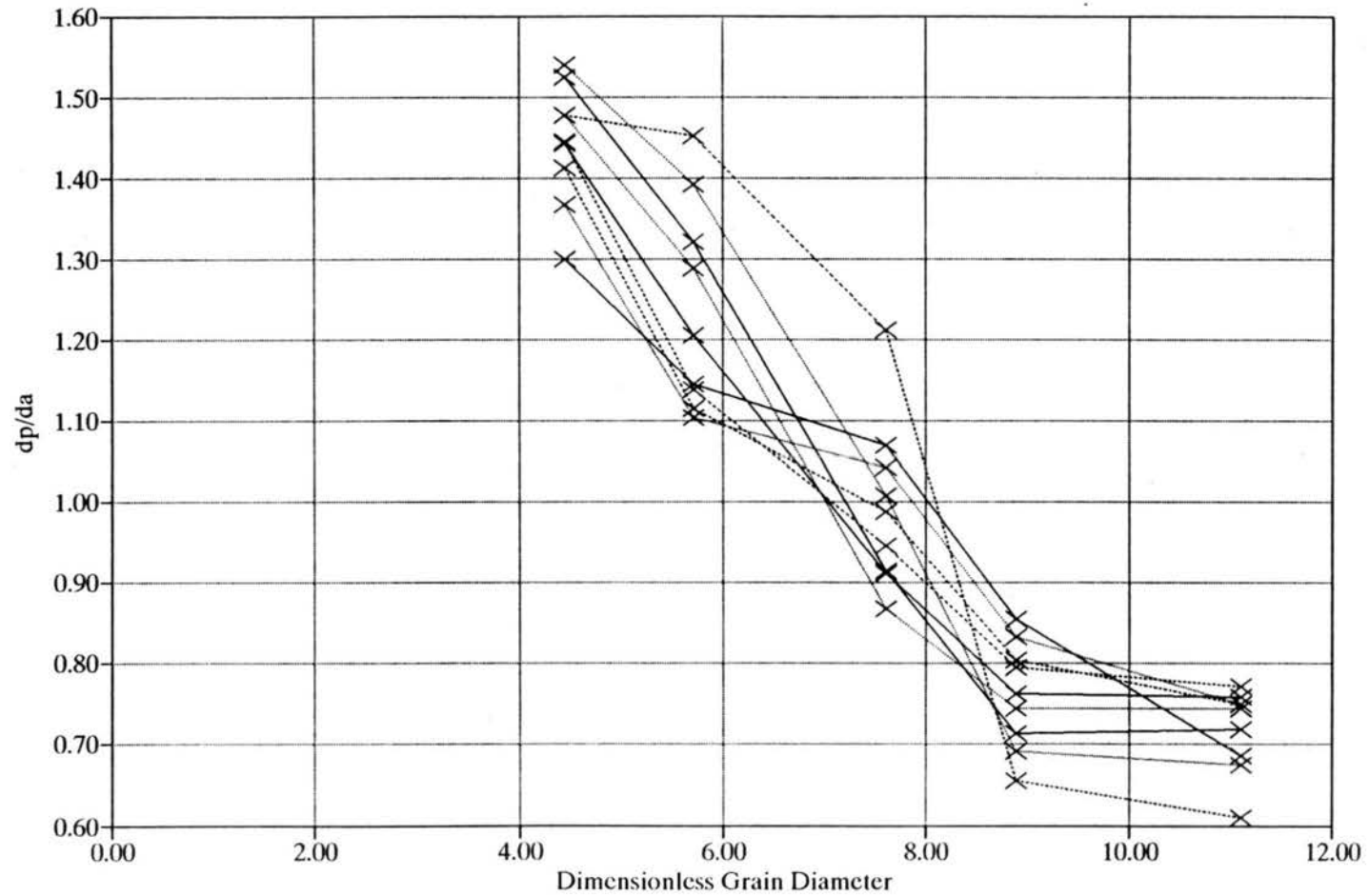


Figure 5.36. Relation between the error in the predicted median grain diameter for each dune layer and the dimensionless grain diameter.

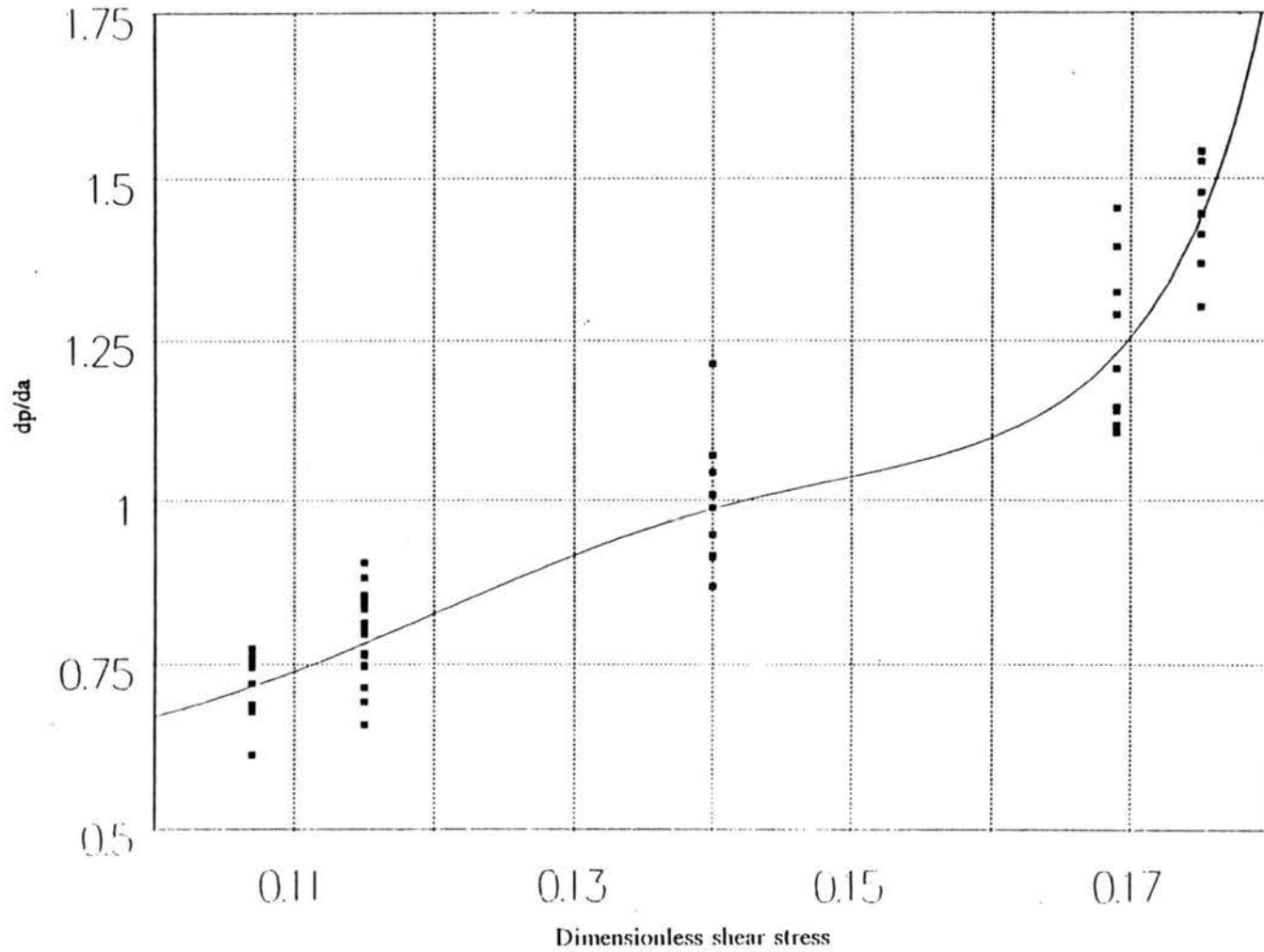


Figure 5.37. Relation between the error in predicting the median diameter for each dune layer and the dimensionless shear stress (due to grain resistance).

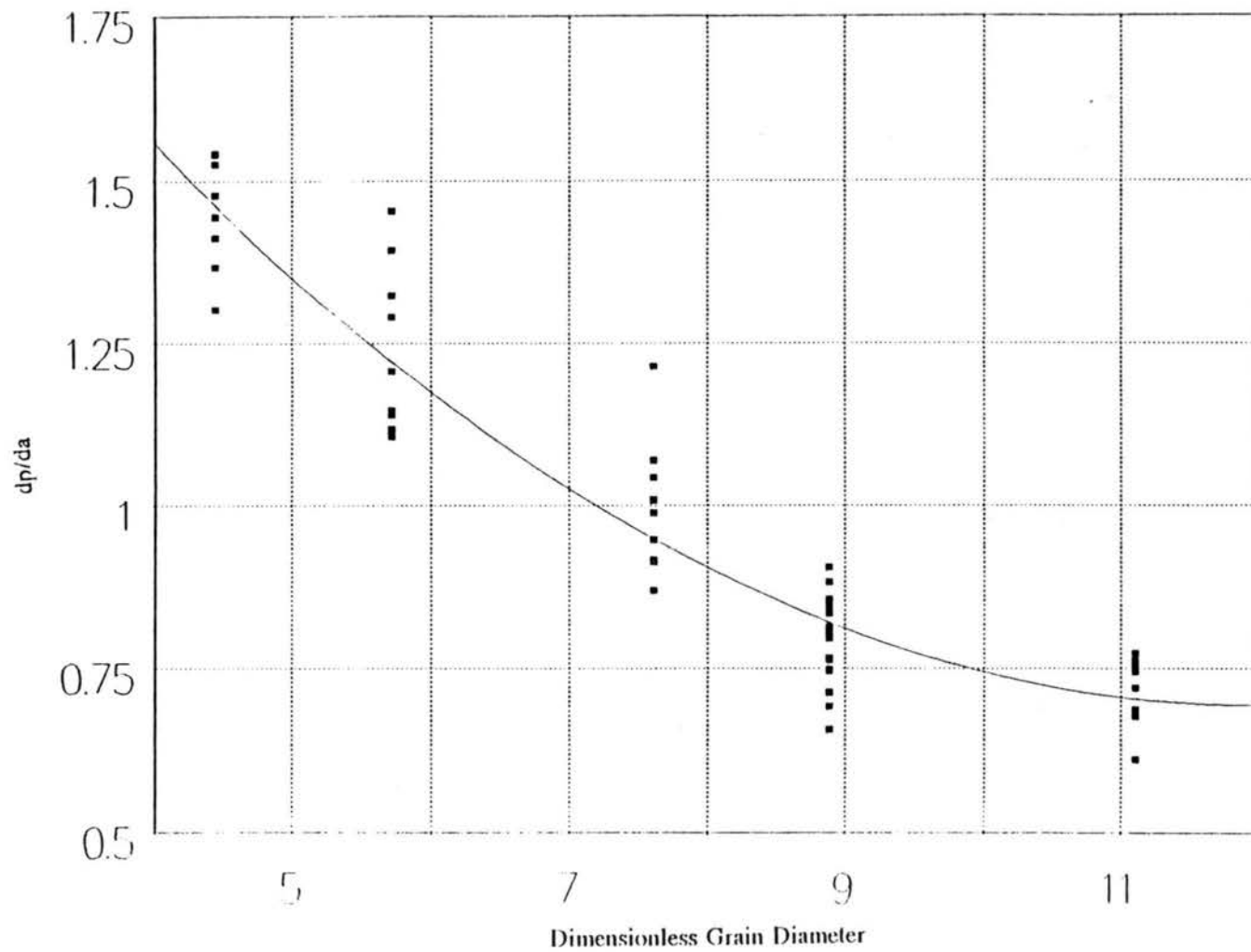


Figure 5.38. Relation between the error in predicting the median diameter for each dune layer and the dimensionless grain diameter.

that for Figure 5.31, using Figures 5.35 and 5.36 as a correction to the values obtained from the prediction. This correction to the predicted values better represents the actual values, as shown in the figures in Appendix A. From these figures it is clear that there is not much difference between the correction values using τ_{*g} and D_* . So, based on the easier calculation, D_* was chosen in the correction factor, see Figures 5.39 through 5.43.

The fall velocities for the median diameters of the mixtures also could be used as a correction factor for the predicted values. Figures A.29 through A.33 in Appendix A show predicted values from Equation 5.10 corrected by the ratio W_m/W_3 , where W_m is the fall velocity for m , the median diameter of mixture m , and W_3 is the fall velocity for median diameter for mixture #3. Note that this correction factor would be similar to Equation 5.18 which involves the dimensionless grain diameter.

5.4 Predicting the Vertical Median Grain Diameter Procedure

The steps to predict the vertical sand size within the dune structure are:

- 1 - Determine the median diameter for the sand mixture (d_{50m}), the geometric standard deviation for the sand mixture (σ_{gm}), and the mean flow velocity (v_m) in the region containing the bedform.
- 2 - Use the standardized average dimensionless back flow velocity diagram at the lee side of the dune, so the velocity at each of the dune layers is known.

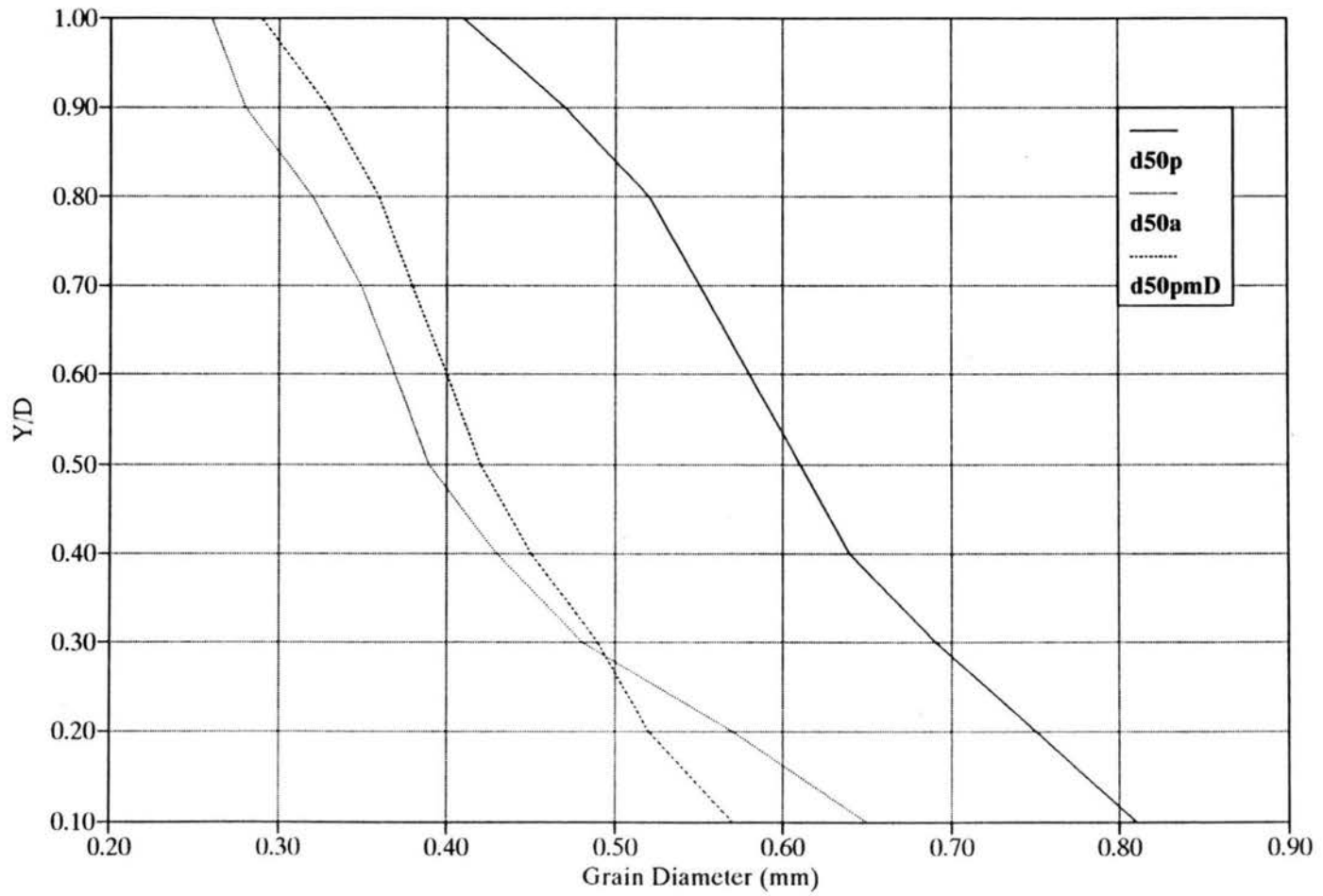


Figure 5.39. Predicted, modified, and actual median grain diameter for a dune layer (Mixture #1).

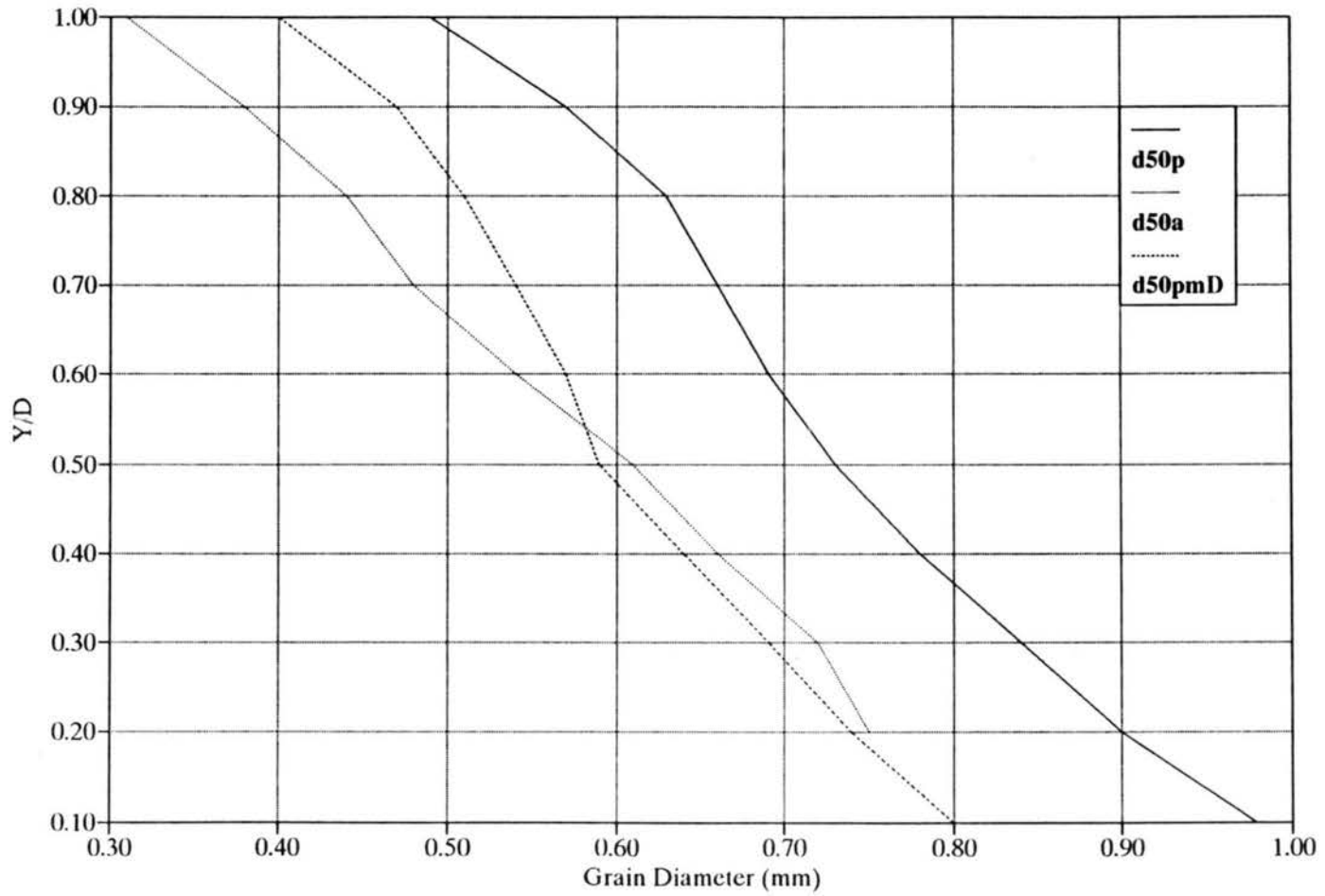


Figure 5.40. Predicted, modified, and actual median grain diameter for a dune layer (Mixture #2).

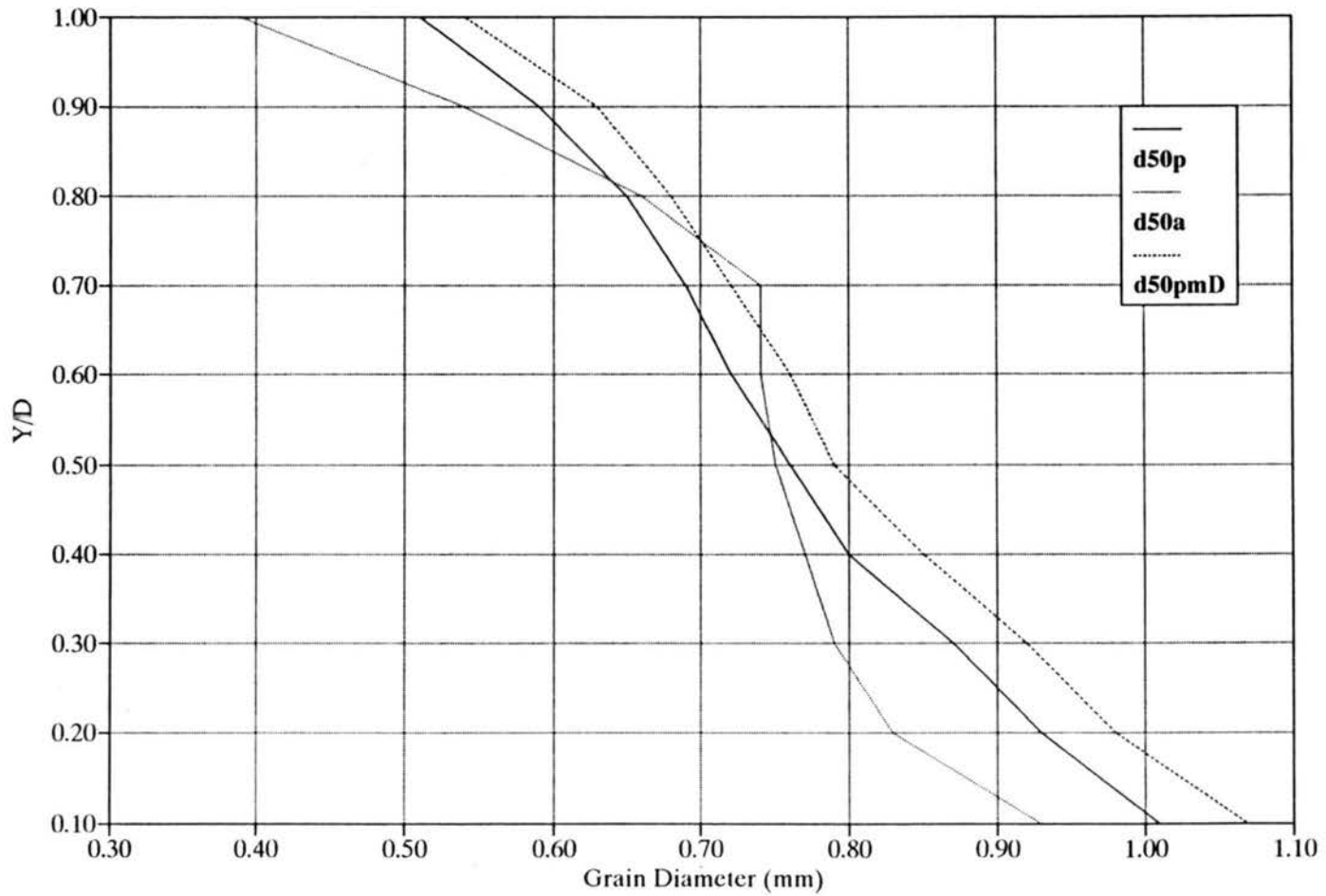


Figure 5.41. Predicted, modified, and actual median grain diameter for a dune layer (Mixture #3).

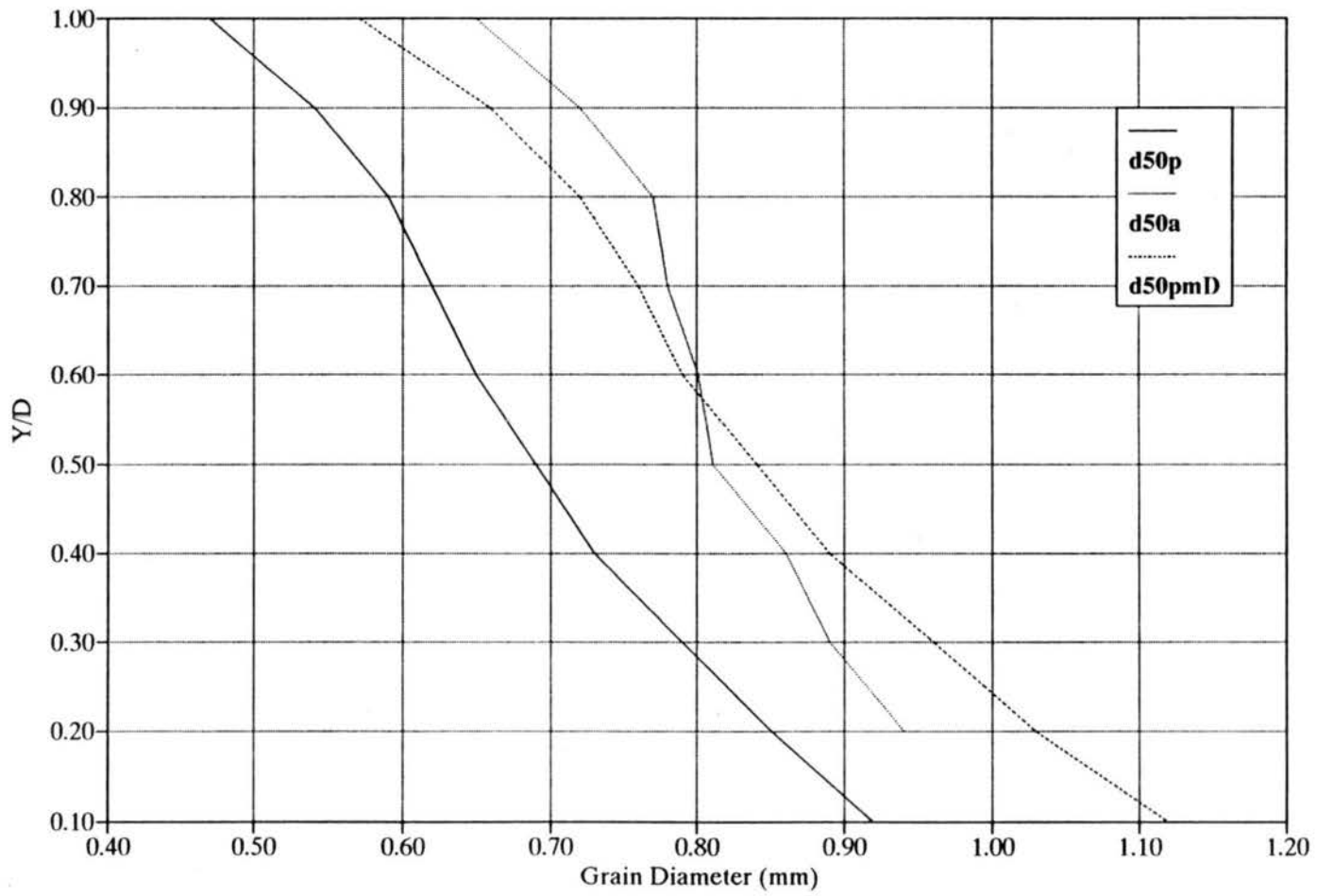


Figure 5.42. Predicted, modified, and actual median grain diameter for a dune layer (Mixture #4).

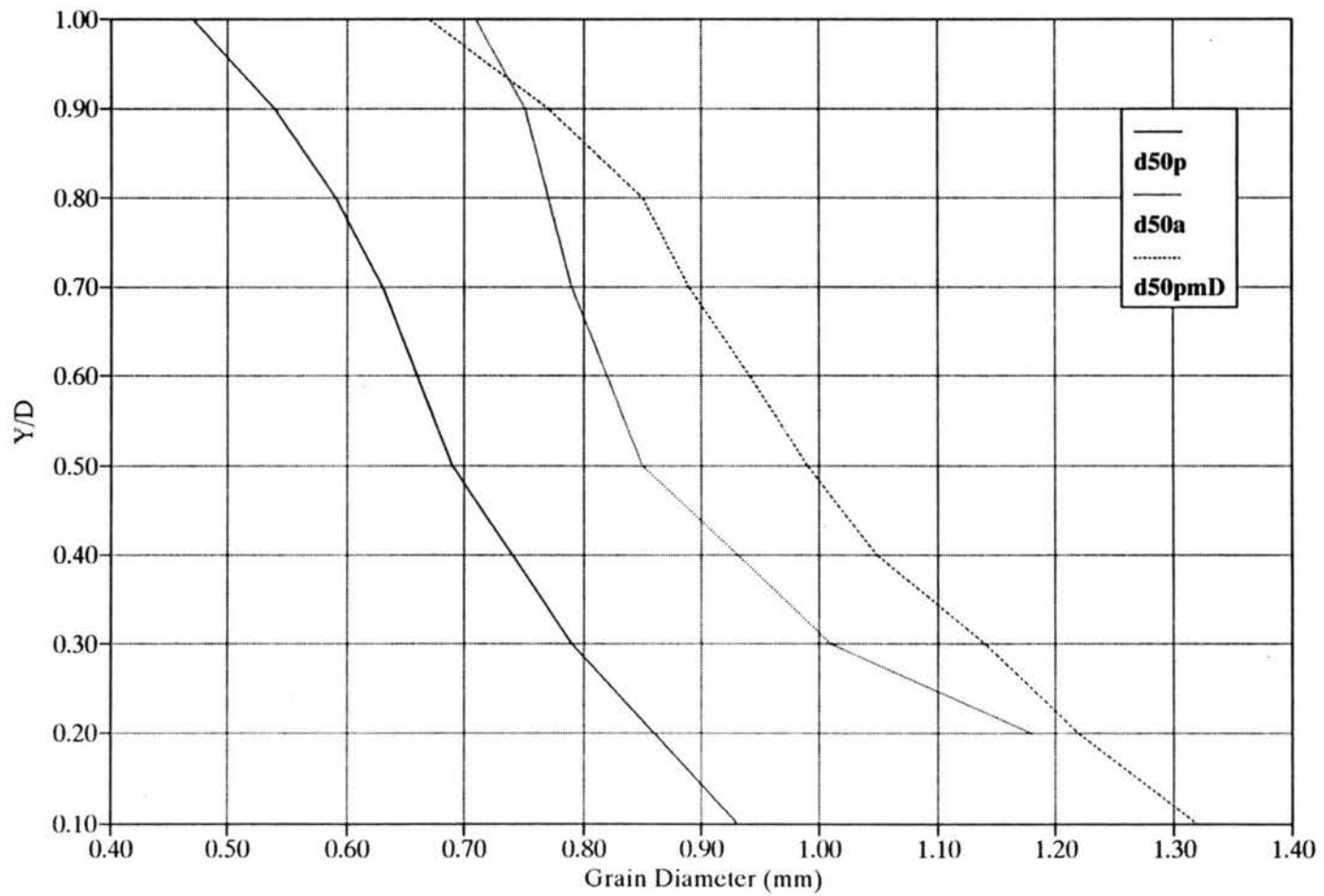


Figure 5.43. Predicted, modified, and actual median grain diameter for a dune layer (Mixture #5).

- 3 - Use the velocity distribution on the lee side of the dune and Equation 5.10 to find the d_{50al} for each layer.
- 4 - After defining the vertical size distribution of the dune, a correction value from Figure 5.38 should be taken, so that the final vertical size distribution can be determined.
- 5 - Use the geometric standard deviation for the sand mixture and Figure 5.44 which contains the standardized values for the average geometric standard deviation of each dune layer over the geometric standard deviation for the sand mixture, to obtain the geometric standard deviation for each dune layer.

5.5 Prediction of Vertical Grain Size for a Three-dimensional Dune

Three-dimensional dunes, which are the type found in natural channel and river beds, have the same vertical sorting phenomena as two-dimensional dunes, as has been shown in this chapter. So it is worth trying the prediction equation which has been developed here based mainly on data from a vertical size distribution of a two-dimensional dunes to predict the vertical grain size of the three-dimensional dune. The vertical grain size data of three-dimensional dunes were collected during an experimental run in an 8 ft. flume described in Section 5.2.4. The objective of the experiment was to study the scour around piers and abutments using a 2.44 m flume that recycled water but not sediment. The sediment discharge was not in equilibrium, meaning that the sediment discharge at the upstream was not equal the sediment discharge at the

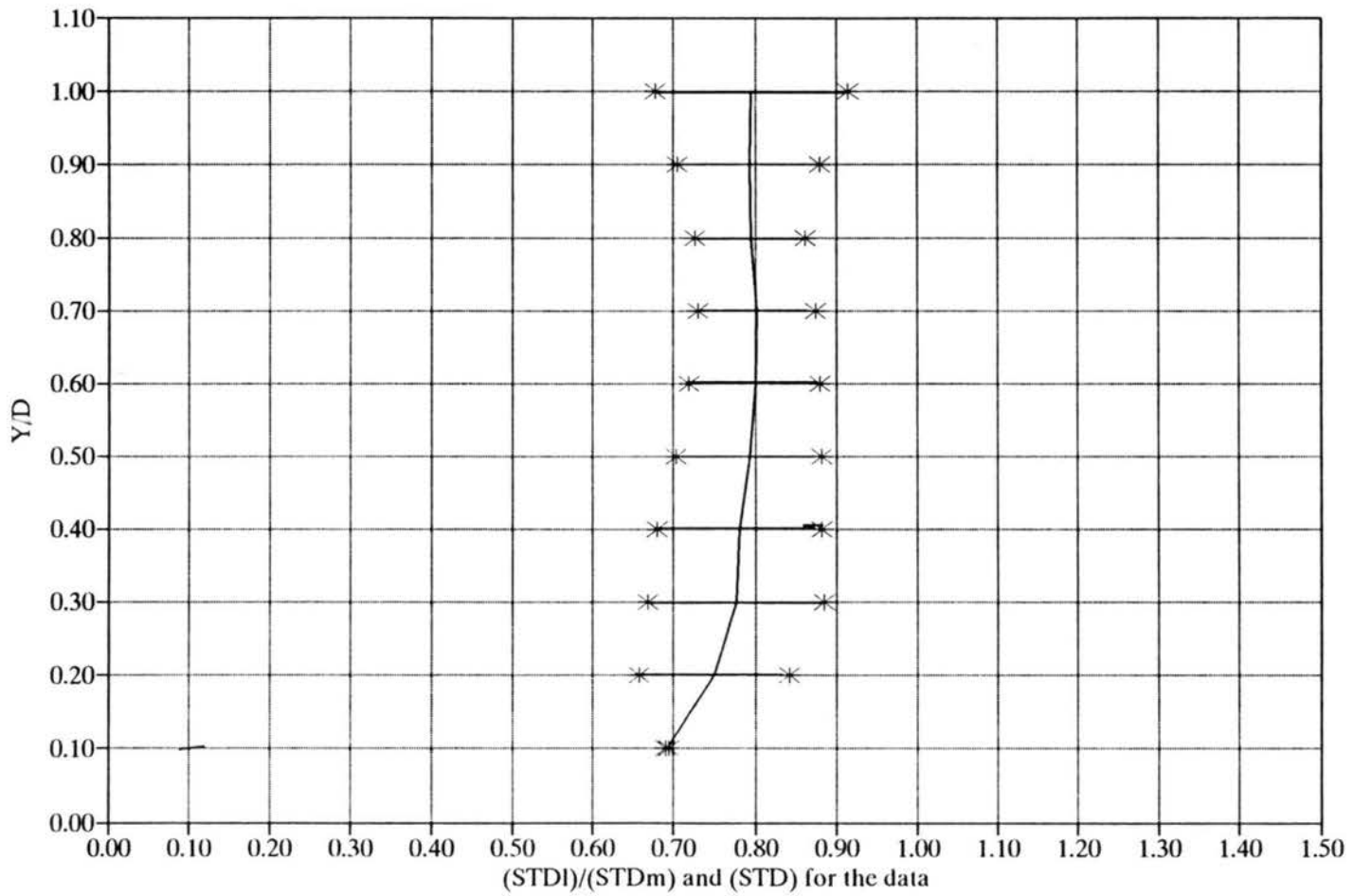


Figure 5.44. Standardized normalized geometric standard deviation in the vertical direction.

downstream end of the flume. The main source for the bed load was the erosion of the upstream bed sediment.

The sampling of the dunes was not by the same method which was presented in Chapter 4. That was because it was not possible to sample the bed before the bed level readings were first taken because to do that the water would have to be drained after the end of each run. The samples were taken as follows: First, the level of the crest of the dune was determined. After that, a very thin steel plate with a sharp edge was used to push slowly into the dune and to get a sample from one layer of the dune. After the first layer was removed, the level of the dune surface was taken. This procedure was repeated until the chosen section of the dune was completely removed. Note that a part of the dune was sampled, not all of it as in the two-dimensional dune because the method which was used here could not allow the whole dune to be sampled.

From the level of the dune crest and the level of the dune surface after removing each layer, the thickness of each layer was calculated. Two dunes with heights of about 0.08 m were on the bed of the flume after the flow was stopped. Each dune was sampled into four layers. The size distribution curves for these two dunes is presented in Appendix A. The hydraulic data of the run and the procedure described in this chapter was used to calculate the vertical grain size for each dune. Note that the mean velocity of the flow was increased by about 14% to represent the velocity in a dune regime because the flume bed was not covered with dunes. This means that the velocity of the flow did not conform to that which was indicated in the formula.

Figure 5.45 shows the actual vertical median grain size diameter (d_{50}) and the calculated vertical median grain size diameter. From the figure, the maximum difference between the actual and the predicted is 13% for the first dune and 30% for the second dune. This difference between the actual and the predicted median grain diameter may be because the whole dune structure was not sampled as in the two-dimensional dunes. Only a portion of each dune was sampled, which may cause an error in the measured median grain diameter, whereas the calibration of the prediction equation was based on the sampling of the whole dune structure. The equilibrium condition of the sediment bed load discharge did not exist which may have produced a fluctuation in the sediment mixture size characteristics which finally affect the sediment structure of the dune.

5.6 Field Data

Not many field data exist to test whether or not the vertical sorting observed in the laboratory in this study and by Brush (1965b) and Ribberink (1983) also occurs in large dunes that form in nature. McKee (1989, Figure 6) collected samples from trenches at the upstream and downstream toes and along the back of the dune shown in Figure 5.46. The dune was 210 m long and about 3 m high.

These samples show a decrease in d_{50} up the face of the dune, with coarser particles accumulated in the lower part of the dune, which agrees with the proposed mechanism described in Chapter 3.

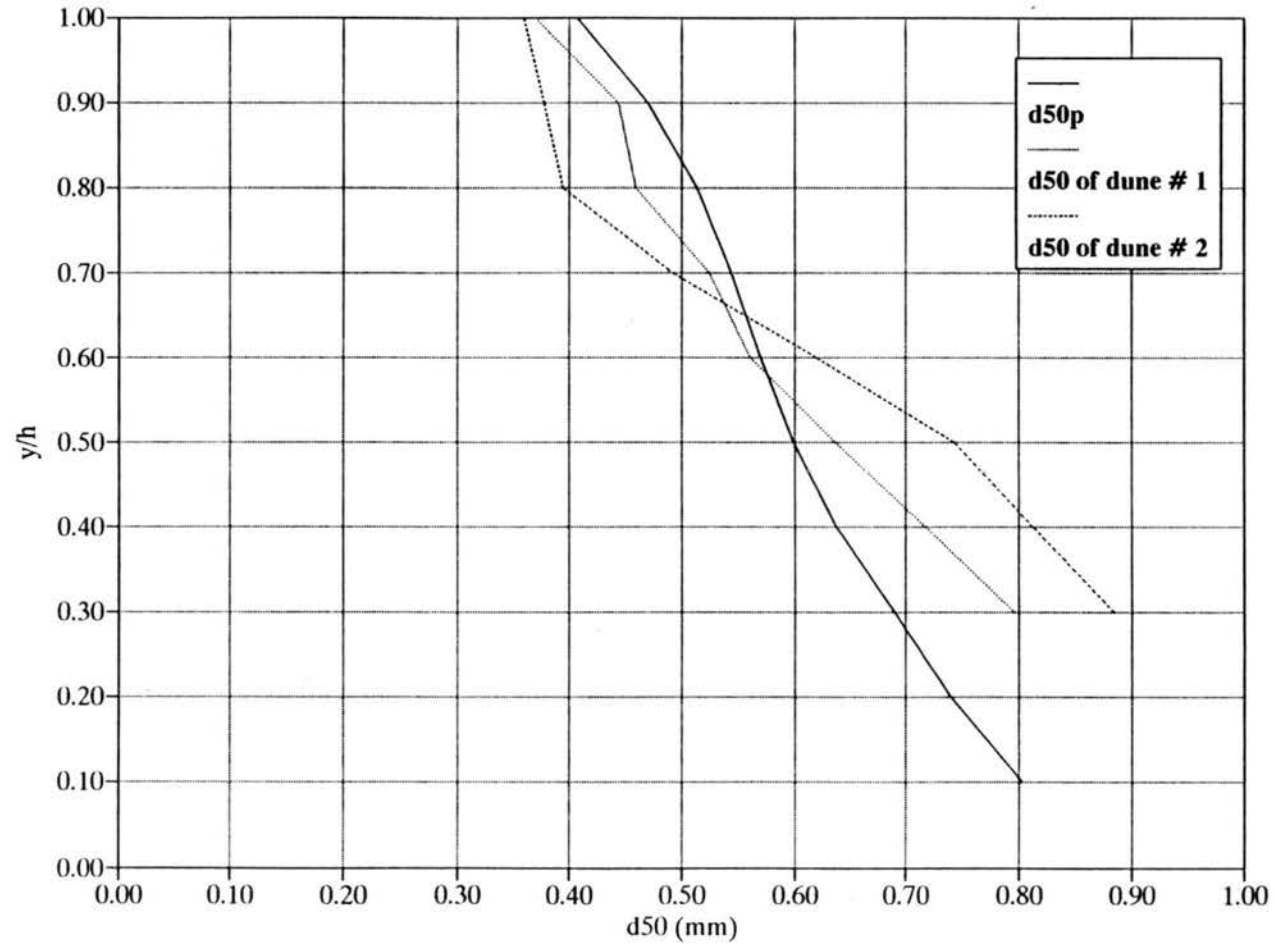


Figure 5.45. Predicted values for the median grain diameter for the 8 foot flume dunes and the actual values.

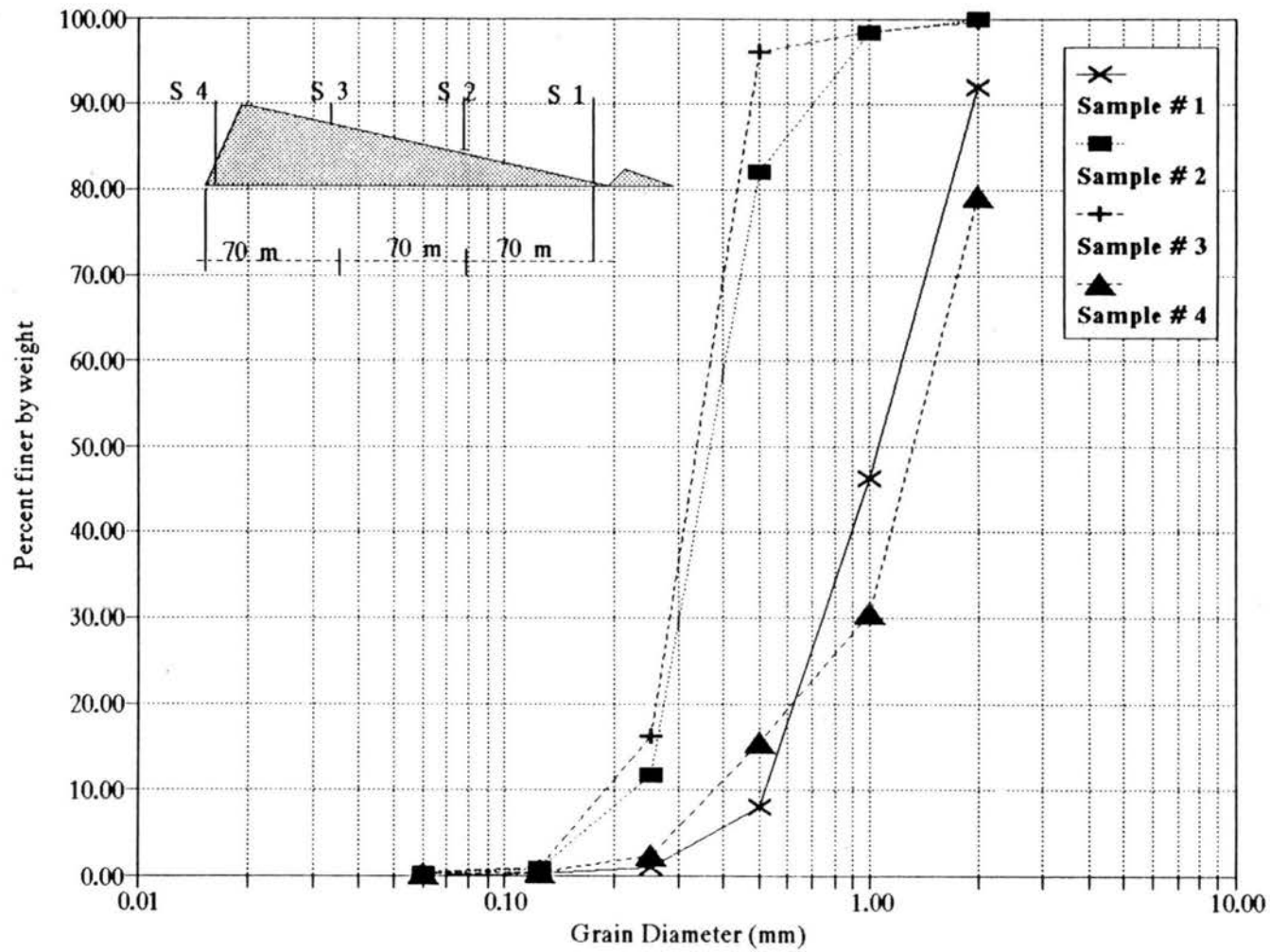


Figure 5.46. Size distribution curves for four samples along the back and the lee face of a water dune (after McKee, 1989).

McKee (1983, Figure 10) also collected samples over a sand dune formed by wind. The median diameters of his samples, plotted in Figure 5.47, show no pattern of sorting, as occurred in water formed sand waves. It is concluded that sorting processes in wind blown sand are not the same as sorting processes in water.

The prediction method developed in this chapter has some limitations, as follows:

- 1 - In this study, the velocity of a sediment particle moving along the lee face slope was not considered. It was included in the velocity term in Equation 5.10. The drag force on the particle will be the result of a relative velocity, $u = v_p + v_f$, where v_p is the particle velocity and v_f is the velocity of the backflow up the face of the dune,
- 2 - There are many other factors which may affect this vertical sorting process, for example, the fluctuation of the backflow velocity, the exact backflow velocity distribution and the turbulence in the lee zone, and
- 3 - The constant, C , accounts for C_g , C_d , and may be other factors which are not known.

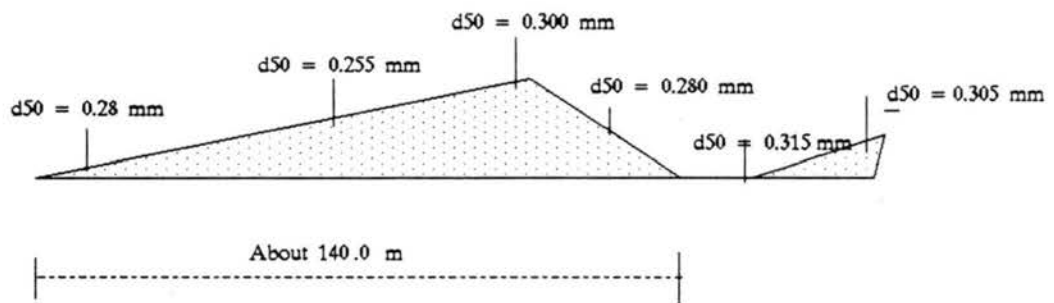


Figure 5.47. Median diameter on a different position and along wind dune (after McKee, 1983).

CHAPTER 6

SUMMARY, CONCLUSIONS, AND RECOMMENDATIONS

6.1 Summary

The main objective of this study was to provide an analytical method to predict the vertical median grain size diameter within two dimensional dune structures. This objective was achieved by conducting a series of physical experiments in a laboratory flume using five different sediment mixtures with known initial gradation.

The median grain diameter (d_{50m}) for the five mixtures was 0.35 mm, 0.47 mm, 0.6 mm, 0.72 mm and 0.86 mm. The geometric standard deviation (σ_{gm}) of the five mixtures was 2.86, 2.33, 2.9, 2.3 and 2.68 respectively. The mixtures were prepared by mixing two different sands whose median grain diameters were between 0.25 mm and 1.2 mm to form the desired sediment mixtures. Three types of experiments were conducted, namely, running water experiments, still water experiments, and air experiments.

In the first type of experiment, running water, the discharge was kept constant during each run. But there was a little difference in the flow depth and water surface slope due to the presence of dunes on the bed. Because this difference was small, they were considered to be almost constant. A uniform flow and sediment discharge over the entire flume length was maintained. The experiment was continued until the dunes had fully developed along the flume. Then the discharge was slowly lowered until the

flow was stopped completely without distorting the dune shape. The flume was not drained so the sampling of each dune into several layers could be done to determine its grading curve.

In the second type of experiment, still water, the flume was filled with water, and the sand mixture was deposited into the flume, foreset by foreset, following one another in a continuous way. The final deposited sand mixture was in a delta shape. This deposit method was to duplicate what occurs during the avalanche process of the sand grains on the lee slope of a running water dune. That was done by using of a funnel with the same width as the flume moving continuously along the flume. After reaching enough length, the deposited sand mixture was sampled through several layer to determine its grading curve.

In the third type of experiment, air, the sand mixture was deposited, as in the still water experiments, foreset by foreset in a delta-type deposit. The deposited sand was sampled while submerged in water in order to sample each layer.

A prediction equation for the vertical median grain diameter within two-dimensional dunes was developed using the experimental data. In addition, a prediction of the geometric standard deviation in the vertical direction using a normalized graph based on the experimental data was presented. A vertical grain size distribution for a three-dimensional dune was also presented. The prediction equation was used to predict a vertical grain size diameter for the three-dimensional dunes as well as for the two-dimensional dunes.

6.2 Conclusions

The main conclusions drawn from the analysis of the results are as follows:

- 1 - Extensive sampling of the bed showed that the sand grains of a sediment mixture tend to rearrange themselves during the deposition of a dune in such way as to develop a vertical reduction in the grain diameter within the dune structure.
- 2 - From the sampling results of each dune layer it can be said that each horizontal dune layer contains an almost constant size distribution of sand grains; in another words, that each layer is composed of homogeneous sand.
- 3 - The normalized geometric standard deviation for each horizontal dune layer decreased upward for mixtures having a median grain diameter of less than 0.6 mm, but for mixtures with a median grain diameter higher than 0.6 mm it increased upward. The mixture which had a median grain diameter of just 0.6 mm showed an increase upward but within a very small range.
- 4 - The median grain diameter of the dune structure is larger than the original mixture. This can be explained by the loss of a small amount of the fine material as a suspended load due to a losses in the flume system.
- 5 - It is possible to predict the vertical median grain diameter within the dune structure for a sediment mixture using the following equation:

$$d_{si} = \frac{u_i^2}{22.53 g \left(\frac{\rho_s}{\rho} - 1 \right)} \quad (6.1)$$

where:

u_i^2 = velocity in the front of the dune at each dune layer,

g = acceleration of gravity,

ρ_s = density of the sediment mixture, and

ρ = density of water.

- 6 - From the results of the still water and air experiments, it is clear that to develop vertical sorting within a deposited sand mixture by avalanche over the lee side needs the lee slope length to be much longer than that for the running water dune.
- 7 - From the still water and air experiment, the role of hydrodynamic forces on the development of the vertical sorting process is very obvious.
- 8 - The geometric standard deviation for the sediment mixture is not an effective factor in the characteristics of the vertical sorting process. On the contrary, median grain diameter of the sediment mixture is an important factor for developing the vertical sorting process.
- 9 - Concerning the effect of the dimensionless shear stress due to grain resistance, the boundary Reynolds number and the dimensionless grain diameter are the most effective parameters in the vertical sorting process. A correction factor depending on the dimensionless grain diameter was used to correct the error in the predicted values of the vertical median grain diameter. It was shown that fall velocity might also be used as a correction factor.

- 10 - The vertical sorting within the dune structure may act on the long-run as a protection layer for the nonmoving bed material. That is due to the formation of the coarsest layer at the bottom of the dune. This layer may act as an armoring layer.

6.3 Recommendations for Future Research

On the basis of the results of this investigation the following recommendations are made for a better understanding of the vertical sorting phenomenon.

- 1 - The main objective of this study was studying the sorting phenomenon. The next step is to study the effect of the vertical sorting process on the dimension of the dune.
- 2 - The study included only five different sediment mixtures to develop of the dune. It is recommended that more than five sediment mixtures be included to enhance the developed equation.
- 3 - Further work is needed to determine the effect of the three dimensional dune data on the vertical sorting process.
- 4 - More research is required to investigate the effect of the dimensionless shear stress due to grain resistance, the boundary Reynolds number and the dimensionless grain diameter on the vertical sorting process.
- 5 - The dune dimensions in this study were almost constant; in another words, there was little difference between the dimensions of the dune from one run to another. It is recommended that a wider range of flow conditions should be

used to generate dunes having a wider spectrum of dimension including large features with secondary waves. Then the effect of the dune dimensions on the vertical sorting could be studied.

- 6 - Further research is needed to study the effect of the bottom layer, which has the coarsest grain diameter of the dune, on the stability of the bed material in the long run.

REFERENCES

- Allen, J.R.L., 1968, The diffusion of grains in the lee of ripples, dunes, and sand deltas, *J. of Sedimentary Petrology*, vol. 38, no. 2, p 621-633.
- Bagnold, R.A., 1941, *The physics of blown sands and desert dunes*, Methuen and Co., London, 165 p.
- Bagnold, R.A., 1954, Experiments on a gravity-free dispersion of large solid spheres in a Newtonian fluid under shear. *Proc. Royal Society of London*, ser. A225, p 49-63.
- Brookfield, M.E. and Ahlbrandt, T.S. (editors), 1983, *Eolian sediments and processes*, Amsterdam, 660 p., Elsevier Science Publishers B.V.
- Brush, L.M., 1965a, Experimental work on primary sedimentary structures. *Society of Economic Paleontologists and Mineralogists Special Publication 12*, p. 17-24, Tulsa, OK.
- Brush, L.R., 1965b, Sediment sorting in alluvial channels, *Society of Economic Paleontologists and Mineralogists, Special Publication 12*, p 25-33, Tulsa, OK.
- Einstein, H.A., 1950, The bedload function for sediment transport in open channel flow. *U.S. Dept. of Agriculture Tech. Bull. no. 1026*, 71 p.
- Einstein, H.A., 1947, Formulas for the transportation of bed-load. *Trans. ASCE*, vol. 107, p 561-577.

- Einstein, H.A., and Barbarossa, N.L., 1952, River channel roughness, Trans. ASCE, vol. 117, p 1121-1146.
- Engelund, F., 1970, Instability of erodible beds, J. of Fluid Mechanics, vol. 42, p 225-244.
- Engelund, F., 1974, Flow and bed topography in channel bends, ASCE, J. of Hydraulic Division, vol. 100, no. HY 11, p. 1631-1648.
- Fredsøe, J., 1978, Meandering and braiding of rivers, J. of Fluid Mechanics, vol. 84, part 4, p 609-624.
- Fredsøe, J., 1982, Shape and dimension of stationary dunes in rivers. ASCE, J. of Hydraulic Eng., vol. 108, no.HY8, p 932-947.
- Fredsøe, J., 1984, Sediment transport in current and waves, Technical University of Denmark, Institute of Hydrodynamics and Hydraulic Eng., series paper no. 35.
- Freythuth, P., 1966, On transition in a separated laminar boundary layer, J. of Fluid Mechanics, vol. 25, p 683-704.
- Gessler, J., 1967, The beginning of bed load movement of mixtures investigated as natural armoring in channels, translation T-5. W.M. Keck Laboratory of Hydraulics and Water Research, California Institute of Tech., Pasadena, CA.
- Gessler, J., 1970, Self stabilizing tendencies of alluvial channels. Proc. ASCE, J. of Waterways and Harbors Division, vol. 96, WW2, p 235-249.
- Gessler, J., 1971, Critical shear stress for sediment mixtures, Proc. of the 14th Congress of the IAHR, Paris, France, paper C1, p 1-8.
- Graf, W.H., 1971, Hydraulics of sediment transport, NY, McGraw-Hill Inc., 513 p.

- Greeley, R. and Iversen, J., 1987, *Wind as a geological process*, Cambridge, Cambridge University Press, 333 p.
- Guy, H.P., Simons, D.B., Richardson, E.V., 1966, Summary of alluvial channel data from flume experiments 1956-61. USGS Professional Paper 462-I.
- Ikeda, S., Yamesaka, M., and Chiyoda, M., 1987, Bed topography and sorting in bends, *ASCE, J. of Hydraulic Eng.*, vol. 113, no. 2, p 190-205.
- International Standards Organization (ISO), 1983, *Measurement of liquid flow in open channel*. Swizerland, 518 p.
- Jopling, A.V., 1964, Laboratory study of sorting processes related to flow separation, *J. of Geophysical Research*, vol. 69, N16, p 3403-3418.
- Jopling, A.V., 1965, Laboratory study of the distribution of grain sizes in cross-bedded deposits, *Soc. Economic paleontologists and Mineralogists, Special Pub. 12*, p 3-65, Tulsa, OK.
- Keulegan, G.H., 1938, *Laws of turbulent flow in open channels*, National Bureau of Standards, *J. of Research*, research paper 1151, vol. 21, p 707-741.
- Kennedy, J.F., 1963, The mechanics of dunes and antidunes in erodible-bed channel, *J. of Fluid Mechanics*, vol. 16, p 521-544.
- Lane, E.W., 1955, The importance of fluvial morphology in hydraulic engineering, *Proc. ASCE*, vol. 81, no. 745.
- McKee, E.D., 1965, Experiments on ripple lamination, *Society of Economic Paleontologists and Mineralogists, Special Pub. 12*, p 66-83, Tulsa, OK.

- McKee, E.D., 1983, Eolian sand bodies of the world: in "Eolian Sediments and Processes" (Brookfield, M.E. and Ahlbrant, T.S., ed.), New York, Elsevier, p. 1-25.
- McKee, E.D., 1989, Sedimentary structure and textures of Rio Orinoco channel sands, Venezuela and Colombia, USGS Water Supply Paper 2326, p .
- Middleton, G.V., (editor), 1965, Primary sedimentary structures and their hydrodynamic interpretation, Society of Economic Paleontologists and Mineralogists, pub. 12, 265 pp, Tulsa, OK.
- Nelson, J.M. and Smith, J.D., 1989, Mechanics of flow over ripples and dunes, J. of Geophysical Research, vol. 94, no. c6, p 8146-8162.
- Odgaard, A.J., 1982, Bed characteristics in alluvial channel bends, Proc. ASCE, vol. 108, no. HY 11, p 1268-1281.
- Rathbun, R.E. and others, 1969, Response of a laboratory alluvial channel to changes of hydraulic and sediment-transport variables, USGS Professional Paper 562-D, 32 p.
- Rathbun, R.E. and Nordin, C.F., 1971, Tracer studies of sediment transport processes, Proc. ASCE, J. of Hydraulic Division, vol. 97, no. HY 9, p 1305-1316.
- Raudkivi, A.J., 1963, Study of sediment ripple formation," Proce. ASCE, vol. 89, p 15-34.
- Reineck, H.E. and Singh, I.B., 1975, Depositional sedimentary environments, New York, Springer-Verlag, 439 p.

- Ribberink, J.S., 1983, Experiments with non-uniform sediment in case of bed-load transport, communications on hydraulics, Department of Civil Engineering, Delft University of Technology, Report no. 83-2.
- Rouse, H. (editor), 1950, Engineering Hydraulics, New York, John Wiley & Sons, 1039 p.
- Shields, A., 1936, Application of similarity principles and turbulence research to bed load movement, Berlin, Uchelen, Pub. No. 167, Translation by California Institute of Tech., Pasadena, CA.
- Simons, D.B., and Richardson, E.V., 1961, Forms of bed roughness in alluvial channel, Proc. ASCE, vol. 87, no. HY 3, p. 87-105.
- Simons, D.B., and Richardson, E.V., 1966, Resistance to flow in alluvial channels, USGS Professional Paper 422-J, 61 p.
- Van Rijn, 1982, The prediction of bedforms and alluvial roughness, Proc. of Euromech 156, Mechanics of Sediment Transport, Istanbul, p 133-135.
- Van Rijn, 1984, Sediment transport part III, Bed forms and alluvial roughness. ASCE, J. of Hydraulic Eng., vol. 110, no. 12, p 1733-1754.
- Vanoni, V.A., and Brooks, N.H., 1957, Laboratory studies of the roughness and suspended load of alluvial streams, Sedimentation Laboratory Report no. E68, California Institute of Tech., Pasadena, CA.
- Yalin, M.S., 1977, Sediment transport, New York, Pergamon Press, 2nd ed., 298 p.

APPENDIX A

SIZE DISTRIBUTION CURVES FOR THE DUNE LAYERS

Predicted, modified (using τ_{*g} and D_*), and actual median grain diameter for dune layers (five mixtures).

Size distribution curves for dune layers (twenty-foot flume).

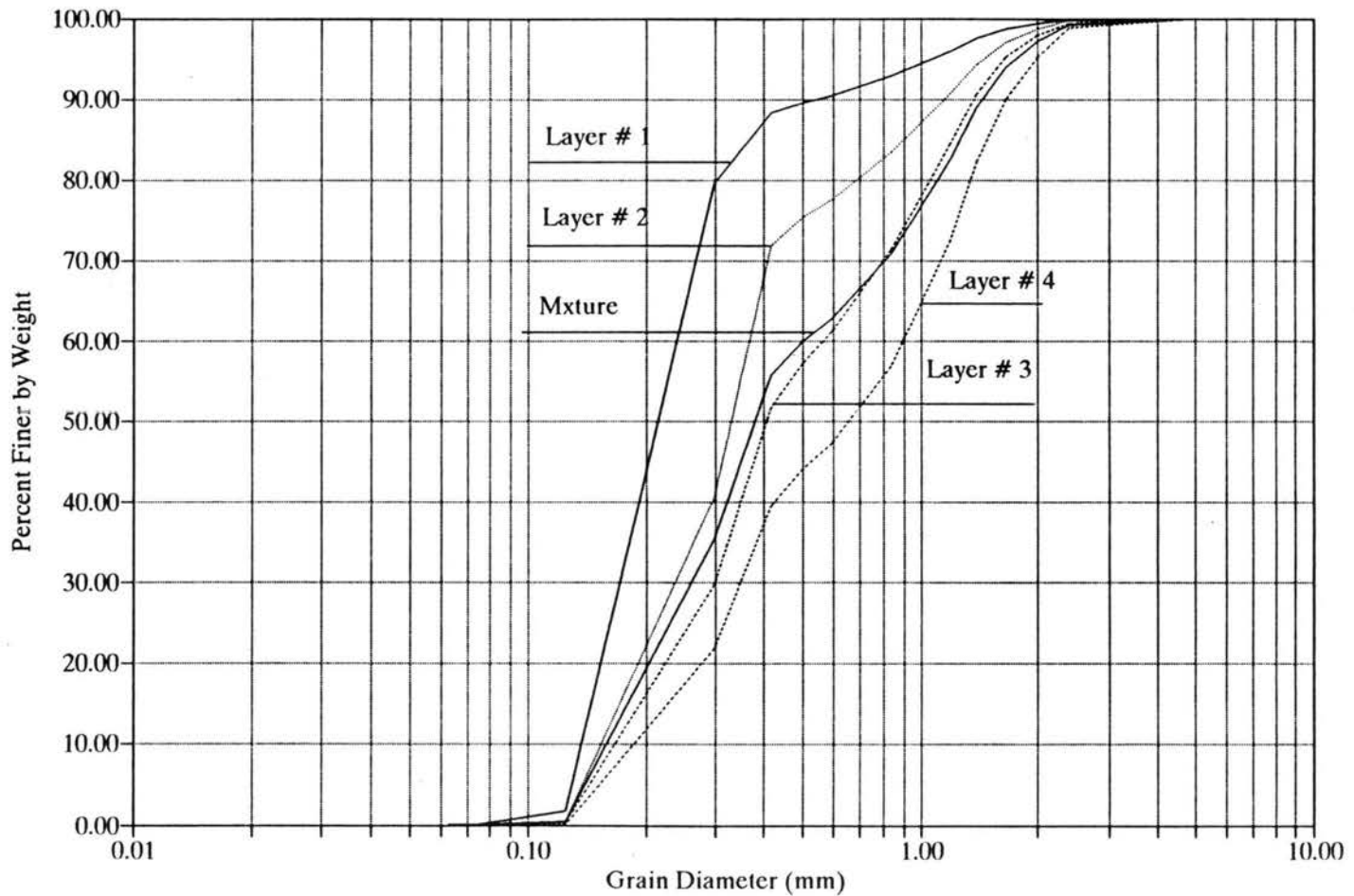


Figure A-1 : Size distribution curves for dune layers (Dune # 2, Mixture # 1)

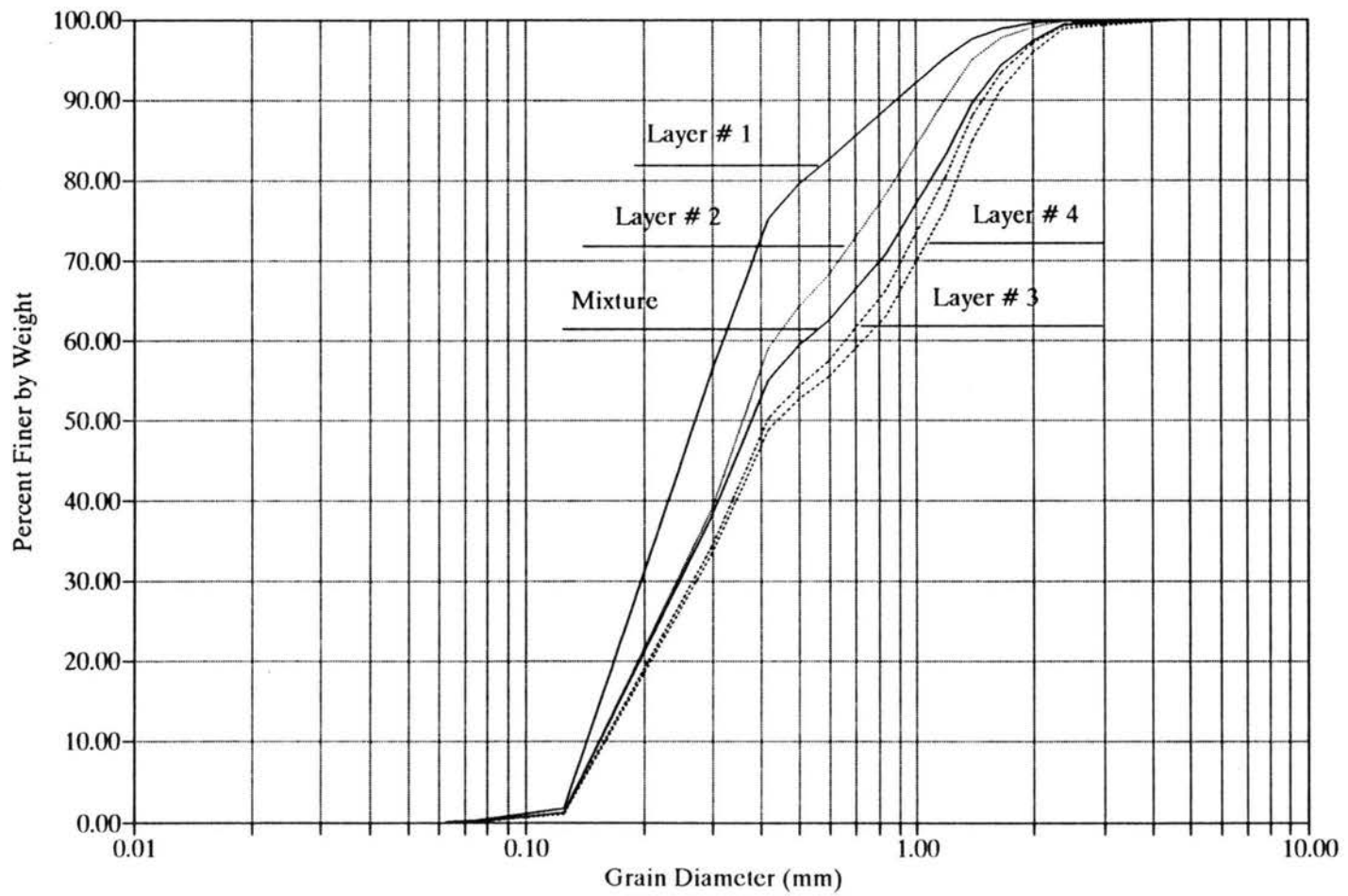


Figure A-2 : Size distribution curves for dune layers (Dune # 3, Mixture # 1)

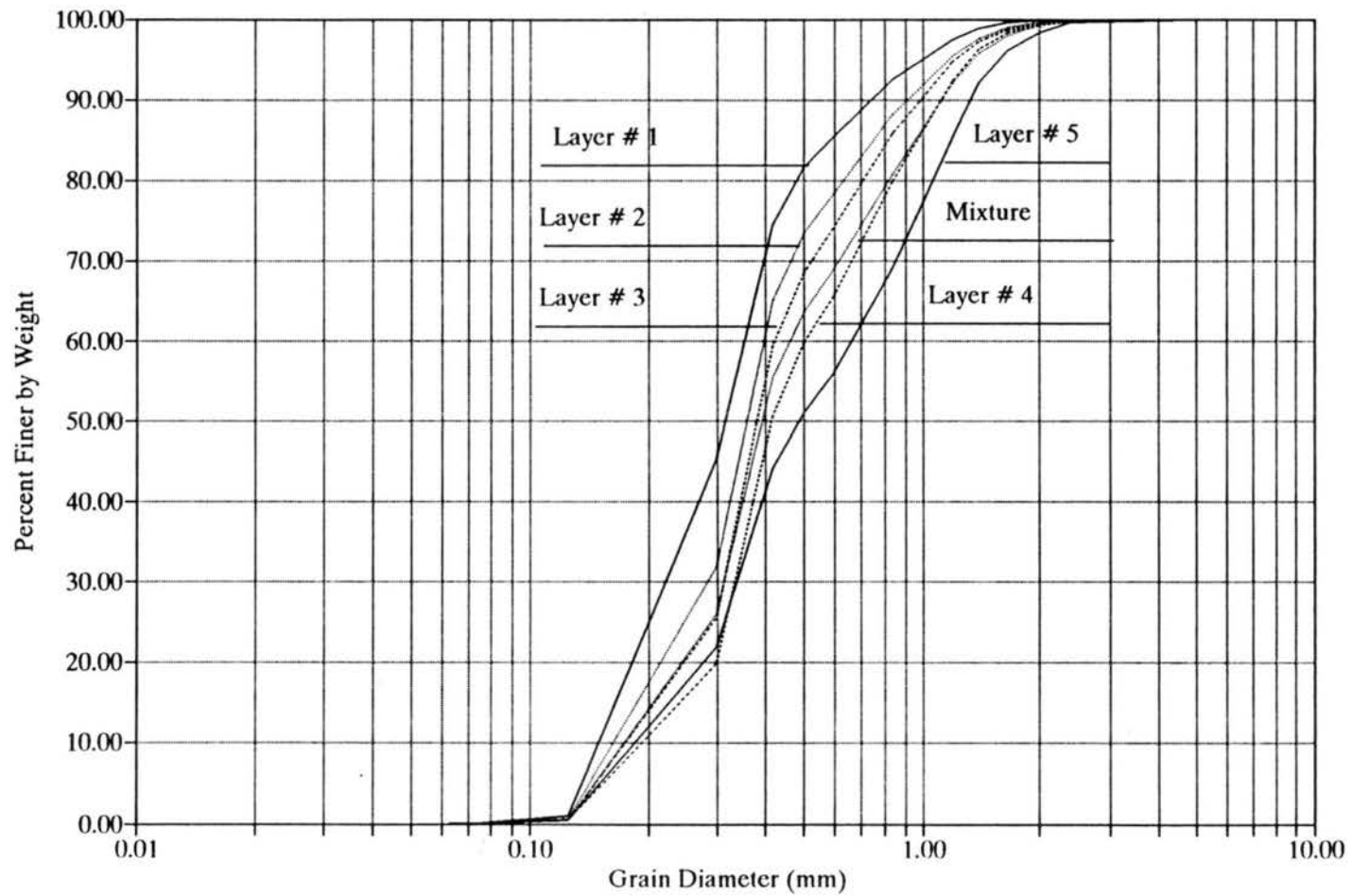


Figure A-3 : Size distribution curves for dune layers (Dune # 4, Mixture # 1)

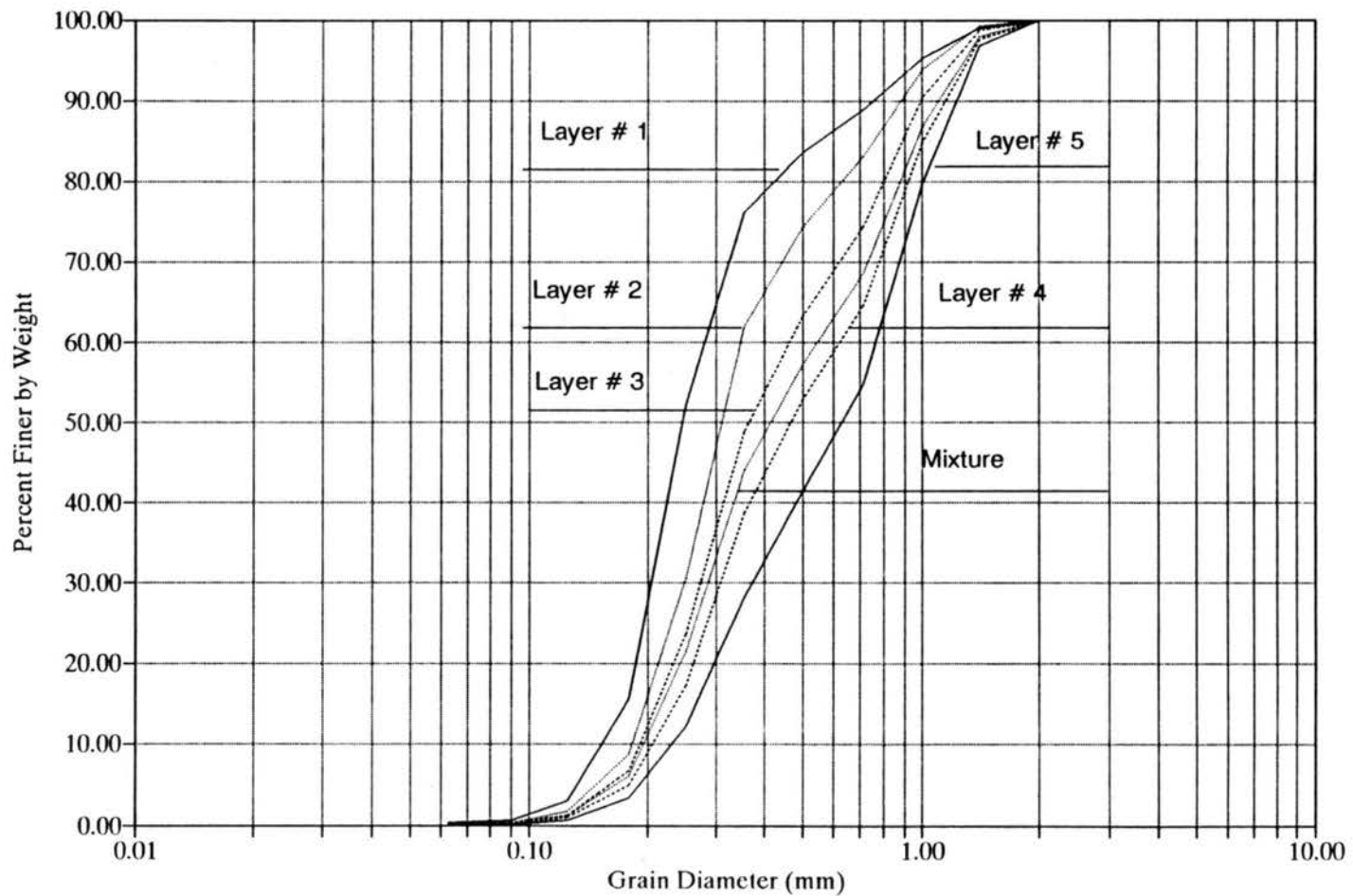


Figure A-4 : Size distribution curves for dune layers (Dune # 1, Mixture # 2).

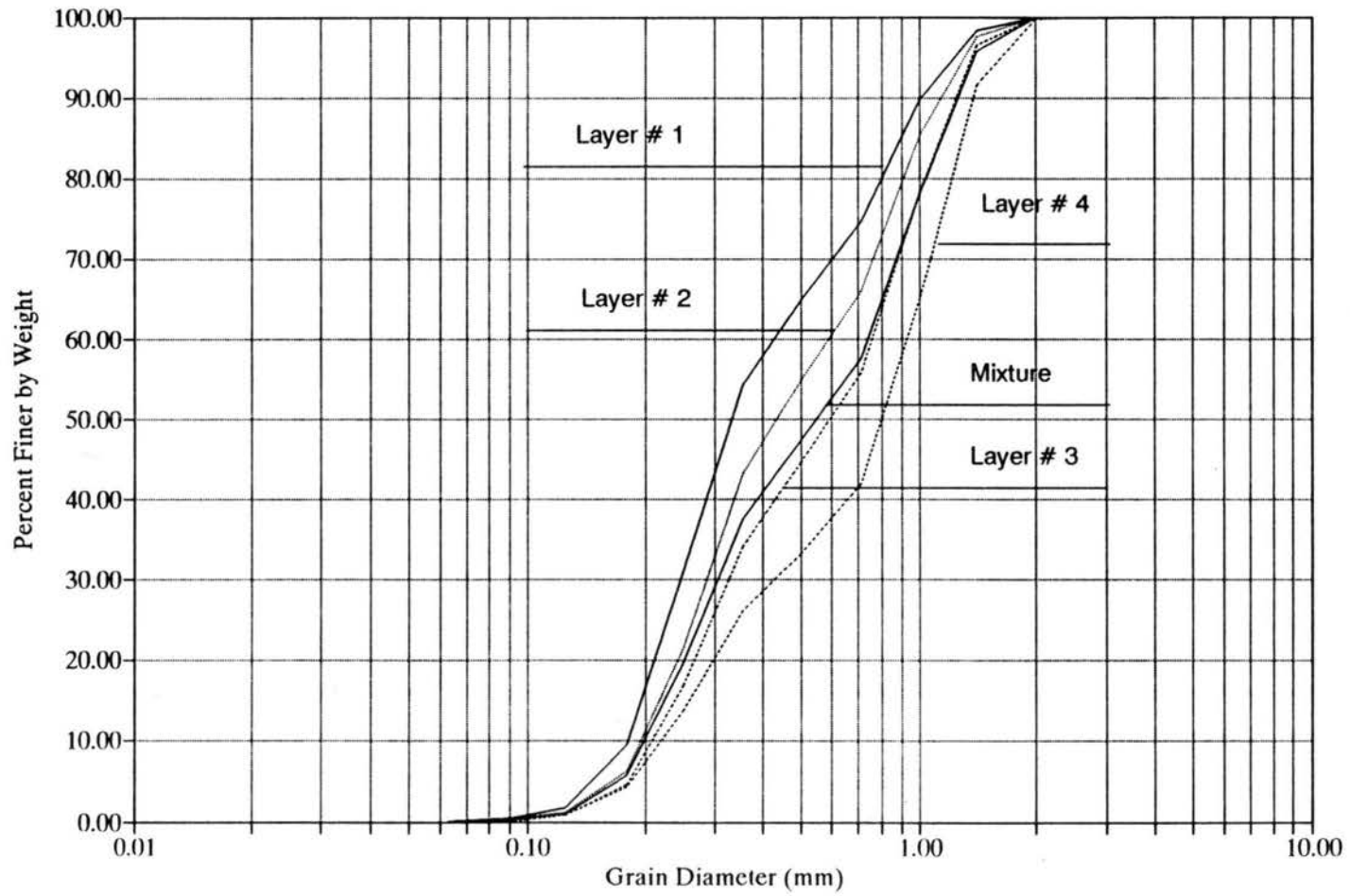


Figure A-5 : Size distribution curves for dune layers (Dune # 2, Mixture # 2).

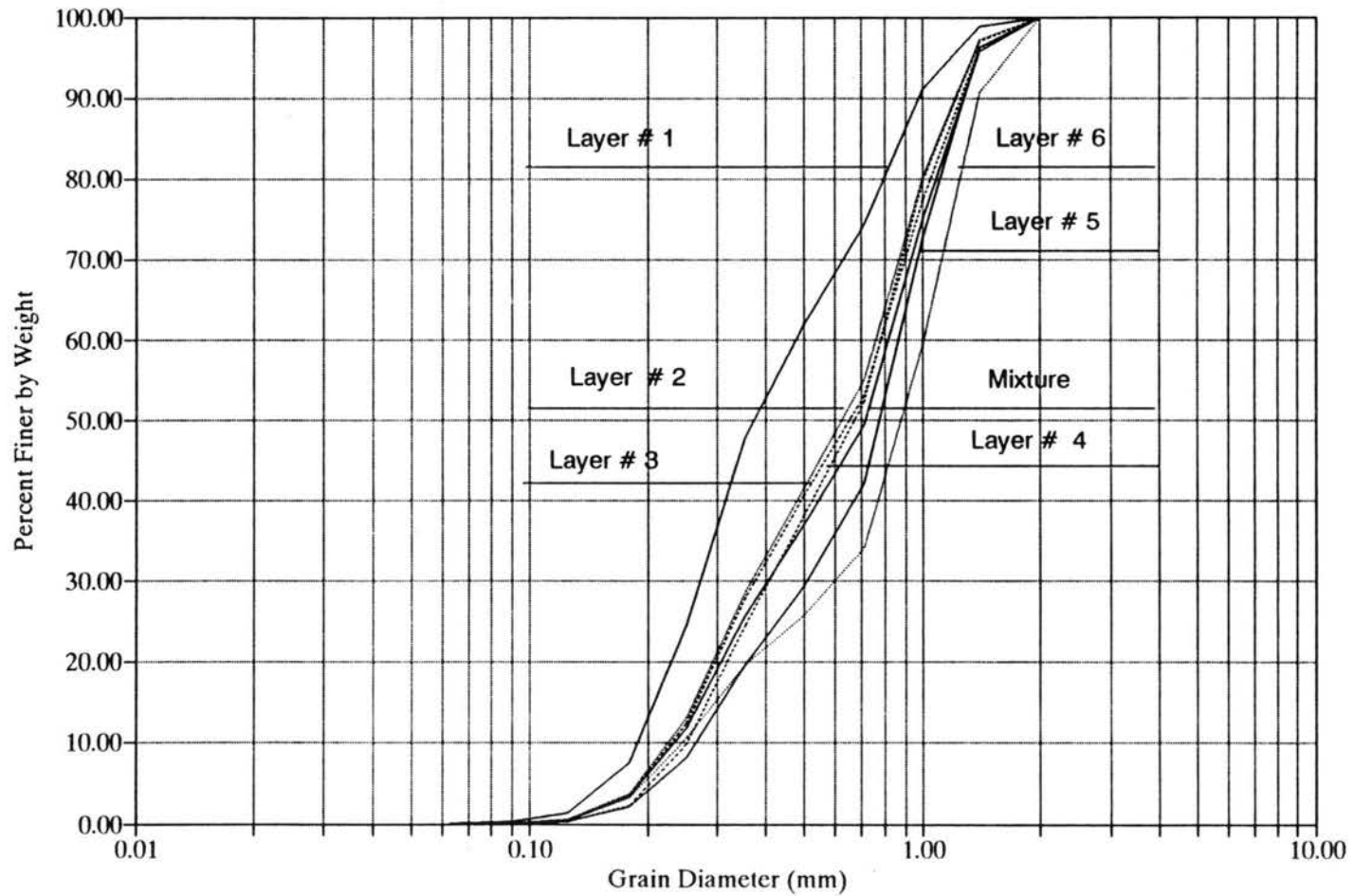


Figure A-6 : Size distribution curves for dune layers (Dune # 3, Mixture # 2).

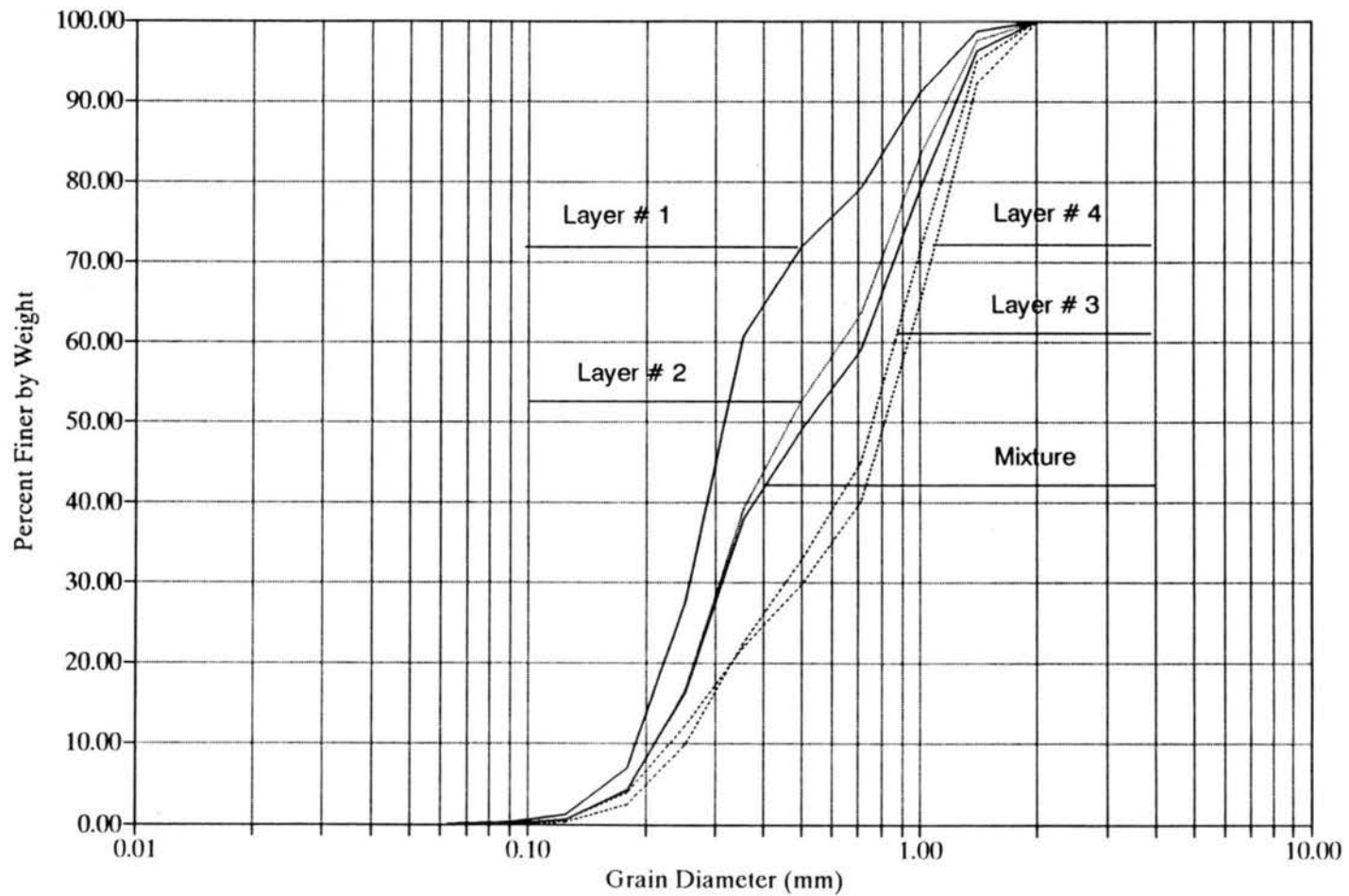


Figure A-7 : Size distribution curves for dune layers (Dune #4, Mixture # 2).

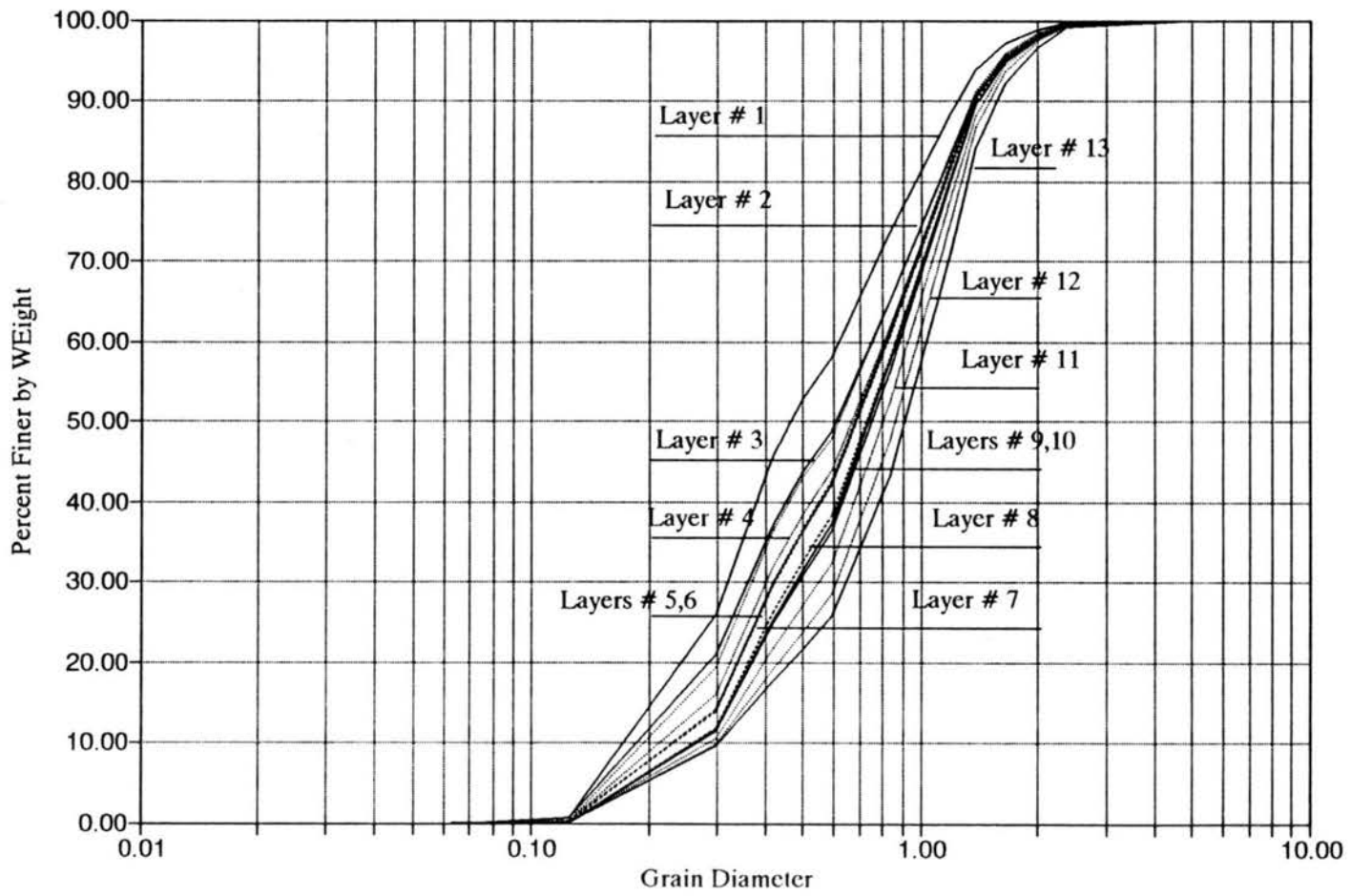


Figure A-8 : Size distribution curves for dune layers (Dune # 1, Mixture # 3).

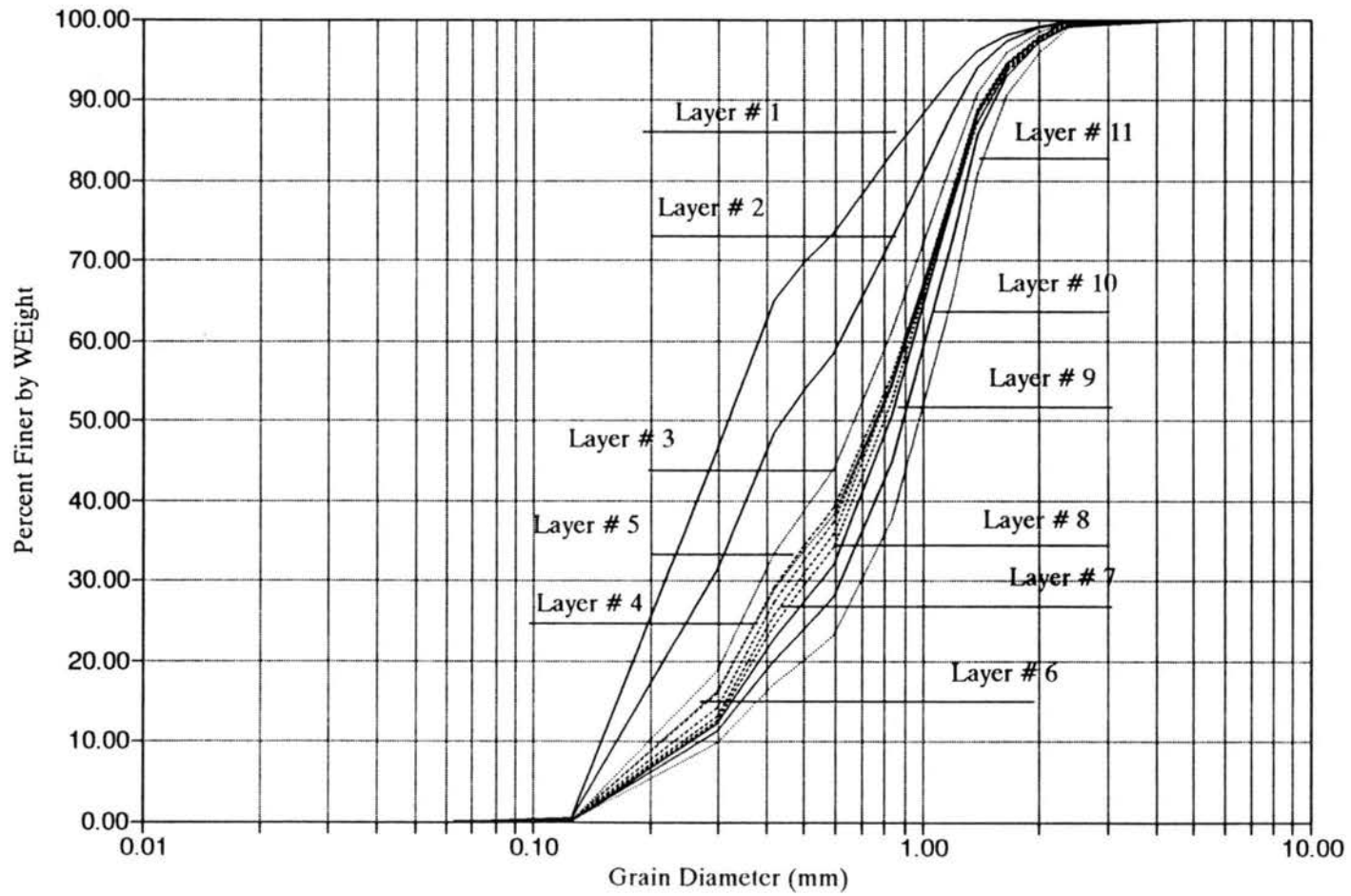


Figure A-9 : Size distribution curves for dune layers (Dune # 2, Mixture # 3).

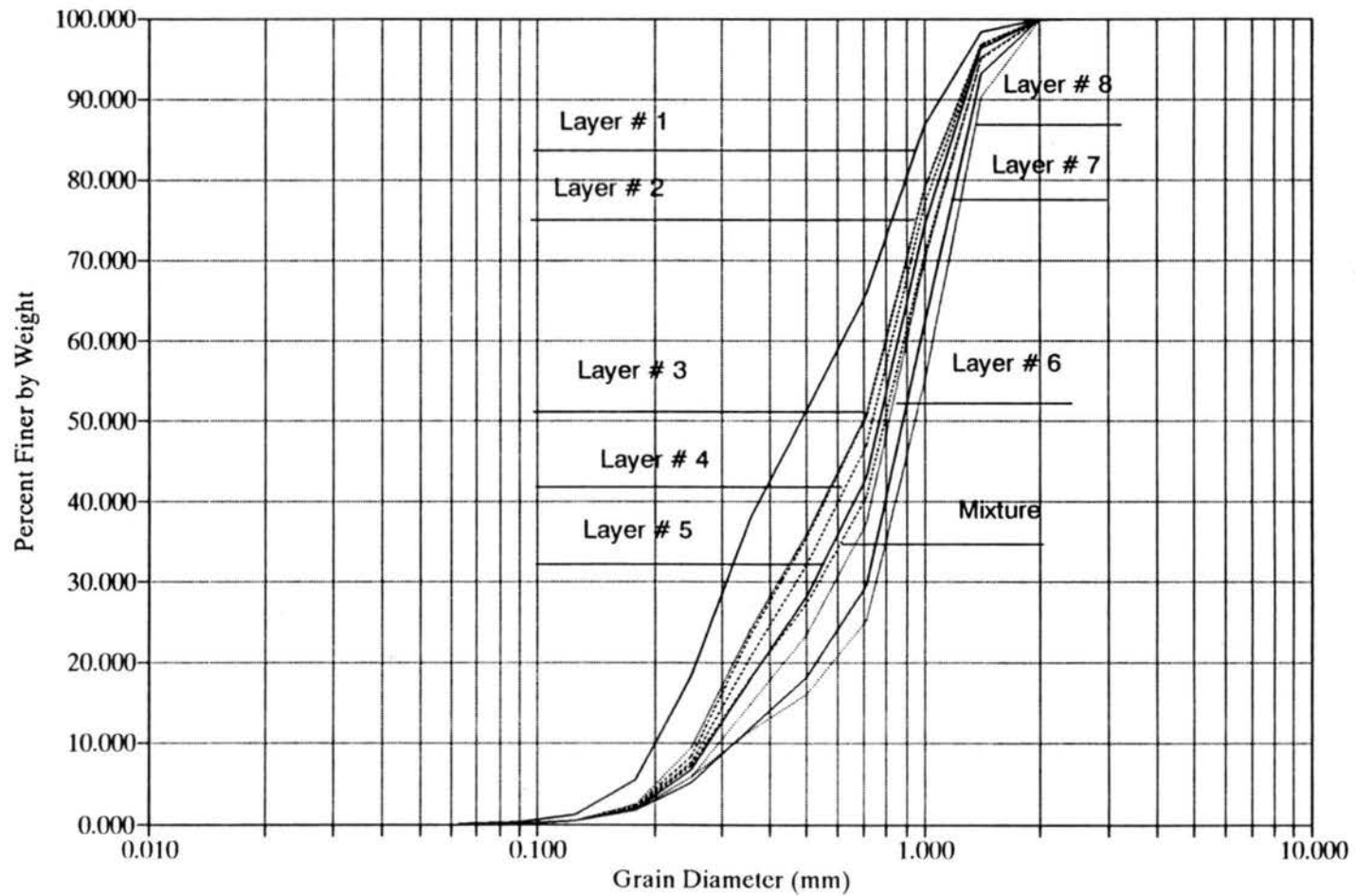


Figure A-10 : Size distribution curves for dune layers (Dune # 1, Mixture 4).

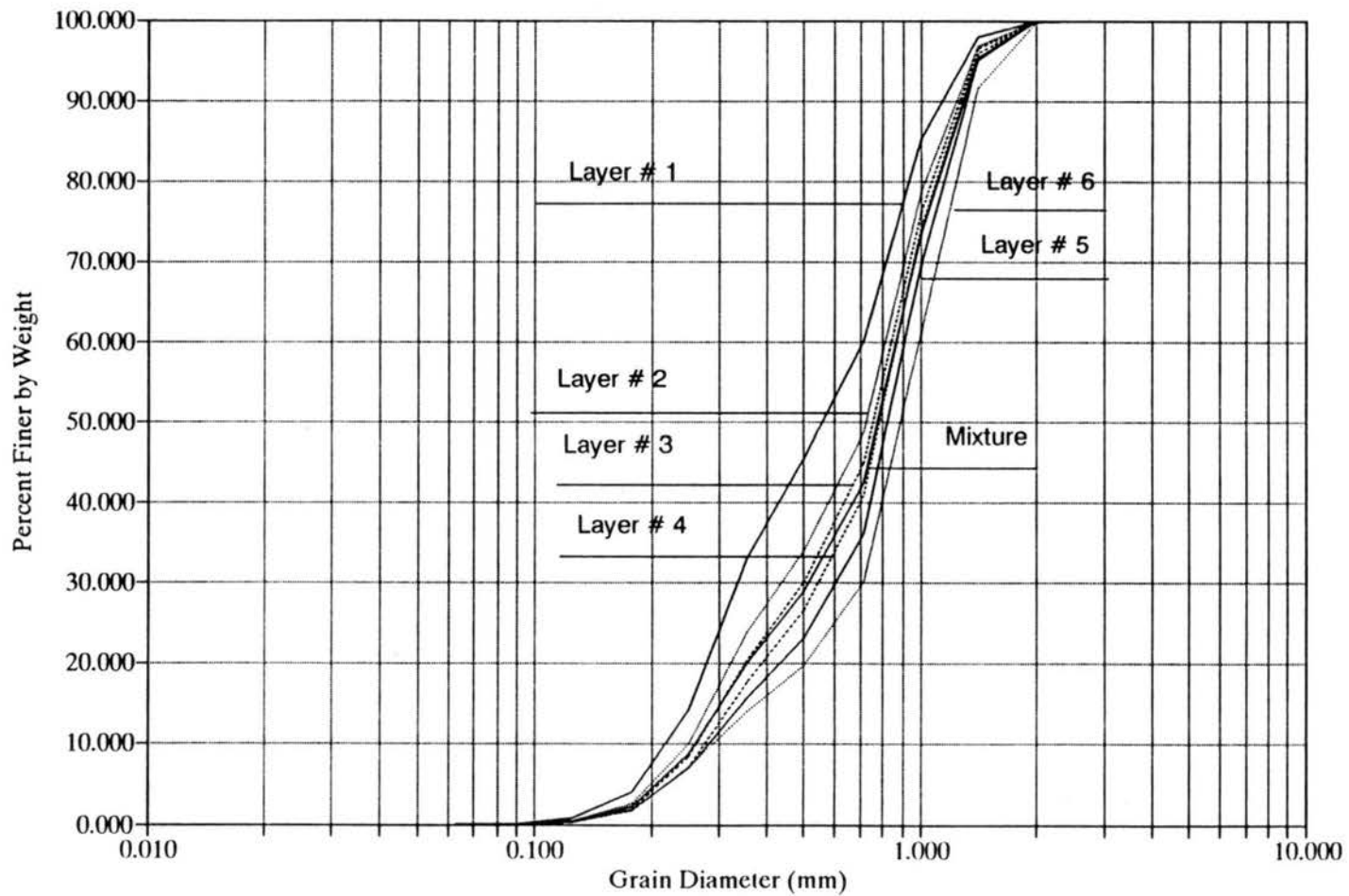


Figure A-11 : Size distribution curves for dune layers (Dune # 2, Mixture # 4).

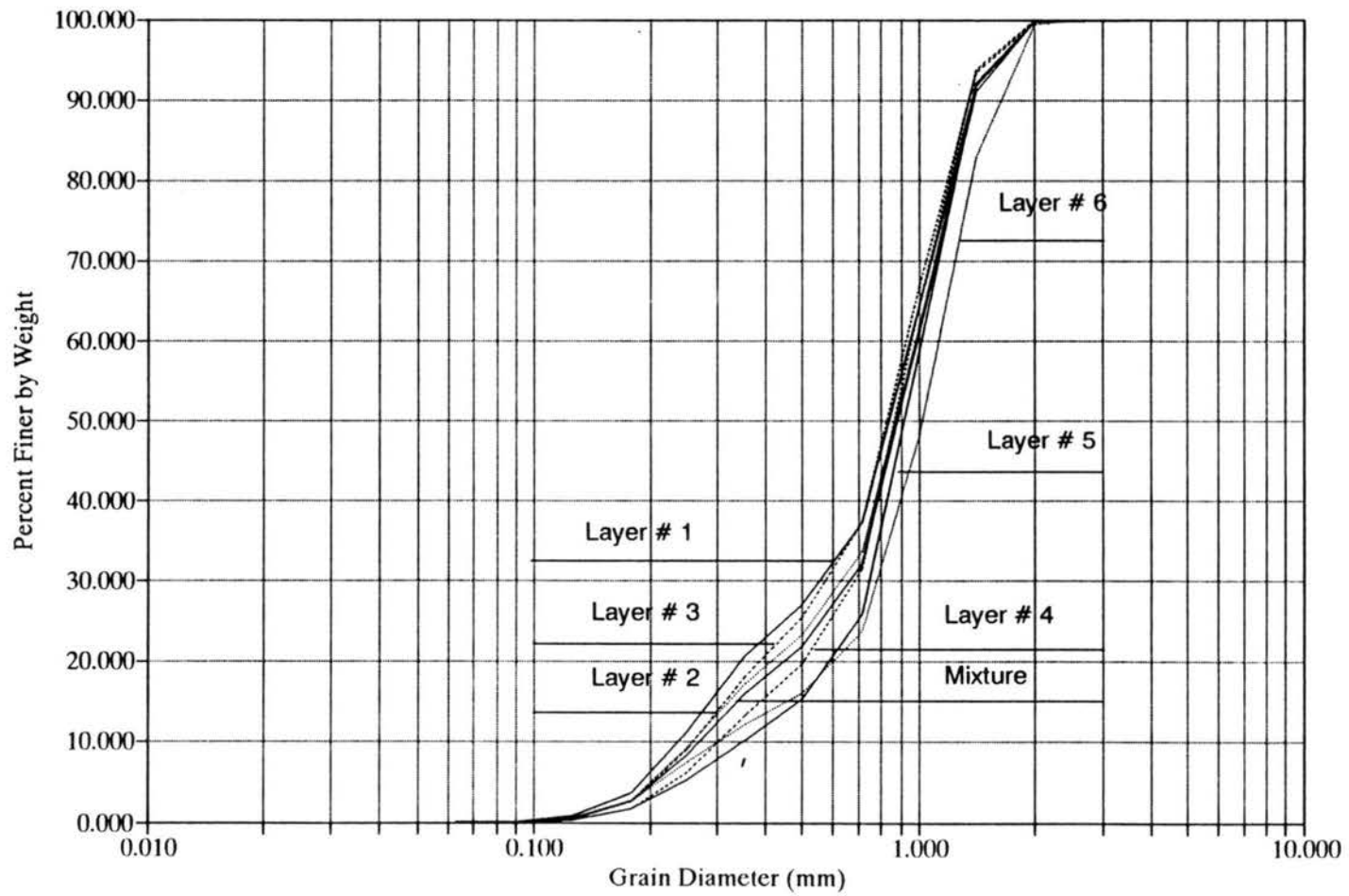


Figure A-12 : Size distribution curves for dune layers (Dune #3, Mixture # 4).

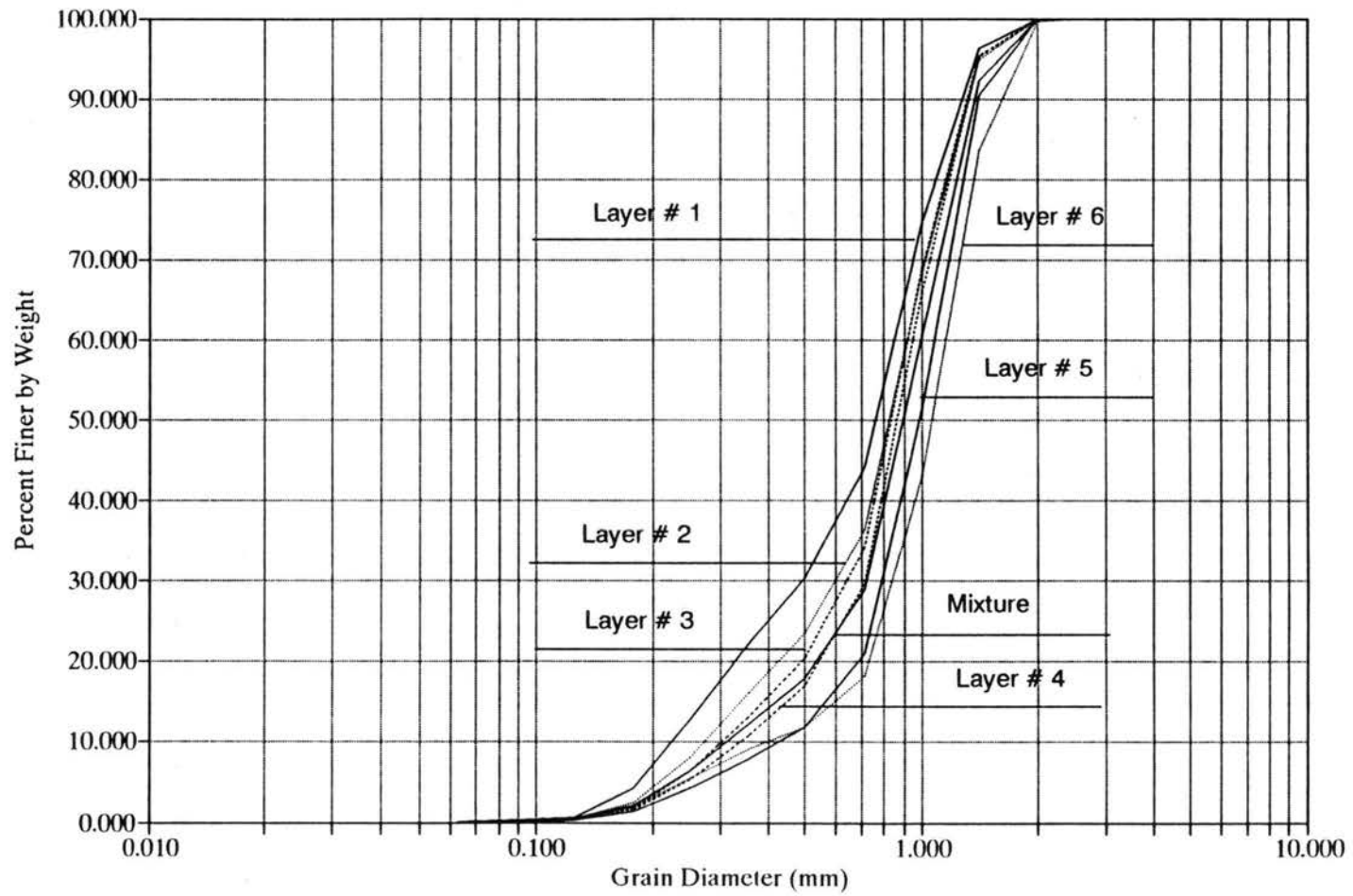


Figure A-13 : Size distribution curves for dune layers (Dune # 4, Mixture # 4).

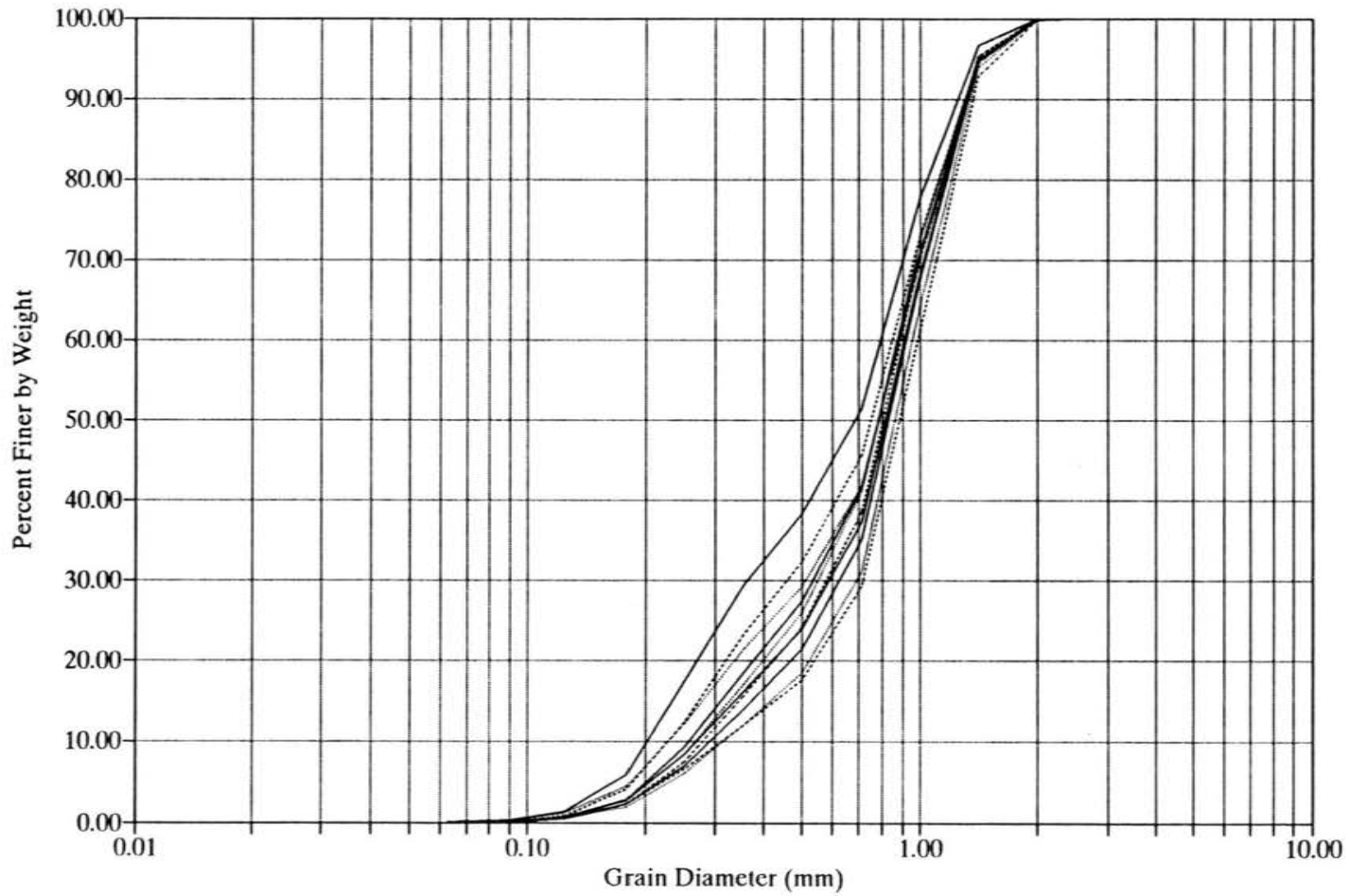


Figure A-14 : Size distribution curves for dune layers (Dune # 1.1, Mixture # 4).

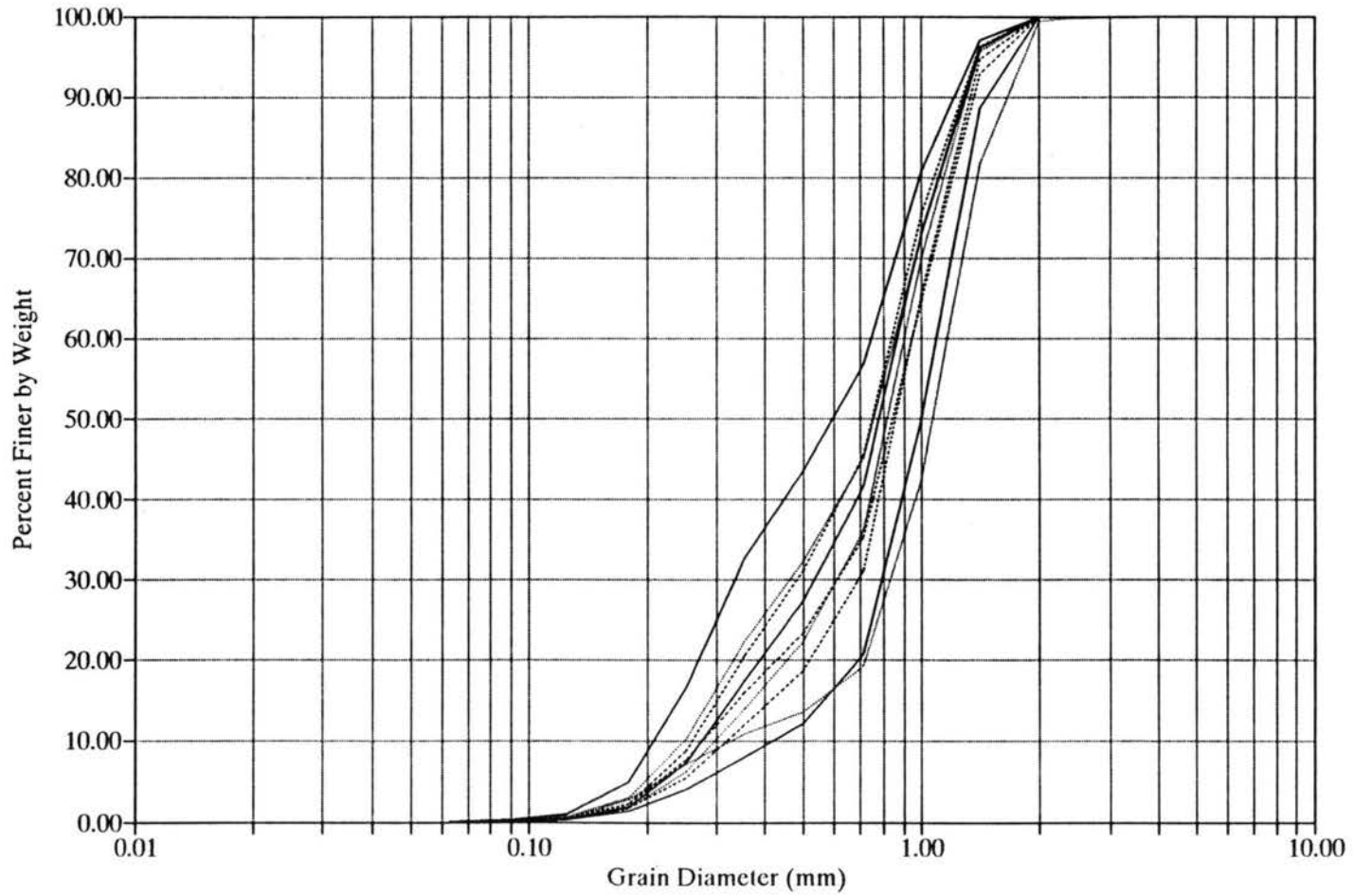


Figure A-15 : Size distribution curves for dune layers (Dune # 2.1, Mixture # 4).

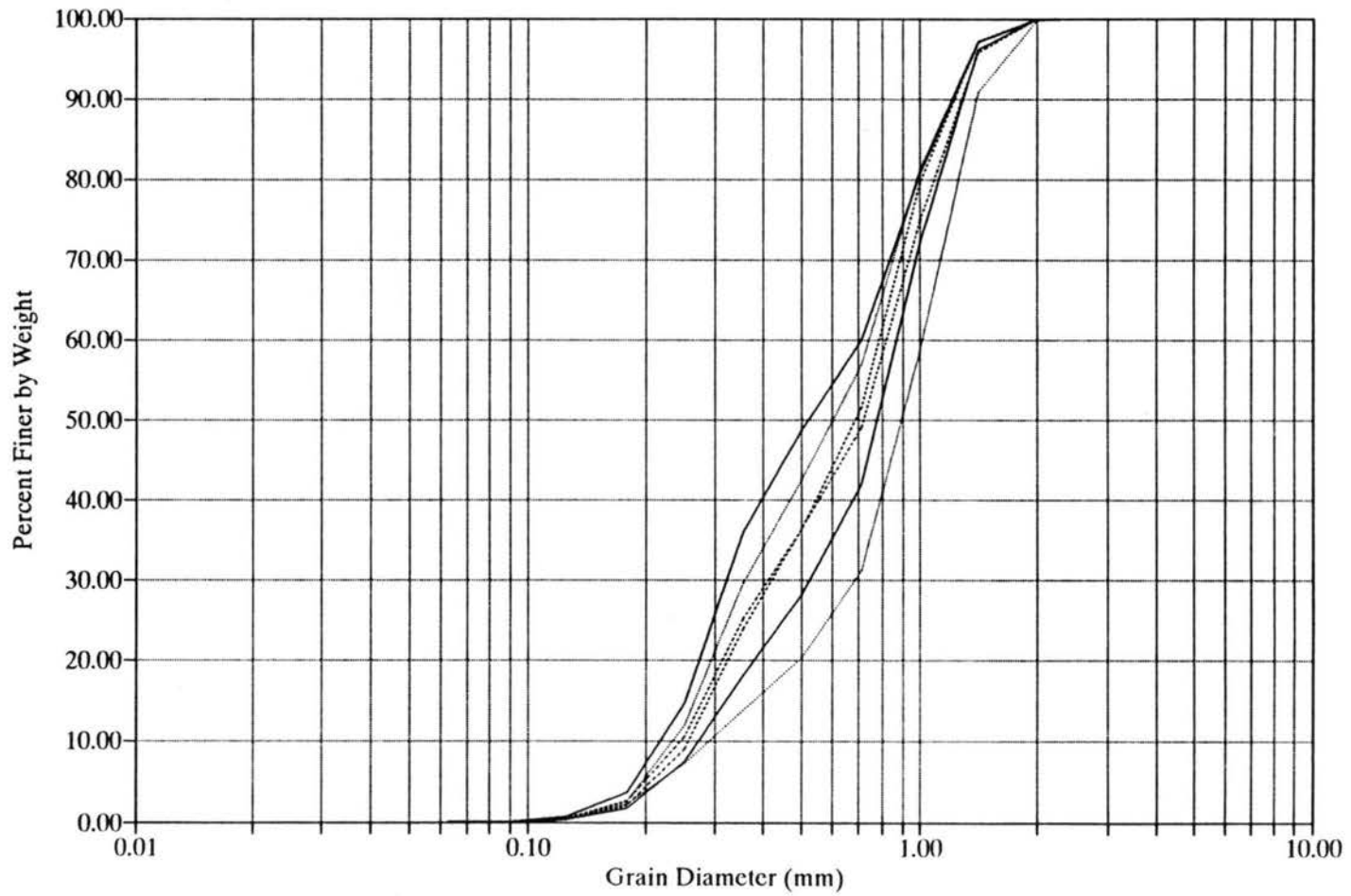


Figure A-16 : Size distribution curves for dune layers (Dune # 3.1, Mixture # 4).

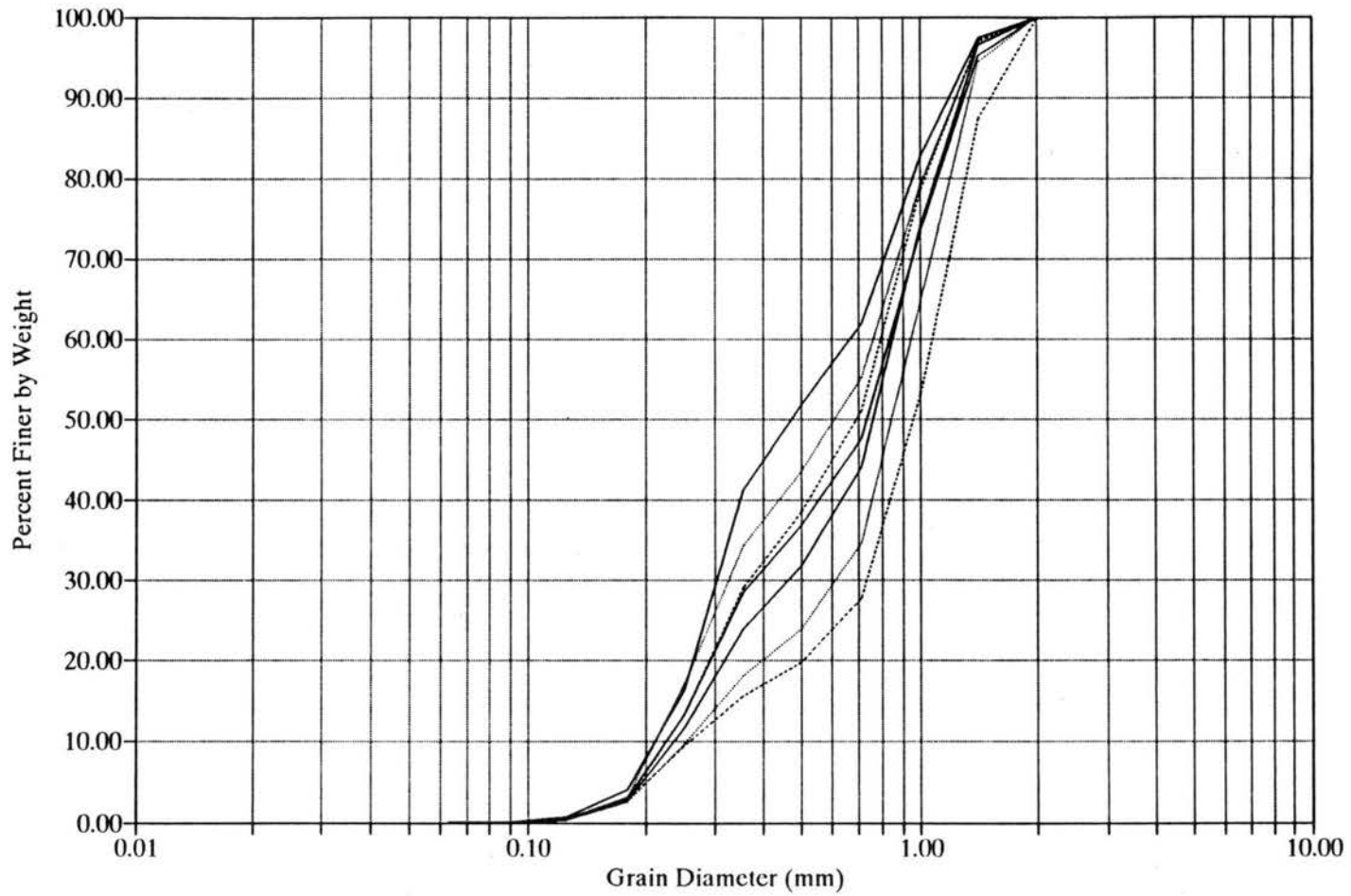


Figure A-17 : Size distribution curves for dune layers (Dune # 4.1, Mixture # 4).

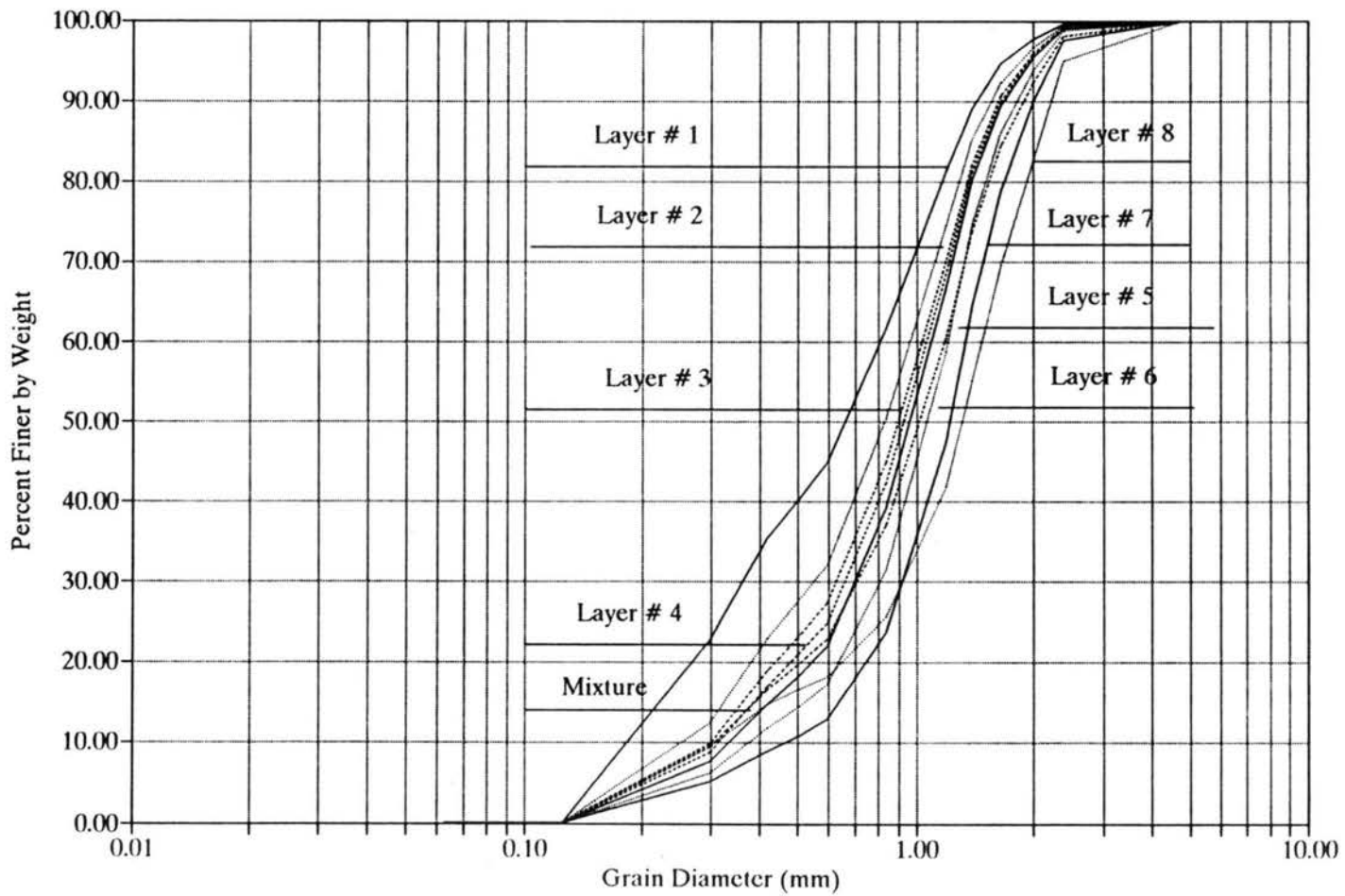


Figure A-18 : Size distribution curves for dune layers (Dune # 1, Mixture 5)

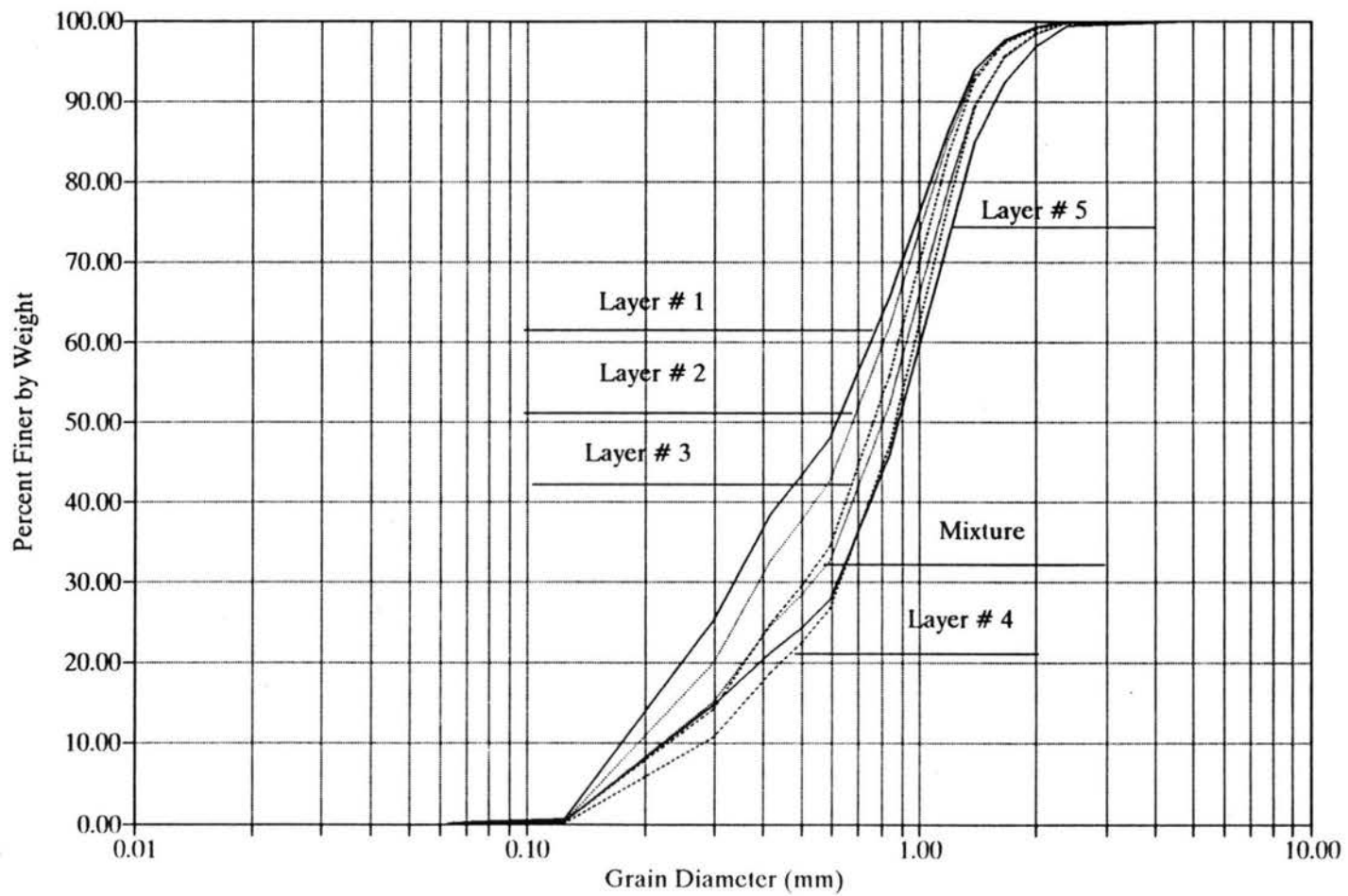


Figure A-19 : Size distribution curves for dune layers (Dune # 2, Mixture # 5)

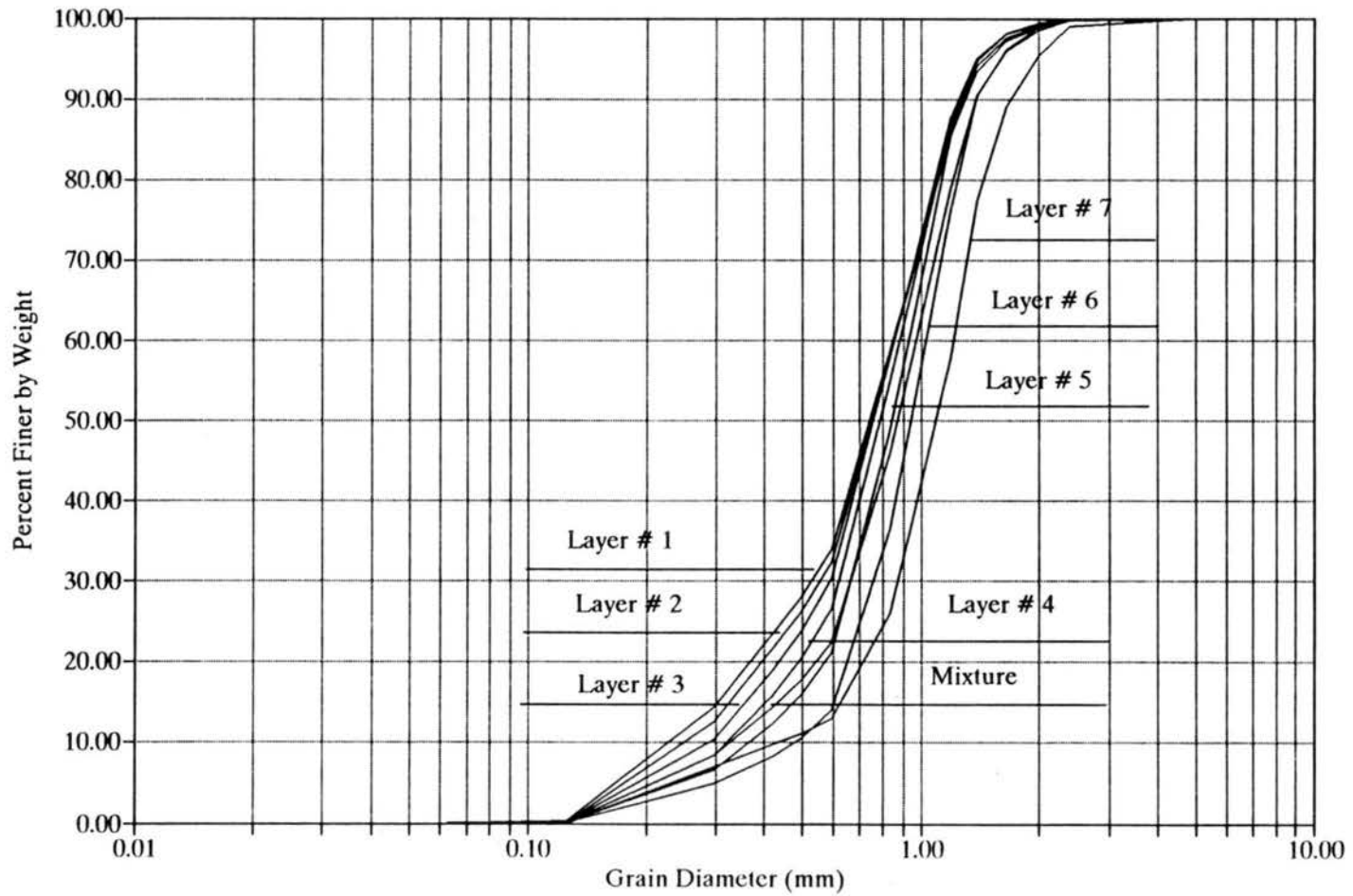


Figure A-20 : Size distribution curves for dune layers (Dune # 3, Mixture # 5)

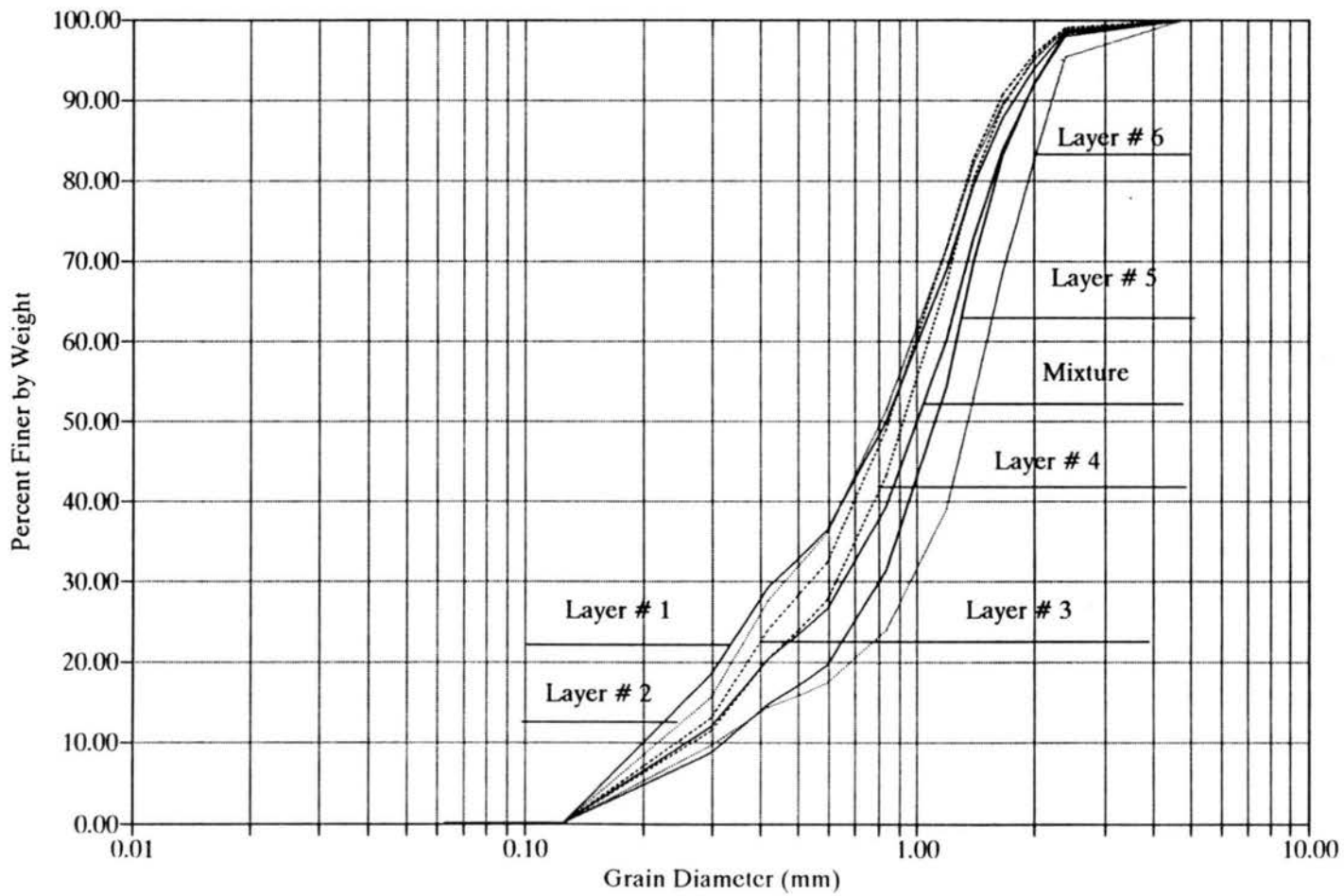


Figure A-21 : Size distribution curves for dune layers (Dune # 4, Mixture # 5)

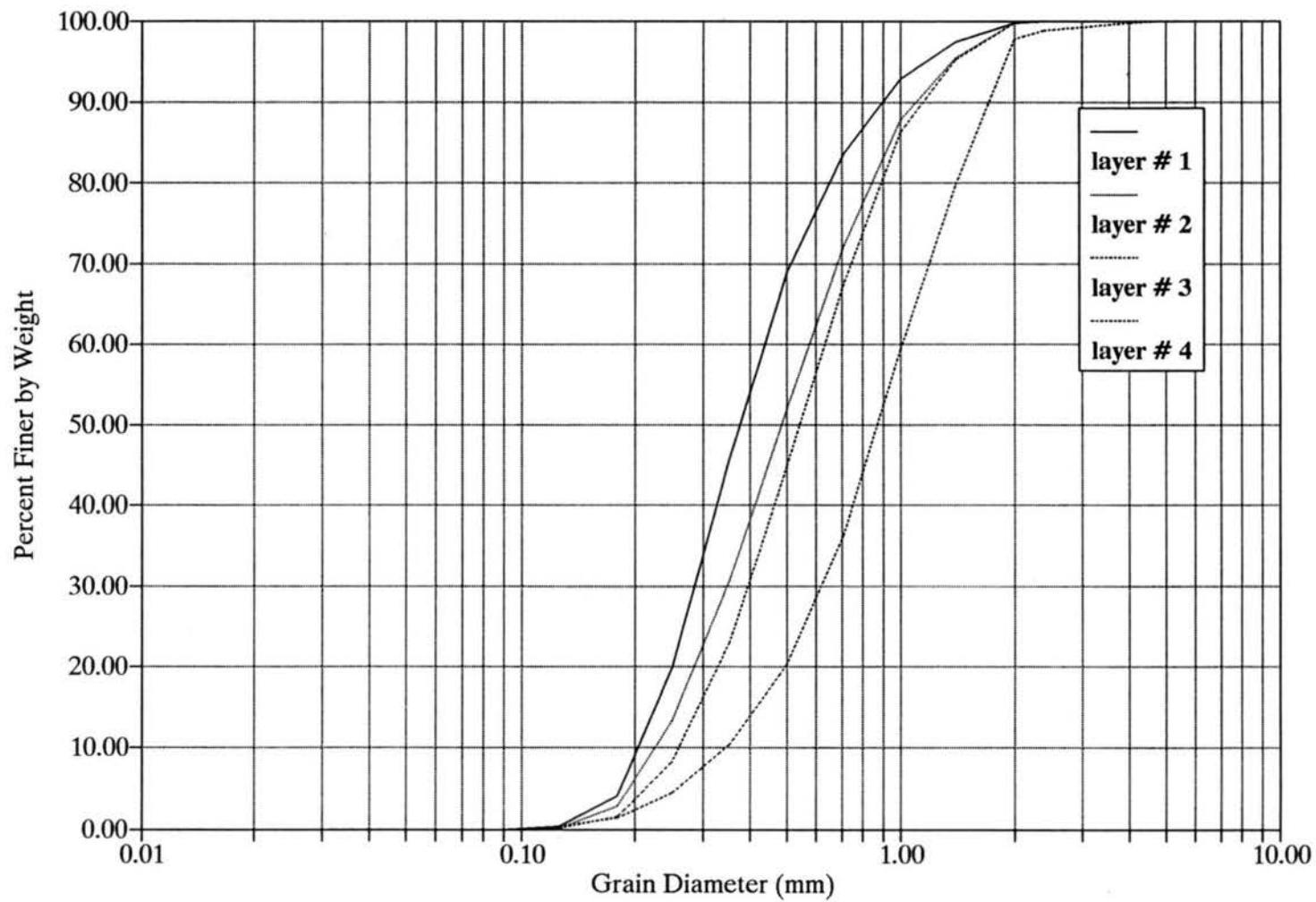


Figure A22 : Size distribution curves for dune layers (20 ft flume, Dune # 1)

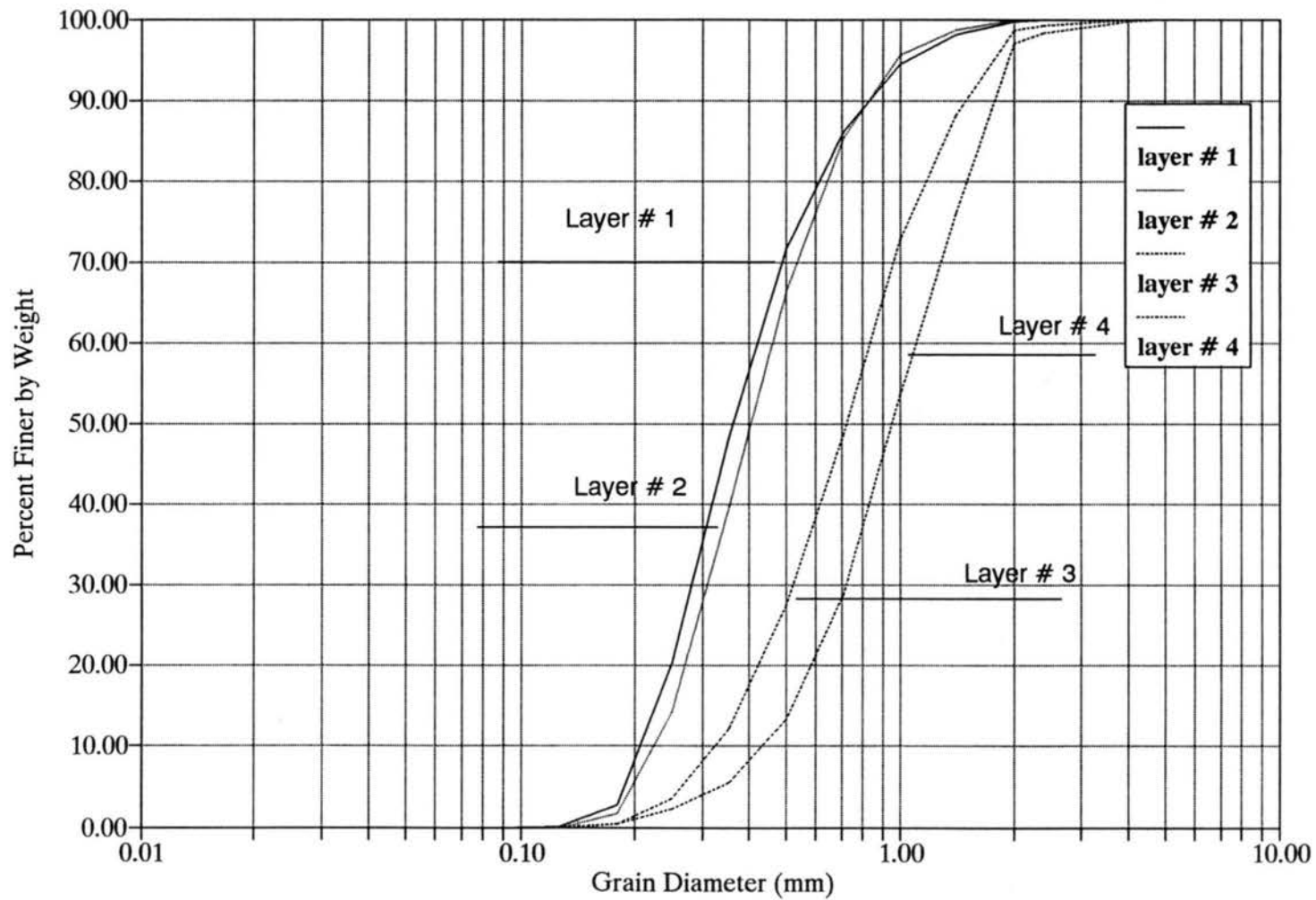


Figure A23 : Size distribution curves for dune layers (20 ft flume, Dune # 2)

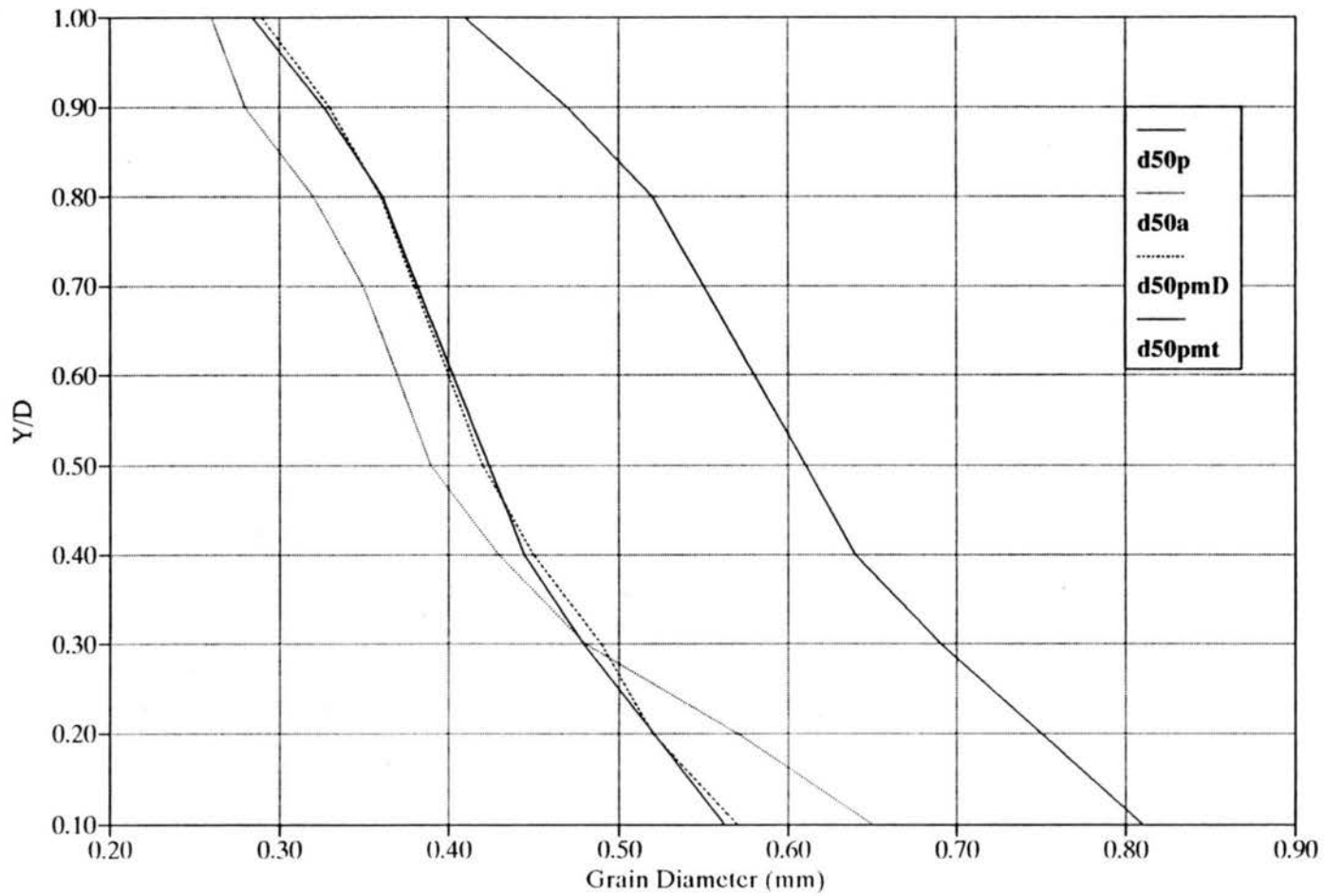


Figure A-24 : Predicted, modified, and actual median grain diameter for a dune layers (mixture number 1).

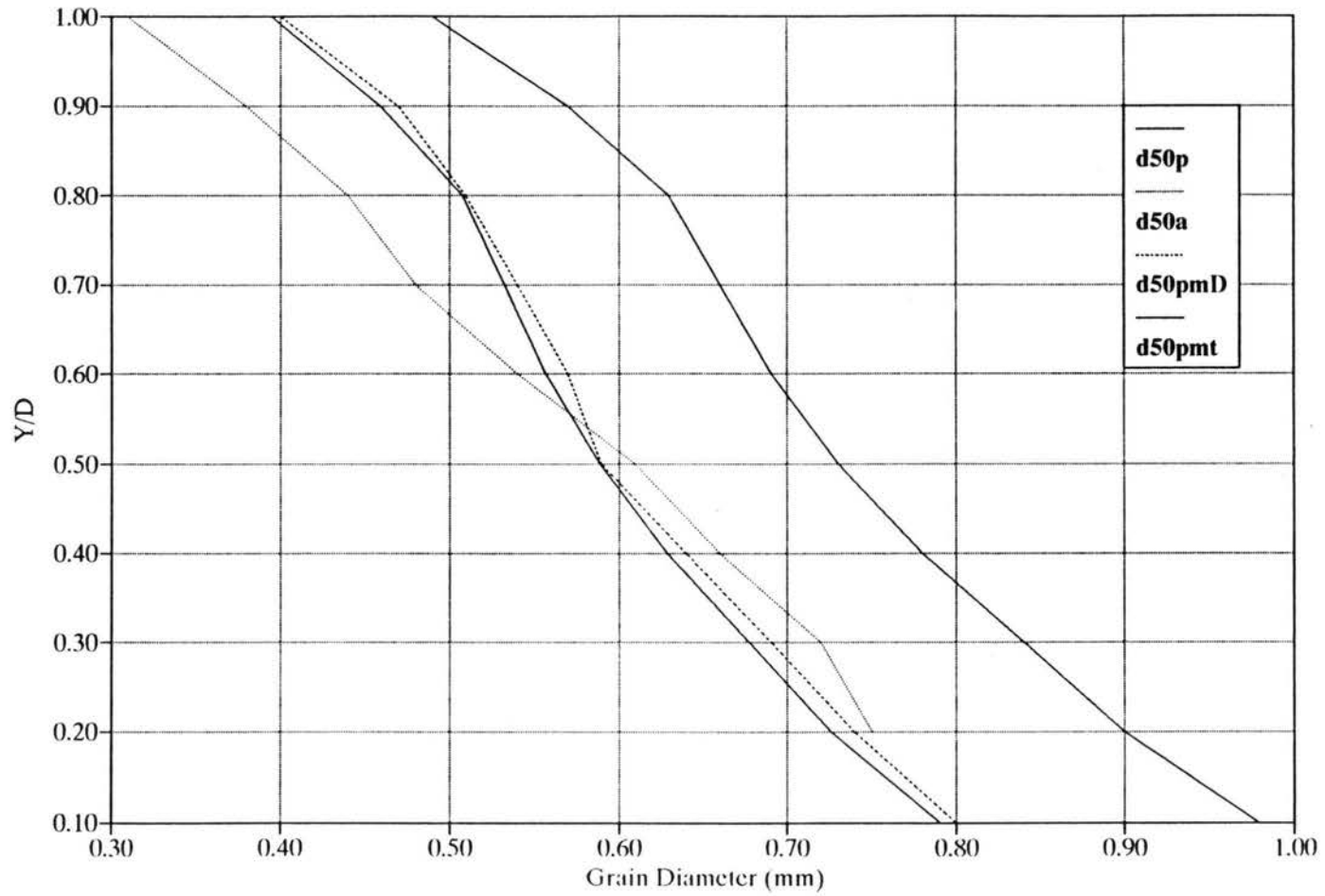


Figure A-25 : Predicted, modified, and actual median grain diameter for a dune layers (mixture number 2).

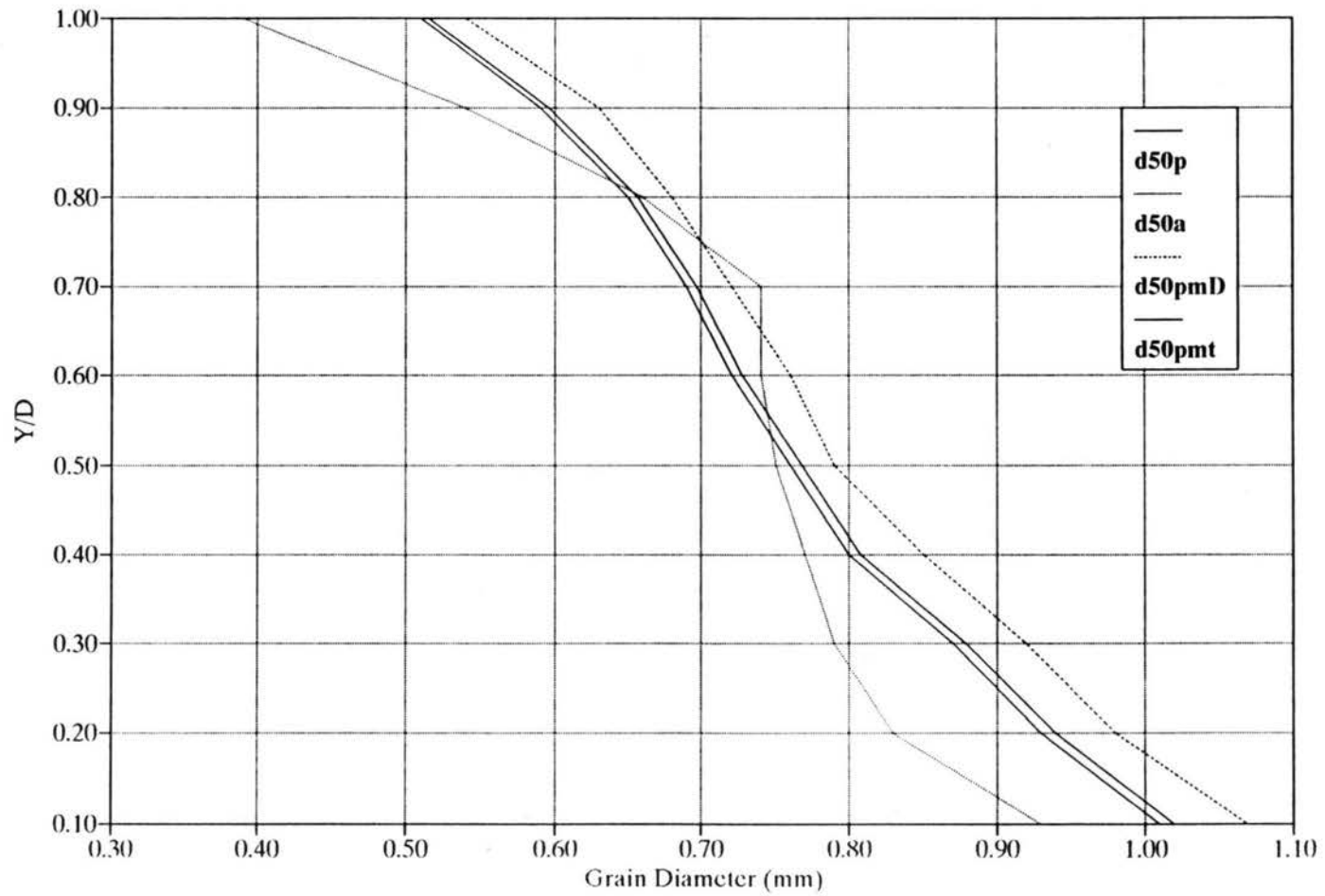


Figure A-26 : Predicted, modified, and actual median grain diameter for a dune layers (mixture number 3).

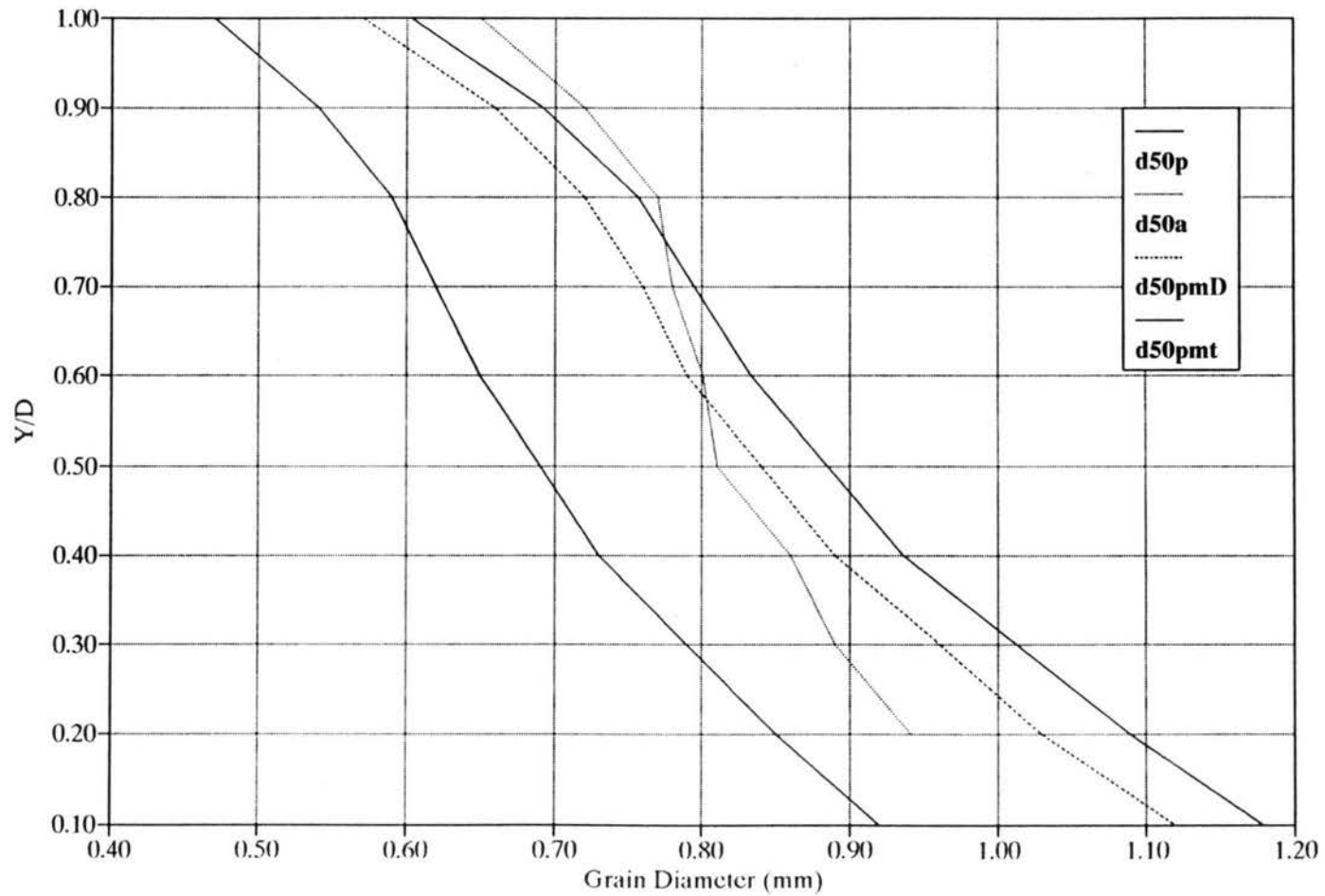


Figure A-27 : Predicted, modified, and actual median grain diameter for a dune layers (mixture number 4).

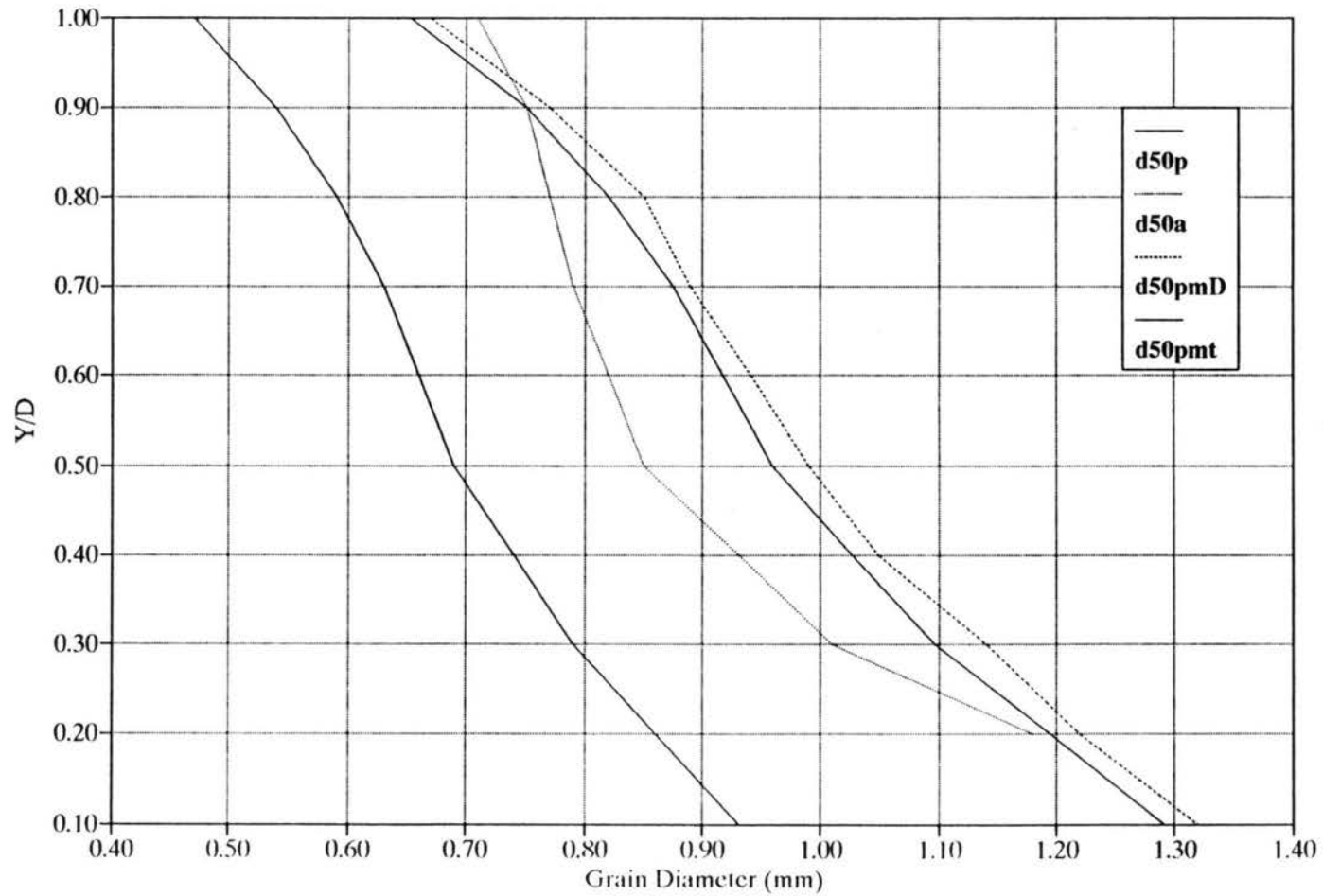


Figure A-28 : Predicted, modified, and actual median grain diameter for a dune layers (mixture number 5).

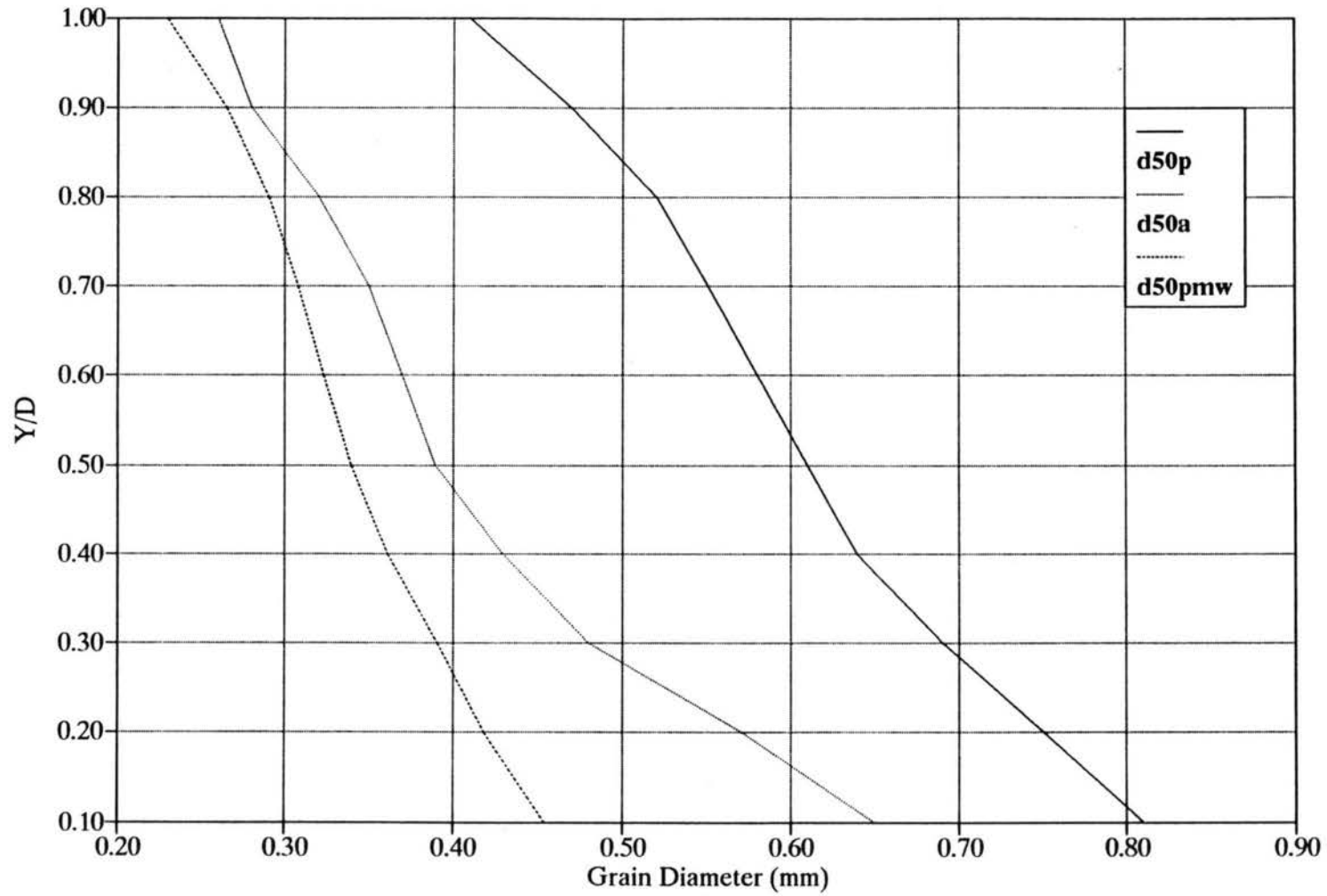


Figure A-29 : Predicted, modified, and actual median grain diameter for a dune layers (mixture number 1).

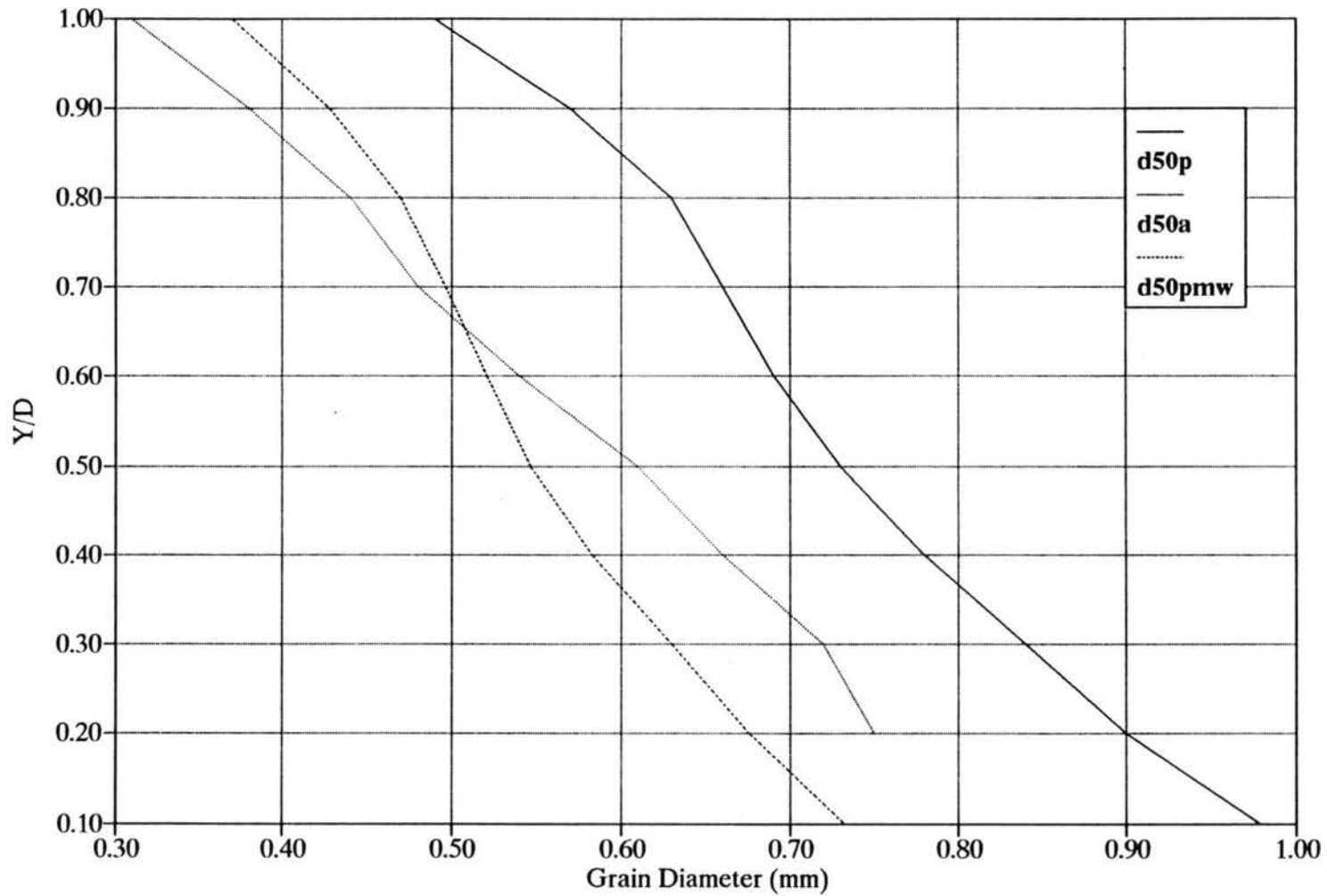


Figure A-30 : Predicted, modified, and actual median grain diameter for a dune layers (mixture number 2).

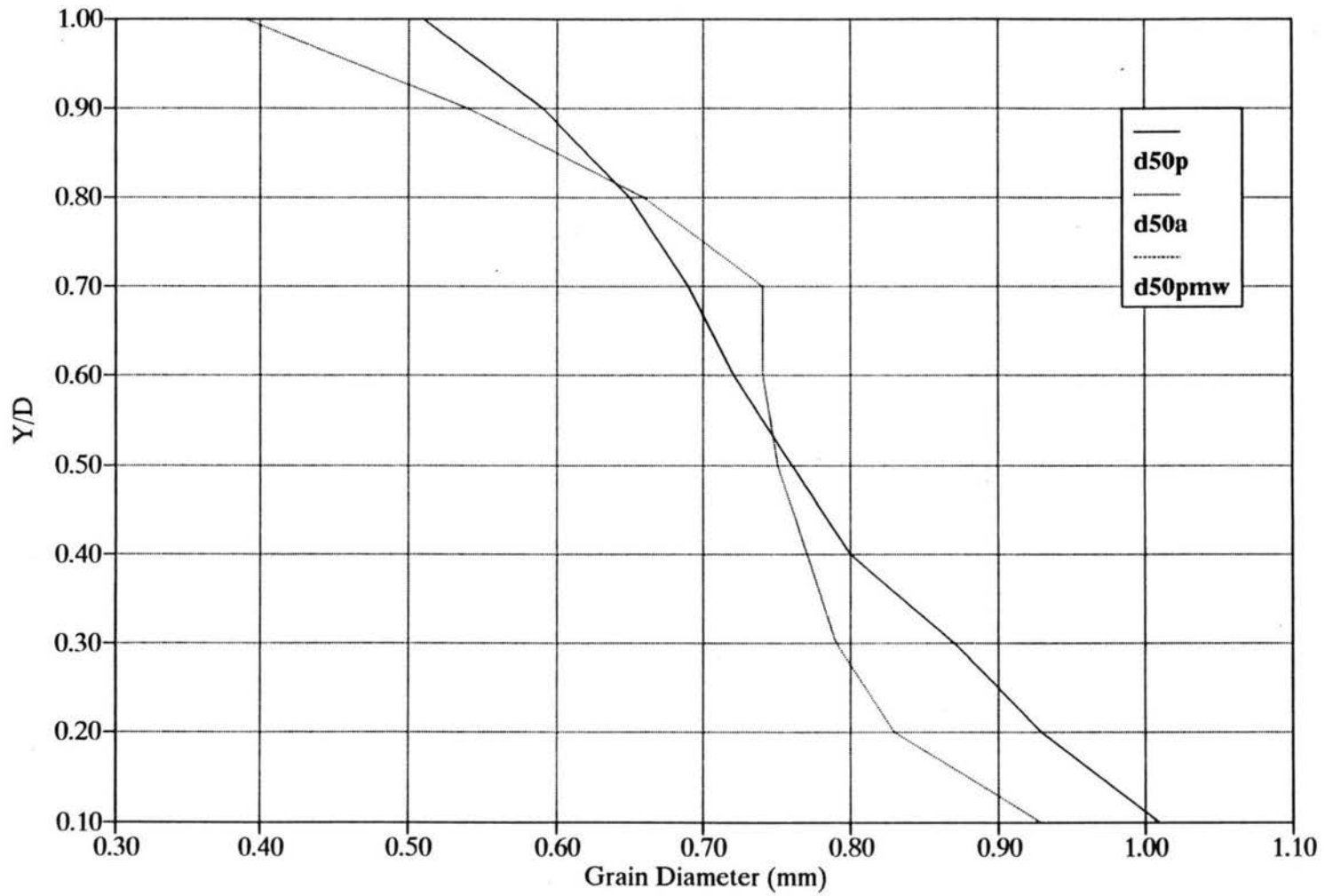


Figure A-31 : Predicted, modified, and actual median grain diameter for a dune layers (mixture number 3).

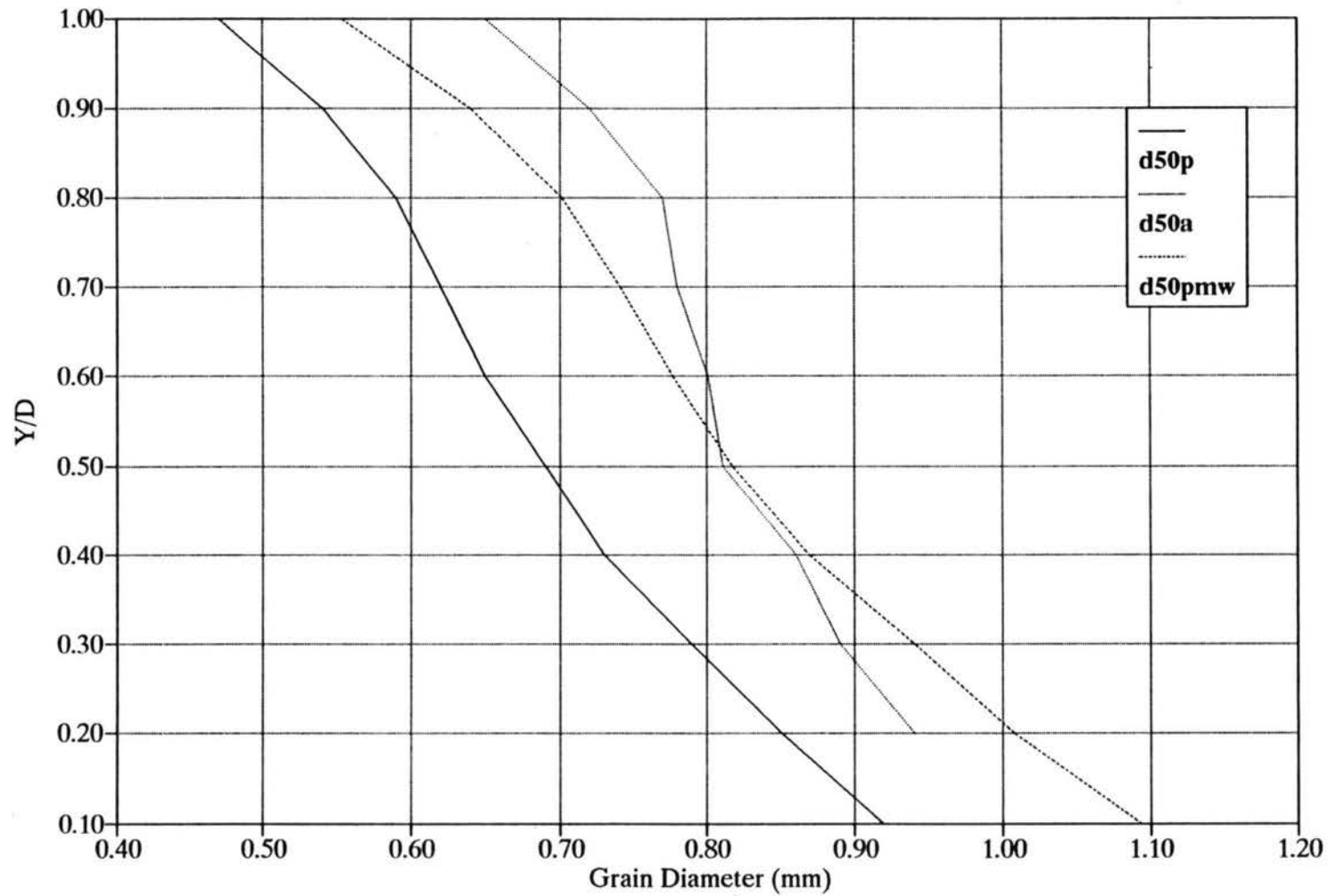


Figure A-32 : Predicted, modified, and actual median grain diameter for a dune layers (mixture number 4).

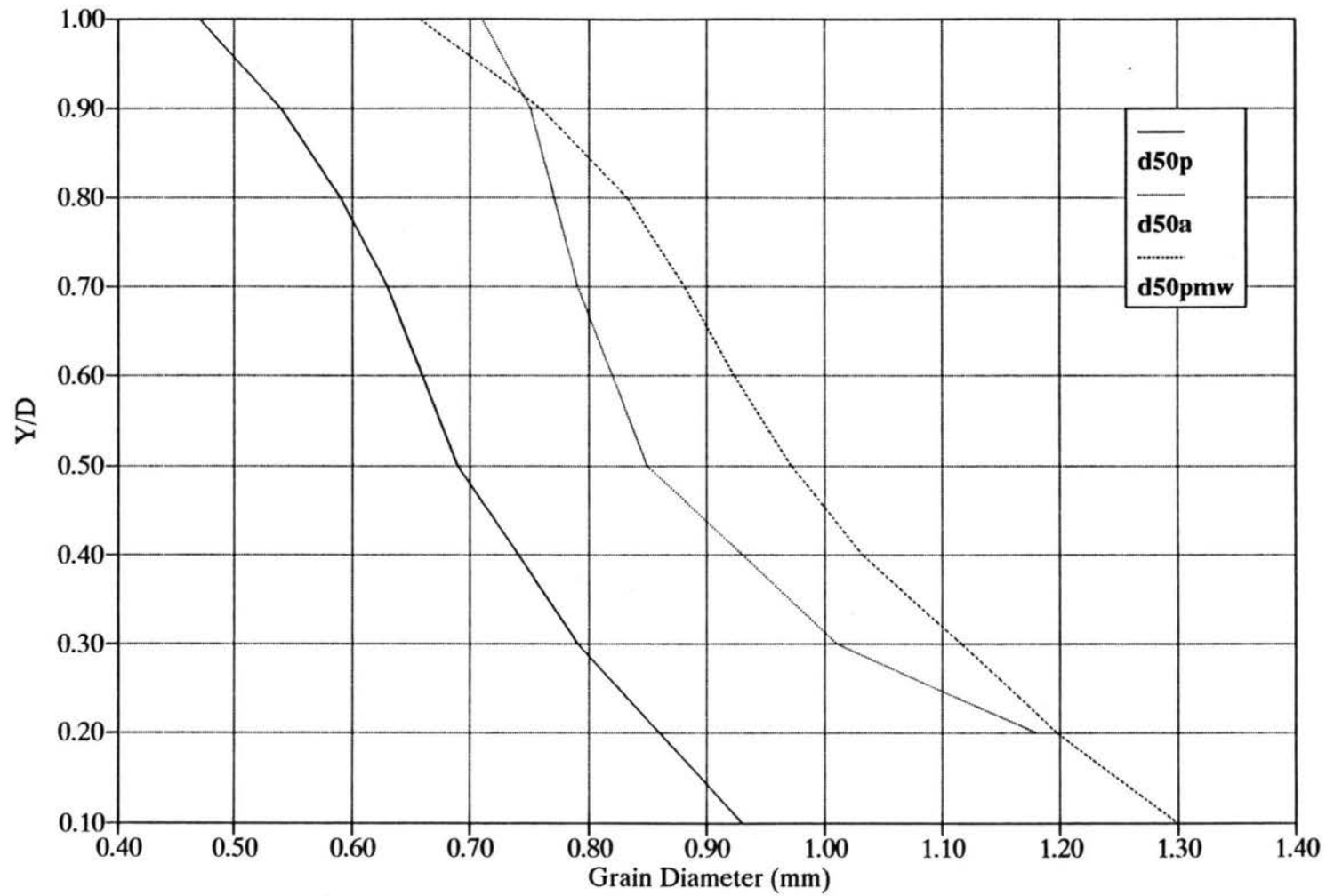


Figure A-33 : Predicted, modified, and actual median grain diameter for a dune layers (mixture number 5).

APPENDIX B

SHEAR STRESS CALCULATIONS

The average bed shear stress considering the influence of the wall can be calculated as:

$$\tau_b = \gamma_w r_b S_e \quad (\text{B.1})$$

where:

τ_b = bed shear stress,

γ_w = specific weight of the fluid,

P = fluid density,

g = acceleration of gravity,

S_e = slope of the energy gradient, and

r_b = hydraulic radius associated with the bed.

The value of r_b can be calculated as follows:

- 1 - Calculate R_e (Reynolds number) and f (friction factor) from the experimental data using the following equations:

$$R = \frac{4 r u}{\nu} \quad (\text{B.2})$$

$$f = \frac{8 g A s_e}{u^2 P} \quad (\text{B.3})$$

where:

r = The hydraulic radius for the whole section,

u = The mean velocity,

ν = The kinematic viscosity of the water,

g = The acceleration of gravity,

A = cross sectional area, and

p = wetted perimeter.

- 2 - Obtain f_w , which is the wall friction factor from Figure B.1 which relates R_e/f value to the f_w .
- 3 - Calculate f_b , which is the bed friction factor, from the following equation:

$$f_b = f + \frac{2d}{b} (f - f_w) \quad (\text{B.4})$$

where:

d = water depth, and

b = flume (channel) width.

- 4 - Calculate r_b from the following equation:

$$r_b = \frac{A_b}{p_b} = \frac{u^2 f_b}{8 g S_e} \quad (\text{B.5})$$

where:

A_b = area related to the bed, and

p_b = wetted perimeter related to the bed.

The bed shear stress can now be calculated using Equation B.1.

Calculation of shear stress due to grain resistance and form drag.

In 1952 an analysis was proposed by Einstein and Barbarossa to calculate the shear stress due to grain resistance and form drag. They considered that the bed shear stress, τ_b , could be divided into two parts.

$$\tau_b = \tau_{bg} + \tau_{bd} \quad (\text{B.6})$$

where:

τ_{bg} = The shear stress which results from grain resistance, and

τ_{bd} = The additional shear stress due to irregularities in the bed such as dunes.

In using the term "shear" it should be recognized that the resistance of the dunes is actually form drag resulting from a pressure differential on the front and back sides of the dune. With the shear stress divided they then divided the hydraulic radius, r_b , into two parts, r_{bg} and r_{bd} , in the following way:

$$r_b = r_{bg} + r_{bd} \quad (\text{B.7})$$

Also the shear velocities u_{*g} and u_{*d} were defined as:

$$u_{*}^2 = u_{*g}^2 + u_{*d}^2 \quad (\text{B.8})$$

$$u_{*g}^2 = g r_{bg} S_e \quad (\text{B.9})$$

The quantity, r_{bg} , is the hydraulic radius which the stream must have in order to flow at the same velocity and slope without dune resistance. The relationship between velocity, u , and r_{bg} was given by the Prandtl-Von Karman logarithmic resistance law for fixed channels as given by Keulegan (1938):

$$\frac{u}{u_{*g}} = 5.75 \log_{10} \left(12.27 \frac{r_{bg}}{k_s} x \right) \quad (\text{B.11})$$

where:

$k_s = d_{65}$ is the grain roughness of the bed, and

$x =$ The correction factor for channels which are not hydrodynamically rough, shown by a graph (see Figure B.2) as a function of k_s/δ_1 as in the following equation:

$$x = f\left(\frac{k_s}{\delta_1}\right) = f\left(\frac{k_s u_{*g}}{11.6 \nu}\right) \quad (\text{B.12})$$

with δ_1 being the thickness of the laminar sublayer, as long as the value of k_s / δ_1 is bigger than 5.00, $x = 1.00$ for all practical purposes. With the use of these equations, r_{bg} and u_{*g} can be determined by trial and error for any set of hydraulic measurements.

In 1957 Vanoni and Brooks modified the above method to avoid having to get r_{b1} and u_{*1} by trial and error. Substituting Equations B.9 and B.12 into Equation B.11, they obtained:

$$\frac{v}{\sqrt{g r_{b1} s_e}} = 5.75 \log_{10} 12.27 \left(\frac{r_{b1}}{k_s}\right) f_1 \left(\frac{k_s \sqrt{g r_{b1} s_e}}{11.6 \nu}\right) \quad (\text{B.13})$$

where, as before, f_1 is defined by a curve. Basically there are three parameters involved:

$$(a) \quad u/u_{*g} = u/\sqrt{g r_{bg} S_e}$$

$$(b) \quad r_{bg}/k_s$$

$$(c) \quad k_s \sqrt{g r_{bg} S_e} / 11.6$$

The solution of Equation B.13 for r_{bg} is laborious because r_{bg} appears in all three of these parameters, so that none of them is known directly before the trial and error solution is started. It is more convenient to change the parameters above to:

$$(A) \quad u/u_{*g} = u/\sqrt{g r_{bg} S_e}$$

$$(B) \quad u/\sqrt{g k_s S_e} = (a)\sqrt{b}$$

$$(C) \quad u^3/g \nu S_e = 11.6 (a)^3 (b) (c) .$$

Consequently, they got the following equation:

$$\frac{u}{\sqrt{g r_{bg} S_e}} = f_2\left(\frac{u}{\sqrt{g k_s S_e}}, \frac{u^3}{g \nu S_e}\right) \quad (\text{B.14})$$

Now, when r_{bg} is unknown, but u , s_e , and k_s are all known, the second and third parameters can be calculated directly and the first parameter involving r_{bg} is readily determined by Equation B.14 without resort to trial and error. Figure B.3 is a graph of this function derived from the Einstein-Barbarossa formulas. When this modified method is used, the values of r_{bg} and r_{bd} can be calculated as follows:

- 1 - Calculate the value of $(u/\sqrt{g k_s s_e})$ and $(u^3/g \nu s_e)$,
- 2 - Take the value of u/u_{*g} from Figure B.3,
- 3 - When the value of u_{*g} is known, the value of r_{bg} can be calculated using

$$r_{bg} = (u_{*g})^2 / g s_e ,$$
- 4 - Therefore, $r_{bd} = r_b - r_{bg}$, and
- 5 - Finally, the shear stress due to grain resistance and form drag can be calculated.

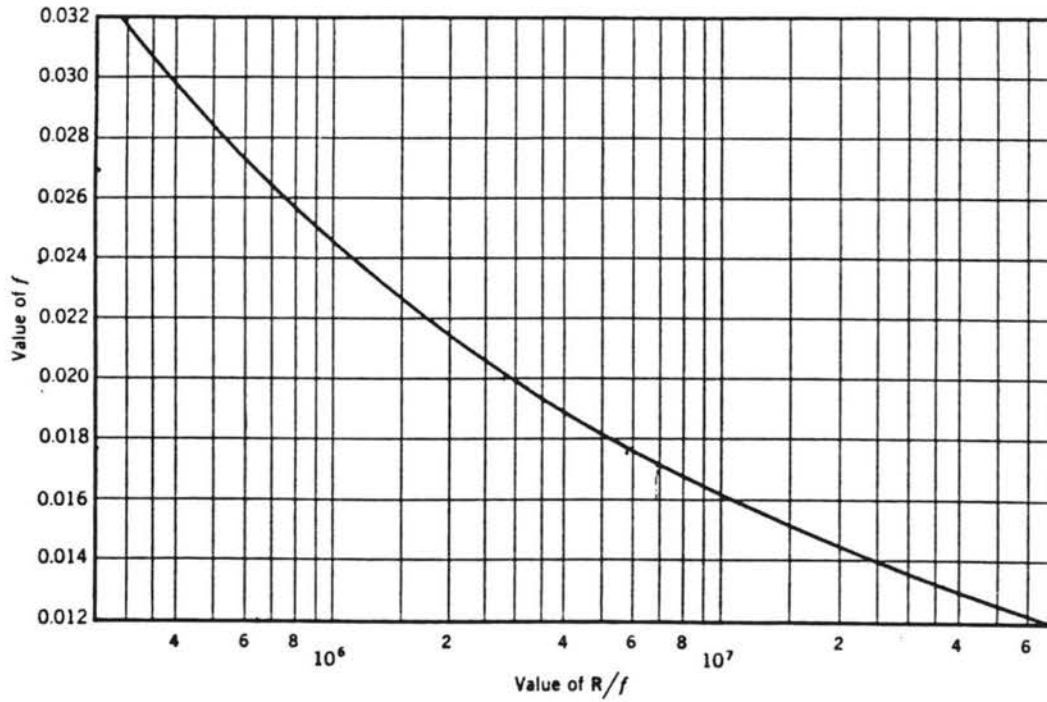


Figure B.1. Friction factor as function of R/f for smooth boundary channel and conduits, for use in side-wall correction calculation (Vanoni and Brooks, 1957).

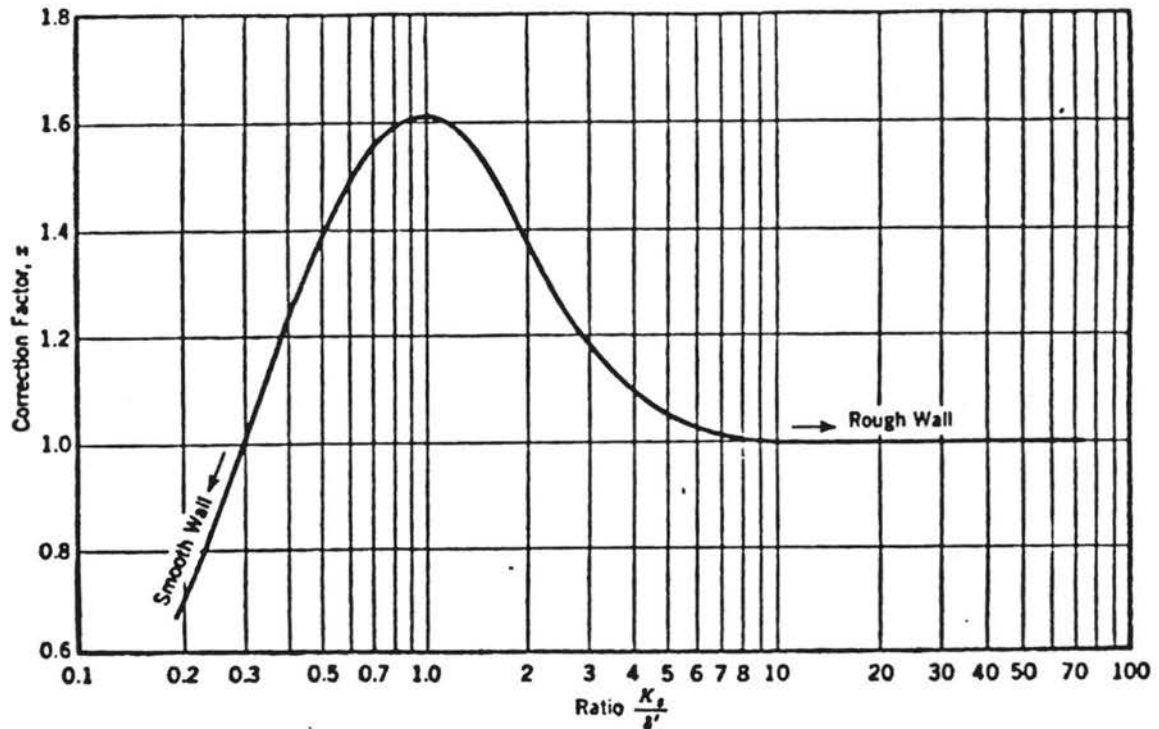


Figure B.2. Correction x in the logarithmic friction formula (Einstein and Barbarossa, 1952).

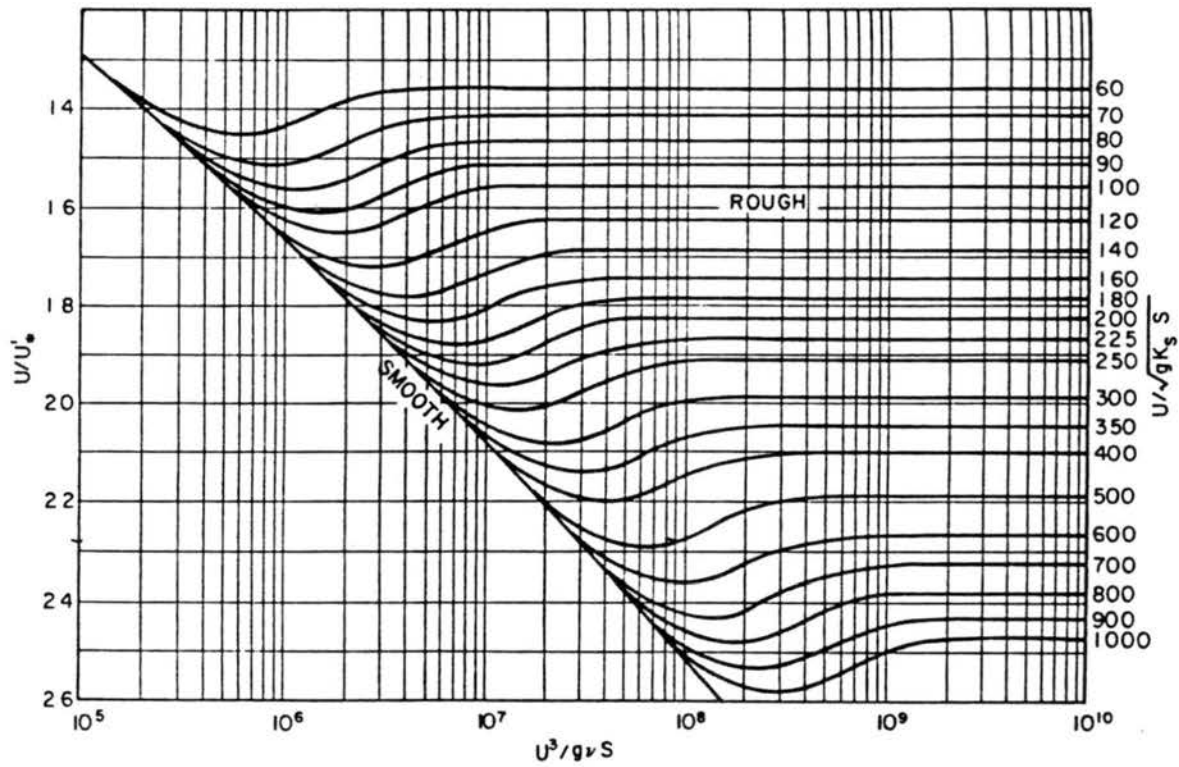


Figure B.3. Curves for graphical solution of Einstein-Barbarossa Equation for determination of r_{bg} and r_{bd} (Vanoni and Brooks, 1957).